UNIVERSITÀ DEGLI STUDI DI ROMA
"LA SAPIENZA"

FACOLTÀ DI SCIENZE MATEMATICHE FISICHE E NATURALI

Dottorato in Fisica - Ph.D. in Physics
XVI ciclo

Kinetically constrained models and glassy dynamics

Candidate:
Dr. *Cristina Toninelli*

Supervisor:
Prof. *Giovanni Jona Lasinio*

October, 2003

Contents

Chapter 1

Introduction

The subject of this thesis is the investigation of the mechanisms underlying the slowing down of dynamics and the occurrence of a dynamical arrest for some physical systems. Experimentally, upon changing physically relevant parameters such as temperature or density the typical times for relaxation to equilibrium of a wide variety of systems increase dramatically. Therefore, after a certain value of the tuned parameter the sample is no more able to equilibrate and freezes in an amorphous phase where dynamics experimentally occurs in a non–stationary regime. One of the most well–know among these phenomena is the so–called *glass transition*, namely the dynamical arrest occurring for a supercooled liquid upon lowering its temperature. Therefore, the overall phenomena related to dynamical arrest are usually referred to as *glassy dynamics*. We emphasize that glass transition is however only a particular case of these *jamming transitions*, which are a more widespread phenomenon. For example, analogous phenomena occur upon increasing the density for granular media, polymer melts and suspensions of colloidal particles and upon lowering the temperature for spin glasses. Despite a great deal of theoretical efforts, these remarkable phenomena are still far from understood. In particular, it is not clear if the slowing down of dynamics is due to an underlying thermodynamic transition or is a purely dynamical phenomenon. More generally, understanding the nature of the physical mechanisms inducing the slowing down of dynamics is still a widely open issue.

In this work we analyze the dynamics of some *kinetically constrained models*. These are models of particles with possible discrete positions on the sites of a lattice and hard core exclusion. The dynamics is given through a stochastic sequence of jumps (for conservative models) or birth–death (for non—conservative models) of particles. The former are referred to as *kinetically constrained lattice gases* and the latter as *kinetically constrained*

spin models. Indeed, it is natural to rewrite non–conservative models as spin models with a spin on each site and a dynamics consisting in a sequence of spin flips. For both models the moves are allowed only if the configuration satisfies some local constraints, namely for some configurations the rate of a given move (particle jump or spin flip) can degenerate to zero. Moreover, these rates are chosen in order to satisfy detailed balance with respect to a trivial measure, which is therefore invariant under dynamics. For kinetically constrained lattice gases this is usually flat measure over all configurations with the same number of particles on a finite lattice and Bernoulli product measure at a given density on the infinite lattice. However, due to the degeneracy of rates, the configuration space is usually broken in different irreducible components, namely there are configurations which cannot be connected one to the other by any path of allowed moves. In this case the invariant measure is not unique. In particular there exist *blocked configurations*, i.e. configurations in which any move is forbidden by the kinetic constraints. Therefore, measure concentrated on these particular configurations are invariant too. The existence of many invariant measure implies a non–trivial relaxation dynamics and in the thermodynamic limit a *dynamical transition* could occur. With this we refer to the possibility that the infinite system undergoes an ergodic/non–ergodic transition. For example, if the kinetic constraints strongly depends on the local density of particles, it could be possible that a kinetically constrained lattice gas is ergodic with respect to Bernoulli product measure in a given density regime and non–ergodic at different densities. Moreover, even if such transition does not take place there could be a different kind of *dynamical arrest*, e.g. a diffusive/non–diffusive transition in the long time behaviour of a tagged particle displacement.

Kinetically constrained models were introduced as simplified models to study glassy dynamics. A very intuitive link among these models and supercooled liquids is that by a proper choice of kinetic rules one can mimic the fact that in a dense liquid a molecule can get trapped by surrounding molecules. This *cage effect* could be at the root of the cooperative behaviour which induces glass transition. In this respect, these are very simplified models since they allow only a discrete choice for the positions of particles. However, there is a deeper reason for studying these models in relation with *glass* and more generally *jamming transition*. The basic Ansatz is that jamming transition is a purely dynamical phenomenon with static correlations playing no role. This is suggested by the fact that, in a small window in the vicinity of the transition, experiments detect a dramatic change in dynamical properties while structural ones remain almost unchanged. In other words, there could exist a dynamical length which diverges while static one remains constant. If this is the case, the key mechanism for glass transition could be captured

by an effective model obtained by performing a coarse graining on the scale of the static length. This rescaled model should have a trivial statics and a very slow relaxation dynamics which could be well reproduced by a kinetically constrained model. Therefore, despite their simplicity, such models could provide a good description of real systems at a mesoscopic level which already contains the key mechanisms for glassy dynamics. In this approach the discrete variable could correspond to e.g. the average of the particle density over the coarse–graining volumes. Of course, a true mapping from the microscopic description to the mesoscopic one is a formidable task. However, studying the dynamics of these models can be a very useful ground to understand the mechanisms underlying jamming transitions in real systems. On the other hand, this study is also a relevant issue in the context of stochastic models of interacting particles.

In recent years several numerical simulations have been performed on these models. For some choices of the kinetic constraints a sluggish and heterogeneous relaxation which is very reminiscent of glassy dynamics has been detected. However, the main issues in understanding these phenomena are still open. In particular, it is not clear if the slowing down of dynamics is related to the presence of a real dynamical transition or is a simple cross over in typical time–scales. More generally, one would like to understand the nature of the collective processes inducing the slowing down of dynamics and its heterogeneous character. Numerical studies are not conclusive on these issues. The difficulty lies in the fact that since dynamics is very slow, one cannot analyze the large time behaviour by means of simulations. Moreover, since the behaviour of these models on finite and infinite lattices can be extremely different, it is difficult to controll finite size effects on numerical results and extrapolate the behaviour of the system in the thermodynamic limit.

In this work we study some of these models by means of analytical tools. In particular we focus on Kob Andersen (KA) [1] and Fredrickson Andersen (FA) [2] models, which are probably the most well–known kinetically constrained models of conservative and non–conservative type, respectively. On infinite lattices, KA dynamics satisfies detailed balance with respect to Bernoulli product measure at any density. The same is true for FA dynamics with respect to canonical measure at any temperature with a simple non–interacting Hamiltonian. For KA model we prove that a dynamical transition occurs in the mean field approximation, namely there exists a critical density above which the system is not ergodic. This transition is destroyed in finite dimensions by exponentially rare processes which occur in sufficiently large systems. More precisely, we identify the cooperative rearrangements which guarantee ergodicity and a strictly positive diffusion coefficient at any

density. Furthermore, we predict the typical length and time scales of these collective processes, which grow extremely rapidly in the high density regime. On the other hand, we predict a cross–over at a finite density to a different relaxation mechanism which should give rise to a substantial range of "critical behaviour" for diffusion coefficient (and relaxation times) near an *apparent* transition. This cross–over, which can be in some cases very sharp, can be regarded as a ghost of the mean field transition surviving in finite dimensions and could explain previous numerical results which claimed the existence of a dynamical transition. To confirm our analytical results we have performed Monte Carlo numerical simulations, which are indeed in good agreement with the theoretical predictions. Moreover, we give a possible explanation of the heterogeneous character of the dynamics which relies on the strong density–dependence of typical relaxation times. For FA model we obtain very similar results. In particular, we calculate a finite critical temperature at which a mean field ergodic/non–ergodic transition takes place. By performing numerical simulations we find indeed that below such temperature the dynamics dysplays the typical character of out of equilibrium glassy dynamics. In the finite dimensional case, irreducibility in the thermodynamic limit was an already proven result. We show that this implies ergodicity (which is not a priori guaranteed for an infinite volume process) and predict typical relaxation times in the low temperature regime, which are in good agreement with numerical simulations.

1.1 Outline of the thesis

This work is organized as follows.

- In Chapter 2 we introduce glass and jamming transition. After recalling the main open issues in understanding the slow relaxation dynamics related to these phenomena, we introduce some of the theoretical approaches. In particular we focus on kinetically constrained lattice models, which are the main subject of present work. After defining such models, we analyze the different forms of dynamical arrests that could take place for these systems and introduce some of the tools we will use to study their dynamics.

- In Chapter 3 we introduce two classes of kinetically constrained lattice gases. First we consider these models on finite d–dimensional hypercubic lattices in contact with boundary sources of particles and give sharp estimates on the velocity of convergence to equilibrium. Then we analyze the models on the infinite lattice. In this case we prove

ergodicity and positiveness of the self diffusion coefficient of a tagged particle at any finite density.

This chapter is based on:

L.Bertini, C.Toninelli *Exclusion processes with degenerate rates: convergence to equilibrium and tagged particle*
preprint number`cond-mat/0304694`.

- In Chapter 4 we recall the definition of Kob Andersen model (KA). We shortly recall previous numerical results which detected a slow and heterogeneous behaviour in the high density regime for . We study the model on d–dimensional hypercubic lattices and prove that in the thermodynamic limit the configuration space is always covered by a single ergodic component at any finite density. In other words, an ergodic/non–ergodic transition cannot take place. On the other hand, on lattices of finite linear size L, the process is never ergodic. However, we identify a density dependent crossover size $\Xi(\rho)$ which separates the regime ($L < \Xi(\rho)$) in which the configuration space breaks into exponentially many ergodic components from the regime ($L > \Xi(\rho)$) in which a single component has almost unit probability.

  This chapter is based on:

  C.Toninelli, G.Biroli, D.S.Fisher *Spatial structures and dynamics of kinetically constrained models for glasses*
  preprint number`cond-mat/ 0306746`

  C.Toninelli, G.Biroli, D.S.Fisher *Kob Andersen model: proof of ergodicity and mean field transition*
  in preparation

- In Chapter 5 we analyze KA model on a Bethe lattice, which provides a mean field approximation of the model on the hypercubic lattice. In this case the scenario is completely different. Indeed we prove that there exists a finite critical density at which the system undergoes an ergodic/non–ergodic transition. This corresponds to a transition from a regime in which all particles can diffuse to a partially frozen phase. The transition has aspects of both first and second order transition and is very similar to the dynamical transition in p–spin models with quenched disorder. The comparison of results for the hypercubic and Bethe lattice case can be a first step towards a better understanding of how the results in other mean field approaches to glass transition (e.g. mode coupling theory and random first order scenario) modify for real systems.

This chapter is based on:

C.Toninelli, G.Biroli, D.S.Fisher *Spatial structures and dynamics of kinetically constrained models for glasses*
preprint number`cond-mat/ 0306746`

C.Toninelli, G.Biroli, D.S.Fisher *Kob Andersen model: proof of ergodicity and mean field transition*
in preparation

- In Chapter 6 we consider dynamics of KA model on hypercubic lattices. First we prove that there is no dynamical diffusive/non–diffusive transition at any finite density, namely the self diffusion coefficient of the tagged particle is strictly positive at any density. Then we analyze the density dependence of the self diffusion coefficient and of the typical relaxation times. In the high density regime diffusion is guaranteed by the cooperative slow motion of rare regions in which vacancies are configured in special ways. The self diffusion coefficient vanishes, for density which goes to one, as the density of these rare regions which goes to zero faster than any power law. Therefore, this collective processes are at the root of the dramatic slowing down of dynamics for this model. By performing Monte Carlo simulations we have checked the validity of these analytical results. On the other hand, by percolation–type arguments we predict a cross over for lower densities to a non–cooperative diffusion mechanism. This should give rise to an *apparent* diffusive/non–diffusive transition due to a substantial range of power law decrease for the self diffusion coefficient near a finite density. The existence of such cross–over provides a possible explanation of the dynamical transition claimed by previous numerical results.
  Finally we give a possible interpretation of the heterogeneous relaxation which occurs in the high density regime.

  This chapter is based on:

  C.Toninelli, G.Biroli, D.S.Fisher *Spatial structures and dynamics of kinetically constrained models for glasses*
  preprint number`cond-mat/ 0306746`

  C.Toninelli, G.Biroli, D.S.Fisher *Relaxation time scales for kinetically constrained lattice models*
  in preparation

  G.Biroli, C.Toninelli *Kob Andersen model: diffusion of the tagged particle*
  in preparation

- In Chapter 7 we recall the definition of Fredrickson Andersen model (FA). For the model on the hypercubic lattice we recall the result of irreducibility in the thermodynamic limit and prove that this implies ergodicity. Then, as for KA model, we estimate the typical relaxation time scales and check by numerical simulations our predictions. Also in this case, the mean field scenario is completely different. Indeed, for the model on the Bethe lattice, we find a dynamical transition which has aspects very similar to those of p–spin models with quenched disorder.

  This chapter is based on:

  G.Biroli, S.Franz, M.Sellitto, C.Toninelli *Fredrickson Andersen model: mean field vs finite dimensions* (tentative title)
  in preparation

- Finally, in Chapter 8 we briefly summarize our results and outline some open problems and possible lines of research.

Chapter 2

Glass transition and kinetically constrained models

In this chapter we introduce glass transition recalling both open problems and some of the theoretical approaches developed to study this phenomenon (section 2.1). In particular we focus on kinetically constrained lattice gases, which are the main subject of present work. After a general definition of the models and a discussion of the relation with glass transition, we give an overview on the key issues one should investigate in connection with the physical problem (section 2.5).

2.1 Glass transition

In the last fifty years there have been several experimental and theoretical efforts to solve a long standing puzzle in condensed matter physics, namely explaining liquid-glass transition and understanding the nature of glasses.

The glass phase, which is a solid state lacking long range order, can be obtained by the following experimental procedure. Take a liquid at high temperature $T \gg T_m$, where T_m is melting temperature, and cool it at a constant rate. If the quench is fast enough with respect to the time needed to enucleate the crystal inside the liquid, crystallization is avoided and the liquid enters a metastable *super-cooled phase* (the true equilibrium phase being the crystal). In this regime, on time scales shorter than those required for crystallization to occur, thermodynamic and structural properties of the liquid depend weakly on temperature and they are smoothly related to those of the liquid above T_m. For example, by plotting the volume as a function of temperature, no unusual behavior arises when T_m is crossed (see figure 2.1). On the other hand dynamical properties, such as the viscosity or the diffusion

constant, show a very pronounced temperature dependence. In particular, as temperature is lowered, typical relaxation time scales increase dramatically. When equilibration times become longer than experimentally accessible time scales, the liquid falls out of equilibrium and becomes a *glass*. Empirically, glass transition temperature T_g is defined as the value at which viscosity reaches the value of 10^{13} Poise (Pa s), which corresponds to a structural relaxation time of the order of one hour. As we will explain in next section, T_g depends on the experimental setting and in particular on the value of the cooling rate. Note that at T_g no true thermodynamic transition occurs, but a dynamical cross over takes place between a regime where the dynamics of the supercooled liquid is stationary[1] and a regime where the system is no more able to equilibrate on experimentally accessible time scales.

A complete theoretical explanation of the mechanism inducing such *dynamical arrest* and other striking phenomena in the vicinity of T_g is still lacking [3]. The first crucial question to be settled is whether the dramatic increase of the relaxation time is due to an underlying equilibrium transition occurring at a temperature $T < T_g$ (and therefore experimentally unaccessible) or else it is a purely dynamical phenomenon. The second possibility is supported by the fact that no static divergent correlation length is experimentally detected and the structural properties show a very small temperature dependence [4]. On the other hand, the existence of a true thermodynamic transition, usually referred to as *ideal glass transition*, is suggested by a conjecture on the behaviour of the entropy that was first suggested by Kauzmann [5]. As usual, the entropy of the supercooled liquid can be obtained by integrating $C(T)/T$ with respect to temperature, where $C(T)$ is the specific heat. Experimental data for specific heat are available only for $T > T_g$, however one can extrapolate them to lower temperatures. The result from the extrapolated data is that the entropy goes to the one of the crystal at a finite temperature $T_K < T_g$. In other words the configuration entropy S_c, defined as the difference among liquid and crystal entropy, goes to zero at $T_K > 0$ with a finite slope. Since a negative configurational entropy does not make sense[2], Kauzmann conjectured that at $T = T_K$ a true thermodynamic transition occurs, with $S_c = 0$ for $T < T_K$. However, it is possible that the configurational entropy below a certain temperature is different form the

[1]Note that at any temperature $T < T_m$ the true equilibrium state of the system is the crystal. However, on time scales shorter than typical crystallization times for $T > T_g$, the supercooled liquid relaxes to a stationary state whose thermodynamic and structural properties can be smoothly achieved from equilibrium ones above T_m. On the other hand, for $T < T_g$, the dynamics of the liquid cannot reach stationarity.

[2]For hard sphere a negative configurational entropy occurs, but this is due to the absence of interaction energy.

extrapolated one and does not vanish at T_K. Note that this putative glass transition would have character of both second and first order transition. It is second order because the derivative of entropy is discontinuous while both entropy and energy are continuous at T_K. On the other hand, since it corresponds to the thermodynamic transition among supercooled liquid and glass phase, there should exist an order parameter which has a jump at T_K. Indeed, the fact that the glass is an amorphous solid state corresponds to a density profile which is not flat as the liquid one but has peaks as for the crystal even if not at periodic positions.

In this section we have illustrated the phenomenon of glass transition occurring by cooling *glass forming liquids*. We emphasize that the latter are not special liquids, indeed in principle all liquids belong to this class. However, for some liquids it is not possible to create a glass because the time for enucleating the crystal is very small and therefore a very high cooling rate would be needed to enter the metastable supercooled phase.[3] Before giving a more detailed explanation of experimental results (section 2.3) and presenting some of the theoretical approaches to glass transition (section 2.4), let us shortly recall some different physical systems in which a transition analogous to supercooled–glass transition occurs.

2.2 Other phenomena of dynamical arrest

Phenomena of dynamical arrest followed by a non–equilibrium dynamics analogous to those occurring for supercooled liquids, take place for very different physical systems. Therefore, also for these systems this arrest is commonly referred to as glass transition and the non–equilibrium phase as glass phase (when ambiguities can arise, real glasses will be referred to as *structural glasses*). In particular we recall polymer melts, which become glassy at sufficiently low temperature; suspension of colloid particles and granular systems, which become glassy at large densities; spin–glasses, where at a finite temperature a transition between a paramagentic and a glassy phase occurs. Let us say a few more words on granular systems and spin glasses. Indeed, some of the models we analyze in our work have been successfully used to study granular media. On the other hand, we introduce spin glasses since we will later compare some of our results with those coming from spin glass models.

Granular media are systems composed by many particles with hard core

[3]Note that the need of a high cooling rate should be matched with the opposite need of sufficiently small cooling rate that enables equilibration of the liquid at each temperature step.

interactions. Moreover, the particles feel an external field due to gravity. Note that for these models thermal excitations are negligible, since $k_B T$ at room temperature is negligible with respect to the energy needed to lift a grain in the presence of gravity. Therefore, the system has an effective zero temperature, and energy is injected by external excitations such as vibrations, shearing and vertical tapping of the system containing the grains, which are non–thermal sources. For example by gently tapping the container the system compactifies (it corresponds in some sense to lowering the temperature in liquids). However the increase of density is very slow and after a finite density ρ_c (with ρ_c well below close packing density), the system gets blocked and density cannot be further increased. This dynamical arrest, commonly referred to as *jamming transition*, shares with glass transition many properties, both in the non–equilibrium regime and in the slow relaxation dynamics for $\rho < \rho_c$.

On the other hand, spin glasses are magnetic alloys formed by an inert material with magnatic impurities at random positions, which are assumed not to vary in the experimental time (quenched disorder). Since the sign of magnetic interactions among impurities is very sensitive to changes in the relative distance and since such distance is random, the interactions has a random sign. Experimentally, by starting at high temperature and performing a cooling procedure, at a finite temperature T_g the system falls out of equilibrium (the non equilibrium phase occurring for $T < T_g$ is the true spin glass phase, while for $T > T_g$ the system is paramagnetic). Again, both the slow relaxation dynamics in the vicinity (above) T_g and the phenomena occurring in the non–equilibrium below T_g are analogous to those described in previous and next section for glass forming liquids.

2.3 Experimental phenomena

In this section we give a more detailed description of some of the remarkable phenomena related to glass transition (for further details see e.g. [6], [7], [4]). We always refer to supercooled liquids–glass transition, but we emphasize that the properties we describe in this section are present with small modifications in all the different above system displaying a *glass–like dynamical arrest*.

Take a liquid at high temperature and cool it at a constant rate $\gamma = -\Delta T/\Delta t$. On each temperature step viscosity relaxes quickly and by extrapolating its asymptotic behavior it is possible define a function $\eta(T)$ for viscosity vs temperature. At sufficiently high temperature, $\eta(T)$ is well fitted for most liquids by an Arrhenius dependence, i.e. by a function

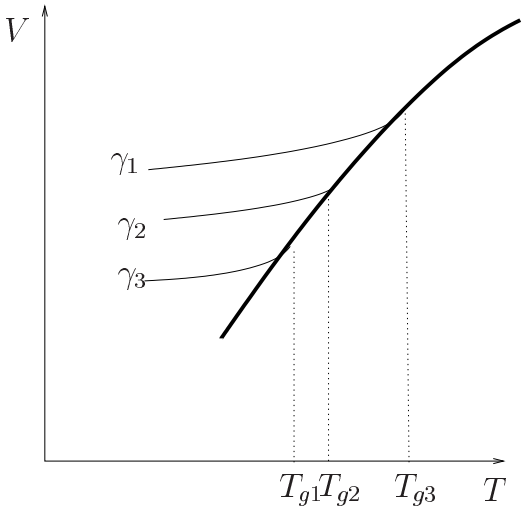

Figure 2.1: Typical plot of the temperature dependence of the volume of a supercooled liquid which is cooled with cooling rate γ_i, with $\gamma_1 > \gamma_2 > \gamma_3$. The bold line is the curve extrapolated from equilibrium data. The experimental curve corresponds at high temperature to the equilibrium one and then departs from it at a cooling rate dependent temperature T_{gi} which is lower for lower cooling rate.

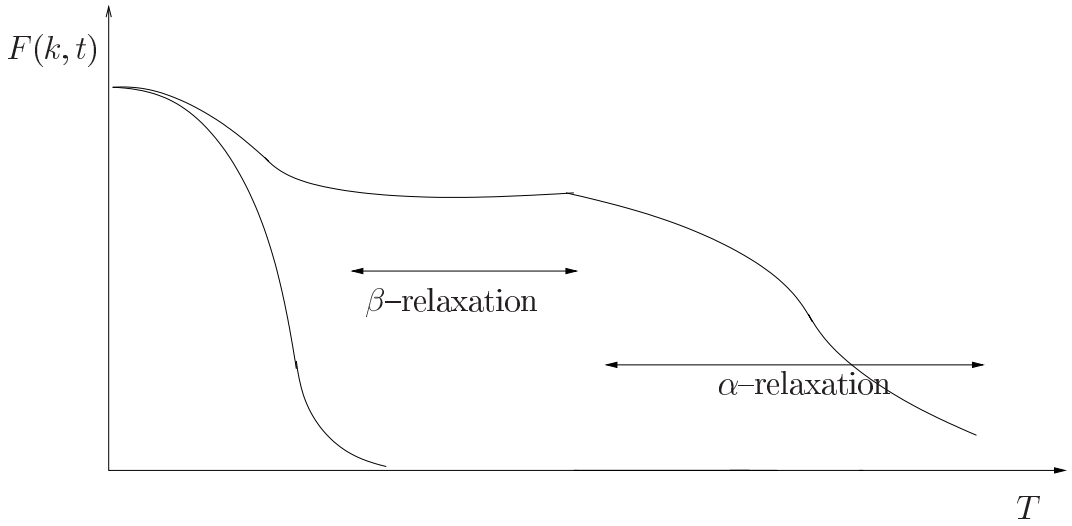

Figure 2.2: Schematic plot of a typical correlation function $F(k,t)$ versus $\log(t)$. The exponential and two step relaxatiuon correspond to the high and low temperature regime, respectively

$$\eta(T) \propto \exp\left(\frac{A}{T}\right) \tag{2.1}$$

with A constant. On the other hand, at lower temperature two possible behaviors can occur. For the so–called *strong liquids* Arrhenius dependence still holds, while for *fragile liquids* it is subsituted by a super–Arrhenius law, i.e. in (2.1) constant A is substituted by a function $A(T)$ which increases by lowering temperature. A natural interpretation of (2.1) is that for relaxation to occur the system must overcome energy barrier of the order of A, therefore a super–Arrhenius behavior suggests the existence of higher and higher barrier for lower temperatures. This is consistent with the idea that such barriers should be inversely proportional to configurational entropy, that is indeed almost constant (in the considered range of temperatures) for strong liquids and decreases for fragile liquids. The exact form of $A(T)$ is still a matter of debate. Fits of some experimental data are in good agreement with an inverse power law of $T - T_0$, with T_0 a finite temperature, which would imply the so called Vogel-Tamman-Fulcher law for viscosity

$$\eta(T) \propto \exp\left(\frac{A}{T - T_0}\right) \tag{2.2}$$

This form suggests the divergence of viscosity and therefore the existence of a dynamical transition at T_0[4] However, since (2.2) comes from the extrapolation of experimental data for temperatures much higher than T_0, one cannot exclude the possibility that at $T > T_0$ a crossover to a different behavior takes place, thus preventing the transition. Note that one cannot settle through experiments the question whether a transition or a cross over takes place, since temperature T_0 is not experimentally reachable. In other words, if the system is in contact with temperature reservoirs at such temperature, it cannot equilibrate and therefore data for viscosity (which is an equilibrium property) are not available at such temperature. Indeed, the minimal experimentally reachable temperature can be derived as follows. Let $\tau(T)$ be the temperature dependent relaxation time of the liquid and t_{exp} the maximal experimentally reachable time. The system can equilibrate only at temperature $T > T_g(t_{exp})$ defined by $\tau(T_g(t_{exp})) = t_{exp}$. In particular, since $\tau(T)$ has at $T = T_0$ the same divergence as $\eta(T)$, $T_g > T_0$. Note that t_{exp} depends on the

[4] As emphasized in previous section, the question whether the glass transition is a true thermodynamic transition or a purely dynamical phenomenon is still debated. Therefore, it is not clear whether the putative divergence of viscosity is a purely dynamical phenomenon or else it corresponds to the existence of a true thermodynamic transition. The second possibility is supported by the experimental observation that T_0 and Kauzmann's temperature T_K are very close for a large variety of systems.

cooling procedure, more precisely it is set by the inverse of γ and therefore T_g itself depends on the cooling procedure. Conventionally *experimental glass transition temperature*, T_g, is defined by choosing experimental time–scales of the order of one hour, which correspond to viscosity of the order of 10^{13} Poise. The prediction of a cooling rate dependent glass transition temperature is very well reproduced by experiments. The temperature at which the system is no more able to equilibrate can be detected by plotting the volume of the liquid as a function of temperature. Indeed, at a finite temperature $T_g(\gamma)$ the volume curve departs from the equilibrium one (see figure 2.1) and $T_g(\gamma)$ is lower for lower γ.

Before turning to the out of equilibrium phenomena occurring below T_g, let us describe the relaxation of microscopic functions in the equilibrium regime. Consider for example the Fourier transform of the density–density correlation function

$$F(k,t) = 1/N < \rho(k,t)\rho(k,0) > \tag{2.3}$$

where N is the number of molecules, the mean is taken over equilibrium Boltzmann Gibbs distribution at temperature T and

$$\rho(k,t) = \sum_{j=1}^{N} \exp\left(ikr_j(t)\right) \tag{2.4}$$

with r_j the position of molecule j at time t. Such a function, the so–called intermediate scattering function, can be studied through experiments of dynamic light scattering. The result is that $F(k,t)$ relaxes in a very different way in the high and low temperature regime as is schematically shown in figure 2.2. At high temperature, after a ballistic regime at short times, the system shows a Debye–relaxation, i.e. $F(k,t)$ is well fitted by an exponential decay. In particular, on large length scales, i.e. for small k, the relaxation is of the form

$$F(k,t) \simeq \exp\left(-k^2 Dt\right) \tag{2.5}$$

namely density fluctuations relaxes diffusively with the macroscopic diffusion coefficient D. On the other hand at low temperatures, after the ballistic regime, $F(k,t)$ shows a plateau and only for much larger times the correlator decays to zero. The time window in which $F(k,t)$ is near the plateau is the so–called β–relaxation, while the regime of relaxation below the plateau is the α–relaxation. Moreover, the final decay at large times is slower than exponential and is well approximated by a stretched exponential or Kohlrausch-Williams-Watts function

$$F(k,t) = \exp\left(-At^{\beta}\right) \tag{2.6}$$

with stretching parameter $\beta < 1$. Typically, both β and A decrease with temperature and $\beta \simeq 0.5$ at T_g. The presence of a plateau (β–relaxation) is usually explained by the so called *cage effect*, which will be further explained in section 2.5. At low temperatures each particle is surrounded by many neighbors, which form a cage around it. Therefore, for short times all the possible displacements of each particle are the small rearrangements occurring inside the cage, thus giving a ballistic relaxation. On the other hand, at long times the particles are able to leave the cage and therefore the correlator relaxes to zero. However, for intermediate times, the particle is trapped by its neighbors and the correlator cannot decay and remains close to the plateau[5]. On the other hand, two different scenarios have been proposed for the explanation of the non–Debye α–relaxation and they are still a matter of debate. The first possibility is that the stretched exponential arises from the superposition of exponential relaxations with different typical times. This should be related to the presence of a very heterogeneous spatial structure, with different regions having different relaxation times. On the other hand, the second scenario suggests that relaxation is homogeneous but intrinsically non–exponential. Of course, since the stretched exponential comes from fits of experimental data which cover a very limited range of time scales, one cannot exclude the possibility that a cross over to an exponential relaxation takes place at longer times. In any case, the ubiquitous presence of a stretched behavior in glasses requires an explanation.

Let us now turn to non–equilibrium dynamics. Recall that when the system reaches T_g, by further lowering temperature it enters (by definition) a non–equilibrium state and it cannot be described by Boltzmann Gibbs distribution. Out of equilibrium properties can be investigated through the study of two times *correlation function* $C(t,t_w)$ and *instantaneous linear response function* $R(t,t_w)$. Given an observable ϕ, such functions are defined respectively as

$$\begin{aligned} C(t,t_w) &= <\phi(t)\phi(t_w)> - <\phi(t)><\phi(t_w)> \\ R(t,t_w) &= \left.\frac{\delta <\phi(t)>}{\delta h(t_w)}\right|_{h=0} \end{aligned} \tag{2.7}$$

[5]This explanation is still debated. In particular, recent experiments have shown that in some cases it is not true that the α–relaxation corresponds to the regime in which the particle is able to leave the cage, but only to make a displacement inside the cage that is much larger than the initial rattling.

where $t > t_w$, $<>$ is the mean over different initial conditions. The formal derivative in the definition of R means that one should compare the free evolution of $\phi(t)$ with the evolution in presence of an instantaneous perturbing external field $h(t) = h\delta(t-t_w)$ conjugated with variable ϕ and set h to zero at the end of the calculation, i.e. keep only the linear order in the perturbation. Therefore, to measure correlation function $C(t, t_w)$, one should let the system evolve from time t_w to a later time t and then compare the configuration at the two times. On the other hand, to measure $R(t, t_w)$ one should perturb at t_w the system with a small instantaneous external field h and then compare its evolution with the evolution in absence of perturbation. On the other hand, one can also define the *integrated linear response function* $\chi(t, t_w)$, which is the response to a step–like perturbation applied from time t_w to time t

$$\chi(t, t_w) = \int_{t_w}^{t} R(t, t')dt' \tag{2.8}$$

For $T > T_g$ the system reaches equilibrium at sufficiently large times, therefore stationarity holds and above functions depend only on the time difference, i.e. $C(t, t_w) = c(t - t_w)$, $R(t, t_w) = r(t - t_w)$, $\chi(t, t_w) = \chi(t - t_w)$. Moreover, they are related trough the fluctuation dissipation relation

$$r(t) = \frac{\partial \chi(t)}{\partial t} = -\frac{1}{T}\frac{\partial}{\partial t}c(t) \tag{2.9}$$

On the other hand, for $T < T_g$, equilibrium cannot be reached and correlation and response depend on the two arguments t and t_w even at very large times. In figure (2.3) we show a typical plot of correlation as a function of $t - t_w$ for different values of t_w, where time zero corresponds to the time at which the quenching procedure from an initial temperature grater than T_g to a final temperature $T < T_g$ has been performed. While for $T > T_g$ curves for different t_w superimpose as in the equilibrium case, for $T < T_g$ this is true only for the initial part of the β–relaxation. On the other hand, the time spent on the plateau and the α–relaxation depend on t_w. In particular, the relaxation of the correlator is slower the larger the value of t_w, which is the *age* of the system (time elapsed since quenching) Therefore, these effect are usually referred to as *aging effects*.

Moreover, in this non–equilibrium regime, fluctuation dissipation relation (2.9) no more holds. To quantify the violation of FDT, one can measure the *violation factor* $X(t, t_w)$ implicitely defined by

$$R(t, t_w) = -\frac{\partial \chi(t, t_w)}{\partial t_w} = \frac{X(t, t_w)}{T}\frac{\partial}{\partial t_w}C(t, t_w) \tag{2.10}$$

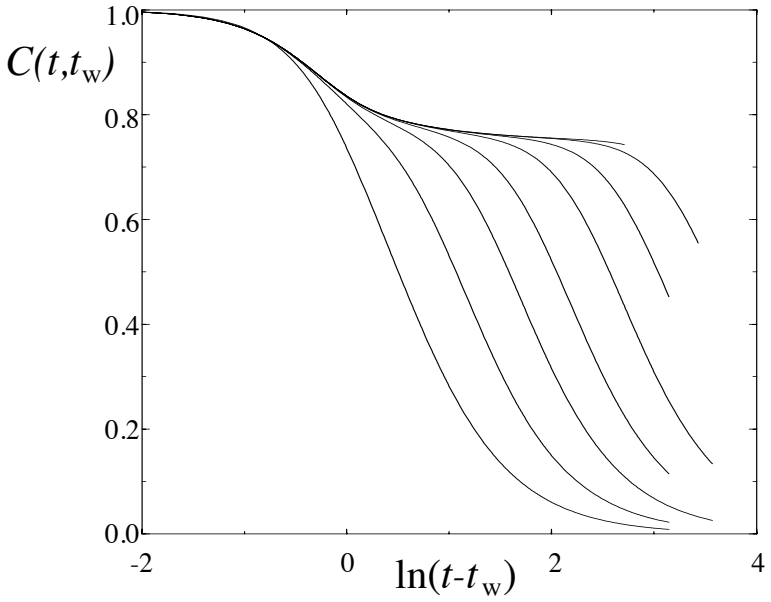

Figure 2.3: The typical form of a two time correlation function plotted as a function of $t - t_w$ with age t_w increasing from left to right.

Indeed, values of $X(t, t_w)$ different from unity mark a violation of FDT. In several mean field models $X(t, t_w)$ becomes a function of a single argument at large t and t_w: taking $t, t_w \to \infty$ with $C(t, t_w) = C$ constant, $X(t, t_w)$ becomes a single valued function of C. In these mean field models, aging can be explained through the existence of one or more time–scales for the model becoming infinite for $t_w \to \infty$. The presence of different time–scales which become separately infinite, identifies different time–sectors and on each of them the effective temperature $T_{eff} = T/X(C)$ is constant and corresponds to the response of a thermometer tuned on this time–scale.
Of course, one of the major goals is to find a substitute of Boltzmann Gibbs distribution for this non–equilibrium regime, i.e. to find a way to compute observables attained dynamically. A proposal in this sense was made by Edwards [10] for granular systems, who suggested that the right ensemble could be the equilibrium measure correspondent to the value of the dynamically reached one time quantities and restricted to *blocked configurations*, i.e. configurations in which no grain can move in the absence of external tapping. In other words, once the mean value of density $\rho(t)$ has been measured, any other observable should be calculated by a using equilibrium measure at density $\rho(t)$ restricted to blocked configurations. Of course, extending this proposal to real glasses is not straightforward, since one should first translate

the concept of *blocked configurations*. Moreover, also for granular systems, there is no clear justification for this choice and its validity is not universally accepted. However, Edward's conjecture has been successfully checked by some numerical experiments for some simplified models of granular media [49].

2.4 Theoretical approaches

Among the most important theoretical approaches to glass transition we recall the followings

1. Microscopic theories. These theories start from first principle kinetic liquid equations and solve them via proper approximations. One of the most successfull among these approaches is mode coupling theory (MCT) [11]. The main ingredient of MCT is the a separation of time scales occurring in supercooled liquids, i.e. the fact that some dynamical processes occur on the microscopic time scale while others, such as relaxation, are on much larger time scales. More precisely, since the density distribution of particles evolve much slower than others variables, the approximation consists in an adiabatic projection of the equation of motion on these *relevant variables*. The main criticism against this theory is that the underlying approximation is rather uncontrolled (note that it is not a perturbative approach). Nevertheless MCT leads to some quantitative predictions that are fulfilled by experiments. One of the main results is the prediction of a dynamical transition taking place at a finite temperature T_{MCT}. More precisely, MCT predicts that the typical time for α–relaxation (see previous section) diverges at T_{MCT} with an inverse power law. However, this putative glass transition would take place in a region where experiments clearly show that the system is still in the liquid phase, i.e. $T_{MCT} \gg T_0$. A possible interpretation of this discrepancy is that T_{MCT} do not correspond to T_0, but to a higher temperature at which for mean filed models a dynamical transition takes place, which is substituted for real system by a crossover. This hypothesis is supported by the following argument. MCT is exact for some mean field models, e.g. p–spin models. Such models display two transitions: a thermodynamic one at T_c and a dynamical one at $T_d > T_c$. The latter, which coincides with the mode coupling transition, is an *ergodic/non–ergodic* transition, i.e. at T_d the configuration space of the system breaks into many disconnected components which are separated by infinitely high barriers. Therefore by starting from an initial configuration inside a given component, the

system can never escape such component and it cannot reach equilibrium. In other words, even at large times the temporal mean of a given observable cannot be substituted with the mean over Boltzmann Gibbs distribution (for a more rigorous definition see section 2.5.1). Since real systems are not mean field, it is natural to expect that these barriers are no longer of infinite height and therefore there is no sharp transition. However, there should be a change in the transport mechanism for the particles, from a flow–like one to a regime in which particles should rearrange in a cooperative way in order that a few of them can hop the barrier. In other words, the sharp transition predicted by MCT, should be substituted by a crossover between two different relaxation mechanisms in real systems.

2. Random first order scenario. In this approach predictions are drawn in analogy with results for fully connected discontinuous spin glass models, e.g. p–spin model with $p > 2$. Recalling the brief introduction to spin glasses in section 2.2, it is immediate to see that a simplified model for such systems is given by representing impurities with Ising spins on the vertices of a cubic lattice with an interaction among nearest neighbor spins which is chosen at random from a Gaussian distribution with zero mean. The mean field version of this model, i.e. a spin model with interaction among any couple of spins, is the so–called Sherrington Kirkpatrick (SK) model. P–spin model is the generalization of SK with interactions among p spins ($p = 2$ reduces to SK). P–spin model with $s > 2$ share with glass forming liquids a similar behaviour. As mentioned in previous paragraph such models display both a dynamical and a thermodynamic transition. The former has a discontinuous order parameter, but a continuous energy and entropy, therefore has a character similar to the putative thermodynamic liquid–glass transition at T_K (see section 2.1). Moreover, for $T \to T_d$ from above the relaxation of dynamics has a two step behavior and for $T < T_d$ aging phenomena occur which are very similar to those of real systems (see section 2.3). However, despite these similarities, due to the presence of quenched disorder it is not immediate to establish a connection of these models with supercooled liquids. A possible explanation [13], [3] for this analogy could lie in the fact that spin glasses share with real glasses the presence of *frustration* inducing a very complex energy landscape. Frustration, which is related in spin glasses to the presence of quenched disorder, could be related for glass forming liquids to the presence of geometrical constraints on the possible positions of particles. Therefore, random first order approach derives predictions for glasses in analogy

with the available results for these spin models.

3. Phenomenological theories. In this approach glass transition is analyzed through the behavior of effective variables of mesoscopic character. In particular we recall free–volume theories, entropic theories and the energy landscape approach [14].

4. Kinetically constrained models. These models share with the phenomenological approach the use of effective mesoscopic variables. However, an Hamiltonian and a dynamical evolution for these variables are explicitely defined and no further approximation is performed. The main limit of this approach lies in the fact that, due to the simplicity of the models, it is not possible to establish a true mapping with real systems. Nevertheless, the study of such models can be a very useful ground to test and develop new ideas. Kinetically constrained models are of two kinds: *spin facilitated Ising models* and *kinetically constrained lattice gases*. The former, introduced in the early eighties by Fredrickson and Andersen [2], are spin models on lattices. The dynamics is given by a Markovian evolution allowing the flip of a chosen spin only if the whole spin configuration obeys some previously chosen rules. Such models can be reformulated as non–conservative particle models with a dynamics allowing birth–death of particles. On the other hand, kinetically constrained lattice gases are conservative models and dynamics is given by a Markovian sequence of particle jumps satisfying both hard core and additional constraints. In the rest of this chapter we give a more detailed introduction to these models which are the main subject of present work. In particular, we focus on the open issues which are relevant in relation with the study of glass transition and other phenomena of dynamical arrest.

2.5 Kinetically constrained lattice gases

Kinetically constrained lattice gases are stochastic lattice gases with hard core exclusion, i.e. systems of particles on a lattice Λ with the constraint that on each site there can be at most one particle. A configuration is therefore defined by giving for each site $x \in \Lambda$ the occupation number $\eta_x \in \{0,1\}$, which represents an empty or occupied site respectively. The dynamics is given by a continuous time Markov process on the configuration space $\Omega_\Lambda = \{0,1\}^{|\Lambda|}$ which consists of a sequence of particle jumps. A particle at site x attempts to jump to a different site y with a fixed rate $c_{x,y}(\eta)$, which in general depends both on $\{x,y\}$ and on the configuration η over the entire

lattice. The discretized time version of the process is the following. At time t choose at random a particle let x be its position, and a site y. At time $t+dt$, the particle has jumped from x to y with probability $c_{xy}(\eta(t))$, while with probability $1-c_{xy}(\eta(t))$ the configuration has remained unchanged. In other words, the probability measure at time t, μ_t, can be derived by the initial measure μ_0 as

$$\mu_t(\eta) = \sum_{\eta' \in \{0,1\}^{|\Lambda|}} \exp(\mathcal{L}t)\, \mu_0(\eta') \tag{2.11}$$

where $\mathcal{L}$, the *generator of the Markov process*, is the operator which acts on local functions $f : \Omega_\Lambda \to \mathbb{R}$ as

$$\mathcal{L}f(\eta) = \sum_{\{x,y\}\subset\Lambda} c_{x,y}(\eta)\,(f(\eta^{xy}) - f(\eta)) \tag{2.12}$$

where we defined

$$(\eta^{x,y})_z := \begin{cases} \eta_y & \text{if } z = x \\ \eta_x & \text{if } z = y \\ \eta_z & \text{if } z \neq x, y \end{cases} \tag{2.13}$$

The simplest model is the symmetric simple exclusion process (SSEP), in which $c_{x,y}(\eta) = \eta_x(1-\eta_y)+\eta_y(1-\eta_x)$ for nearest neighbors $\{x,y\}$, $c_{x,y}(\eta) = 0$ otherwise. Therefore, only nearest neighbor jumps are allowed and there are no further kinetical constraints besides hard core. The definition *kinetically constrained* more properly refers to models in which jump rates impose additional requirements in order for the nearest neighbor move to be allowed. In other words, the rate $c_{x,y}(\eta)$ can be zero for some choices of the configuration η and the couple $\{x,y\}$ even if $\eta_x = 1$ $\eta_y = 0$, thus preventing the jump of a particle from site x to final empty site y. From the above definition it is immediate to see that dynamics preserves the number of particles, i.e. the hyperplanes with fixed number N of particles $\Omega_{\Lambda,N} := \{\eta \in \Omega_\Lambda \ \sum_{x\in\Lambda} \eta_x = N\}$ are invariant under dynamics. Moreover, the rates are chosen in order to satisfy detailed balance w.r.t. uniform measure $\nu_{\Lambda,N}$ on such hyperplanes. In other words condition $c_{x,y}(\eta) = c_{y,x}(\eta^{xy})$ is satisfied for any choice of η and the couple $\{x,y\}$. This implies that the generator is reversible with respect to $\nu_{\Lambda,N}$ and therefore $\nu_{\Lambda,N}$ is stationary[6]. Note that $\nu_{\Lambda,N}$ is nothing else

[6]Let $\mu(g,h)0\sum_{\eta\in\Omega}\mu(\eta)g(\eta)h(\eta)$. $\mathcal{L}$ is reversible with respect to μ if, for any functions f and g, equality $\mu(g,\mathcal{L}f) = \mu(f,\mathcal{L}g)$ holds. By a direct calculation it is possible to check that detailed balance implies reversibility with respect to $\nu_{\Lambda,N}$, therefore the choice $g(eta) = 1$ $\forall\eta$, implies $\mu(\mathcal{L}f) = 0$ $\forall f$. This, together with (2.11) implies that $\nu_{\Lambda,N}$ is invariant under time evolution.

than canonical measure with zero Hamiltonian, i.e. with this choice of the rules there are no static interactions beyond hard core and an equilibrium transition cannot occur. However, it is possible that a dynamical transition occurs for some choices of the rules. The possible forms of such transition will be explained in detail in the rest of the chapter. However, we emphasize since now that the degeneracy of the rates implies that $\nu_{\Lambda,N}$ is not the unique invariant measure, i.e. the system is not ergodic on $\Omega_{\Lambda,N}$ and this will have several consequences on dynamics inducing a very different behavior with respect to SSEP case.

The reason which motivated the introduction of kinetically constrained lattice gases to study glassy dynamics is the following. Consider a molecule in a dense liquid: the presence of surrounding particles can create geometrical constraints inhibiting its motion, i.e. a molecule can be caged by its neighbors and the cage must be opened to allow its motion. These local constraints might produce, for a finite value of density, a cooperative behavior inducing a slowing down of dynamics and this could be the mechanism underlying glass transition. Therefore, kinetically constrained lattice models for glasses are devised by choosing jump rates which encode this *cage effect*. A deeper justification behind the use of such models to study glass transition and more general jamming transition lies in the ansatz that these transitions are a purely dynamical phenomenon and static correlations play no role (see e.g. [15] and [16]). This conjecture is supported by the fact that, in a small experimental window in the vicinity of the transition, dynamical properties vary enormously while structural ones remain almost unchanged. This suggests that there could exist a dynamical length which diverges while static one remains constant. If this is the case, it is natural to expect that, by a coarse graining on the scale of the static length, the real systems reduce to a kinetically constrained model. In other words, by a proper choice of kinetic rules, these models would provide a mesoscopic description of real systems (the discrete variable could correspond to e.g. the average of the particle density over the coarse–graining volumes). Of course, a true mapping from the microscopic description to the mesoscopic one is a formidable task. Nevertheless, despite their simplicity and discrete character, these models might capture, at least at a mesoscopic level, some of the key dynamical ingredients of real glasses. Indeed, some of these models display a slow dynamics and a whole phenomenology that is very reminiscent the behavior of glass forming liquids in the vicinity of the glass transition [15]. Therefore, it is important to unveil the mechanism inducing the slowing down of dynamics in such models and to investigate whether this is due to the presence of a dynamical transition. In the rest of the chapter, we analyze in some detail different possible forms of dynamical arrest that could occur in these particle

systems.

2.5.1 Irreducibility and ergodicity

As we already mentioned, jump rates are chosen in order that to satisfy detailed balance w.r.t. uniform measure $\nu_{\Lambda,N}$ on hyperplanes $\Omega_{\Lambda,N}$ with N particles, which is therefore a stationary measure. However, due to the presence of degenerate rates, usually there exist configurations which can not be connected one to the other using moves allowed by the dynamics and therefore $\Omega_{\Lambda,N}$ breaks into disconnected components, i.e. the Markov chain correspondent to the process is *reducible*. This implies that the invariant measure in not unique and therefore ergodicity does not hold with respect to any of these invariant measure. In other words there are subsets of the configuration space that are left invariant by the dynamics and it is not true that starting form any initial distribution it relaxes at large times on the invariant one, which is a necessary condition to substitute temporal means with mean over the invariant measure.

A natural question is whether in the thermodynamic limit irreducibility and/or ergodicity are recovered.
To settle this question one should study the asymptotic behavior $\nu_\infty(\mathcal{E})$ for $|\Lambda| \to \infty$, $N \to \infty$ at fixed density $\rho = N/|\Lambda|$ of the probability $\nu_{\Lambda,N}(\mathcal{E})$, where $\mathcal{E}$ is the *maximal irreducible component*. We say that the process is irreducible in the thermodynamic limit if $\nu_\infty(\mathcal{E}) = 1$, irreducible otherwise. Note that $\lim_{|\Lambda|,N\to\infty,N/|\Lambda|=\rho} \nu_{\Lambda,N} \equiv \nu_{\infty,\rho}(\mathcal{E})$ depends on density, therefore there could exists a finite density ρ_c below which irreducibility holds and above which the configuration space breaks into many disconnected components. In this case we say that an irreducible/non–irreducible transition takes place at a ρ_c.
A strictly related issue is whether ergodicity holds for the process on the infinite lattice with respect to Bernoulli product measure $\mu_\rho \equiv \prod_i \rho^{\eta(x)}(1-\rho)^{1-\eta(x)}$, which is invariant for the models on such lattices (the product is over all the sites of the lattice). For a finite volume system irreducibility of the Markov chain implies that there exists one and only one invariant measure and that under time evolution any initial measure reaches the invariant one in the large time limit. Therefore, irreducibility implies that ergodicity holds. However, for infinite systems, irreducibility does not a priori imply ergodicity (for example Ising model is irreducible but not ergodic at the equilibrium transition). On the other hand, a sufficient condition to establish ergodicity on infinite lattices is the validity of the mixing property

$$\lim_{t\to\infty} \int d\mu_\rho(\eta) \left[P_t f(\eta) - \mu_\rho(f)\right]^2 = 0 \quad \text{for any } f \in L_2(\mu_\rho) \tag{2.14}$$

where $P_t = \exp \mathcal{L}t$ is the semigroup associated to the Markov process, see equation (2.11). By spectral theorem, (2.14) holds if and only if zero is a simple eigenvalue of the generator, i.e. if the only functions f such that $\mathcal{L}f(\eta) = 0$ are constant almost surely in $L_2(\mu_\rho)$. This implies there cannot exist an invariant region of the configuration space whose probability is different from zero and one. Indeed, the characteristic function of this region would be a non constant eigenvector of $\mathcal{L}$ with zero eigenvalue. Note that this corresponds to the natural idea that ergodicity breaking is related to the existence of disconnected regions of the configuration space in which the system can get trapped for infinite time. An ergodic/non–ergodic transition occurs at ρ_c if the process is ergodic for $\rho < \rho_c$ and not ergodic for $\rho > \rho_c$.

Investigating the presence of such transition for kinetically constrained models is particularly relevant since ergodicity breaking is one of the possible explanations for the dynamical arrest in glass forming liquids. In particular, the transition predicted in mean field approximation both for spin models and in MCT (see section 2.4) is an ergodic/non–ergodic transition.

2.5.2 Diffusion of the tagged particle

A different kind of dynamical arrest, which could take place even in the density regime where ergodicity holds, is diffusive/sub–diffusive transition.

Consider a kinetically constrained model on the infinite lattice $\Lambda = \mathbb{Z}^d$ and start at time zero from the equilibrium distribution, so that the process will be stationary. Then single out one particle, the tracer, and analyze its motion. In the density regime where the process is ergodic one can repeat the arguments in [18, 19] and show that under a diffusive rescaling the position of the tracer at time t, $\vec{x}(t)$, converges to a Brownian motion with diffusion coefficient $D_S(\rho)$. More precisely, $\lim_{\epsilon\to 0} \epsilon\vec{x}(\epsilon^{-2}t) = \sqrt{2D_S}\ \vec{b}(t)$, where $\vec{b}(t)$ is standard Brownian motion and the self diffusion matrix $D_S(\rho)$ is given by the variational formula ([17])

$$(\vec{l}\cdot D_S(\rho)\vec{l}) = \inf_f \left[\frac{1}{2} \sum_{\{y\neq 0\}\subset\Lambda} \mu_{\rho,0} \left(c_{0,y}(\eta)(1-\eta(y))[\sum_{i=1}^{d} (\vec{l}\cdot\vec{d}) + f(\tau_{-y}\eta^{0y}) - f(\eta)]^2 \right) \right.$$
$$\left. + \frac{1}{4} \sum_{\substack{\{x,y\}\subset\Lambda \\ x\neq 0, y\neq 0}} \mu_{\rho,0} \left(c_{x,y}(\eta)[f(\eta^{xy}) - f(\eta)]^2 \right) \right] \tag{2.15}$$

where $(\vec{a}\cdot\vec{b})$ is Euclidean scalar product, $\tau_{-y}\eta$ is the configuration obtained translating the configuration η of y, $\mu_{\rho,0}$ is the Bernoulli measure at density ρ conditioned to the existence of a particle in the origin and the infimum is over all real–valued local functions f, i.e. functions which depend on a finite number of occupation variables. For spatially hysotropic systems, as the one we will deal with, the self diffusion matrix is usually proportional to identity, the proportionality coefficient being the so–called *self diffusion coefficient*. For future purposes it is useful to define the two sums in (2.15) as $D_1(\rho, f)$ and $D_2(\rho, f)$

$$\begin{aligned} D_1(\rho,f) &= \frac{1}{2}\sum_{\{y\neq 0\}\subset\Lambda}\mu_{\rho,0}\left(c_{0,y}(\eta)(1-\eta(y))[\sum_{i=1}^{d}(\vec{l}\cdot\vec{d})+f(\tau_{-y}\eta^{0y})-f(\eta)]^2\right) \\ D_2(\rho,f) &= \frac{1}{4}\sum_{\substack{\{x,y\}\subset\Lambda\\ x\neq 0,y\neq 0}}\mu_{\rho,0}\left(c_{x,y}(\eta)[f(\eta^{xy})-f(\eta)]^2\right) \end{aligned} \tag{2.16}$$

It is immediate to notice that $D_1(\rho, f) \geq 0$ and $D_2(\rho, f) \geq 0$ at any density ρ, and therefore $D_S(\rho) \geq 0$. However, for the tagged particle process to be diffusive, D_S should be strictly positive. A diffusive/sub–diffusive transition takes place at ρ_c if $D_S > 0$ for $\rho < \rho_c$ and $D_S = 0$ for $\rho \geq \rho_c$. The existence of such transition could again be related with glass transition. Indeed experimental data for supercooled liquids suggest that the ratio of the mean square displacement of a tracer over time, $< x(t)^2 > /t$, vanishes at the glass transition [4] (here we use $<>$ for the mean over equilibrium measure).

In the rest of this section we will outline the proof of the well known result $D_S > 0$ at any density $\rho < 1$ for simple exclusion process in $d = 2$ [18]. The proof, which can be extended to any dimension $d > 2$, uses as a key ingredient the fact that jumps from occupied to neighboring empty sites are always allowed and cannot be trivially extended to kinetically constrained models. We emphasize that this is not only a technical difficulty since, due to the presence of kinetic constraints, the tagged particle could in principle get *trapped* and the diffusion coefficient turn to zero at sufficiently high density. Analyzing the proof for SSEP is a useful ground for a deeper understanding of the difficulties that arise for kinetically constrained models and to understand the ideas behind the proofs of diffusivity we will construct both for the two classes of models introduced in chapter 3 and for Kob Andersen model (chapter 6).

SSEP for $d = 2$: proof of positive self-diffusion coefficient

The physical mechanism behind diffusion of the tagged particle in SSEP is the following. Since a particle can always move to an empty site, the tagged particle can move whenever a vacancy passes by and therefore the typical relaxation time $\tau \simeq 1/D_S$ should be of order τ_v/ρ_v, with $\rho_v = 1 - \rho$ being the vacancy concentration and τ_v the relaxation time of a single vacancy. Moreover, since a vacancy can always move in an otherwise totally filled lattice, τ_v is finite and density independent. Therefore, for $\rho < 1$, τ should be finite and D_S positive, with a density dependence well fitted by $1 - \rho$ at high density.

The strategy of the proof is the following. Instead of dealing directly with the variational formula (2.15), one defines a proper auxiliary model and proceeds in two steps. First, one establishes that $D_S^{aux} > 0$; second, one proves that $D_S \geq cD_S^{aux}$ with c a positive constant. In principle such strategy can be generalized to any stochastic lattice gas, the major difficulty is finding a proper auxiliary process in order that the above two sentences are true and that they can be directly proved.

For SSEP a suitable auxiliary process is the following. Let η be the configuration and x the position of the tagged particle

(i) The tagged particles can jump from x to $x + e_1$. The rate of the jump is one if $\eta(x + e_1) = 0$, zero otherwise;

(ii) The tagged particles can jump from x to $x - e_1$. The rate of the jump is one if $\eta(x - e_1) = 0$, zero otherwise;

(iii) The occupation variables of site $x - e_1$ can be exchanged with the one of site $x + e_1$. The rate of the exchange is one;

(iv) All other moves are not allowed.

It is immediate to check that, if in the configuration $\eta(0)$ at time zero the tagged particle has a vacancy on the right or left neighboring, then at each subsequent time there will be a vacancy either in $x(t) - e_1$ or $x(t) + e_1$, where $x(t)$ is the position of the tagged particle in the configuration $\eta(t)$ evolute of $\eta(0)$ at time t. Moreover, since one can always move this neighboring vacancy from $x(t) - e_1$ to $x(t) + e_1$ and viceversa (move (iii) above), the jump of the tagged particle to any of the two neighbors in direction e_1 can always be performed via a sequence of at most two moves. Therefore, since the condition we are requiring on the initial configuration has a probability $1 - \rho^2$ which is finite even in the high density limit, it follows that D_S^{aux} is

strictly greater than zero. This ends the first step of the proof. In particular, for $\rho \to 1$, $D_S^{aux} \geq (1-\rho)k$ with k a density independent positive constant.

Let us now turn to the second step, namely establishing inequality $D_S > cD_S^{aux}$, with $c > 0$. Since move (iii) for the auxiliary process is not allowed for SSEP, some work is required to establish such inequality. The basic idea is to show that all the moves allowed for the auxiliary process can be performed through a proper finite sequence of elementary nearest neighbors jumps which are allowed in the SSEP case. If this is true, it is natural to expect above inequality among the diffusion coefficients, which can be rigorously established. Let us outline the proof. Consider the second term, D_2, of the variational formula (2.15) which yields for the auxiliary process

$$D_2^{aux} = \frac{1}{4} < \left(f(\eta^{-e_1,e_1}) - f(\eta)\right)^2 >_0 \tag{2.17}$$

and let us define a path of neighboring sites $x_0, \dots x_4$ joining e_1 and $-e_1$ as follows: $x_0 \equiv e_1$, $x_1 \equiv e_1 + e_2$, $x_2 \equiv e_2$, $x_3 \equiv e_2 - e_1$, $x_4 \equiv -e_1$. By recalling definition (2.13) and letting the exchange operator $T_{x,y}$ be

$$T_{x,y}\eta = \eta^{x,y} \tag{2.18}$$

we immediately obtain the following equivalence

$$\eta^{-e_1,e_1} = T_{x_1,x_0}Tx_2, x_1T_{x_3,x_2}Tx_3, x_4T_{x_2,x_3}Tx_1, x_2T_{x_0,x_1}\eta \tag{2.19}$$

Therefore, term $f(\eta^{-e_1,e_1}) - f(\eta)$ in (2.17) can be rewritten by a telescopic sum as

$$\begin{aligned} f(\eta^{-e_1,e_1}) - f(\eta) &= (f(T_{x_1,x_0}\eta_6) - f(\eta_6)) + (f(T_{x_2,x_1}\eta_5) - f(\eta_5)) \\ &+ (f(T_{x_3,x_2}\eta_4) - f(\eta_4)) + (f(T_{x_3,x_4}\eta_3) - f(\eta_3)) \\ &+ (f(T_{x_2,x_3}\eta_2) - f(\eta_2)) + (f(T_{x_1,x_2}\eta_1) - f(\eta_1)) \\ &+ (f(T_{x_0,x_1}\eta_0) - f(\eta_0)) \end{aligned} \tag{2.20}$$

where we have defined $\eta_0, \dots \eta_6$ as $\eta_0 \equiv \eta$, $\eta_1 \equiv \eta_0^{x_0,x_1}$, $\eta_2 \equiv \eta_1^{x_1,x_2}$, $\eta_3 \equiv \eta_2^{x_2,x_3}$, $\eta_4 \equiv \eta_3^{x_3,x_4}$, $\eta_5 \equiv \eta_4^{x_3,x_2}$, $\eta_6 \equiv \eta_5^{x_2,x_1}$. Then, by using (2.20) and Cauchy–Scharwz inequality we obtain

$$\big(f(\eta^{-e_1,e_1}) - f(\eta)\big)^2 \;\le\; 7\Bigg[\sum_{j=0}^{3}\big(f(T_{x_j,x_{j+1}}\eta_j) - f(\eta_j)\big)^2 + \sum_{j=1}^{3}\big(f(T_{x_j,x_{j+1}}\eta_{7-j}) - f(\eta_{7-j})\big)^2\Bigg] \tag{2.21}$$

Since the sequence $\eta_0, \dots \eta_6$ has been chosen in order that the exchanges in the right hand side are all nearest neighbor exchanges, SSEP rate $c_{x_j,yx_{j+1}}(\eta_j)$ is one when η is such that $f(T_{x_j,x_{j+1}}\eta_j) - f(\eta_j) \neq 0$ and the same is true for the exchanges in the second term. Therefore, we can rewrite above inequality by introducing in the right hand side the corresponding jump rates for SSEP

$$\big(f(\eta^{-e_1,e_1}) - f(\eta)\big)^2 \;\le\; 7\Bigg[\sum_{j=0}^{3} c_{x_j,x_{j+1}}(\eta_j)\big(f(T_{x_j,x_{j+1}}\eta_j) - f(\eta_j)\big)^2 + \sum_{j=1}^{3} c_{x_j,x_{j+1}}(\eta_{7-j})\big(f(T_{x_j,x_{j+1}}\eta_{7-j}) - f(\eta_{7-j})\big)^2\Bigg] \tag{2.22}$$

Multiplying above inequality by $1/4$ and averaging over Bernoulli measures conditioned to have the origin occupied yields, for any real–valued local functions f,

$$\frac{1}{4} < \big(f(\eta^{-e_1,e_1}) - f(\eta)\big)^2 >_0 \;\le\; \frac{1}{4}\,14 \sum_{\substack{\{x,y\}\subset\Lambda \\ \mathrm{d}(x,y)=1}} < (f(\eta^{x,y}) - f(\eta))^2 >_0 \tag{2.23}$$

which recalling (2.15) and (2.17) gives

$$D_2^{aux}(\rho, f) \le 14\; D_2(\rho, f) \tag{2.24}$$

for any ρ and f. Note that factor 14 comes from the fact that the shortest path needed to reconstruct the moves of the auxiliary process is composed of 7 elementary moves allowed by SSEP (see formula (2.19)) and an overall factor 2 comes from the fact that in this sequence each move of SSEP is used at most twice. On the other hand, since the tagged particle jumps with the same rate for the auxiliary process and for SSEP, the first term of the variational expression (2.15) for D_S is the same for the two processes, i.e.

$$D_1^{aux}(\rho, f) = D_1(\rho, f) \tag{2.25}$$

for any ρ and f. Therefore

$$D_S(\rho) \geq \frac{1}{14}\, D^{aux}(\rho) > 0 \tag{2.26}$$

at any density $\rho < 1$. In order to obtain D_2 in (2.23) from the average of right hand side of equation (2.21), we used the changes of variables $\eta \to \eta_i$ and the invariance of equilibrium measure under exchange of occupation numbers. We emphasize that the proof uses as a key ingredients that the tagged particle can jump to any nearest neighbor empty site and that a particle can be exchanged with a vacancy next nearest neighbor to it by means of a configuration independent path composed of a fixed finite number of allowed moves.

2.5.3 Relaxation to equilibrium

Another interesting issue, in the regime where ergodicity holds, is the analyses of relaxation towards equilibrium for the model either on finite and on infinite lattices.

For finite lattices the quantities which give the velocity of convergence to equilibrium are the spectral gap and the logarithmic Sobolev constant with respect to equilibrium measure. Let us recall the definition of such quantities. The spectral gap of a Markov generator $\mathcal{L}$ with respect to a measure μ is defined as the smallest eigenvalue of $-\mathcal{L}$ on the subspace of $L_2(\mu)$ orthogonal to the constant functions, namely

$$\mathrm{gap}(\mathcal{L}) \equiv \inf_{f \in \mathbb{I}^\perp} -\frac{\mu(f\mathcal{L}f)}{\mu(f - \mu(f))^2} \tag{2.27}$$

where we recall that the action $\mathcal{L}f$ of the generator on a function f was defined in (2.12) and $\mu(fg)$ is the mean value of the scalar product among the two functions, i.e. $\mu(fg) = \sum_\eta \mu(\eta) f(\eta) g(\eta)$. For finite systems above definition implies [20] that the gap is the smallest positive constant C_g such that, for any real-valued local function f, inequality

$$||P_t f - \mu(f)||_{L_2(\mu)} \leq ||f - \mu(f)||_{L_2(\mu)} \exp\{-tC_g\} \tag{2.28}$$

holds, where we recall that $P_t = \exp \mathcal{L}t$ is the semigroup associated to the evolution of the process (see equation (2.11)). In other words, the gap is the worst mean velocity (and 1/gap the slowest relaxation time) of convergence to equilibrium. Note that definition (2.27) implies that $\mathrm{gap}(\mathcal{L})$ is strictly greater

than zero when ergodicity holds. Moreover, the variational characterization (2.27) implies that

$$E_\mu\big(f(\eta(0)); f(\eta(t))\big) \leq \exp\Big\{ - tC_g \Big\} \, \big\| f - \mu f \big\|^2_{L_2(\mu_{\Lambda,\rho})} \tag{2.29}$$

for any function f, where E is the mean over the stationary process with initial measure μ. This means that the worst velocity of decay to zero of any two time correlation function is given by C_g.
On the other hand, the logarithmic Sobolev constant is defined as the smallest constant C_s such that, for any real–valued local f, inequality

$$\mu(f^2 \log \frac{f^2}{\mu(f^2)}) \leq C_s \, (-\mu(f \mathcal{L} f)) \tag{2.30}$$

holds. Above definition implies (se e.g. [21]) inequality

$$\mu\Big(P_t f \log P_t f\Big) \leq \exp\Big\{ - \frac{4\,t}{C_s} \Big\} \mu\big(f \log f\big) \tag{2.31}$$

for any real function f such that $f > 0$ and $\mu(f) = 1$, i.e. for any f which is a probability density w.r.t. μ. In other words, the logarithmic Sobolev constant controls the exponential decay of the relative entropy with respect to equilibrium measure.
The dependence of both these velocities in system size and particle number is well known for the SSEP case. In particular, one can prove [38, §8] that the spectral gap on $L_2(\nu_{\Lambda,N})$ goes with $1/\ell^2$ for large ℓ uniformely in N, where ℓ is the linear size of Λ and N the number of particles. The logarithmic Sobolev constant, on the other hand, goes as ℓ^2. Let us give a rough explanation of such results. Consider a lattice gas with hard core constraints and *long jumps*, i.e. with jump rates $c_{x,y}(\eta) = 1$ for any choice of $\{x, y\}$, even if not nearest neighbor. In this case $\nu_{\Lambda,N}$ is invariant and the gap with respect to this measure is size independent, as it is natural to expect since every site is connected to any other and can be easily checked using variational formula (2.27). Let $\mathcal{L}^{long}$ be the generator of the process with long jumps. By using path arguments analogous to those in previous section, one can rewrite the exchange of occupation variables in non nearest neighbors sites appearing in $\mathcal{L}^{long}$ as a sequence of nearest neighbor exchanges allowed by the SSEP process. Since any nearest neighbor exchange is allowed by SSEP, the length of such path is at most ℓ. Therefore, by using telescopic sums and Cauchy Schwartz, one can obtain inequality

$$-\nu_{\Lambda,N}(f, \mathcal{L} f) \leq -\ell^2 \nu_{\Lambda,N}(f, \mathcal{L}^{long} f) \tag{2.32}$$

for any function f, which implies $\mathrm{gap}(\mathcal{L}) \geq \mathrm{gap}(\mathcal{L}^{long})/\ell^2$ and therefore $\mathrm{gap}(\mathcal{L}) \geq c/\ell^2$ for SSEP, with c independent from ℓ. By taking as a test function $f(\eta) = \sum_{x\in\Lambda}(\eta_x - \rho)\cos(\pi x/2\ell)$ and using definition (2.27), an upper bound with the same $1/\ell^2$ form immediately follows.
As we already stressed, kinetically constrained models on finite lattices are not ergodic due to the existence of blocked configurations and therefore both the gap and the inverse of the logarithmic Sobolev constant are trivially zero. On the other hand, an interesting issue is the behavior of typical relaxation times towards equilibrium for kinetically constrained models on finite lattices with boundary sources, i.e. with the addition in generator (2.12) of a term allowing birth and death of particles at the boundary with rate ρ and $1-\rho$ respectively. This corresponds to adding to the generator (2.12) a term

$$\mathcal{L}_{\text{bound.}} f(\eta) = \sum_{\substack{x\in\Lambda, y\notin\Lambda \\ \mathrm{d}(x,y)=1}} c_x(\eta)(f(\eta^x) - f(\eta)) \tag{2.33}$$

with

$$(\eta^x)_z := \begin{cases} 1-\eta_z & \text{if } z = x \\ \eta_z & \text{if } z \neq x \end{cases} \tag{2.34}$$

and

$$c_x(\eta) = (1-\rho)\eta_x + \rho(1-\eta_x) \tag{2.35}$$

Note that the number of particles is no more conserved by the dynamics generated by $\mathcal{L} + \mathcal{L}_{\text{bound.}}$ and the invariant measure is Bernoulli product measure $\mu_{\rho,\Lambda}$ at density ρ instead of canonical measure $\nu_{N,\Lambda}$. The dependence on ℓ of both the gap and logarithmic Sobolev constant (with respect to $\mu_{\rho,\Lambda}$) for the SSEP model with the addition of the boundary term (5.14) are the same as without sources. Therefore, since for other kinetically constrained model jump rates are always greater or equal than those of SSEP and the equilibrium measure is the same, the gap of any such model should go to zero at least as $1/\ell^2$ and the logarithmic Sobolev constant should go to infinity at least as ℓ^2. However, the true dependence on ℓ could in principle be different and it is also possible that a different dependence on the density appears. Indeed the gap, which is density independent for SSEP, usually depends on the density for these models. Therefore it is possible that at a finite density a crossover between regimes with a different dependence of the gap on ρ occurs. Recalling that the gap represents the worst mean velocity of relaxation to equilibrium, this would correspond to a cross over from a faster to a slower relaxation to equilibrium for models on finite lattices with boundary sources.

Let us now turn to models on infinite lattices $\Lambda = \mathbb{Z}^d$. In this case a quantity which gives informations on the velocity of convergence to equilibrium is the structure function $S(k,t)$, i.e. the Fourier transform of the density–density correlation function in the stationary state

$$S(k,t) \equiv \sum_{x\in\mathbb{Z}^d} \exp\{ikx\} \left[\mu_\rho(\eta_x(t)\eta_0(0)) - \rho^2\right] \tag{2.36}$$

which is the discrete analogous of (2.3). In the SSEP case, the time dependence of $S(k,t)$ is exponential at large time and small wave number. More precisely, in the small ϵ limit, the following scaling form holds

$$S(\epsilon k, \epsilon^{-2}t) \simeq \exp\{-k^2 D(\rho)t\} \tag{2.37}$$

with $D(\rho) = \mathbb{1}$. A rough explanation of above result, which can be rigorously proved [17], is the following. Since

$$\mu_t(f) = \sum_{\eta\in\Omega} f(\eta)\mu_t(\eta) = \sum_{\eta\in\Omega} f(\eta) \sum_{\eta'\in\Omega} \mu_0(\eta')(\eta \exp(\mathcal{L}t)\eta') \tag{2.38}$$

it follows that

$$\frac{d}{dt}S(\epsilon k, \epsilon^{-2}t) = \epsilon^{-2} \sum_{x\in\mathbb{Z}^d} \exp\{ik\epsilon x\} \left[\mu_\rho((\mathcal{L}\eta_x(\epsilon^{-2}t))\eta_0(0)) - \rho^2\right] \tag{2.39}$$

By using (2.12) we can rewrite $\mathcal{L}\eta_x$ in the right hand side as

$$\mathcal{L}\eta_x = \sum_{y\in\Lambda} c_{x,y}(\eta)(\eta_y - \eta_x) = \sum_{y\in\Lambda} j_{x,y}(\eta) \tag{2.40}$$

where $j_{x,y}(\eta)dt$ is the number of particles which jump in time dt from x to y minus those which jump form y to x, or in other words the infinitesimal current among x and y. The choice of the jump rates of SSEP (see section 2.5), i.e. the fact that $c_{x,y}(\eta)$ is always one when $\eta_x \neq \eta_y$ and $\{x,y\}$ are nearest neighbors, yields $j_{x,y} = 0$ for $\{x,y\}$ non–nearest neighbors and

$$j_{x,x+e_i}(\eta) = [\tau_x - \tau_{x+e_i}](\eta_x) \tag{2.41}$$

Therefore the sum over y in (2.40) can be rewritten as

$$\sum_{y\in\Lambda} j_{x,y}(\eta) = [2\tau_x - \tau_{x+e_1} - \tau_{x-e_1}](\eta_x) \tag{2.42}$$

The operator in parenthesis in the right hand side above is the discrete version of the Laplacian, therefore in the limit of small ϵ by inserting (2.42) in (2.40) and (2.39) and integrating twice by parts we finally obtain

$$\frac{d}{dt}S(\epsilon k, \epsilon^{-2}t) = -k^2 S(\epsilon k, \epsilon^{-2}t) \tag{2.43}$$

from which (2.37) immediately follows. Note we have used the fact that the current among neighboring sites can be written as (2.41). When the less restrictive condition

$$j_{x,y}(\eta) = j_1(\eta) = [\tau_x - \tau_y]h(\eta) \tag{2.44}$$

holds, with h a local function, results (2.37) can be established again with a density dependent diffusion constant

$$D(\rho)_{\alpha,\beta} = \frac{1}{4\sum_x S(x,0)} \sum_{x\in\Lambda} x_\alpha x_\beta \mu_\rho(c_{0,x}) \tag{2.45}$$

Models satisfying (2.44) are known as *gradient models*, since the particle current can be rewritten as the gradient of a local function. This is a key ingredient in the proof of (2.37) (see [17] Sec II 2.10), indeed a key step of the proof is the substitution of a sum of currents with a gradient over function h followed by a double integration by parts. Note that the same ingredient was necessary in the above rough explanation for the SSEP case. On the other hand, for non–gradient models proving that the scaling limit (2.37) holds is in generally not trivial and its validity is not a priori guaranteed. However, the Green–Kubo formula gives the form the diffusion coefficient should satisfy provided the scaling limit holds

$$D_{\alpha,\beta} = \frac{1}{2\sum_x S(x,0)} \int_{-\infty}^{+\infty} dt \lim_{\Lambda\to\mathbb{Z}^d} \frac{1}{|\Lambda|} \mu_{\Lambda,\rho}(j_{\Lambda,\alpha}(\eta(t)) j_{\Lambda,\beta}(\eta(0))) \tag{2.46}$$

For kinetically constrained models, it is a priori possible that relaxation is slower than exponential or else it could be exponential below a critical density and slower than exponential above it. This could explain why for some models a stretched exponential rather than exponential behavior is detected above a finite density in the time scale accessible by numerical experiments. However, it is more likely that also for these systems (2.37) holds, but that the asymptotic behavior arises only after a very long density dependent relaxation time. More precisely, it is possible that the scaling regime in which (2.37) holds is smaller the higher the density and there could be a crossover

at a finite density to a more rapid decrease of the width of such regime with $1-\rho$. Therefore, above such cross over density numerical experiment will always be in the pre–asymptotic regime were (2.37) does not hold. This transition or crossover could again be related to a similar behavior in glass forming liquids, where the long time behavior of relaxation functions is well fitted by an exponential at high temperature and by a *stretched exponential* (or Kolhlrausch-Williams-Watts function) at low temperature [8], [9] (see section4.2).

2.5.4 Evolution of density profiles

A different kind of dynamical arrest could be related to the time evolution of density profiles. Consider for example a model on a finite lattice Λ with boundary sources at a density ρ. It is immediate to check that the only invariant measure is Bernoulli product measure with density ρ. A natural issue is the study of the evolution of initial states with constant density $\rho(0) \neq \rho$ or with a position–dependent slowly varying density. Note that such states are locally in equilibrium, therefore they are locally time invariant and it is natural to expect their evolution to be rather slow, the slower the larger the length scale on which the density varies appreciably. Moreover, since we expect the process to be diffusive, if we let ϵ^{-1} be the typical spatial scale on which the density changes, the correspondent time scale should be of the order ϵ^{-2}. By defining the rescaled space and time scales

$$\begin{aligned} q &= \epsilon^{-1} x \\ \tau &= \epsilon^{-2} t \end{aligned} \tag{2.47}$$

and recalling that the number of particles is locally conserved, it is natural to expect that the density $\rho(q,\tau)$ satisfies a continuity law

$$\frac{\delta \rho(q,\tau)}{\delta \tau} + \nabla j(q,\tau) = 0 \tag{2.48}$$

where the current $j(q,\tau)$ should be related to the density gradient by Fick's diffusion law

$$j(q,\tau) = -D(\rho(q,\tau)) \nabla \rho(q,\tau) \tag{2.49}$$

with the density dependent macroscopic diffusion coefficient $D(\rho)$ which appears in the relaxation of density density correlation (2.37). Note that the diffusion coefficient $D(\rho)$ do not correspond to the self diffusion coefficient

$D_S(\rho)$ of a tagged particle, neither the positiveness of one of them guarantees the positiveness of the other (for example for the SSEP model in $d = 1$, $D_S = 0$ and $D(\rho) = 1$). Therefore, combining (2.48) and (2.49) we expect the evolute of density at time τ to be the solution of

$$\frac{\delta\rho(q,\tau)}{\delta\tau} = \nabla\left[D(\rho(q,\tau))\nabla\rho(q,\tau)\right] \tag{2.50}$$

with condition $\rho(\tau, q) = \rho$ at the boundary. The *proof of the hydrodynamic limit* consists in establishing the validity of the above parabolic equation. In other words, one should prove that starting from a local–equilibrium state with a given density profile, the state at later times is again a local–equilibrium state, with density profile determined by the solution of (2.50). The hydrodynamic limit can be rigorously proven for SSEP and for gradient models such that the jump rates do not degenerates with respect to those of SSEP, i.e. there do not exists configurations η such that $c_{x,y}(\eta) = 0$ if $\{x, y\}$ are nearest neighbors and either site x or y is empty. The extension of the result to non–degenerate non–gradient models involve some technical difficulties, see ([22]) for some solvable cases. On the other hand, for kinetically constrained models the rates degenerate and extending the proof of the hydrodynamic limit for these models (even when they are of gradient type) is not a trivial task. In general, it is neither obvious which equation should determine $\rho(t)$ at later times. A possible candidate is a diffusion equation of porous media type, i.e. with a macroscopic diffusion coefficient $D(\rho)$ vanishing for a finite density. This would give rise to a sort of *macroscopic arrest*, correspondent to the fact that density profiles above a certain density no more evolve. We emphasize that the difficulties which arise when one tries to establish (2.50) for kinetically constrained models are not purely technical. Indeed, it is a priori possible that local equilibrium is not conserved, or in other words there is no density profile at later times. In order to clarify this issue, let us briefly recall how the proof of (2.50) works for non–degenerate gradient models and which are the difficulties arising for kinetically constrained models.

Consider a gradient model in $d = 1$ on a lattice Λ with N sites, let $\epsilon = 1/N$, i.e. let the macroscopic rescaled lattice be $[0, 1]$. Moreover, define the *empirical density* as

$$\rho_N(\tau, q) = \frac{1}{N}\sum_{x\in\Lambda} \eta_x(N^2 t)\delta(q - \frac{x}{N}) \tag{2.51}$$

and the scalar product with any test function $G(q)$ as

$$< \rho_N, G > (\tau) = \int_0^1 du \rho_N(\tau, u) G(u) \tag{2.52}$$

Note that for $G = 1$ we have

$$< \rho_N, 1 > (\tau) = \frac{1}{N} \sum_{x \in \Lambda} \eta_x(N^2 t) \tag{2.53}$$

which is the mean density. To compute the evolution of $< \rho_N, G > (\tau)$ we use 2.40 which gives

$$\frac{d}{d\tau} E_{\mu_\tau} < \rho_N, G >= E_{\mu_\tau} \mathcal{L} < \rho_N, G > (\tau) \tag{2.54}$$

where E_{μ_τ} is the expectation value over the evoluted μ_τ at time $\tau = tN^2$ of the initial measure. Therefore, using definition (2.51) and result (2.40) and integrating twice by parts we find

$$\frac{d}{d\tau} E_{\mu_\tau} < \rho_N, G >= E_{\mu_\tau} \frac{1}{N} \sum_{x \in \Lambda} h(\eta_x(N^2 t)) \Delta G(\frac{x}{N}) \tag{2.55}$$

In the SSEP case, where $h(\eta) = \eta_x$, above equation yields

$$\frac{d}{d\tau} E_{\mu_\tau} < \rho_N, G >= E_{\mu_\tau} < \rho_N, \Delta G > \tag{2.56}$$

which integrating twice by parts and using the fact that G is a generic test function, corresponds to heat equation for the density. For different models, if one could substitute $\sum_x 1/N h(\eta_x(N^2 t)$ with $h(\rho(q, \tau))$ in the right hand side of (2.55), this would give again a closed differential equation for the density

$$\frac{d}{d\tau} \rho(q, \tau) = \Delta(h(\rho(q, \tau))) \tag{2.57}$$

i.e. equation (2.50) would hold with

$$D(\rho) = \nabla h(\rho) \tag{2.58}$$

Note that this form for $D(\rho)$, together with equation (2.44) give Fick's law (2.49). However, substituting the argument of h in (2.55) with density is possible only under some proper conditions which guarantee that the system is locally in equilibrium at any macroscopic time and therefore the mean over an observable can be substituted by Bernoulli measure with spatially varying density. This condition holds when the rates do not degenerate with respect to those of SSEP which allows to establish the parabolic (2.57) for these

models. On the other hand, for kinetically constrained models *the rates degenerate* and therefore the system can get trapped locally in a blocked configuration rather than reaching Bernoulli measure correspondent to the local density. Therefore it is possible that local equilibrium does not survive during evolution if the constraints are too strict (which usually correspond to high density). Therefore the substitution above is not a priori allowed and in general one cannot find a closed equation for density evolution.

2.6 Spin facilitated Ising models

Spin facilitated Ising models or kinetically constrained spin models, are models of spins on a lattice Λ. A configuration is defined by giving for each site $x \in \Lambda$ the state of a spin $\sigma_x = \{-1, 1\}$ which represent an up or down spin respectively. The dynamics is given by a continuous time Markov process on the configuration space $\Omega_\Lambda = \{-1, 1\}^{|\Lambda|}$ which consists of a sequence of spin flips. More precisely, the spin at site x attempts to flip with a fixed rate $c_x(\eta)$, which depends both on x and on the configuration η over the entire lattice. In other words, the discretized time version of the process is the following. At time t choose at random a site x. At time $t + dt$, the spin in x has flipped with probability $c_x(\eta(t))$, while with probability $1 - c_x(\eta(t))$ the configuration has remained unchanged. These models can be easily reformulated as non–conservative particle system introducing variables $\eta_x = \{0, 1\}$, with 1 and 0 representing and up and down spin, respectively and a dynamics composed of a sequence of birth and death of particles. With this convention, which we will adopt in the following, the dynamics is given by a continuous time Markov process on the configuration space $\Omega_\Lambda = \{0, 1\}^{|\Lambda|}$ with generator

$$\mathcal{L}f(\eta) = \sum_{\{x\} \subset \Lambda} c_x(\eta) \left(f(\eta^x) - f(\eta) \right) \tag{2.59}$$

where we recall that η^x is configuration η with $\eta_x \to 1 - \eta_x$ (see (2.34). The flip rates $c_x(\eta)$ are chosen in order to satisfy detailed balance with respect to the product Gibbs measure $\mu_{\Lambda,T}$ with non–interacting Hamiltonian $H = \sum_x f(\eta_x)$ at a given temperature T, namely

$$\mu_{\Lambda,T}(\eta) = \prod_{x \in \Lambda} \left(\frac{\exp(\beta f(1))}{\exp(\beta f(1)) + \exp(\beta f(0))} \right)^{\eta_x} \left(\frac{\exp(\beta f(0))}{\exp(\beta f(1)) + \exp(\beta f(0))} \right)^{1-\eta_x} \tag{2.60}$$

with $\beta = 1/T$. The definition *kinetically constrained* refers to models in which rates impose some constraints in order for the flip to be allowed, i.e.

$c_x(\eta)$ degenerates to zero for some choices of η. As for kinetically constrained lattice gases, the degeneracy of the rates usually implies that $\mu_{\Lambda,T}$ is not the unique invariant measures, i.e. the system is not ergodic on Ω_Λ.

Spin–facilitated Ising models where introduced by Friedrickson and Andersen in the early eighties. The original idea was to mimic the fact that in a supercooled liquid there can be low–density regions that facilitate rearrangements and high–density regions that block the dynamics. Indeed, as for kinetically constrained lattice gases, despite their simplicity such models could provide a mesoscopic descriptions which contains the key ingredients of glass transition (for a further discussion on the connection with glassy dynamics we refer to the introduction and to section 2.5). Again, numerical simulations show that with a proper choice of kinetic constraints, these models display a slow and heterogeneous relaxation dynamics which is very reminiscent of the behaviour of supercooled liquids in the vicinity of glass transition. Therefore, understanding the mechanisms which induce the slowing down of dynamics for these spin models can be a useful ground towards a deeper understanding of real systems. The natural questions one would like to answer and the mathematical techniques which are used are essentially those explained in previous sections. Of course, since there is not a locally conserved quantity there is no analogous for the hydrodynamic equation which gives the macroscopic evolution of density profiles (see section 2.5.4) and since particles can be created and destroyed there is no analogous of the self diffusion coefficient for a tagged particle (see section 2.5.2).

Chapter 3

Sharp results: velocity of convergence to equilibrium and tagged particle

In this chapter we introduce two classes of kinetically constrained models and consider them on a finite hypercubic lattice $\Lambda \in \mathbb{Z}^d$ of linear size ℓ in contact with particle reservoirs at the boundary. We prove that, as for SSEP, the inverse of the spectral gap and the logarithmic Sobolev constant grows as ℓ^2. However, the density dependence of both velocities, is different from the SSEP case. Then we analyze the process on the infinite lattice. First we prove that such process is ergodic, then we study the displacement of a tagged particle on the stationary process. In dimension larger than two we prove that, in the diffusive scaling limit, it converges to a Brownian motion with non–degenerate diffusion coefficient.

3.1 Definition of the models

We define two kinetically constrained models on an hypercubic d–dimensional lattice, $\Lambda := [1, \ell]^d \cap \mathbb{Z}^d$, where ℓ is a positive integer.

The first model has jump rates $c^{(1)}_{xy}(\eta) = 0$ if $\{x, y\}$ are not nearest neighbors and

$$c^{(1)}_{x,x+e_i}(\eta) := \begin{cases} 0 & \text{if } \eta_{x-e_i} + \eta_{x+2e_i} = 2, \quad \{x - e_i, x, x + e_i, e + 2e_i\} \in \Lambda \\ 1 & \text{otherwise} \end{cases} \tag{3.1}$$

where we let e_i, $i = 1, \dots, d$ be the coordinate unit vectors. In other words, the exchange across the bond $\{x, x+e_i\}$ is suppressed if the neighboring sites

in the ith direction are both occupied. Note that exchanges across the bonds $\{x, x+e_i\}$ such that either $x-e_i \in \Lambda^c$ or $x+2e_i \in \Lambda^c$ are not suppressed, where we denote by Λ^c the complement of Λ on $\mathbb{Z}^d$, i.e. $\Lambda^c = \mathbb{Z}^d \setminus \Lambda$.

The second model has jump rates $c^{(2)}_{xy}(\eta) = 0$ if $\{x, y\}$ are not nearest neighbors and

$$c^{(2)}_{x,y}(\eta) := \begin{cases} 0 & \text{if} \sum_{\substack{d(\{z\},\{x,y\})=1 \\ z\in\Lambda}} \eta_z > 2d-1 \\ 1 & \text{otherwise} \end{cases} \tag{3.2}$$

where we let $d(A,B)$ be the distance among set A and B, i.e. $\mathrm{d}(A,B) = \inf\{|x-y|\,,\ x\in A, y\in B\}$. In other words, the exchange across bond $\{x,y\}$ is suppressed if more than one half of $d(2d-1)$ neighboring sites of the couple $\{x,y\}$ are occupied. Note that for $d=1$ we have $c^{(1)}_{x,y} = c^{(2)}_{x,y}$.

Note that such dynamics preserves the total number of particles in Λ and satisfies detailed balance with respect to flat measure $\nu_{\Lambda,N}$ on hyperplanes $\Omega_{\Lambda,N}$ with fixed number of particles, which is therefore stationary. However - since the rates degenerate - blocked configuration exist and the generator is not ergodic on all the hyperplanes of Ω_Λ with fixed total number of particles. For instance, if $d=1$, all configurations η in which the distance between all the empty sites is three or more do not evolve. On the other hand, by adding sources of birth and death of particles at the boundary, i.e. by adding a term of the form (2.33), it is not difficult to show that the generator for both the models is irreducible, namely there is positive probability of going from any configuration to any other. Therefore the process is ergodic and the unique invariant measure is $\mu_{\Lambda,\rho}$, i.e. Bernoulli product measure with density ρ. As explained in section 2.5.3, an interesting issue is to study the gap and logarithmic Sobolev constant for such processes. An estimate of such quantities, and therefore of the typical velocity of convergence to equilibrium for the model with boundary sources, will be given in section 3.2. On the other hand, in section 3.3 we address the study of the model on the infinite lattice. First we prove that ergodicity holds at any density (no ergodic–non/ergodic transition), then we prove that the self diffusion coefficient of a tagged particle is always strictly positive (no diffusive/non–diffusive transition). In this chapter we will use a mathematical language that will be replaced in next chapters by a less rigorous formulation of results. Indeed we believe that, writing explicitely proofs and results for these models, will provide a useful ground to understand the tools and ideas used in future chapters where we deal with more complicated models for which the results of this chapter cannot be readily extended.

3.2 Models on finite lattices

In this section we prove a lower and upper bound on the spectral gap and logarithmic Sobolev constant of the generator of both the models in $L_2(\mu_{\Lambda,\rho})$. We show that, for any $\rho \in (0,1)$, the asymptotic behavior for $\ell \to \infty$ is, respectively, ℓ^{-2} and ℓ^2. This is the same behavior as for SSEP (see section 2.5.3). On the other hand, a different density dependence arises.

3.2.1 Spectral gap

Let us recall that the generators we are considering are the operators which acts on local functions $f : \eta \in \Omega \to \mathbb{R}$ as

$$\mathcal{L}_\Lambda^{(k)} f(\eta) = \sum_{\substack{\{x,y\}\subset\Lambda \\ \mathrm{d}(x,y)=1}} c_{x,y}^{(k)}(\eta)\nabla_{xy} f(\eta) + \sum_{\substack{x\in\Lambda, y\notin\Lambda \\ \mathrm{d}(x,y)=1}} c_x(\eta)\nabla_x f(\eta) \tag{3.3}$$

where we have introduced $\nabla_{xy} f := T_{xy} f - f$ and $\nabla_x f := T_x f - f$, with exchange and birth/death operators T_{xy} and T_x acting on configuration as $T_{x,y}(\eta) \equiv \eta^{x,y}$ and $T_x \eta \equiv \eta^x$ (recall that jump rates $c_{xy}^{(i)}(\eta)$ have been defined in (3.1), (3.2) and birth/death rates $c_x(\eta)$ in (2.35)). We use the suffix Λ in the generator to indicate that it is defined on the lattice Λ and distinguish with the generator on infinite lattice $\mathbb{Z}^d$ which we denote simply by $\mathcal{L}$.

Our first results is a lower bound on the spectral gap of $L_\Lambda^{(k)}$, $k = 1, 2$. Let us define the Dirichlet form associated to $\mathcal{L}_\Lambda^{(k)}$ as

$$\begin{aligned} \mathcal{E}_{\Lambda,\rho}^{(k)}(f) &:= -\mu_{\Lambda,\rho}(f L_\Lambda^{(k)} f) \\ &= \frac{1}{2}\Bigg\{ \sum_{\substack{\{x,y\}\subset\Lambda \\ \mathrm{d}(x,y)=1}} \mu_{\Lambda,\rho}\big[c_{x,y}^{(k)}(\nabla_{x,y} f)^2\big] + \sum_{\substack{x\in\Lambda, y\notin\Lambda \\ \mathrm{d}(x,y)=1}} \mu_{\Lambda,\rho}\big[c_x(\nabla_x f)^2\big] \Bigg\} \end{aligned} \tag{3.4}$$

therefore variational definition of the spectral gap can be rewritten as

$$\mathrm{gap}(\mathcal{L}) \equiv \inf_{f\in\mathbb{I}^\perp} \mathcal{E}_{L,\rho}\mu(f - \mu(f))^2 \tag{3.5}$$

Theorem 3.2.1. *For any $\rho \in (0,1)$ and $k = 1, 2$ there exists a constant $C = C(d, \rho, k)$ such that for any ℓ and for any function $f : \Omega_\Lambda \to \mathbb{R}$ we have*

$$\mu_{\Lambda,\rho}(f; f) \le C\,\ell^2\,\mathcal{E}_{\Lambda,\rho}^{(k)}(f) \tag{3.6}$$

Remark 1. Thanks to the variational characterization of the spectral gap, the bound (3.6) is equivalent to $\mathrm{gap}(L_\Lambda^{(k)}) \geq C^{-1}\ell^{-2}$.

Remark 2. By taking as test function $f(\eta) = \sum_{x\in\Lambda}(\eta_x - \rho)\cos\frac{\pi x}{2\ell}$ and using $c_{x,y}^{(k)} \leq 1$ for any x, y and $k = 1, 2$, a simple computation shows that for each $\rho \in (0,1)$ there exist a constant $C = C(d, k, \rho)$ such that $\mathrm{gap}(L_\Lambda^{(k)}) \leq C\ell^{-2}$. Hence $\mathrm{gap}(L_\Lambda^{(k)}) \asymp \ell^{-2}$ as in the case of the simple exclusion.

Remark 3. As discussed in the introduction, the correct dependence of the spectral gap on the density ρ has some interest. For simplicity we discuss it only in the case $k = 1$, namely for the rates chosen as in (3.1). It is a corollary of our analysis that the gap goes to zero as $\rho \uparrow 1$ as a power law of exponent between 1 and 2. More precisely the following two inequalities hold. There exists a constant $C_1 = C_1(d)$ such that for any $\rho \in (0,1)$ and any ℓ we have $\mathrm{gap}(L_\Lambda^{(1)}) \geq (1-\rho)^2 C_1/\ell^2$. For each integer $\ell \geq 5$, there exists a constant $C_2 = C_2(d, \ell)$ such that $\mathrm{gap}(L_\Lambda^{(1)}) \leq C_2(1-\rho)$. The lower bound follows from the proof of Theorem 3.2.1; the upper bound is obtained easily by using as test function $f(\eta) = \eta_x$ with $x \in \Lambda$ such that $\mathrm{d}(x, \Lambda^c) \geq 3$.

Remark 4. As previously discussed, the process generated by L_{bulk} is not irreducible on the hyperplanes with fixed number of particles, $\Omega_{\Lambda,N} := \{\eta \in \Omega_\Lambda : \sum_{x\in\Lambda}\eta_x = N\}$. In the one–dimensional case, $d = 1$ (recall that in such a case $c^{(1)} = c^{(2)}$), is however not difficult to check that L_{bulk} is irreducible on the set

$$\widetilde{\Omega}_{\Lambda,N} := \{\eta \in \Omega_{\Lambda,N} : \exists\, x, y \in \Lambda,\, x \neq y\,, \mathrm{d}(x,y) \leq 2 \text{ such that } \eta_x = \eta_y = 0\}$$

and L_{bulk} satisfies detailed balance w.r.t. the conditional measure $\widetilde{\nu}_{\Lambda,N}(\cdot) := \mu_{\Lambda,\rho}(\cdot|\widetilde{\Omega}_{\Lambda,N})$. A natural question is then the asymptotic behavior of the spectral gap of L_{bulk} in $L_2(\widetilde{\nu}_{\Lambda,N})$, a reasonable guess is that for each $N \leq \ell - 2$ we still have $\mathrm{gap}(L_{\mathrm{bulk}}) \asymp \ell^{-2}$. This conjecture is supported by the fact that if $N = |\Lambda| - 2 = \ell - 2$, i.e. in the highest density case, we have a single pair of neighboring empty sites which performs a random walk. We are not able to prove the above conjecture in general, but only in the trivial situation in which $N < |\Lambda|/3 = \ell/3$. In such a case, for ℓ large enough, we have $\widetilde{\Omega}_{\Lambda,N} = \Omega_{\Lambda,N}$; therefore the statement follows easily by a comparison with the exclusion process with long exchanges, see [38, Lemma 8.1], and a minor modification of the argument in Lemma 3.2.2 below.

Remark 5. By considering the same models with the strength of the sources slowed down of a factor $1/\ell$ (i.e. by multiplying rates c_x by $1/\ell$ in (3.3), our proof gives the same estimate for both gap and logarithm Sobolev constant. This come from the fact that a factor ℓ in the second term would not modify the the passage from (3.9) to (3.6).

The key step in the proof of Theorem 3.2.1 is the following lemma, which is in the same spirit of the path lemmata in [37, 38, 41].

Lemma 3.2.2. *For $k = 1, 2$ and each $x \in \Lambda$ let*

$$U_x^{(k)} := \big\{ y \in \Lambda \,:\, 1 \le y_1 \le x_1 - 1\,,\ |y_i - x_i| \le r^{(k)},\ i = 2, \dots, d \big\}$$

where $r^{(1)} := 0$ and $r^{(2)} := 1$. Then, for each $k = 1, 2$ and $\rho \in (0, 1)$, there exists a constant $A = A(d, k, \rho)$ such that for any ℓ

$$\mu_{\Lambda,\rho}\big(c_x(\nabla_x f)^2\big) \le A\Big\{ \ell \sum_{y \in U_x^{(k)}} \mu_{\Lambda,\rho}\big(c^{(k)}_{y,y+e_1}(\nabla_{y,y+e_1} f)^2\big) + \sum_{\substack{y:\, y_1 = 1 \\ y \in U_x^{(k)}}} \mu_{\Lambda,\rho}\big(c_y(\nabla_y f)^2\big) \Big\} \tag{3.7}$$

for any $x \in \Lambda$ and any function f on Ω_Λ.

Postponing the proof of the lemma above, let us first show how it implies, together with a comparison argument with Glauber dynamics, Theorem 3.2.1.

Proof of Theorem 3.2.1. Let us introduce the product (Glauber) dynamics in Ω_Λ defined by the generator

$$L_\Lambda^G f(\eta) := \sum_{x \in \Lambda} c_x(\eta) \nabla_x f(\eta) \tag{3.8}$$

where c_x has been defined in 2.35. The generator L_Λ^G is self–adjoint in $L_2(\mu_{\Lambda,\rho})$; since it is a product dynamics, it is immediate to check its spectral gap is 1. For each function f on Ω_Λ we thus get

$$\begin{aligned}
\mu_{\Lambda,\rho}(f; f) &\le -\mu_{\Lambda,\rho}(f L_\Lambda^G f) = \frac{1}{2} \sum_{x \in \Lambda} \mu_{\Lambda,\rho}\big(c_x(\nabla_x f)^2\big) \\
&\le \frac{A}{2} \sum_{x \in \Lambda} \Big\{ \ell \sum_{y \in U_x^{(k)}} \mu_{\Lambda,\rho}\big(c^{(k)}_{y,y+e_1}(\nabla_{y,y+e_1} f)^2\big) + \sum_{\substack{y:\, y_1 = 1 \\ y \in U_x^{(k)}}} \mu_{\Lambda,\rho}\big(c_y(\nabla_y f)^2\big) \Big\} \\
&\le \frac{A}{2} \ell (2r^{(k)} + 1)^{d-1} \Big\{ \ell \sum_{\substack{\{x,y\} \subset \Lambda \\ \mathrm{d}(x,y) = 1}} \mu_{\Lambda,\rho}\big(c^{(k)}_{x,y}(\nabla_{x,y} f)^2\big) + \\
&\quad \sum_{\substack{x \in \Lambda, y \notin \Lambda \\ \mathrm{d}(x,y) = 1}} \mu_{\Lambda,\rho}\big(c_x(\nabla_x f)^2\big) \Big\}
\end{aligned} \tag{3.9}$$

where we used the variational characterization of the spectral gap, Lemma 3.2.2 and elementary inequalities. We thus get the bound (3.6) with $C = A(2r^{(k)} + 1)^{d-1}$. □

We are left with the proof of the lemma. The basic idea is to use first $L_{\text{bound.}}$ to empty a few sites at the boundary. Then - via careful moves - we show how this cluster of holes can be shifted, using exchanges with non zero rate, and used to flip the occupation number in x. Finally we shift the cluster back to the boundary and use again $L_{\text{bound.}}$ to reconstruct the initial configuration near the boundary.

Proof of Lemma 3.2.2. We discuss first the case of $k = 1$ which corresponds to the rates (3.1). We assume also that $x_1 \geq 4$, otherwise the proof is much easier.

Given $\eta \in \Omega_\Lambda$ and $x \in \Lambda$ let us define $S_x\eta \in \Omega_\Lambda$ as the configuration given by

$$(S_x\eta)_y := \begin{cases} 0 & \text{if } y = (1, x_2, \dots, x_d) \\ 0 & \text{if } y = (2, x_2, \dots, x_d) \\ 1 - \eta_x & \text{if } y = (3, x_2, \dots, x_d) \\ \eta_y & \text{otherwise} \end{cases} \tag{3.10}$$

Moreover, for $y \in \mathbb{Z}^d$ we define

$$\begin{aligned} T_y^L &:= T_{y+e_1,y+2e_1} T_{y,y+e_1} T_{y-e_1,y} \\ T_y^R &:= T_{y,y+e_1} T_{y+e_1,y+2e_1} T_{y+2e_1,y+3e_1} \end{aligned} \tag{3.11}$$

Note that T_y^L moves the occupation number in $y - e_1$ to $y + 2e_1$ while the configuration in $y, y + e_1, y + 2e_1$ is shifted by one in the direction $-e_1$. Analogously T_y^R moves the occupation number in $y + 3e_1$ to y while the configuration in $y, y + e_1, y + 2e_1$ is shifted by one in the direction e_1.

For $x \in \Lambda$, we let $\gamma_i := (ie_1, x_2, \dots, x_d)$, $i = 1, \dots x_1 - 1$ and define

$$\overline{S}_x\eta := \big(T^L_{\gamma_2} \cdots T^L_{\gamma_{x_1-3}}\big) T_{x-e_1,x} \big(T^R_{\gamma_{x_1-4}} \cdots T^R_{\gamma_1}\big) S_x\eta \tag{3.12}$$

It is not difficult to check that $(\overline{S}_x\eta)_y = 0$ if $y = \gamma_1$ or $y = \gamma_2$, $(\overline{S}_x\eta)_y = \eta_x$ if $y = \gamma_3$, $(\overline{S}_x\eta)_y = 1 - \eta_x$ if $y = x$, and $(\overline{S}_x\eta)_y = \eta_y$ otherwise.

For $x \in \Lambda$ with $x_1 \geq 4$ we write

$$\nabla_x f(\eta) = \big[f(\eta^x) - f(\overline{S}_x\eta)\big] + \big[f(\overline{S}_x\eta) - f(S_x\eta)\big] + \big[f(S_x\eta) - f(\eta)\big] \tag{3.13}$$

We start by considering the second term in decomposition above; we claim that

$$\sum_{\eta \in \Omega_\Lambda} \mu_{\Lambda,\rho}(\eta) c_x(\eta) \big[f(\overline{S}_x\eta) - f(S_x\eta)\big]^2 \tag{3.14}$$

$$\leq 18(1-\rho)^{-2}(2x_1 - 7) \sum_{i=1}^{x_1-1} \mu_{\Lambda,\rho}\Big[c^{(1)}_{\gamma_i,\gamma_{i+1}} \big(\nabla_{\gamma_i,\gamma_{i+1}} f\big)^2\Big] \tag{3.15}$$

To prove the above bound, let us introduce the path

$$\zeta_i := \begin{cases} S_x\eta & i=0 \\ T^R_{\gamma_i}\cdots T^R_{\gamma_1}S_x\eta & i=1,\dots,x_1-4 \\ T_{x-e_1,x}\big(T^R_{\gamma_{x_1-4}}\cdots T^R_{\gamma_1}\big)S_x\eta & i=x_1-3 \\ \big(T^L_{\gamma_{2x_1-5-i}}\cdots T^L_{\gamma_{x_1-3}}\big)T_{x-e_1,x}\big(T^R_{\gamma_{x_1-4}}\cdots T^R_{\gamma_1}\big)S_x\eta & i=x_1-3+1,\dots,2x_1-7 \end{cases} \tag{3.16}$$

By (3.12) we have $\zeta_{2x_1-7} = \overline{S}_x\eta$. Note also that, for each $\eta\in\Omega_\Lambda$ and $0\le i\le x_1-4$, the configuration ζ_i is guaranteed to be empty at the sites γ_{i+1} and γ_{i+2}. Moreover, for each $\eta\in\Omega_\Lambda$ and $0\le j\le x_1-4$ the configuration ζ_{x_1-3+j} is guaranteed to be empty at the sites γ_{x_1-2-j} and γ_{x_1-3-j}. This will allow us to move the configuration ζ_i to the configuration ζ_{i+1} using exchanges with non zero $c^{(1)}$ rate.

By telescopic sums and Cauchy–Schwartz, we get

$$\big[f(\overline{S}_x\eta)-f(S_x\eta)\big]^2 = \Big(\sum_{i=1}^{2x_1-7}\big[f(\zeta_i)-f(\zeta_{i-1})\big]\Big)^2 \le (2x_1-7)\sum_{i=1}^{2x_1-7}\big[f(\zeta_i)-f(\zeta_{i-1})\big]^2 \tag{3.17}$$

We consider only the case $1\le i\le x_1-4$, the others are analogous. We then have $\zeta_i = T^R_{\gamma_i}\zeta_{i-1}$; recalling (3.11), again by telescopic sums and Cauchy–Schwartz, we get

$$\begin{aligned} &\big[f(\zeta_i)-f(\zeta_{i-1})\big]^2 = \big[f(T^R_{\gamma_i}\zeta_{i-1})-f(\zeta_{i-1})\big]^2 \\ &\quad\le 3\Big\{\big[f(T_{\gamma_i,\gamma_i+e_1}T_{\gamma_i+e_1,\gamma_i+2e_1}T_{\gamma_i+2e_1,\gamma_i+3e_1}\zeta_{i-1})-f(T_{\gamma_i+e_1,\gamma_i+2e_1}T_{\gamma_i+2e_1,\gamma_i+3e_1}\zeta_{i-1})\big]^2 \\ &\qquad+\big[f(T_{\gamma_i+e_1,\gamma_i+2e_1}T_{\gamma_i+2e_1,\gamma_i+3e_1}\zeta_{i-1})-f(T_{\gamma_i+2e_1,\gamma_i+3e_1}\zeta_{i-1})\big]^2 \\ &\qquad+\big[f(T_{\gamma_i+2e_1,\gamma_i+3e_1}\zeta_{i-1})-f(\zeta_{i-1})\big]^2\Big\} \\ &\quad= 3\Big\{c^{(1)}_{\gamma_i,\gamma_i+e_1}(T_{\gamma_i+e_1,\gamma_i+2e_1}T_{\gamma_i+2e_1,\gamma_i+3e_1}\zeta_{i-1})\big[\nabla_{\gamma_i,\gamma_i+e_1}f(T_{\gamma_i+e_1,\gamma_i+2e_1}T_{\gamma_i+2e_1,\gamma_i+3e_1}\zeta_{i-1})\big]^2 \\ &\qquad+c^{(1)}_{\gamma_i+e_1,\gamma_i+2e_1}(T_{\gamma_i+2e_1,\gamma_i+3e_1}\zeta_{i-1})\big[\nabla_{\gamma_i+e_1,\gamma_i+2e_1}f(T_{\gamma_i+2e_1,\gamma_i+3e_1}\zeta_{i-1})\big]^2 \\ &\qquad+c^{(1)}_{\gamma_i+2e_1,\gamma_i+3e_1}(\zeta_{i-1})\big[\nabla_{\gamma_i+2e_1,\gamma_i+3e_1}f(\zeta_{i-1})\big]^2\Big\} \end{aligned} \tag{3.18}$$

where we used that

$$\begin{aligned} c^{(1)}_{\gamma_i+2e_1,\gamma_i+3e_1}(\zeta_{i-1}) &= c^{(1)}_{\gamma_i+e_1,\gamma_i+2e_1}(T_{\gamma_i+2e_1,\gamma_i+3e_1}\zeta_{i-1}) \\ &= c^{(1)}_{\gamma_i,\gamma_i+e_1}(T_{\gamma_i+e_1,\gamma_i+2e_1}T_{\gamma_i+2e_1,\gamma_i+3e_1}\zeta_{i-1}) = 1 \end{aligned}$$

by construction of the path ζ_i, see the remark below (3.16).

In order to prove the bound 3.14 we consider only the last term on the r.h.s. of (3.18), the other can be analyzed in the same way. Given $A \subset \Lambda$, $\xi \in \Omega_A$, $x \in A$, and $g : \Omega_\Lambda \to \mathbb{R}$ we observe that, since $\mu_{\Lambda,\rho}$ is a product measure and c_x is given in (2.35),

$$\begin{aligned}\sum_{\eta\in\Omega_\Lambda} \mu_{\Lambda,\rho}(\eta)\,\eta_x\,c_x(\eta)\,g(\eta_{\Lambda\setminus A}\,\xi) &= \sum_{\eta\in\Omega_\Lambda} \mu_{\Lambda,\rho}(\eta)\,(1-\eta_x)\,c_x(\eta)\,g(\eta_{\Lambda\setminus A}\,\xi)\\ &= \rho(1-\rho)\mu_{\Lambda,\rho}\big(g\,\big|\,\eta_A=\xi\big)\end{aligned} \tag{3.19}$$

Recalling definitions (3.10) and (3.16), we thus get

$$\begin{aligned}&\sum_{\eta\in\Omega}\mu_{\Lambda,\rho}(\eta)c_x(\eta)c^{(1)}_{\gamma_i+2e_1,\gamma_i+3e_1}(\zeta_{i-1})\big[\nabla_{\gamma_i+2e_1,\gamma_i+3e_1}f(\zeta_{i-1})\big]^2\\ &=\sum_{\eta\in\Omega}\mu_{\Lambda,\rho}(\eta)\eta_x c_x(\eta)c^{(1)}_{\gamma_i+2e_1,\gamma_i+3e_1}(\zeta_{i-1})\big[\nabla_{\gamma_i+2e_1,\gamma_i+3e_1}f(\zeta_{i-1})\big]^2\\ &+\sum_{\eta\in\Omega}\mu_{\Lambda,\rho}(\eta)[1-\eta_x]c_x(\eta)c^{(1)}_{\gamma_i+2e_1,\gamma_i+3e_1}(\zeta_{i-1})\big[\nabla_{\gamma_i+2e_1,\gamma_i+3e_1}f(\zeta_{i-1})\big]^2\\ &=\rho(1-\rho)\Big\{\mu_{\Lambda,\rho}\Big(c^{(1)}_{\gamma_i+2e_1,\gamma_i+3e_1}\big[\nabla_{\gamma_i+2e_1,\gamma_i+3e_1}f\big]^2\,\Big|\,\eta_x=1,\eta_{\gamma_i}=\eta_{\gamma_{i+1}}=\eta_{\gamma_{i+2}}=0\Big)\\ &+\mu_{\Lambda,\rho}\Big(c^{(1)}_{\gamma_i+2e_1,\gamma_i+3e_1}\big[\nabla_{\gamma_i+2e_1,\gamma_i+3e_1}f\big]^2\,\Big|\,\eta_x=\eta_{\gamma_i}=\eta_{\gamma_{i+1}}=0,\eta_{\gamma_{i+2}}=1\Big)\Big\}\end{aligned} \tag{3.20}$$

We now observe that for any positive function $g : \Omega_\Lambda \to \mathbb{R}$ we have

$$\begin{aligned}&\mu_{\Lambda,\rho}(g)\ge\mu_{\Lambda,\rho}(\eta_x=1,\eta_{\gamma_i}=\eta_{\gamma_{i+1}}=\eta_{\gamma_{i+2}}=0)\,\mu_{\Lambda,\rho}\big(g\,\big|\,\eta_x=1,\eta_{\gamma_i}=\eta_{\gamma_{i+1}}=\eta_{\gamma_{i+2}}=0\big)\\ &+\mu_{\Lambda,\rho}(\eta_x=\eta_{\gamma_i}=\eta_{\gamma_{i+1}}=0,\eta_{\gamma_{i+2}}=1)\,\mu_{\Lambda,\rho}\big(g\,\big|\,\eta_x=\eta_{\gamma_i}=\eta_{\gamma_{i+1}}=0,\eta_{\gamma_{i+2}}=1\big)\\ &\qquad=\rho(1-\rho)^3\Big\{\mu_{\Lambda,\rho}\big(g\,\big|\,\eta_x=1,\eta_{\gamma_i}=\eta_{\gamma_{i+1}}=\eta_{\gamma_{i+2}}=0\big)\\ &\qquad\qquad+\mu_{\Lambda,\rho}\big(g\,\big|\,\eta_x=\eta_{\gamma_i}=\eta_{\gamma_{i+1}}=0,\eta_{\gamma_{i+2}}=1\big)\Big\}\end{aligned}$$

so that from (3.20) we get

$$\begin{aligned}&\sum_{\eta\in\Omega_\Lambda}\mu_{\Lambda,\rho}(\eta)c_x(\eta)c^{(1)}_{\gamma_i+2e_1,\gamma_i+3e_1}(\zeta_{i-1})\big[\nabla_{\gamma_i+2e_1,\gamma_i+3e_1}f(\zeta_{i-1})\big]^2\\ &\qquad\le(1-\rho)^{-2}\,\mu_{\Lambda,\rho}\Big(c^{(1)}_{\gamma_i+2e_1,\gamma_i+3e_1}\big[\nabla_{\gamma_i+2e_1,\gamma_i+3e_1}f\big]^2\Big)\end{aligned} \tag{3.21}$$

The bound (3.14) follows from (3.17), (3.18), and (3.21). Note that the extra factor 2 comes from the return path, $x_1 - 4 \le i \le 2x_1 - 7$.

Let us now consider the last term on the r.h.s. of (3.13); we claim that

$$\sum_{\eta\in\Omega}\mu_{\Lambda,\rho}c_x(\eta)\big[f(S_x\eta)-f(\eta)\big]^2$$
$$\le\frac{6}{(1-\rho)^2}\Big\{3\mu_{\Lambda,\rho}\big(c_{\gamma_1}[\nabla_{\gamma_1}f]^2\big)+2\mu_{\Lambda,\rho}\big(c_{\gamma_1,\gamma_2}[\nabla_{\gamma_1,\gamma_2}f]^2\big)+\mu_{\Lambda,\rho}\big(c_{\gamma_2,\gamma_3}[\nabla_{\gamma_2,\gamma_3}f]^2\big)\Big\} \tag{3.22}$$

To prove the above bound let us define $T_x^+\eta$ as the configuration given by $(T_x^+\eta)_x=1$ and $(T_x^+\eta)_y=\eta_y$ for $y\neq x$; analogously we let $T_x^-\eta$ be the configuration given by $(T_x^-\eta)_x=0$ and $(T_x^-\eta)_y=\eta_y$ for $y\neq x$. Recalling (3.10) we then have

$$\begin{aligned}f(S_x\eta)-f(\eta)=\eta_x\Big[&\eta_{\gamma_1}\nabla_{\gamma_1}f(\eta)+\nabla_{\gamma_1,\gamma_2}f(T^-_{\gamma_1}\eta)+\eta_{\gamma_2}\nabla_{\gamma_1}f(T_{\gamma_1,\gamma_2}T^-_{\gamma_1}\eta)\\&+\nabla_{\gamma_2,\gamma_3}f(T^-_{\gamma_1}T_{\gamma_1,\gamma_2}T^-_{\gamma_1}\eta)+\nabla_{\gamma_1,\gamma_2}f(T_{\gamma_2,\gamma_3}T^-_{\gamma_1}T_{\gamma_1,\gamma_2}T^-_{\gamma_1}\eta)\\&+\eta_{\gamma_3}\nabla_{\gamma_1}f(T_{\gamma_1,\gamma_2}T_{\gamma_2,\gamma_3}T^-_{\gamma_1}T_{\gamma_1,\gamma_2}T^-_{\gamma_1}\eta)\Big]\\+(1-\eta_x)\Big[&(1-\eta_{\gamma_1})\nabla_{\gamma_1}f(\eta)+\nabla_{\gamma_1,\gamma_2}f(T^+_{\gamma_1}\eta)+\eta_{\gamma_2}\nabla_{\gamma_1}f(T_{\gamma_1,\gamma_2}T^+_{\gamma_1}\eta)\\&+\nabla_{\gamma_2,\gamma_3}f(T^-_{\gamma_1}T_{\gamma_1,\gamma_2}T^+_{\gamma_1}\eta)+\nabla_{\gamma_1,\gamma_2}f(T_{\gamma_2,\gamma_3}T^-_{\gamma_1}T_{\gamma_1,\gamma_2}T^+_{\gamma_1}\eta)\\&+\eta_{\gamma_3}\nabla_{\gamma_1}f(T_{\gamma_1,\gamma_2}T_{\gamma_2,\gamma_3}T^-_{\gamma_1}T_{\gamma_1,\gamma_2}T^+_{\gamma_1}\eta)\Big]\end{aligned} \tag{3.23}$$

By using Schwartz inequality and the fact that the telescopic decomposition in (3.23) has been arranged so that all the exchanges have non zero $c^{(1)}$ rate, we get

$$\begin{aligned}[f(S_x\eta)-f(\eta)]^2\le 6\Big\{&\eta_x\,\eta_{\gamma_1}[\nabla_{\gamma_1}f(\eta)]^2+(1-\eta_x)(1-\eta_{\gamma_1})[\nabla_{\gamma_1}f(\eta)]^2\\&+\eta_x c^{(1)}_{\gamma_1,\gamma_2}(T^-_{\gamma_1}\eta)[\nabla_{\gamma_1,\gamma_2}f(T^-_{\gamma_1}\eta)]^2+(1-\eta_x)c^{(1)}_{\gamma_1,\gamma_2}(T^+_{\gamma_1}\eta)[\nabla_{\gamma_1,\gamma_2}f(T^+_{\gamma_1}\eta)]^2\\&+\eta_x\eta_{\gamma_2}[\nabla_{\gamma_1}f(T_{\gamma_1,\gamma_2}T^-_{\gamma_1}\eta)]^2+(1-\eta_x)\eta_{\gamma_2}[\nabla_{\gamma_1}f(T_{\gamma_1,\gamma_2}T^+_{\gamma_1}\eta)]^2\\&+\eta_x c^{(1)}_{\gamma_2,\gamma_3}(T^-_{\gamma_1}T_{\gamma_1,\gamma_2}T^-_{\gamma_1}\eta)[\nabla_{\gamma_2,\gamma_3}f(T^-_{\gamma_1}T_{\gamma_1,\gamma_2}T^-_{\gamma_1}\eta)]^2\\&+(1-\eta_x)c^{(1)}_{\gamma_2,\gamma_3}(T^-_{\gamma_1}T_{\gamma_1,\gamma_2}T^+_{\gamma_1}\eta)[\nabla_{\gamma_2,\gamma_3}f(T^-_{\gamma_1}T_{\gamma_1,\gamma_2}T^+_{\gamma_1}\eta)]^2\\&+\eta_x c^{(1)}_{\gamma_1,\gamma_2}(T_{\gamma_2,\gamma_3}T^-_{\gamma_1}T_{\gamma_1,\gamma_2}T^-_{\gamma_1}\eta)[\nabla_{\gamma_1,\gamma_2}f(T_{\gamma_2,\gamma_3}T^-_{\gamma_1}T_{\gamma_1,\gamma_2}T^-_{\gamma_1}\eta)]^2\\&+(1-\eta_x)c^{(1)}_{\gamma_1,\gamma_2}(T_{\gamma_2,\gamma_3}T^-_{\gamma_1}T_{\gamma_1,\gamma_2}T^+_{\gamma_1}\eta)[\nabla_{\gamma_1,\gamma_2}f(T_{\gamma_2,\gamma_3}T^-_{\gamma_1}T_{\gamma_1,\gamma_2}T^+_{\gamma_1}\eta)]^2\\&+\eta_x\eta_{\gamma_3}[\nabla_{\gamma_1}f(T_{\gamma_1,\gamma_2}T_{\gamma_2,\gamma_3}T^-_{\gamma_1}T_{\gamma_1,\gamma_2}T^-_{\gamma_1}\eta)]^2\\&+(1-\eta_x)\eta_{\gamma_3}[\nabla_{\gamma_1}(f(T_{\gamma_1,\gamma_2}T_{\gamma_2,\gamma_3}T^-_{\gamma_1}T_{\gamma_1,\gamma_2}T^+_{\gamma_1}\eta)]^2\Big\}\end{aligned} \tag{3.24}$$

By recalling the definition (2.35) we have $1-\eta_y\le\rho^{-1}c_y(\eta)$ and $\eta_y\le(1-\rho)^{-1}c_y(\eta)$ for any $\eta\in\Omega_\Lambda$ and $y\in\Lambda$. We next estimate separately each

term on the r.h.s. of (3.24). Let us consider only the last two terms, the others are easier. We have

$$\begin{aligned}\sum_{\eta\in\Omega_\Lambda}\mu_{\Lambda,\rho}(\eta)\,c_x(\eta)\Big\{&\eta_x\,\eta_{\gamma_3}[\nabla_{\gamma_1}f(T_{\gamma_1,\gamma_2}T_{\gamma_2,\gamma_3}T^-_{\gamma_1}T_{\gamma_1,\gamma_2}T^-_{\gamma_1}\eta)]^2\\&+(1-\eta_x)\,\eta_{\gamma_3}[\nabla_{\gamma_1}(f(T_{\gamma_1,\gamma_2}T_{\gamma_2,\gamma_3}T^-_{\gamma_1}T_{\gamma_1,\gamma_2}T^+_{\gamma_1}\eta)]^2\Big\}\\ \le{}&(1-\rho)^{-1}\Big\{(1-\rho)\,\mu_{\Lambda,\rho}(\eta_x)\mu_{\Lambda,\rho}\big(c_{\gamma_1}[\nabla_{\gamma_1}f]^2\,\big|\,\eta_x=1,\eta_{\gamma_2}=\eta_{\gamma_3}=0\big)\\&+\rho\,\mu_{\Lambda,\rho}(1-\eta_x)\mu_{\Lambda,\rho}\big(c_{\gamma_1}[\nabla_{\gamma_1}f]^2\,\big|\,\eta_x=\eta_{\gamma_2}=0,\eta_{\gamma_3}=1\big)\Big\}\\ \le{}&(1-\rho)^{-2}\mu_{\Lambda,\rho}\big(c_{\gamma_1}[\nabla_{\gamma_1}f]^2\big)\end{aligned}\tag{3.25}$$

where we used that, as in (3.21), for any positive function $g:\Omega_\Lambda\to\mathbb{R}$

$$\mu_{\Lambda,\rho}\big(g\,\big|\,\eta_x=1,\eta_{\gamma_2}=\eta_{\gamma_3}=0\big)+\mu_{\Lambda,\rho}\big(g\,\big|\,\eta_x=\eta_{\gamma_2}=0,\eta_{\gamma_3}=1\big)\le\tag{3.26}$$

$$\frac{1}{\rho(1-\rho)^2}\,\mu_{\Lambda,\rho}\big(g\big)\tag{3.27}$$

By analogous computations for the other terms, (3.22) follows.

Finally, to bound the first term on the r.h.s. of (3.13), it is enough to change variable $\eta\mapsto\eta^x$. Indeed, noting $\bar S_x\eta^x=S_x\eta$, we get

$$\sum_{\eta\in\Omega_\Lambda}\mu_{\Lambda,\rho}(\eta)c_x(\eta)\big[f(\eta^x)-f(\bar S_x\eta)\big]^2=\sum_{\eta\in\Omega_\Lambda}\mu_{\Lambda,\rho}(\eta)c_x(\eta)\big[f(\eta)-f(S_x\eta)\big]^2\tag{3.28}$$

For x such that $x_1\ge 4$, the bound (3.7), with the constant A given by $A=180(1-\rho)^{-2}$ now follows from (3.13), (3.14), (3.22), and (3.28). The case in which $1\le x_1\le 3$ can be proven directly by the same steps leading to (3.22).

In the case $k=2$, namely for the choice (3.2) of the exchange rates, we give only a rough sketch of the proof, which is very similar to the case $k=1$. Indeed, it is enough to define the configuration $S_x\eta$, analogous to (3.10), as

$$(S_x\eta)_y:=\begin{cases}0 & \text{if } \ y\in Q_1((3,x_2,\dots,x_d))\\ 1-\eta_x & \text{if } \ y=(1,x_2,\dots,x_d)\\ \eta_y & \text{otherwise}\end{cases}\tag{3.29}$$

where $Q_1(x):=\{y\in\mathbb{Z}^d\,:\,\max_{i=1,\dots,d}|x_i-y_i|\le 1\}$ is the cube of side 3 centered in x. The configuration $S_x\eta$ can then be shifted using exchanges with non zero $c^{(2)}$ rates by means of a suitable path, depicted in Fig. 3.1 for $d=2$. The proof is finally completed by the same arguments given for the choice (3.1). □

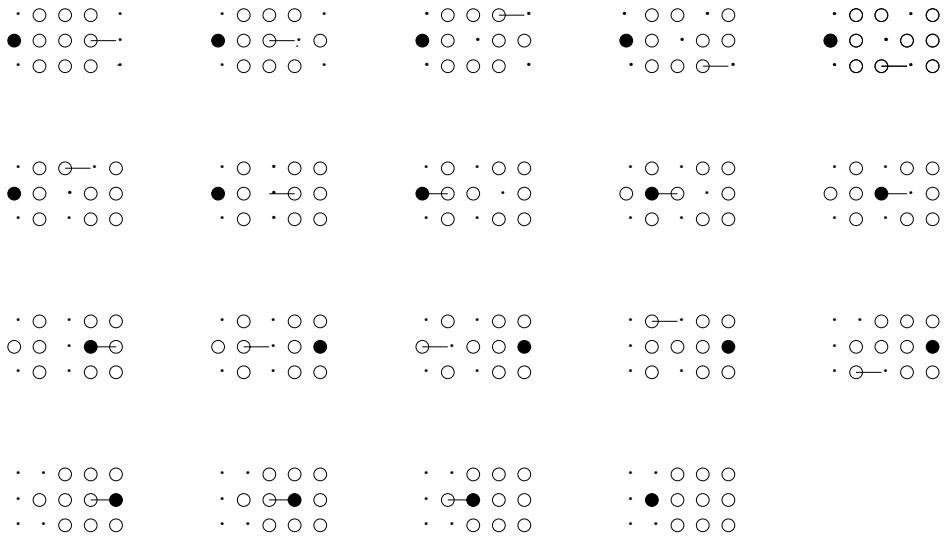

Figure 3.1: *The shifting path.* ∘ denotes sites guaranteed empty, • denotes $1 - \eta_x$, · denotes an arbitrary occupation number, and — denotes the bond exchanged in the next move.

3.2.2 Log–Sobolev inequality

In this section we show how the techniques introduced in the proof of the spectral gap can be used to prove a logarithmic Sobolev inequality for the same processes.

Recall that a Markov process with reversible measure μ and Dirichlet form $\mathcal{E}$ is said to satisfy a logarithmic Sobolev inequality with constant c_{LS} iff for any function f we have

$$\mu\left(f^2 \log \frac{f^2}{\mu(f^2)}\right) \le c_{\mathrm{LS}}\, \mathcal{E}(f) \tag{3.30}$$

(we used definition (3.3) and (3.4)).

Theorem 3.2.3. *For each $k = 1, 2$ and $\rho \in (0,1)$ there exists a constant $C = C(d,k,\rho)$ such that for any ℓ and for any function $f : \Omega_\Lambda \to \mathbb{R}$ we have*

$$\mu_{\Lambda,\rho}\left(f^2 \log \frac{f^2}{\mu_{\Lambda,\rho}(f^2)}\right) \le C\, \ell^2\, \mathcal{E}^{(k)}_{\Lambda,\rho}(f) \tag{3.31}$$

Proof of Theorem 3.2.3. Let L^G_Λ be the generator on Ω_Λ introduced in (3.8); then, see e.g. [21], for any $\rho \in (0,1)$ it satisfies the logarithmic Sobolev inequality (3.30) with c_{LS} given by $C_1(\rho) := (1-2\rho)^{-1} \log[(1-\rho)/\rho]$ (we understand $C_1(1/2) = 2$) uniformly in ℓ. By (3.7) and (3.9) the bound (3.31), with $C = C_1(\rho)\, A\, (2r^{(k)} + 1)^{d-1}$ (recall $A = A(d,\rho,k)$ is the constant in Lemma 3.2.2), follows. □

3.3 Models on infinite lattices

In this section we consider the models in infinite volume. We first introduce the infinite volume dynamics and prove that the correspondent generators $\mathcal{L}^{(k)}$, $k = 1, 2$ are ergodic for each $\rho \in [0, 1]$ in $L_2(\mu_\rho)$, where μ_ρ is the Bernoulli measure on Ω. Then, for $d \geq 2$, we prove the invariance principle for the position of the tagged particle, namely that $\varepsilon x(\varepsilon^{-2}t)$ converges in distribution, as $\varepsilon \to 0$, to a Brownian motion with strictly positive diffusion coefficient.

3.3.1 Ergodicity

In order to discuss the diffusive behavior of the tagged particle we need to introduce the infinite volume dynamics, i.e. to define the process on $\Lambda = \mathbb{Z}^d$. The configuration space is then $\Omega = \{0, 1\}^{\mathbb{Z}^d}$, a function $f : \Omega \longrightarrow \mathbb{R}$ is called a *local* function if it depends only on finitely many η_x. The generator of the process acts on local functions as

$$\mathcal{L}^{(k)} f(\eta) = \sum_{\substack{\{x,y\}\subset\mathbb{Z}^d \\ \mathrm{d}(x,y)=1}} c^{(k)}_{x,y}(\eta)\nabla_{x,y} f(\eta) \tag{3.32}$$

where $c^{(k)}$, $k = 1, 2$ has been defined in (3.1),(3.2). Note that $c^{(k)}$ are translationally covariant in the sense that $c^{(k)}_{x+y,x+y+e}(\vartheta_y\eta) = c^{(k)}_{x,x+e}(\eta)$. Moreover, for each $\rho \in [0, 1]$ and$k = 1, 2$, the generator $\mathcal{L}^{(k)}$ is self adjoint in $L_2(\mu_\rho)$, where μ_ρ is the Bernoulli measure in Ω with density ρ. In the following we prove that, for each $\rho \in [0, 1]$ and $k = 1, 2$, the generator $\mathcal{L}^{(k)}$ is ergodic in $L_2(\mu_\rho)$, namely that 0 is a simple eigenvalue of $\mathcal{L}^{(k)}$(see section 2.5.1).

Proposition 3.3.1. *For each $\rho \in [0, 1]$ and $k = 1, 2$ we have that zero is a simple eigenvalue of the generator $\mathcal{L}^{(k)}$ considered on $L_2(\mu_\rho)$.*

Proof. Let

$$\mathcal{E}^{(k)}_\rho(f) = \frac{1}{2} \sum_{\substack{\{x,y\}\subset\mathbb{Z}^d \\ \mathrm{d}(x,y)=1}} \mu_\rho\big[c^{(k)}_{x,y}(\nabla_{x,y} f)^2\big] \tag{3.33}$$

be the Dirichlet form of the generator $\mathcal{L}^{(k)}$. To show that zero is a simple eigenvalue of $\mathcal{L}^{(k)}$ we should check that $\mathcal{E}^{(k)}_\rho(f) = 0$ implies f constant μ_ρ–a.s. This is trivially true for $\rho = 0, 1$. For $\rho \in (0, 1)$ it is enough to show that $\mathcal{E}^{(k)}_\rho(f) = 0$ implies $\mu_\rho(\nabla_{x,y} f)^2 = 0$ for each $\{x, y\} \subset \mathbb{Z}^d$ with $\mathrm{d}(x, y) = 1$. Indeed, this implies that $\tilde{\mu}(\eta) = f(\eta)\mu(\eta)$ is an exchangeable measure and using DeFinetti's theorem (see [43] and [42]) on the decomposition of

exchangeable measures into product measures we conclude that $\tilde{\mu}$ coincides with μ, i.e. f is indeed constant μ_ρ–a.s.

We discuss in some detail the case $k = 1$. Let $x \in \mathbb{Z}^d$ and consider the bond $\{x, x + e_i\}$, $i = 1, \dots, d$. For $n = 1, 2, \dots$ we introduce the events

$$B^n_{x,i} := \big\{\eta \in \Omega \,:\, \eta_{x+ne_i} = \eta_{x+(n+1)e_i} = 0\big\} \qquad B_{x,i} := \bigcup_{n\geq 1} B^n_{x,i}$$

By noting that $\mu_\rho(B_{x,i}) = 1$, we have

$$\mu_\rho(\nabla_{x,x+e_i} f)^2 = \mu_\rho\big([\nabla_{x,x+e_i} f]^2 \mathbb{1}_{B_{x,i}}\big) \leq \sum_{n=1}^{\infty} \mu_\rho\big([\nabla_{x,x+e_i} f]^2 \mathbb{1}_{B^n_{x,i}}\big) \tag{3.34}$$

Let $\gamma_h := x + he_i$, $h = 0, 1, \dots$; given $\eta \in B^n_{x,i}$ we can find a path $\eta = \zeta_0, \dots, \zeta_N = \eta^{x,x+e_i}$ where $\zeta_{j+1} = \zeta_j^{\gamma_h,\gamma_{h+1}}$ for some $h = 0, 1, \dots$ and $c^{(1)}_{\gamma_h,\gamma_{h+1}}(\zeta_j) = 1$. It is in fact possible to construct a path analogous to the one introduced in the proof of Lemma 3.2.2; note that the two sites γ_n and γ_{n+1} are empty by the definition of the event $B^n_{x,i}$. Since $\mathcal{E}^{(1)}_\rho(f) = 0$ implies

$$\mu_\rho\big(c^{(1)}_{\gamma_h,\gamma_{h+1}} [\nabla_{\gamma_h,\gamma_{h+1}} f]^2\big) = 0 \quad \text{for any } h = 0, 1, \dots$$

by telescopic sums and Cauchy–Schwartz in (3.34) we get $\mu_\rho(\nabla_{x,x+e_i} f)^2 = 0$.

Recalling Figure 3.1 it is straightforward to modify the argument given above to cover also the case $k = 2$. □

3.3.2 Diffusion of the tagged particle

We now turn to the discussion of the asymptotic behavior of a tagged particle. Consider the process $\eta(t)$ generated by $\mathcal{L}^{(k)}$ and condition that at time zero the origin is occupied; tag the particle at the origin and denote by $x(t)$ its position at time t. The pair $\big(\eta(t), x(t)\big)$ is then a Markov process on the state space $\big\{(\eta, x) \in \Omega \times \mathbb{Z}^d \,:\, \eta_x = 1\big\}$ with generator

$$\begin{aligned} \mathcal{A}^{(k)} F(\eta, x) \;:=\; & \sum_{\substack{y\in\mathbb{Z}^d \\ \mathrm{d}(x,y)=1}} c^{(k)}_{x,y}(\eta)(1-\eta_y)\big[F(\eta^{x,y}, y) - F(\eta, x)\big] \\ & + \sum_{\substack{\{y,z\}\subset\mathbb{Z}^d\setminus\{x\} \\ \mathrm{d}(y,z)=1}} c^{(k)}_{y,z}(\eta)\big[F(\eta^{y,z}, x) - F(\eta, x)\big] \end{aligned} \tag{3.35}$$

Let $\Omega_0 := \{\eta \in \Omega \,:\, \eta_0 = 1\}$ and $\mu_{\rho,0}$ be the Bernoulli measure on Ω_0 with marginal $\mu_{\rho,0}(\eta_x = 1) = \rho$, $x \in \mathbb{Z}^d \setminus \{0\}$. We shall consider the

process $\big(\eta(t), x(t)\big)$ generated by $\mathcal{A}^{(k)}$ with initial condition $x(0) = 0$ and $\eta(0)$ distributed according to $\mu_{\rho,0}$. Let $\xi(t) := \vartheta_{-x(t)}\eta(t)$ be the process as seen from the tagged particle, we have that $\xi(t)$ is itself a Markov process on the configuration space Ω_0 with generator

$$\begin{aligned}\mathcal{A}_0^{(k)} f\,(\xi) \;:=\; & \sum_{\substack{y\in\mathbb{Z}^d\\ \mathrm{d}(0,y)=1}} c_{0,y}^{(k)}(\xi)(1-\xi_y)\big[f(\vartheta_{-y}\xi^{0,y}) - f(\xi)\big] \\ & + \sum_{\substack{\{x,y\}\subset\mathbb{Z}^d\setminus\{0\}\\ \mathrm{d}(x,y)=1}} c_{x,y}^{(k)}(\xi)\nabla_{x,y} f(\xi) \end{aligned} \tag{3.36}$$

A straightforward computation shows that $\mathcal{A}_0^{(k)}$ is self–adjoint in $L_2(\mu_{\rho,0})$; moreover, by the same argument as in Proposition 3.3.1, it is also ergodic in $L_2(\mu_{\rho,0})$. We can therefore apply the same proof as the one given in [18,19] for non–degenerate rates and conclude that the rescaled position of the tagged particle, $\varepsilon x(\varepsilon^{-2}t)$, converges in distribution, as $\varepsilon \to 0$, to a d–dimensional Brownian motion with diffusion matrix $2\,D_{\mathrm{self}}^{(k)}$, where $D_{\mathrm{self}}^{(k)} = D_{\mathrm{self}}^{(k)}(\rho)$ satisfies the variational formula

$$\begin{aligned} & r\cdot D_{\mathrm{self}}^{(k)}(\rho) r = \\ & \frac{1}{2}\inf_{f\ \mathrm{local}} \int \mu_{\rho,0}(d\xi)\,\Big\{ \sum_{\substack{y\in\mathbb{Z}^d\\ \mathrm{d}(0,y)=1}} c_{0,y}^{(k)}(\xi)(1-\xi_y)\big[r\cdot y + f(\vartheta_{-y}\xi^{0,y}) - f(\xi)\big]^2 \\ & + \sum_{\substack{\{x,y\}\subset\mathbb{Z}^d\setminus\{0\}\\ \mathrm{d}(x,y)=1}} c_{x,y}^{(k)}(\xi)[\nabla_{x,y} f(\xi)]^2\Big\} \end{aligned} \tag{3.37}$$

where $r \in \mathbb{R}^d$ and $\cdot$ is the inner product in $\mathbb{R}^d$.

The main result of this Section is that, for $d \geq 2$ and each $\rho \in [0,1)$, the diffusion matrix $D_{\mathrm{self}}^{(k)}(\rho)$ is strictly positive as in the case of simple exclusion [18, 19].

Theorem 3.3.2. *For each $d \geq 2$, $k = 1, 2$ and $\rho \in [0,1)$ there exists a real $c = c(d,k,\rho) > 0$ such that $r\cdot D_{\mathrm{self}}^{(k)}(\rho) r \geq c\, r\cdot r$ for any $r \in \mathbb{R}^d$.*

As discussed in section 2.5.2, the behavior of $D_{\mathrm{self}}^{(k)}(\rho)$ as $\rho \uparrow 1$ has some interest. Note that for SEP it vanishes linearly. For these models, an upper bound of the form $D_{\mathrm{self}}^{(k)}(\rho) \leq C_0(1-\rho)^2\mathbb{1}$ is easily obtained by using a constant test function f in (3.37). In the case $k = 1$, the best lower bound we have found is $D_{\mathrm{self}}^{(k)}(\rho) \geq c_0(1-\rho)^4$ where c_0 does not depend on ρ. This can be obtained with the same strategy of Theorem 3.3.2 and some further efforts,

i.e. with a more complicated path (the path described above gives indeed a worst upper bound $D^{(k)}_{\rm self}(\rho) \geq c'_0(1-\rho)^4$.

Let us fix a direction in $\mathbb{R}^d$, say e_1 and define the following subsets of $\mathbb{Z}^d \setminus \{0\}$

$$\begin{aligned} R^{(1)}_0 &:= \big\{x \in \mathbb{Z}^d \setminus \{0\} \,:\, \max_{i=1,2} |x_i| = 1\,,\; x_i = 0\,, i = 3, \dots, d\big\} \\ R^{(1)}_{\pm 1} &:= \big\{x \in \mathbb{Z}^d \setminus \{0\} \,:\, x_1 = \pm 2\,,\; |x_2| \leq 1\,,\; x_i = 0\,, i = 3, \dots, d\big\} \end{aligned} \tag{3.38}$$

and

$$\begin{aligned} R^{(2)}_0 &:= \big\{x \in \mathbb{Z}^d \setminus \{0\} \,:\, x_1 = 0\,,\; \max_{i=2,\dots,d} |x_i| \leq 3\big\} \\ R^{(2)}_{\pm 1} &:= \big\{x \in \mathbb{Z}^d \setminus \{0\} \,:\, x_1 = \pm 1\,,\; \max_{i=2,\dots,d} |x_i| \leq 3\big\} \end{aligned} \tag{3.39}$$

Given $\xi \in \Omega_0$, we next define $\xi^{+,-,(k)}$ as the configuration obtained from ξ by exchanging the occupation numbers in $R^{(k)}_{+1}$ with the corresponding ones in $R^{(k)}_{-1}$, namely

$$\big(\xi^{+,-,(1)}\big)_x := \begin{cases} \xi_x & \text{if } \; x \notin R^{(1)}_{+1} \cup R^{(1)}_{-1} \\ \xi_{x \mp 4e_1} & \text{if } \; x \in R^{(1)}_{\pm 1} \end{cases} \tag{3.40}$$

and

$$\big(\xi^{+,-,(2)}\big)_x := \begin{cases} \xi_x & \text{if } \; x \notin R^{(2)}_{+1} \cup R^{(2)}_{-1} \\ \xi_{x \mp 2e_1} & \text{if } \; x \in R^{(2)}_{\pm 1} \end{cases} \tag{3.41}$$

We finally introduce the events

$$\mathcal{B}^{(k)}_{\pm} := \big\{\xi \in \Omega_0 \,:\, \xi_{R^{(k)}_0} = 0\,,\; \xi_{R^{(k)}_{\pm 1}} = 0\big\}\,, \qquad \mathcal{B}^{(k)} := \mathcal{B}^{(k)}_{+} \cup \mathcal{B}^{(k)}_{-} \tag{3.42}$$

and note that $\xi \in \mathcal{B}^{(k)}_{+}$ iff $\xi^{+,-,(k)} \in \mathcal{B}^{(k)}_{-}$.

Lemma 3.3.3. *For each $d \geq 2$, $k = 1, 2$, and $\rho \in [0, 1)$ there exists a real $a = a(d, k, \rho) > 0$ such that for any $r \in \mathbb{R}^d$ we have*

$$\begin{aligned} r \cdot D^{(k)}_{\rm self}(\rho) r \geq (r \cdot e_1)^2 \, \frac{a}{2} \inf_{f \text{ local}} \int \mu_{\rho,0}\big(d\xi \big| \mathcal{B}^{(k)}\big) \Big\{ \big[f(\xi^{+,-,(k)}) - f(\xi)\big]^2 \\ + \sum_{y=\pm 1} \mathbb{I}_{\{\xi_{R^{(k)}_y} = 0\}}(\xi) \big[y + f(\vartheta_{-ye_1} \xi^{0,ye_1}) - f(\xi)\big]^2 \Big\} \end{aligned} \tag{3.43}$$

Proof. We discuss in some detail the case $k = 1$. We note that if $\xi \in \mathcal{B}^{(1)}$ and $y = \pm 1$ we have

$$c^{(1)}_{0,ye_1}(\xi)[1 - \xi_{ye_1}] \geq \mathbb{1}_{\{\xi_{R^{(1)}_y}=0\}}(\xi)$$

since $\mu_{\rho,0}(\mathcal{B}^{(1)}) \geq (1-\rho)^{11}$, by the same argument as in (3.21), from (3.37) we then get

$$\begin{aligned} r{\cdot}D^{(1)}_{\text{self}}(\rho)r \geq (r{\cdot}e_1)^2 \frac{1}{2} \inf_{f \text{ local}} \Big\{ \int \mu_{\rho,0}(d\xi) \sum_{\substack{\{x,y\}\subset\mathbb{Z}^d\setminus\{0\} \\ \mathrm{d}(x,y)=1}} c^{(1)}_{x,y}(\xi)[\nabla_{x,y} f(\xi)]^2 \\ + (1-\rho)^{11} \int \mu_{\rho,0}\big(d\xi \big| \mathcal{B}^{(1)}\big) \sum_{y=\pm 1} \mathbb{1}_{\{\xi_{R^{(1)}_y}=0\}}(\xi) \big[y + f(\vartheta_{-ye_1}\xi^{0,ye_1}) - f(\xi)\big]^2 \Big\} \end{aligned} \tag{3.44}$$

Let $T_1, \dots, T_{16}$ be the chain of exchanges depicted in Figure 3.2, T_i exchanges the occupation numbers in the bond b_i. Note that if $\xi \in \mathcal{B}^{(1)}_+$ the path $\zeta^+_0 := \xi$, $\zeta^+_1 := T_1\zeta^+_0$, …, $\zeta^+_{16} := T_{16}\zeta^+_{15} = \xi^{+,-,(1)}$ is such that $c^{(1)}_{b_i}(\zeta^+_{i-1}) = 1$, $i = 1, \dots, 16$. For $\xi \in \mathcal{B}^{(1)}_-$ we define analogously $\zeta^-_0 := \xi$, $\zeta^-_1 := T_{16}\zeta^-_0$, …, $\zeta^-_{16} := T_1\zeta^-_{15} = \xi^{+,-,(1)}$ which is such that $c^{(1)}_{b_{17-i}}(\zeta^-_{i-1}) = 1$, $i = 1, \dots, 16$.

We then have

$$\begin{aligned} &\big[f(\xi^{+,-,(1)}) - f(\xi)\big]^2 \mathbb{1}_{\mathcal{B}^{(1)}}(\xi) \\ &\quad \leq \mathbb{1}_{\mathcal{B}^{(1)}_+}(\xi)\big[f(\xi^{+,-,(1)}) - f(\xi)\big]^2 + \mathbb{1}_{\mathcal{B}^{(1)}_-}(\xi)\big[f(\xi^{+,-,(1)}) - f(\xi)\big]^2 \\ &\quad = \mathbb{1}_{\mathcal{B}^{(1)}_+}(\xi)\big[\sum_{i=1}^{16} f(\zeta^+_i) - f(\zeta^+_{i-1})\big]^2 + \mathbb{1}_{\mathcal{B}^{(1)}_-}(\xi)\big[\sum_{i=1}^{16} f(\zeta^-_i) - f(\zeta^-_{i-1})\big]^2 \\ &\quad \leq 16 \sum_{i=1}^{16} \Big\{ c^{(1)}_{b_i}(\zeta^+_{i-1})\big[\nabla_{b_i} f(\zeta^+_{i-1})\big]^2 + c^{(1)}_{b_{17-i}}(\zeta^-_{i-1})\big[\nabla_{b_{17-i}} f(\zeta^-_{i-1})\big]^2 \Big\} \end{aligned} \tag{3.45}$$

By integrating w.r.t. $\mu_{\rho,0}$ the above inequality and taking into account that in the chain of exchanges T_i, $i = 1, \dots, 16$ each bond is used at most twice we get

$$\begin{aligned} \mu_{\rho,0}\big(\mathcal{B}^{(1)}\big) \int \mu_{\rho,0}\big(d\xi \big| \mathcal{B}^{(1)}\big) \, \big[f(\xi^{+,-,(1)}) - f(\xi)\big]^2 \\ = \int \mu_{\rho,0}(d\xi) \, \big[f(\xi^{+,-,(1)}) - f(\xi)\big]^2 \mathbb{1}_{\mathcal{B}^{(1)}}(\xi) \\ \leq 64 \int \mu_{\rho,0}(d\xi) \sum_{\substack{\{x,y\}\subset\mathbb{Z}^d\setminus\{0\} \\ \mathrm{d}(x,y)=1}} c^{(1)}_{x,y}(\xi)[\nabla_{x,y} f(\xi)]^2 \end{aligned} \tag{3.46}$$

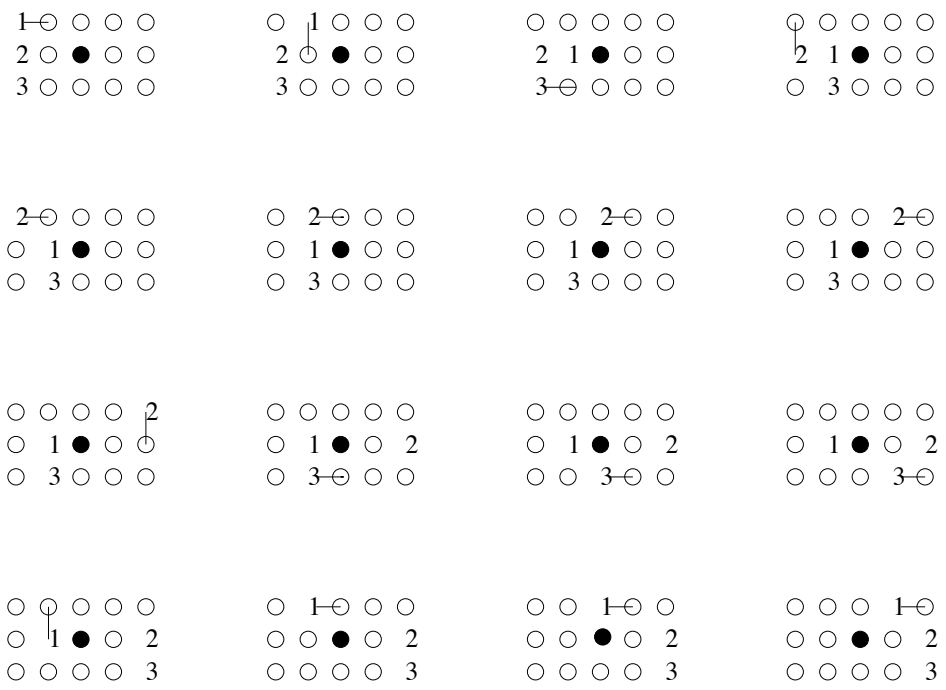

Figure 3.2: *Chain of exchanges* $T_1, \ldots, T_{16}$ *for* $k = 1$. The picture represents sites in the plane e_1, e_2, $\bullet$ denotes site 0 and — in the i–th figure denotes the bond exchanged by T_i. If the sites denoted by $\circ$ are empty then the starting configuration is in $\mathcal{B}_+^{(1)}$. In such a case 1,2, and 3 denote the occupation numbers in $R_-^{(1)}$ which, step by step, are moved to $R_+^{(1)}$ by using only allowed exchanges.

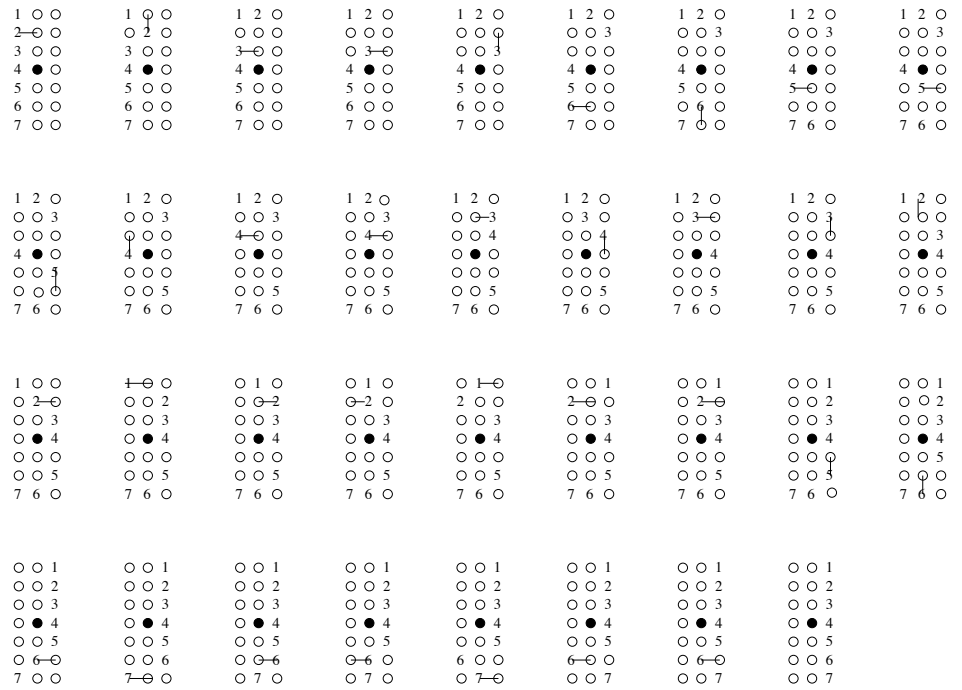

Figure 3.3: *Chain of exchanges* $T_1, \dots, T_{35}$ *for* $k = 2$. • denotes site 0 and — in the i–th figure denotes the bond exchanged by T_i.

which inserted in (3.44) concludes the proof with $a(d, 1, \rho) = 2^{-6}\,(1-\rho)^{11}$.

The case $k = 2$ is proven by the same arguments; in this case, for $d = 2$, the required chain of exchanges $T_1, \dots, T_{35}$ is depicted in Figure f:path3. □

Proof of Theorem 3.3.2 (sketch). Thanks to Lemma 3.3.3, it is enough to prove that the right hand side of (3.43) is strictly positive for $r \cdot e_1 \neq 0$. By the variational formula (3.37), it can be interpreted as the self diffusion coefficient of a one dimensional auxiliary process which we next describe in the fixed frame of reference.

The configuration space is $\big\{(y, \eta) \in \mathbb{Z} \times \Omega : \vartheta_{-ye_1}\eta \in \mathcal{B}^{(k)}\big\}$. Let $y(t) \in \mathbb{Z}$ be the position of the tagged particle and $\eta(t)$ be the particles configuration. At time $t = 0$ the tagged particle is at the origin, $y(0) = 0$, and $\eta(0) \in \mathcal{B}^{(k)}$ is distributed according to $\mu_{\rho,0}\big(\cdot \big| \mathcal{B}^{(k)}\big)$. Then the tagged particle jumps to the right, resp. left, with rate one if $\vartheta_{-y(t)e_1}\eta(t) \in \mathcal{B}^{(k)}_+$, resp. if $\vartheta_{-y(t)e_1}\eta(t) \in \mathcal{B}^{(k)}_-$. Moreover, with rate one, $\eta(t)$ is exchanged to $\vartheta_{y(t)e_1}\big[(\vartheta_{-y(t)e_1}\eta(t))^{+,-,(k)}\big]$, namely the occupation numbers in $\vartheta_{y(t)e_1}R^{(k)}_-$ are exchanged with the ones in $\vartheta_{y(t)e_1}R^{(k)}_+$.

The proof of the Theorem can now be completed as in the case of non–

degenerate rates, see [17][II.6.3], by showing that there exists a real $c > 0$ such that for any $t > 0$ and $\eta \in \mathcal{B}^{(k)}$ we have $\mathbb{E}_{(0,\eta)}\big(y(t)^2\big) \geq ct$. Here $\mathbb{E}_{(0,\eta)}$ denotes the distribution of the auxiliary process with initial condition $(0, \eta)$. □

3.4 A conjecture for hydrodynamic limit

Another relevant issue is the evolution of macroscopic density profiles. As already mentioned in section 2.5.4, for models with degenerate rates establishing the hydrodynamical limit [17] is not a trivial task. For these models a natural candidate for the hydrodynamic limit is a parabolic equation of porous media type degenerating when the density approaches one. In particular, though neither the first nor the second model are of gradient type, the former can be turned into a gradient models by slightly changing the rates, i.e. defining new rates $\tilde{c}^{(1)}_{x,y}(\eta)$ as $\tilde{c}^{(1)}_{x,x+e_i}(\eta) := 1 - 1/2(\eta_{x-e_i} + \eta_{x+2e_i})$. Note that this is a slight modification, in the sense that it does not modifies the degeneracy of the rates (it modifies the value of the positive rates but when $c_{x,y}(\eta)$ is zero also $\tilde{c}_{x,y}(\eta)$ is zero and viceversa). It is immediate to check that with this choice of the rates the model is gradient and, by the arguments in 2.5.4, *if* the initial state is a local equilibrium state and *if* local equilibrium is conserved by temporal evolution, the following parabolic differential equation holds for density evolution

$$\frac{d}{d\tau}\rho(q,\tau) = \nabla((1-\rho)\nabla\rho) \tag{3.47}$$

which is a porous media equation with diffusion coefficient vanishing at unit density. Equations of this form have been widely studied in different contexts. Note that this equation cannot holds for any choice of the initial condition admitting a density profile. Consider for instance the models described above in $d = 1$ with periodic boundary conditions and take an initial configuration given by a sequence of two occupied sites and one empty on $x \in [0, N/2]$ and three occupied and one empty in the rest of the lattice. This configuration has a density profile is invariant for the microscopic dynamic, however the associated density profile

$$\rho(q,0) = \begin{cases} \frac{2}{3} & \text{for } \ q \in [0,1/2] \\ \\ \frac{3}{4} & \text{for } \ q \in [1/2,1] \end{cases} \tag{3.48}$$

evolves diffusively reaching for infinite time $\rho(q,\infty) = 17/12$ according to (3.47). Indeed, the initial density profile is bounded away from 1 and therefore is not affected by the degeneracy. Therefore, at variance with exclusion

processes with non–degenerate rates, the hydrodynamic behavior cannot hold for any initial state. On the other hand such phenomenon is somehow exceptional and we expect a hydrodynamic behavior (3.47) for a suitable large class of initial conditions.

Our conjecture is that (3.47) holds provided the initial state has a density profile and moreover has a density of *double holes*, i.e. couples of vacancies at a distance less or equal to two. Indeed, (3.47) holds if one can substitute a mean of a function of local occupation variables with the same function evaluated on the local value of density (see section 2.5.4)[1]. In other words (3.47) holds if the measure relaxes in any macroscopically small volume λ into a superposition of canonical measures $\nu_{\lambda,n}$. Therefore, we should rule out the possibility that the system is locally blocked in a different stationary measure. Recalling remark 4 in section 3.2.1, this is guaranteed if there is at least a double hole in the volume λ. Therefore, our conjecture is quite reasonable and to turn it into a proof one should prove that the initial local density of double holes is conserved at any subsequent time. Note that double holes are created and destroyed by the dynamics, therefore even if they can move freely they do not perform a random walk and proving above statement is not trivial.

A different connection of these models with the (3.47) and with more degenerate porous media equations is derived in appendix A.

3.5 Conclusions

The models introduced in this chapter do not display at any density $\rho < 1$ a dynamical ergodic/non–ergodic transition. The key ingredient behind all the results is that for these models there exists a finite cluster of vacancies that can freely move into an otherwise totally filled lattice. Therefore the mechanism underlying diffusion is the same as for SSEP, with the role of vacancies substituted by finite clusters of vacancies. Indeed, these models behave like a *renormalized* SSEP model with a different density dependence in typical times and diffusion constant. Though dynamics for these models becomes slower at higher density, the lack both of a dynamical transition[2] and of a crossover among different diffusion or relaxation mechanisms renders them not suitable to study glass transition. In this respect, the study of

[1] Technically, the point that is missing with respect to the non degenerate case, is the proof of the *replacement lemma* [22]

[2] We did not analyze the behavior of density density fluctuation, but we believe there are no further difficulties to generalize SSEP results to these models. In other words no stretched exponential relaxation should appear.

these models can be regarded as a preliminary work in order to develop the necessary tools for the analysis of more difficult kinetically constrained modeel, e.g. the ones considered in next chapters. On the other hand, the models we have introduced in this chapter can be interesting by themselves in the context of stochastic interacting particle systems and in connection with the study of porous media equation (see previous section and appendix A).

Chapter 4

Kob Andersen model on hypercubic lattices: ergodicity

After defining Kob Andersen (KA) model on d-dimensional hypercubic lattices $\Lambda \in \mathbb{Z}^d$ and recalling previous results, we prove that an ergodic / non-ergodic transition *cannot take place* at any finite density $\rho \in [0,1]$. In other words, in the thermodynamic limit $\Lambda \to \mathbb{Z}^d$ a single ergodic component covers the whole configuration space. On the other hand, on finite lattices of linear size L, the system is not ergodic at any density. However, we estimate a density dependent characteristic size $\Xi(\rho)$ which separates the regime $(L \gg \Xi(\rho))$ in which the maximal ergodic component has probability almost one from the regime $(L < \Xi(\rho))$ in which finite size effects are important and there is not a dominant ergodic component.

4.1 Definition of the model

Let $\Lambda \in \mathbb{Z}^d$ be an hypercubic $d-$dimensional lattice and $m = 0, \dots, 2d-1$, KA model is a kinetically constrained lattice model with jump rates

$$c_{x,y}(\eta) := \begin{cases} 1 & \text{if } \sum_{\substack{z\in\Lambda, z\neq y \\ \mathrm{d}(x,z)=1}} \eta_z \leq m \text{ and } \sum_{\substack{z\in\Lambda, z\neq x \\ \mathrm{d}(y,z)=1}} \eta_z \leq m \\ 0 & \text{otherwise} \end{cases} \tag{4.1}$$

namely a particle can move only if both before and after the move it has no more than m neighboring particles. Note that for $m = 2d-1$ the trivial symmetric simple exclusion case is recovered. For future purposes it is useful to reformulate the rule in term of motion of vacancies. Indeed, as can be easily verified, the above definition corresponds to *vacancies* moving only if the initial and final sites have at least $s = z - m - 1$ neighboring vacancies,

with $z = 2d$ the coordination number of the lattice. Therefore the model is completely defined by the choice of the couple d, m or equivalently d, s.

Note that the rates satisfy detailed balance with respect to $\nu_{\Lambda,N}$, i.e. uniform measure on the hyperplanes with fixed number of particles. However, as for the models introduced in previous chapter, there exist configurations that are blocked under the dynamics, $\nu_{\Lambda,N}$ is not the unique invariant measure on the hyperplane and the process is never ergodic. For example, in the case $d = 2$ $s = 1$, a configuration which has a double row of sites completely filled belongs to a different ergodic component with respect to any other configuration which does not contain such structure. Indeed, one can directly check that the particles belonging to the double row can never move.

4.2 Previous results

KA model was introduced in [1] to test the conjecture that *cage effect* (see section 2.5) can induce in glass forming liquids a dynamical arrest responsible for glass transition. Indeed, the jump rates (4.1), are devised in order to mimic the geometric constraints imposed by sourrounding particles on the possible rearrangements of a given molecule. In [1] numerical simulations were performed for the three–dimensional case with $s = 2$. The self-diffusion coefficient of a tagged-particle was analyzed and the results were fitted with good agreement with a power law vanishing at a finite density, $D_s \propto (\rho - \bar{\rho})^{\alpha}$ with $\alpha \simeq 3.1$ and $\bar{\rho} \simeq 0.881$. The time relaxation of density-density correlations was well fitted with an inverse power law diverging at the same density. Moreover the form of such relaxation, which is exponential at low density, becomes stretched exponential when approaching such density from below. Since both results are strongly suggestive of a dynamical glass transition at $\rho = \bar{\rho}$, later works were performed to investigate whether other typical features of "glassy dynamics" are present (indeed in all the results cited below the same case $d = 3$, $s = 2$ was considered).

In [47] numerical simulations were performed showing that the dynamics of this model has an heterogeneous character at high density. More precisely, the four point correlation function plotted as a function of time displays a maximum that grows as an inverse power of $\rho - 0.881$. The position of the maximum also grows for large times as a power of the same quantity thus indicating that dynamics remain correlated for longer and longer times at high density. In [48] the same model with the addition of boundary sources of particle was studied. In this case, by quenching the density of the sources above $\bar{\rho}$, a non–equilibrium regime was reached and aging effects similar to those arising in glasses were detected. In [49] the relationship between

configurational entropy of blocked configurations and effective temperature was investigated to test Edward's hypothesis (see section 2.3). The numerical results are compatible with this hypothesis.

From above described results it emerges that the dynamics of three–dimensional KA model with $s = 2$ is sluggish and heterogeneous at high density and displays a whole range of behavior which is very reminiscent of glassy dynamics. At first sight this could seem strange since KA model is very similar to the models we have introduced in previous chapter and for which we established a rescaled SSEP behaviour (see section 3.5). Furthermore the degeneracy of KA and previous models is not comparable, indeed there are moves that are allowed for KA and not for the other models and viceversa. However, there is an important difference we emphasize from now and whose relevance will become clearer in the rest of the work. While in the models of previous chapter it was possible to identify a proper finite cluster of holes that can freely move into an otherwise totally filled lattice, this is not true for three–dimensional KA model with $s = 2$. Therefore, all the previous results cannot be readily extended to this model. Note that this is not only a technical difficulty, indeed we will find that KA model displays a different relaxation dynamics due to the fact that diffusion involves the cooperative motion of large clusters of vacancies.

4.3 Open issues and outline of results

Despite the above mentioned numerical investigations, many issues remain open in understanding the behaviour of KA models. In particular it is not clear if the slowing down of dynamics is related to the existence of a dynamical ergodic/non–ergodic transition occurring at a finite density or to a different form of dynamical arrest (e.g. a vanishing of the diffusion coefficient or a divergence of the relaxation time for the density density correlation function) or else a simple crossover in typical time scales occurs. More generally, one would like to understand the nature of the cooperative mechanism which induces the slowing down of dynamics.

The first issue we have addressed is whether an ergodic/non–ergodic transition for the $d = 3$ $s = 2$ model or for other choices of the parameters. The result is that, for any spatial dimension d and any choice of the parameter s, an ergodic/non–ergodic transition cannot take place at any finite density $\rho \in [0, 1]$. In other words, the sluggish behavior detected by previous simulations in the original cubic case with $s = 2$ cannot be the mark of an ergodic/non–ergodic transition.

On the other hand, on finite size systems the process is never ergodic. More-

over, at any fixed size L the probability $\mu_\rho(\mathcal{E})$ of the maximal ergodic component goes to zero for $\rho \to 1$. Therefore, since $\lim_{L\to\infty}\lim_{\rho\to 1}\mu_\rho(\mathcal{E}) = 0$ and $\lim_{\rho\to 1}\lim_{L\to\infty}\mu_\rho(\mathcal{E}) = 1$, by sending simultaneously $L \to \infty$ and $\rho \to 1$ the limit will depend on the relative speed convergence. By analyzing the probability of the maximal ergodic component we identify a threshold which separates the two regimes. The form of the threshold depends on the spatial dimension d and on the choice of the parameter s. For the original cubic case with $s = 2$ it is $L \sim \exp\exp\left(c/(1-\rho)\right) \equiv \Xi(\rho)$. Therefore, by fixing the density ρ and varying the size of the system, $\Xi(\rho)$ is the size at which a crossover occurs which separates two different regimes: for $L \gg \Xi(\rho)$ the maximal ergodic component has probability almost one, while for $L \ll \Xi(\rho)$ no single component dominates. In other words in the former regime the system is *almost* in the thermodynamic limit, while in the latter finite size effects become important. Therefore, the knowledge of the crossover length is a key ingredient when studying numerical results since it gives the order of magnitude of the typical size one should consider (once the density has been fixed) in order to avoid finite size effects. On the other hand, by considering a system of fixed size L and varying its density, ergodicity *almost* holds in the regime $\rho < \rho_c(L) = 1 - (c/log\log L)$, namely for smaller sizes finite size effects become relevant at lower values of density.

The fact that ergodicity holds does not rule out the possibility of different kinds of dynamical arrests (see chapter 2). In particular, a diffusive/sub–diffusive transition could occur at a finite density, thus explaining the divergence of typical times and the vanishing of self diffusion coefficient detected by the above mentioned numerical results [1]. In order to investigate this possibility we have studied the large time behaviour of the tagged particle displacement. The result of this analysis is that the self diffusion coefficient D_S is strictly positive at any density $\rho < 1$, i.e. a diffusive/sub–diffusive cannot take place. Moreover, this analysis unveils the presence of the collective processes which are responsible for diffusion at high density. The characteristic time scale of this slow cooperative dynamics can be calculated, with the result that it increases for $\rho \to 1$ faster than any inverse power of $1 - \rho$. On the other hand, by percolation–type arguments, we predict that a crossover to a different diffusion mechanism occurs at a finite density. This crossover should give rise to a substantial range of critical dependence of the diffusion coefficient in the vicinity of an apparent transition at a finite density. This could explain the vanishing of the self diffusion coefficient and divergence of relaxation times claimed by the above mentioned numerical results (see previous section).

Another open issue is understanding the root of the dynamical heterogeneities detected by numerical simulations. From the above described sce-

nario, we expect that in the large time limit dynamics is dominated by the slow relaxation of rare dense regions and we give a possible explanation of the heterogeneous relaxation.

Finally, it would be interesting to establish the connection, if any, of KA model with the scenarios proposed by other theoretical approaches to glass transition. As already mentioned, mode coupling theory [11] and results for fully connected spin glasses [12] predict the existence of an ergodicity breaking transition at a finite temperature T_d. Since these approaches are both mean field, to establish a possible connection we have studied KA model on a Bethe lattice, which is usually a good realization of mean field approximation and whose tree like structure enables analytic calculations. The scenario which emerges for this mean field approximation (namely in infinite dimensions) is completely different from the one on hypercubic lattices (namely in finite dimensions). Indeed, at a finite critical density $\rho_c < 1$ an ergodic/non–ergodic transition takes place which corresponds to the transition from a diffusive to a partially frozen phase. However, even if this transition is destroyed in finite dimension by cooperative rearrangements, a ghost of such transition survives in the dynamics. This corresponds to above mentioned cross–over in typical diffusion times. Furthermore, by analyzing the mean field transition we find that it has aspects of both first order and second order transition and is analogous to the one found in the mode coupling approximation and for p-spin models. The knowledge of both mean field and finite dimensional results for KA could be a useful ground to develop new ideas on the nature of the so called *activated processes* that should smooth the mean field mode coupling or p–spin transition in real systems.

In the rest of this chapter we will focus on the ergodicity proof for the finite dimensional case. The analysis of KA on the Bethe lattice will be developed in chapter 5, while diffusion coefficient, typical time–scales and dynamical heterogeneities will be discussed in chapter 6.

4.4 Ergodicity for d=2, s=1

In this section we analyze the model on a two–dimensional hypercubic lattice, namely a square lattice, with parameter $s = 1$. We prove that, for any density $\rho \in [0, 1]$, an ergodic/ non–ergodic transition *cannot take place* (see section 2.5.1 for a precise definition of such transition). This is also true for a generic choice of d and s, as we will prove in next sections. Indeed the only two possibilities are the following. The process in the thermodynamic limit is ergodic at any finite density, i.e. $\rho_c = 1$, else it is never ergodic, i.e. $\rho_c = 0$.

Let us outline the strategy of the proof. First, we consider the model on

a finite square lattice Λ^2 and identify a component of the configuration space $\Omega = \{0,1\}^{\Lambda^2}$ which is irreducible, i.e. any two configuration belonging to such component can be connected one to the other by a sequence of elementary moves with positive rate. Then we prove that in the thermodynamic limit the probability of this component, w.r.t. Bernoulli product measure $\mu_{\Lambda^2,\rho}$ at any density, goes to one. By applying an argument similar to one in section 3.3.2, it is then easy to prove that this implies ergodicity for the infinite volume system $\Lambda^2 = \mathbb{Z}^2$. In this and next three sections we outline the first and second step of the proof for all the possible choices of d and s, leaving to section 4.8 the last step, which is independent from the choice of the parameters.

Consider KA model on a square lattice $\Lambda^2 \in \mathbb{Z}^2$ with linear size L and periodic boundary conditions. Let *framed* configurations be those with all the boundary sites empty (see figure 4.1) and *frameable* those that by an allowed sequence of elementary moves can reach a *framed* configuration. Any two framed configurations with the same number of particles can be connected one to the other by a sequence of moves allowed by the dynamical rules. This can be checked as follows. Consider a couple of neighboring sites $\{i,j\}$. To prove above claim it is enough to show that for any choice of the framed configuration, there exists a sequence of moves which allows the exchange of occupation variables in sites i and j. Let $j = i + e_1$. Starting from bottom right corner and top right corner it is possible to raise the bottom and top rows of holes respectively, as shown in figure 4.2. This procedure can be iterated till the row which contains sites i and j is "sandwiched" between two rows of holes (see figure 4.3). At this point one can perform the initially chosen jump, since the number of neighboring vacancies for i and j is greater or equal to two, therefore the jump is allowed. Then the initial configuration in the rest of the lattice can be restored by moving backward the two rows of holes. Therefore all the framed configurations with the same number of particles belong to the same irreducible component. However, this is not the set of configurations we are looking for, since the probability of such component goes to zero in the thermodynamic limit. Indeed the requirement of having the external frame empty is very restrictive and the probability to fulfill it, w.r.t. Bernoulli measure $\mu_{\Lambda^2,\rho}$, is $(1-\rho)^{4L}$, which goes to zero for $L \to \infty$. However, there is a larger irreducible component which contains the previous one, namely the set $\mathcal{F}$ of above defined frameable configurations. Indeed, any two frameable configurations can be connected by a path which goes through the two correspondent framed configurations. Therefore, next step is proving that the probability of frameable configurations with density ρ, $\mu_{\Lambda^2,\rho}(\mathcal{F})$, goes to one in the limit $L \to \infty$.

Consider a four by four configuration which has at the center a two by

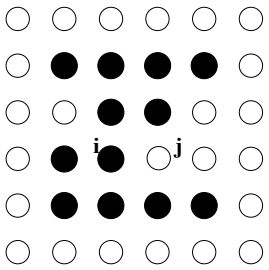

Figure 4.1: A generic 6 by 6 framed configuration. Filled dots stand for occupied sites; empty dots for vacant sites. We indicate with i and j a couple of neighboring sites where the jump from i to j cannot be directly performed. In figure 4.2 and 4.3 we draw a sequence which allow to perform the move

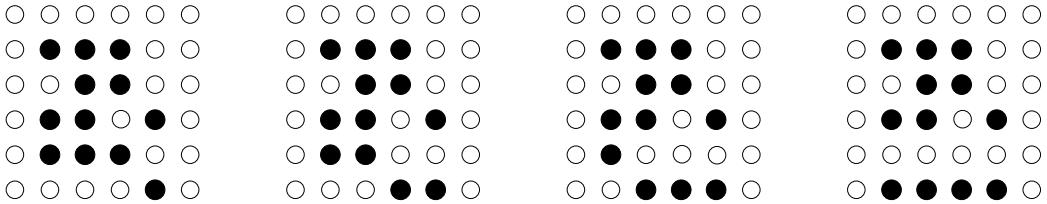

Figure 4.2: Sequence of allowed elementary moves connecting configuration in figure 4.1 to a configuration with the bottom row of holes raised of one unit.

two square of holes and in the next shell at least two holes adjacent to each side of the inner square. It is easy to check (see figure 4.4) that such four by four configuration is frameable. This procedure can be iterated to grow an L by L frameable configuration starting from a two by two nucleus of vacancies and requiring at least two vacancies in each side of any subsequent shell. Therefore $\mu_{\Lambda^2,\rho}(\mathcal{F})$ is bounded from below by the probability, $\mu_{\Lambda^2,\rho}(\mathcal{F}^0)$, of frameable configurations constructed with the above *growing procedure* from a two by two nucleus of vacancies centered in the origin (see figure 4.5):

$$\mu_{\Lambda^2,\rho}(\mathcal{F}) \geq \mu_{\Lambda^2,\rho}(\mathcal{F}^0) = (1-\rho)^4 \prod_{l=1}^{(L-2)/2} (1-\rho^{2l}-2l\rho^{2l-1}(1-\rho))^4 \qquad (4.2)$$

Note that the large L behaviour of $\log\left(\mu_{\Lambda^2,\rho}(\mathcal{F}^0)\right)$ is determined by $4\log(1-\rho)+4\sum_{l=1}\log(1-\rho^{2l}-2l\rho^{2l-1}(1-\rho)) \simeq 4\log(1-\rho)-4\sum_{l=1}(\rho^{2l}+2l\rho^{2l-1}(1-\rho))$, which is a converging series for any $\rho<1$. Therefore, $\mu_{\Lambda^2,\rho}(\mathcal{F}^0)$ converges to a well defined limit when $L\to\infty$ at fixed density. Due to the divergence of the series in $\rho=1$, some additional care is required in order to analyze the

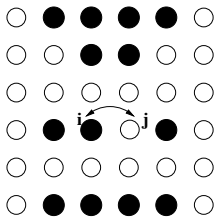

Figure 4.3: Configuration which can be reached from the one in figure 4.1 by the sequence in figure 4.2 and analogous moves lowering top row of holes by two units. Sites i and j are now "sandwiched" between two rows of holes and the jump can be performed. Then the initial configuration of figure 4.1 can be restored on the other sites.

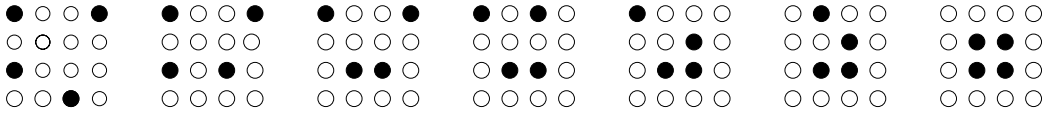

Figure 4.4: Growing procedure: form a 2 by 2 to a 4 by 4 framed configuration

behavior when $\rho \to 1$ and $L \to \infty$. Let $a(x) \equiv \log(1-\rho^{2x}-2x\rho^{2x-1}(1-\rho))$. Since $a(x)$ is increasing in x, the following inequality holds:

$$\begin{aligned} &4a(1)+4\int_1^{\frac{L-2}{2}} dl \log(1-\rho^{2l}-2l\rho^{2l-1}(1-\rho)) \leq \\ &\log \mu_{\Lambda^2,\rho}(\mathcal{F}^0) - 4\log(1-\rho) \leq \\ &4\int_2^{\frac{L-2}{2}+1} dl \log(1-\rho^{2l}-2l\rho^{2l-1}(1-\rho)) \end{aligned} \tag{4.3}$$

where the last term can be rewritten by using the changes of variables $y=\rho^{2l}$ and developing for $\rho \simeq 1$ as

$$\lim_{L\to\infty} \int_2^{\frac{L}{2}} dl \log(1-\rho^{2l}-2l\rho^{2l-1}(1-\rho)) \simeq \frac{1}{2(1-\rho)} \int_0^1 dy \frac{\log(1-y+y\log y)}{y} \tag{4.4}$$

Therefore, combining (4.3) and (4.4) and using $\lim_{\rho\to 1}(1-\rho)\log(1-\rho)=0$ yields

$$\lim_{\rho\to 1}\lim_{L\to\infty}(1-\rho)\log\mu_{\Lambda^2,\rho}(\mathcal{F}^0) = 2\int_0^1 dy \frac{\log(1-y+y\log y)}{y} \tag{4.5}$$

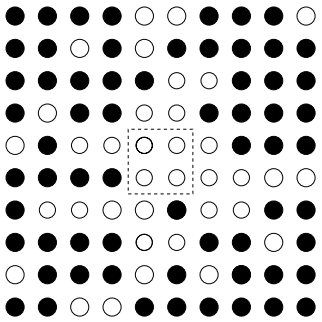

Figure 4.5: An 8 by 8 frameable configuration obtained with the growing procedure. The dashed square indicates the position of the initial two by two seed. Note that, due to the requirement of having two vacancies in each side of any subsequent shell, the density of the configuration should be very small near the seed where the shell is small, but can be high far enough.

i.e., when $\rho \to 1$ and $L \to \infty$,

$$\mu_{\Lambda^2,\rho}(\mathcal{F}^0) \simeq \exp - \left(\frac{2C(2,1)}{1-\rho} \right) \tag{4.6}$$

with $C(2,1) = -\int_0^1 dy \frac{\log(1-y+y\log y)}{y} \simeq 4.48$ (2 and 1 stands for the values of parameters d and s, respectively).
Moreover it is possible to determine a characteristic length $\xi(\rho,2,1)$ such that $\mu_{\Lambda^2,\rho}(\mathcal{F}^0)$ depends weakly on L for $L \gg \xi(\rho)$. Indeed, since

$$\begin{aligned} \log \mu_{\infty,\rho}(\mathcal{F}^0) - \log \mu_{\Lambda^2,\rho}(\mathcal{F}^0) &\simeq \frac{2}{1-\rho} \int_1^{\rho^L} dy \frac{\log(1-y+y\log y)}{y} \\ &\simeq \frac{2}{1-\rho} \int_1^{\rho^L} dy(-1+\log y) \\ &= \frac{2}{1-\rho} \left(\rho^L \log[\rho^L] - 2\rho^L \right) \\ &\simeq \frac{-4\rho^L}{1-\rho} \end{aligned} \tag{4.7}$$

$\mu_{\Lambda^2,\rho}(\mathcal{F}^0) \simeq \mu_{\infty,\rho}(\mathcal{F}^0)$ for $L \gg -\log(1-\rho)/(1-\rho) \equiv \xi(\rho,2,1)$. Therefore ξ is the minimal linear size of a square such that, if the configuration is frameable inside this region, with probability almost one the requirements on each subsequent shell needed to grow it frameable till infinite size are satisfied. In other words, ξ is such that with probability almost one there are always at least two vacancies on any line of length $l \geq \xi$.

By considering all the possible positions for the initial nucleus of the growing procedure[1], it follows that the probability that a square of size L is frameable, $\mu_{\Lambda^2,\rho}(\mathcal{F})$, goes to one for $L \to \infty$. The proof of this statement will be illustrated in section 4.8, let us sketch since now the key ideas. From above definition of ξ, the requirements needed to further expand a frameable square of size $L \gg \xi$ are satisfied almost with probability one. Therefore, events that on different squares of size ξ one can grow frameable configurations, are almost independent. By considering the possible $O(L^2/\xi^2)$ squares of size ξ inside Λ, it is immediate to conclude that $\mu_{\infty,\rho}(\mathcal{F})$ is almost one for $L \gg \xi\sqrt{\mu_{\infty,\rho}(\mathcal{F}^0)} \equiv \Xi_u(\rho, 2, 1)$ and goes to one for $L \to \infty$. Since the events that Λ is frameable starting from different nuclei at distance ξ are not independent, some additional work is required to turn this argument into a proof (see section 4.8).

Note that the whole proof is simply based on two ingredients: fact that configurations with a special frame of holes belong to the same irreducible component; this frame can be created by starting from a finite nucleus of vacancies and expanding to larger sizes by satisfying a requirement that becomes less and less severe at each step. Therefore, the strategy is not very specific of the above choice of the rules and can be readily extended to different models. In particular, in next sections we will show that it can be adapted to all the different KA models. In the following we will refer to *core of a frameable region* as the region of linear size ξ centered around the initial nucleus of the growing procedure. Note that, due to the constraint of having at least two vacancies on rows of length $l \leq \xi$, such regions have a density which is lower than the mean density of the whole configuration and are therefore very rare. Nevertheless, the density of cores $1/\mu_{\Lambda^2,\rho}(\mathcal{F}^0) \sim 1/\Xi_u^2$ is always positive at any ρ. From above proof, it emerges that this rare regions with vacancies configured in special ways are at the root of the mechanism which restores ergodicity in the thermodynamic limit. Moreover, as will be elucidated in chapter 6, their cooperative motion is the only effective mechanism for diffusion in the high density regime.

As already noticed in section 4.1, KA model in not ergodic at any density on a finite lattice. However, as a by–product of the ergodicity proof, we have obtained that if the linear size L of the lattice is such that $L \gg \Xi_u(\rho, 2, 1)$ the maximal ergodic component has probability almost one (in section 4.23 we will prove that the convergence to one for $L \geq \Xi_u(\rho)$ is at least exponential). In other words in this regime, though the model is not ergodic,

[1]Recall that we are considering the model on a finite lattice with periodic boundary conditions. Therefore any point can be considered as the starting point for the growing construction.

a single ergodic component dominates. By explicitating above definition of $\Xi_u(\rho, 2, 1)$, its density dependence can be rewritten as

$$\Xi_u(\rho, 2, 1) \simeq \exp\left(\frac{C(2,1)}{1-\rho}\right) \tag{4.8}$$

On the contrary, it is immediate to check that for $L \ll \Xi_u$ the probability that a configuration is frameable is almost zero. However, from above arguments we cannot exclude the existence of a different ergodic component with probability almost one (which would correspond to a different ergodicity restoring mechanisms which is not taken into account by previous procedure). We will come back to this issue in section 4.9, where we will outline a different argument establishing a characteristic length Ξ_l, which has the same density dependence as Ξ_u, such that for $L \leq \Xi_l$ we are guaranteed that the configuration space is broken into exponentially many ergodic components and none of them dominates.

4.5 Ergodicity for d=3, s=2

In this section we prove that in the case $d = 3$ $s = 2$, namely for the choice originally made by Kob and Andersen, ergodicity holds in the thermodynamic limit at any density $\rho < 1$. This case is also included in the proof we will give in section 4.7, which holds for any d and s. However the analysis of this three-dimensional case can be useful since it introduces in a relatively simple case the technique we use to extend ergodicity results from smaller to larger values of d and s.

Consider a cubic lattice $\Lambda^3 \in \mathbb{Z}^3$ with linear size L. Let *framed* configurations be those with all the boundary sites empty and *frameable* those that by an allowed sequence of elementary moves can reach a *framed* configuration. Again, frameable configurations with the same number of particles belong to the same irreducible component and the probability $\mu_{\Lambda^3,\rho}(\mathcal{F})$ that a configuration belongs to this component goes to one in the thermodynamic limit. This can be checked by noticing that in a framed configuration the bottom and top planes of vacancies can be raised and lowered whatever the internal configuration. Therefore one can again "sandwhich" any couple of neighboring sites among two planes of vacancies and exchange their occupation numbers. In other words, with a procedure analogous to the one previously devised for the case $d = 2$ $s = 1$, one can directly check that frameable configurations belong to the same irreducible component (the role of empty rows in previous proof is now played by empty planes). Moreover, also in this case one can define a *growing procedure* which enables to construct a frameable

configuration of linear size L starting by an initial nucleus of vacancies and satisfying at any subsequent shell a requirement which is less and less restrictive for larger sizes. Consider a cube of linear size four, which has at the center an empty cube of linear size two. If adjacent to each side of the internal cube there is a four by four square which is frameable according to the definition for the $d = 2$ $s = 1$ case, the whole cube of size four is frameable. This procedure can be iterated to grow an L by L by L frameable configuration starting from an empty cube of size two and requiring that in each subsequent shell all the squares are frameable Therefore, letting $\mu_{\Lambda^3,\rho}(\mathcal{F}^0)$ be the probability of frameable configurations grown from a nucleus in the origin, the following lower bound for $\mu_{\Lambda^3,\rho}(\mathcal{F})$ follows

$$\mu_{\Lambda^3,\rho}(\mathcal{F}) \geq \mu_{\Lambda^3,\rho}(\mathcal{F}^0) = (1-\rho)^{L'^3} \prod_{l=0}^{(L-L')/2} \left(\mu_{\Lambda_l^2,\rho}(\mathcal{F})\right)^6 \qquad \forall L' \tag{4.9}$$

where Λ_l^2 is a square lattice of linear size $L' + 2l$. From results in previous section we know that $\mu_{\Lambda_l^2,\rho}(\mathcal{F})$ is almost one for $L' \gg \Xi_u(\rho, 2, 1)$ and goes to one for $|\Lambda_l| \to \infty$. If the convergence to one were sufficiently fast, from (4.9) we would conclude that for $L \gg \Xi_u(\rho, 2, 1)$ the probability $\mu_{\Lambda^3,\rho}(\mathcal{F}^0)$ does not depend on L and

$$\mu_{\Lambda^3,\rho}(\mathcal{F}^0) \simeq (1-\rho)^{\Xi_u(\rho,2,1)^3} \tag{4.10}$$

Let $\xi(\rho, 3, 2) \equiv \Xi_u(\rho, 2, 1)$, we can again divide the cubic lattice Λ^3 in $(L/\xi(\rho, 3, 2))^3$ smaller cubes of linear size $\xi(\rho, 3, 2)$. Since the probabilities of growing frameable configurations starting with nuclei inside different cubes are almost independent, we conclude again that $\mu_{\Lambda,\rho}(\mathcal{F})$ is almost one for $L \gg \xi(\rho, 3, 2)(1-\rho)^{\Xi_u(\rho,2,1)^3} \equiv \Xi_u(\rho, 3, 2)$ and goes to one for $L \to \infty$. Therefore, in the thermodynamic limit the irreducible component of frameable configurations has unit probability. We postpone to section 4.23 the prove of the fast convergence to one of the probability of the frameable set for $d = 2$ $s = 1$ (the proof will be given for the case $s = 1$ and any d) and to section 4.7 the proof of the above argument on independent frameable configurations. Note that we have found as for the two–dimensional case a typical size ξ such that if a configuration is frameable inside a cube of linear size ξ, with probability almost one it can be grown frameable to infinite size. Again, we let the *core* of a frameable region be the cube of size ξ around the initial empty nucleus of the growing procedure.

As for the square lattice case, though on finite lattices the process is not ergodic, we find that for $L \gg \Xi_u(\rho, 3, 2)$ the ergodic component of frameable configurations has probability almost one (in section 4.7 we will prove that

for $L \geq \Xi_u(\rho, 3, 2)$ the convergence to one is at least exponential). Note that above expression for $\Xi_u(\rho, 3, 2)$ can be rewritten, up to log corrections as

$$\Xi_u(\rho, 3, 2) = \exp\ \Xi_u(\rho, 2, 1) = \exp\exp\left(\frac{C(2,1)}{1-\rho}\right) \tag{4.11}$$

The fact that the three dimensional length is the exponential of the two–dimensional one is not a pure coincidence. Indeed, it is a consequence of the fact that on each step of the three–dimensional growing procedure we require a two–dimensional frameable configuration. Again, the fact that for $L \ll \Xi_u(\rho, 3, 2)$ the probability of a frameable configuration is almost zero is not sufficient to conclude that in this regime all ergodic components have small probability and none dominates. However, the argument outlined in section 4.7 will allow us to conclude that this is ture and there exists a crossover length separating the two different regimes.

4.6 Ergodicity for any d, s=1

Consider KA model on an hypercubic d–dimensional lattice Λ^d with parameter $s = 1$. Let *framed* configurations be those with all the hyperedges of dimension 1 empty and *frameable* be again those reachable from a framed one. In the case $d = 3$, for example, they correspond to the hyperplanes

$x_1 = 1, x_2 = 1; x_1 = L, x_2 = 1; x_1 = 1, x_2 = L; x_1 = L, x_2 = L;$

$x_1 = 1, x_3 = 1; x_1 = L, x_3 = 1; x_1 = 1, x_3 = L; x_1 = L, x_3 = L;$

$x_2 = 1, x_3 = 1; x_2 = L, x_3 = 1; x_2 = 1, x_3 = L; x_2 = L, x_3 = L$

Again, all frameable configurations belong to the same irreducible component. Consider for example a framed configuration in the case $d = 3$ and chose a permutation of two particles in neighboring sites $\{i, j\}$ belonging to a plane parallel to the upper one. By starting from corners, the bottom frame can be raised till framing the plane which contains the couple $\{i, j\}$. Then, after applying on this plane the same sandwich technique as for $d = 2$ $s = 1$, the permutation can be performed.

The generalization of the growing technique which enables to construct larger and larger frameable configurations starting form an empty nucleus, can be done by using the following observation. Given a frameable hypercube of linear size L, the number of vacancies needed in the subsequent shell to expand it to size $L + 2$ is 2^{d-1} for each of the 2^d faces. Therefore, the probability $\mu_{\Lambda^d,\rho}(\mathcal{F})$ that a system is frameable can be bounded from below

by $\mu_{\Lambda^d,\rho}(\mathcal{F}^0)$, with

$$\mu_{\Lambda^d,\rho}(\mathcal{F}^0) = (1-\rho)^{2d} \prod_{l=4}^{\infty} \left(1 - \sum_{i=0}^{2^{d-1}-1} \frac{l^{d-1}!}{(l^{d-1}-i)!i!} \rho^{l^{d-1}-i} (1-\rho)^i \right)^{2^d} \tag{4.12}$$

where the product is just on l even. In the limit $\rho \to 1$, $L \to \infty$ (4.12) gives:

$$\mu_{\Lambda^d,\rho}(\mathcal{F}^0) \simeq \exp\left(-\frac{c(d)}{(1-\rho)^{\frac{1}{d-1}}} \right) \tag{4.13}$$

where

$$c(d) = -2^{d-1}(d-1) \int_0^1 \frac{dy}{y(\log y)^{\frac{d-2}{d-1}}} \log\left(1 - y \left(\sum_{i=0}^{2^{d-1}-1} \frac{(-\log y)^i}{i!} \right) \right) \tag{4.14}$$

Let

$$\xi(\rho, d, 1) \equiv \left(-\frac{\log(1-\rho)}{1-\rho} \right)^{1/(d-1)} \tag{4.15}$$

by using (4.12), one can directly check that $\mu_{\Lambda^d,\rho}(\mathcal{F}^0)$ remains almost constant with L for $L \gg \xi$. Therefore, by considering the $O\left(L^d/\xi^d\right)$ possible positions for the starting nucleus of $2d$ vacancies, it seems reasonable to conclude that for $L \gg \Xi(\rho, d, 1)$ with

$$\Xi_u(\rho, d, 1) \propto \exp\left(\frac{c(d)}{d(1-\rho)^{\frac{1}{d-1}}} \right) \tag{4.16}$$

the probability that a configuration is frameable is almost one and goes to one in the thermodynamic limit. Above statement comes from considering that the probability that the whole configuration is frameable is given by the number of possible sub-lattices of linear size ξ multiplied by the probability that a the configuration is frameable by starting with an empty nucleus inside such sub-lattice. Therefore, this argument is not completely correct since events that the configuration is frameable by starting from two different sub-lattices are not independent. However it is possible to turn this argument into a proof thanks to the fact that the frameability requirements become more and more weak on larger sizes and therefore, if a configuration is frameable till size ξ, the probability of growing it frameable till infinity is almost one.

Let us sketch the above argument in some detail. Consider the Λ^d hypercubic lattice of linear size L and divide it in $(L/l_2)^d$ hypercubes of linear size

l_2. At the center of each of these hypercubes consider a smaller hypercube Λ_1 of size $l_1 = l_2/2$. The probability that the lattice is frameable can be bounded using the probability that the lattice can be made frameable starting from one of the L^d/l_2^d hypercubes of linear size l_1. Therefore $\mu_{\Lambda^d,\rho}(\mathcal{F}) \geq P_1 P_2 P_3$, where P_1 the probability that at least one of the hypercubes of size l_1 is frameable, P_2 is the probability that this frameable hypercube can be expanded until the size l_2 (requiring 2^{d-1} vacancies for each shell from size l_1 to size l_2), P_3 is the probability that the frameable hypercube of size l_2 can be expanded until the size L (requiring 2^{d-1} vacancies on each shell from size l_2 to L except in the region of space occupied by the other hypercubes of size l_1). The following equations hold:

$$\begin{aligned}
P_1 &= 1-(1-\mu_{\Lambda_1^d,\rho}(\mathcal{F}^0))^{\frac{L^d}{l_2^d}} \simeq 1-\exp\left(-\mu_{\Lambda_1^d,\rho}(\mathcal{F}^0)\frac{L^d}{l_2^d}\right) \\
P_2 &= \prod_{l=l_1}^{l_2}\left(1-\sum_{i=0}^{2^{d-1}-1}\frac{l^{d-1}!}{(l^{d-1}-i)!i!}\rho^{l^{d-1}-i}(1-\rho)^i\right)^{2^d} \\
P_3 &= \prod_{l=l_2}^{L}\left(1-\sum_{i=0}^{2^{d-1}-1}\frac{(l^{d-1}(1-\frac{l_1^{d-1}}{l_2^{d-1}}))!}{(l^{d-1}(1-\frac{l_1^{d-1}}{l_2^{d-1}})-i)!i!}\rho^{l^{d-1}(1-\frac{l_1^{d-1}}{l_2^{d-1}})-i}(1-\rho)^i\right)^{2^d}
\end{aligned} \tag{4.17}$$

By choosing $l_1 \simeq \xi(\rho,1,d)$, above equations give

$$\begin{aligned}
P_1 &\simeq 1-\exp\left(-\exp\left(-\frac{c(d)}{(1-\rho)^{\frac{1}{d-1}}}\right)\frac{L^d}{l_2^d}\right) \\
P_2 &\simeq 1 \\
P_3 &\simeq 1
\end{aligned} \tag{4.18}$$

therefore $\mu_{\Lambda^d,\rho}(\mathcal{F}) \simeq 1$ by requiring the second term in the right hand side of P_1 to be zero, which is equivalent to condition $L \gg \Xi_u(\rho,d,s)$, with $\Xi_u(\rho,d,s)$ defined in (4.16).

Exponential convergence

In this section we prove that the probability for a configuration to be frameable approaches one (at least) exponentially fast in the linear size L, i.e.

$$\mu_{\Lambda,\rho}(\mathcal{F}) \geq 1 - C\exp\left(-\frac{L}{\Xi_u(\rho,d,1)}\right) \tag{4.19}$$

for $L \geq \Xi_u(\rho, 2, 1)$. Indeed, as already mentioned in the end of section 4.5, such exponential convergence is a necessary ingredient to extend to higher dimensions the ergodicity proof established for the square lattice case.

We sketch two possible ways of doing the proof of (4.19) in the case $d = 2$ $s = 1$, which can be easily extended to any other dimension d for $s = 1$, by noticing that in order for such configuration to be frameable it is sufficient that the $d-1$–dimensional boundary is framed and so on.

(i)The first way of doing the proof is through a percolation-like argument, in the same spirit as the one in [27]. Consider a square lattice Λ^2 of linear size L, divide it in smaller squares of sizes l and focus on one of this sublattices, Λ_l^2. If the four neighboring squares of Λ_l^2 along all the independent directions are framed, then the smallest square which includes all these squares can be framed (see figure 4.6). In these way we can grow frameable objects. Moreover, one can directly check that if the non frameable squares of size l on the boundary of Λ^2 form only finite clusters, the whole configuration can be framed. Therefore

$$1 - \mu_{\Lambda^2,\rho}(\mathcal{F}) \leq P_{perc}(\frac{L}{l}, \mu_{\Lambda_l^2,\rho}(\mathcal{F}), 2) \tag{4.20}$$

where we let $P_{perc}(l, p, 2)$ be the probability of conventional site percolation for a square lattice of linear size l, when occupation probability $1-p$. Standard site-percolation estimates yeld following inequality for P_{perc} [27]

$$P_{perc}(l, p, d) \leq \sum_{j=l}^{\infty} 4(1-p)^j 4^{j-1} = \frac{4}{3}\frac{(3(1-p))^{l-1}}{1-3(1-p)} \tag{4.21}$$

If condition

$$\mu_{\Lambda_l^2,\rho}(\mathcal{F}) > 1 - \frac{1}{3e} \tag{4.22}$$

holds, by using (4.20) and (4.21) we find

$$\mu_{\Lambda^2,\rho}(\mathcal{F}) \geq 1 - Ce^{-L/l} \tag{4.23}$$

with a proper positive constant C. Since (4.22) holds for $l = \Xi(\rho, 2, 1)$, inequality (4.19) is proven for the case $d = 2$.

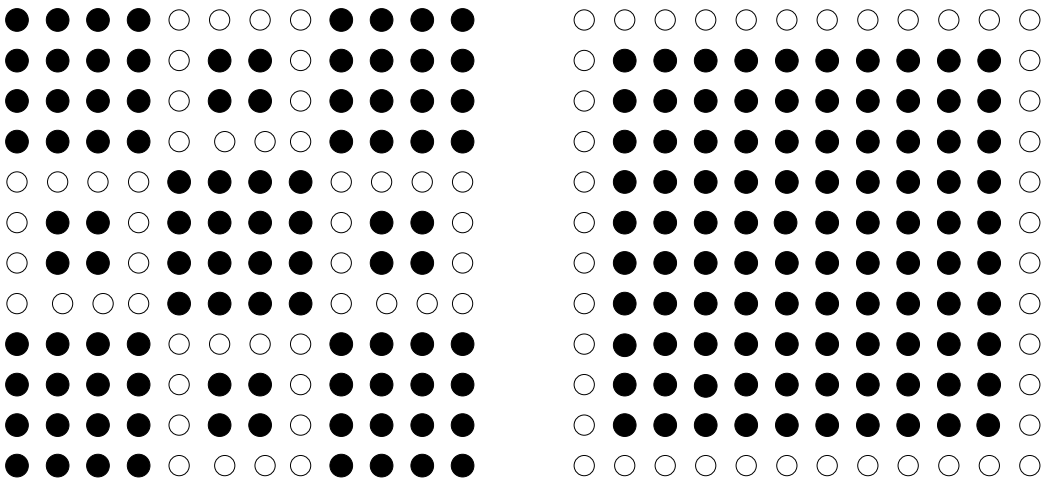

Figure 4.6: The two configurations above can be connected by a sequence similar to the one in figure 4.2: starting by the corners which connect two empty edges one can move the latter up, down, right and left till reaching the final configuration.

(ii)A different way to establish inequality (4.19) for the two–dimensional case is through a sort of renormalization group approach. Consider a square lattice Λ^2_{2L} of linear size $2L$ and divide it in four squares of linear size L. If all the four squares, or at least three of them, are frameable, then the whole lattice is frameable too. Therefore the following iterative inequality holds:

$$\mu_{\Lambda^2_{2L},\rho}(\mathcal{F}) \geq \left(\mu_{\Lambda^2_L,\rho}(\mathcal{F})\right)^4 + 4\left(\mu_{\Lambda^2_L,\rho}(\mathcal{F})\right)^3 (1 - \mu_{\Lambda^2_L,\rho}(\mathcal{F})) \tag{4.24}$$

Moreover, if condition

$$(1 - \mu_{\Lambda^2_L,\rho}(\mathcal{F})) \leq \frac{1}{10e} \tag{4.25}$$

holds, then

$$\mu_{\Lambda^2_{2L},\rho}(\mathcal{F}) \geq 1 - 10(1 - \mu_{\Lambda^2_L,\rho}(\mathcal{F}))^2 \tag{4.26}$$

which also implies condition (4.25) when L goes to $2L$. Therefore, we can iterate inequality (4.26) finding

$$\mu_{\Lambda^2_{2^n L},\rho}(\mathcal{F}) \geq 1 - 1/10\left(10(1 - \mu_{\Lambda^2_L,\rho}(\mathcal{F}))\right)^{2^n} \geq 1 - \frac{1}{10}e^{\frac{-2^n L}{L}} \tag{4.27}$$

Since for $L > \Xi(\rho, 2, 1)$ condition (4.25) holds, inequality (4.27) is established for any integer n. Therefore, we have riderived inequality (4.23)[2] in the case $d = 2$.

4.7 Ergodicity for any d,s

Consider KA model with parameter s on a d–dimensional hypercubic lattice Λ^d. It is immediate to check that in all the cases $s \geq d$, the system is not ergodic in the thermodynamic limit at any density $\rho > 0$. Indeed, all d-dimensional hypercubes of any size which are completely occupied by particles are forever blocked (for example in the case $d = 2$ $s = 2$ the jumps rates impose that any two by two square of four particles can never move). Therefore, a configuration chosen at random with probability $\mu_{\Lambda^d,\rho}$, has with unit probability a finite fraction of forever blocked particles. This implies that two configurations have with probability one a finite fraction of sites on which they cannot be rendered equal, thus they belong to different irreducible components. In other words, at any density $\rho > 0$ ergodicity does not hold. For the $s = 1$ case we already established in previous section that ergodicity holds in the thermodynamic limit at any density $\rho < 1$. On the other hand the cases $s = 0$ corresponds to SSEP, where ergodicity trivially holds at any density (note that SSEP process is ergodic at any density even on finite size lattices). Therefore, the only cases left to be considered are those with $1 < s < d$, for which we will prove that in the thermodynamic limit ergodicity holds at any density $\rho < 1$. The proof of ergodicity will be performed through a generalization of the idea used in section 4.5 to extend the results from the case $d = 2$ $s = 1$ to $d = 3$ $s = 2$.

Let *framed* configurations be those having all hyperedges of dimension s empty. In a more formal way they are defined as the configuration having all the sites empty on the hyperplanes:

$$\{x_{P_1} = 1, L\} \times \{x_{P_2} = 1, L\} \times \ldots \{x_{P_{d-s}} = 1, L\} \tag{4.28}$$

where $P_1, \ldots P_{d-s}$ is a generic $(d-s)$-uple obtained from $1, \ldots, d$. For example the $s = 2, d = 3$ case corresponds to the planes:

$x_1 = 1; x_1 = L; x_2 = 1; x_2 = L; x_3 = 1; x_3 = L$.

It's easy to show that, inside a frameable hypercube, any jump of a particle to a neighboring empty site can be achieved by the generalization of the "sandwich technique" discussed previously. Consider an hypercube of size

[2]By this second argument we have obtained the result only for $L = 2^n \Xi(\rho, 2, 1)$. However there is nothing special with these values, they just come from our iterative procedure.

$l+2$ which is frameable till size l. If adjacent to each side there is a $d-1$ -dimensional hypercube which is frameable for the $d-1$ $s-1$ model, than the d-dimensional hypercube is frameable till size $l+2$. Therefore, to bound from below the probability that a d-dimensional hypercube is frameable for the choice s, $\mu_{\Lambda^d,\rho}(\mathcal{F}_{(s)})$, we can estimate the probability $\mu_{\Lambda^d,\rho}(\mathcal{F}^0_{(s)})$ that an hypercube of linear size l centered in the origin is empty and that starting from it any subsequent shell is frameable for the $d-1$, $s-1$ model:

$$\mu_{\Lambda^d,\rho}(\mathcal{F}_{(s)}) \geq \mu_{\Lambda^d,\rho}(\mathcal{F}^0_{(s)}) = (1-\rho)^{l^d} \prod_{k=l+1}^{L} \mu_{\Lambda_k^{d-1},\rho}(\mathcal{F}_{(s-1)}) \tag{4.29}$$

where Λ_k^{d-1} is the $(d-1)$–dimensional lattice of linear size k. If there exists a length $\Xi_u(\rho,d,s)$ such that

$$\mu_{\Lambda^d,\rho}(\mathcal{F}_{(s-1)}) \geq 1 - C\exp\left(-\frac{L^d}{\Xi_u^d}\right) \quad \text{for} \quad L \gg \Xi_u(\rho,s-1,d-1) \tag{4.30}$$

then, by choosing $l \gg \Xi_u(\rho,d-1,s-1)$ the product on k in (4.29) would become close to one and $\mu_{\Lambda^d,\rho}(\mathcal{F}^0_{(s)})$ would be approximatively given by the probability of finding a starting empty nucleus of linear size $\Xi_u(\rho,d-1,s-1)$, namely

$$\mu_{\Lambda^d,\rho}(\mathcal{F}^0_{(s)}) \simeq (1-\rho)^{\Xi_u(\rho,d-1,s-1)^d} \tag{4.31}$$

Therefore, by considering all the possible positions for the empty nucleus and applying an argument analogous to the one used in the two–dimensional case, we would find that $\mu_{\Lambda^d,\rho}(\mathcal{F}_{(s)})$ goes to one for $L \to \infty$ and is almost one for $L \gg \Xi_u(\rho,d,s)$ where

$$\Xi_u(\rho,d,s) = \left((1-\rho)^{\Xi_u(\rho,d-1,s-1)^d}\right)^{\frac{1}{d}} \tag{4.32}$$

From results in previous section, in the case $s=1$ and for any $d \geq 2$, condition (4.30) hold with $\Xi_u(\rho,d,1)$ given by (4.16). Therefore above argument can be applied iteratively and ergodicity in the thermodynamic limit is proved for the generic case s,d with $1 < s < d$[3]. Moreover, even if on finite lattices the configuration space is always broken into many disconnected components, (4.32) defines a length above which a single ergodic component (frameable configurations) dominates, i.e. has probability almost one. By iteratively

[3]Note that the iterative arguments starts from $s=1$, $d>1$ and does not cover the cases $s \geq d$. As already explained in the beginning of the section, in this cases ergodicity does not hold at any density.

solving this equation with initial condition (4.16), we find for $\Xi_u(\rho, d, s)$ the following density dependence

$$\Xi_u(\rho, d, s) = \exp^{\circ s} \frac{C(d,s)}{(1-\rho)^{d-s}} \tag{4.33}$$

where $\exp^{\circ s}$ is the exponential iterated s times.

4.8 Irreducibility vs ergodicity

In previous sections we have proved that irreducibility holds in the thermodynamic limit for the generic case s, d with $1 < s < d$, i.e. there exists an irreducible component (frameable configurations) which has unit probability. However, as we recalled in section 2.5.1, this is not sufficient to establish ergodicity for the infinite volume system. In this section we prove that for this models irreducibility implies ergodicity (third step of the strategy outlined in section 4.4). We will follow the same strategy as in section 3.3.2. Since the proof is the same for any choice of d and s, in the rest of this section we drop indices d and s. Recalling the definition in section 2.5.1, proving ergodicity corresponds to show that for each $\rho \in [0,1]$, zero is a simple eigenvalue in $L_2(\mu_\rho)$ for the generator $\mathcal{L}$ defined in (2.12) and (4.1). In other words, we should prove that if f is eigenvector with zero eigenvalue of $\mathcal{L}$, then f is constant almost surely with respect to μ_ρ. For this purpose it is sufficient to prove that $f(\eta) = f(\eta^{x,y})$ for any x, y almost surely with respect to μ_ρ, i.e. $\mu_\rho(f(\eta^{xy}) - f(\eta)) = 0$. Indeed, this implies that the measure $\tilde{\mu} = f\mu$ is exchangeable (i.e. invariant under exchange of finitely many variables) and DeFinetti's theorem on the decomposition of exchangeable measures on product measures ([42, 43]) allows us to conclude that $\tilde{\mu} = \mu$, i.e. f is constant almost surely with respect to μ_ρ.

By enumerating frameable configurations as $\eta_1, \ldots, \eta_{N_\mathcal{F}}$ and using the result $\mu_\rho(\mathcal{F}) = 1$ established in previous sections, the following inequality is readily established

$$\mu_\rho(\nabla_{x,y} f)^2 = \mu_\rho\big([\nabla_{x,y} f]^2 \mathbb{I}_\mathcal{F}\big) \leq \sum_{n=1}^{N_\mathcal{F}} \mu_\rho\big([\nabla_{x,y} f]^2 \mathbb{I}_{\eta_n}\big) \tag{4.34}$$

where $\nabla_{x,y} f \equiv f(\eta^{x,y}) - f(\eta)$. From the properties of frameable configurations, for any configuration $\bar{\eta} \in \mathcal{F}$ one can always find an allowed path $\eta_0 = \bar{\eta}, \ldots, \eta_N = \bar{\eta}^{x,y}$ connecting $\bar{\eta}$ to $\bar{\eta}^{x,y}$, i.e. such that $\eta_{i+1} = \eta_i^{z,w}$ for some couple of neighboring sites $\{z, w\}$ and $c_{z,w}(\eta_i) = 1$. Therefore, by telescopic sums and Cauchy–Schwartz inequality, each term in the sum can be bounded

from above by a sum of terms $\mu_\rho\big(c_{z,w}[\nabla_{z,w}f]^2\big)$, i.e. elementary exchanges multiplied by the correspondent rate. On the other hand, the hypothesis that f is eigenvector of $\mathcal{L}$ with zero eigenvalue, implies that $\mu_{\Lambda,\rho}(f\mathcal{L}f)$ is zero. Moreover, using the symmetry of jump rates $c_{x,y}(\eta) = c_{y,x}(\eta)$

$$\mu_{\Lambda,\rho}(f\mathcal{L}f) = -\frac{1}{2}\sum_{\eta}\mu_{\Lambda,\rho}(\eta)\sum_{\{x,y\}\subset\Lambda} c_{x,y}(\eta)(\nabla_{x,y}f)^2 \tag{4.35}$$

therefore

$$\mu_\rho\big(c_{x,y}[\nabla_{x,y}f]^2\big) = 0 \quad \text{for any } x, y \tag{4.36}$$

By combining this equation with (4.34) and above observation, we conclude that $\mu_\rho(\nabla_{x,y}f)^2 = 0$, which ends the proof.

4.9 Bootstrap percolation and crossover length

In previous sections we have proven that for any choice of parameters d and s, with $s < d$, ergodicity holds in the thermodynamic limit. On the other hand the model on finite lattice is always non ergodic. However, we have determined a density dependent characteristic length $\Xi_u(\rho, d, s)$ such that for for $L \gg \Xi(\rho, s, d)$ the probability that a configuration is frameable is almost one (more precisely it goes to one at least exponentially fast, see inequality (4.30)), therefore the ergodic frameable component almost covers the configuration space. On the other hand, for $L \ll \Xi(\rho, s, d)$ the probability of a frameable configuration is almost zero. However, this is not by itself sufficient to rule out the possibility that another ergodic component dominates. In this section, by using known results for a different problem, we prove that indeed there exists a size $\Xi_l(\rho, d, s)$ with the same density dependence as $\Xi_u(\rho, d, s)$, such that for $L \ll \Xi_l(\rho, d, s)$ the number of ergodic components is exponential in the system size and each of them have probability almost zero. In other words there exists a density dependent length $\Xi(\rho, d, s)$ with $\Xi_l(\rho, d, s) < \Xi(\rho, d, s) < \Xi_u(\rho, d, s)$ which separates two different regimes. Let us state more clearly what we mean by crossover length. Consider the probability $\mu_{\Lambda,\rho}(\mathcal{E})$ of the maximal ergodic component for a system Λ of finite size L and density ρ. The ergodicity proof implies that $\lim_{\rho\to 1}\lim_{L\to\infty}\mu_{\Lambda,\rho}(\mathcal{E})$ is one, while if one takes the limits in the inverse order the result is zero. On the other hand, by sending $L \to \infty$ and $\rho \to 1$ simultaneously, the result depends on the relative speed of convergence and the threshold regime is given by $L \sim \Xi(\rho)$. Since numerical simulations are always performed on finite size lattices, the knowledge of the crossover length is a useful information in the

interpretation of numerical results. Indeed, this means in some sense that for $L \gg \Xi$ we are almost in the thermodynamic limit while for $L \ll \Xi$, even if L is large, finite size effects are important and the system do not behave as the infinite volume one (for further discussion on this subject and on the consequences on dynamics, see chapter 6).

Let us explain how the lower bound for the crossover length can be obtained. We recall that according to KA rules a particle can move only if it has no more than m nearest neighbors occupied both in the initial and final position, which corresponds to a vacancy moving if it has at least $s = 2d - m - 1$ neighboring vacancies both in the initial and final position. Consider a d-dimensional hypercubic lattice Λ and sort a configuration at random with Bernoulli measure at density ρ. Then remove all the particles that have no more than m neighbors and iterate the procedure until no more particles can be removed. As already noticed by Kob and Andersen for the $d = 3$ $s = 2$ case, all the particles that eventually remain at the end of the procedure are forever blocked with respect to KA rules, namely starting from the same initial configuration and running dynamics they can never move since they will always have more than m neighbors. The procedure defined above is nothing else but *bootstrap percolation* [4] [23], [24], [25] and rigorous results have been established for the probability $\mu^B_{\Lambda^d,\rho}$ that a cluster of particles remains at the end of the procedure. Indeed, from the recent results in [27], the following behavior holds: $\mu^B_{\Lambda,\rho}$ is very small for $L < L^B(\rho, d, s) \equiv \exp^{\circ s}(\frac{K(d,s)}{v^{d-s}})$; $\mu^B_{\Lambda,\rho}$ converges exponentially fast to one for $L > L^B(\rho, d, s)$. Moreover, for the values of s and d we are focusing on, if something remains at the end of the procedure it should be a system-spanning cluster (i.e. connecting two boundaries of the system). Therefore, for $L < L^B(\rho, d, s)$ a randomly sorted configuration has with probability almost one a system spanning cluster of forever blocked particles and no ergodic component can have probability almost one. As a consequence, the lower bound

$$\Xi(\rho, d, s) \geq \Xi_l(\rho, d, s) \equiv L^B(\rho, d, s) \tag{4.37}$$

follows. Note that the density dependence of such lower bound is the same as for the upper bound (4.33), the difference being that constant $K(d, s)$ replaces $C(d, s)$.

For the $d = 2$ $s = 1$ case, it has recently been established [28] the exact value of the bootstrap percolation constant, $K(2, 1) = \pi^2/6$. On the other

[4] To related this procedure with usual bootstrap percolation we should exchange variable ρ with $1 - \rho$. Indeed usual bootstrap procedure correspond to start form a configuration at density ρ, iteratively injecting particles in empty sites having less than m neighbors and looking for eventual remaining clusters of empty sites.

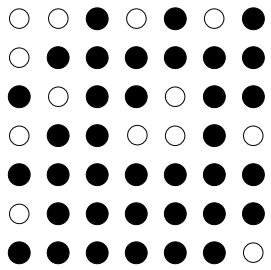

Figure 4.7: A 7 by 7 optimally framed configuration.

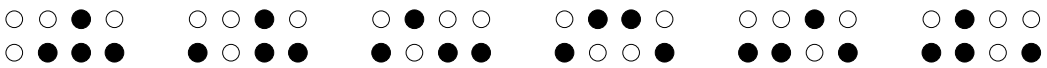

Figure 4.8: The basic moves by which the three vacancy corner can move along the row.

hand, from (4.6), $C(2,1) \simeq 4.48$. Therefore inequalities $K(2,1) < C(2,1)$ and $\Xi_u(\rho,2,1) > \Xi_l(\rho,2,1)$ hold. In next section we will explain how, by devising a different framing technique, it is possible to determine a smaller upper bound for $\Xi(\rho,2,1)$ which turns out to be equal to the above lower bound from bootstrap percolation. In other words, we establish the exact value of the crossover length $\Xi(\rho,2,1) = \Xi_l(\rho,2,1)$.

4.10 Optimal framing and exact crossover length in d=2, s=1

Consider KA model on a square lattice Λ with parameter $s = 1$. Define a $W \times H$ rectangle (with $W + H$ even) to be *optimally framed* if it has $\frac{1}{2}(W + H)+1$ vacancies arranged along alternate sites of two perpendicular sides with an additional one in the corner, plus any number of additional vacancies, see figure 4.7. *Optimally frameable* configurations are those that, with allowed moves, can be reached from an optimally framed one. Optimally frameable configurations belong all to the same irreducible component, since any nearest neighbor jump within an optimally frameable rectangle can be accomplished with all other particles returned to their starting positions. The sequence of moves allowing a generic exchange can be constructed by considering the basic moves in figure (4.8) which allow both to move the group of three vacancies along the row containing the alternated vacancies and those in figure (4.9) which enable to lower and raise this particular row trhogh the lattice.

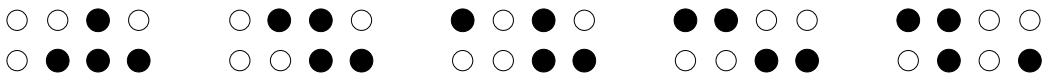

Figure 4.9: The basic move by which the row of alternating vacancies and particles can be lowered.

Consider a framed $W\times H$ rectangle. The following statements can be checked by direct inspection: if there is a vacancy in a line next-nearest neighbor to one of its edges parallel to direction x or y, the rectangle can be expanded to a $W\times(H+2)$ or $(W+2)\times H$ framed rectangle, respectively; if there is a vacancy next nearest neighbor along a diagonal from a corner it is expandable to a $(W+1)\times(H+1)$ framed rectangle; if there is a vacancy in the line segment next to one of its edges parallel to direction x or y it is expandable into a $W\times(H+1)$ or $(W+1)\times H$ framed rectangle, respectively. Therefore, starting from a nucleus of three vacancies in a two-by-two square, this procedure can be iterated to grow larger frameable rectangles as long as the needed vacancies are present. Let Q_k^ℓ be the probability that, given a $(k-2)\times l$ optimally frameable rectangle, it can be expanded to an optimally frameable $k\times l$ rectangle including $(k-1)$th and kth columns. From above observations and developing ρ^ℓ in the large density limit as $\rho^\ell \simeq e^{-\ell(1-\rho)}$, we obtain the following recursive equations

$$Q_{k+2}^\ell = Q_{k+1}^\ell(1-e^{-v\ell}) + Q_k^\ell e^{-v\ell}(1-e^{-v\ell}) \tag{4.38}$$

Defining the ratios of successive Qs by

$$R_k^\ell \equiv \frac{Q_{k+1}^\ell}{Q_k^\ell} \tag{4.39}$$

equation (4.38) gives

$$R_{k+1}^\ell = (1-e^{-v\ell}) + \frac{e^{-v\ell}(1-e^{-v\ell})}{R_k^\ell} \tag{4.40}$$

Since the least unlikely way to expand a rectangle is roughly isotropic, at any scale $k \approx l$. Moreover, the ratios of probabilities for successive expansions along the same axis will vary slowly in the dominant range of length scales, therefore a reasonable ansatz is

$$R_{k+1}^\ell \approx R_k^\ell \approx R(\ell) \tag{4.41}$$

By substituting (4.41) in (4.40), we find

$$R(\ell) \simeq \frac{1-\mathcal{E}}{2} + \frac{1}{2}\sqrt{1+2\mathcal{E}-3\mathcal{E}^2} \tag{4.42}$$

where

$$\mathcal{E} = e^{-v\ell} \tag{4.43}$$

By considering that the rectangle has to be expanded to infinity in all four directions, we find the following estimate for the probability $\mu_{\infty,\rho}(\mathcal{O})$ that a nucleus of three vacancies can be expanded to an infinite frameable rectangle

$$\mu_{\infty,\rho}(\mathcal{O}) \simeq \left[\prod_{n=1}^{\infty} R(2n)\right]^4 \simeq \exp\left[2\sum_{\ell=1}^{\infty} \ln R(\ell)\right] \tag{4.44}$$

which, by replacing the sum over ℓ by an integral and changing variables, gives

$$\mu_{\infty,\rho}(\mathcal{O}) \simeq \exp -\frac{2c_\infty}{1-\rho} \tag{4.45}$$

where

$$c_\infty = -\int_0^1 \frac{d\mathcal{E}}{\mathcal{E}} \ln\left[\frac{1-\mathcal{E}}{2} + \frac{1}{2}\sqrt{1+2\mathcal{E}-3\mathcal{E}^2}\right] \tag{4.46}$$

The knowledge of $\mu_{\infty,\rho}(\mathcal{O})$ gives, as in previous sections, an upper bound for the crossover length $\Xi(\rho, d, s)$

$$\Xi(\rho, 2, 1) \leq \exp \frac{c_\infty}{2(1-\rho)} \tag{4.47}$$

Now the constant c_∞ (4.46) has exactly the same value as the bootstrap constant $K(1,2)$ in [28]. Thus, since the upper bound obtained by the above framing procedure coincides with the lower bound provided by bootstrap results, this gives the *exact* value of crossover length. Therefore, this framing seems to capture the real mechanism which restores ergodicity and for this reason we refer to it as *optimal framing*.

4.11 Conclusions

In this chapter we have proved that KA model on an hypercubic lattice in any dimension d and for any choice of the parameter s does not display an ergodic/non–ergodic transition at a finite density $\rho \in [0,1]$. For the choice $s = 0$, the SSEP case is recovered and ergodicity trivially holds at any finite density. On the other hand, for $s \geq d$ at any density there exists with finite probability a set of particles that are forever blocked. Therefore, it is

immediate to establish that the model is always non–ergodic. The interesting cases correpond to the intermediate choice $0 < s < d$. By constructing an irreducible component and proving that its probability with respect to Bernoulli measure at any density goes to one in the thermodynamic limit, we establish that for this choice of the parameters the system is always ergodic. These cases include the $d = 3$ $s = 2$ model originally introduced by Kob and Andersen for which previous numerical results (see section **??**) suggest the possibility of an ergodic/non–ergodic transition at a finite density. Since we construct explicitely the irreducible component, the proof unveils the rare processes which guaranty ergodicity in the thermodynamic limit. This will be a key ingredient to establish the typical relaxation and diffusion time scales and to understand the mechanism which induces the slow and heterogeneous dynamics at high density (see chapter 6). We also emphasize that the proof is not too specific of the considered rules and the same strategy can be easily extended to other models with different choices of the local kinetic constraints. The key ingredients we use are the following: on a finite lattice one can define a particular configuration of vacancies at the boundary–a frame–which enables any pair exchange inside a configuration; this frame can be constructed by starting from an empty nucleus and imposing on each subsequent concentric shell (from the nucleus to the boundary) a requirement which becomes less and less restrictive on larger shells. Therefore, the probability of continuing such construction till the boundary becomes independent on the size of the system after a certain typical size and does not vanish in the thermodynamic limit.

Furthermore, since on any finite lattice there exist blocked configurations and the model is not ergodic, we have analyzed the probability of the maximal ergodic component at a fixed density ρ for different system sizes L. The result is that there exists a crossover length $L \sim \Xi(\rho)$ with $\Xi(\rho) = \exp^{0s} c/(1-\rho)^{d-s}$ (with $\exp^{0s}$ the s–times iterated exponential). This separates the large size regime in which the configuration space is covered almost entirely by a single ergodic component and the small size regime in which it is decomposed into many disjoint parts. A comparison with bootstrap percolation results allows us to explain the latter regime with the arising of system–spanning clusters of forever blocked particles.

Chapter 5

KA model on a Bethe lattice

In this chapter we analyze KA model on a Bethe lattice, i.e. a random graph with fixed connectivity. The scenario in this mean field model is completely different from that of the hypercubic lattice case discussed in previous chapter. Indeed, we prove that there exists a finite critical density ρ_c at which an ergodic/non–ergodic transition takes place in the thermodynamic limit. More precisely, ρ_c separates the regime ($\rho < \rho_c$) in which the configuration space is covered by a single ergodic component and all particles can diffuse, from the regime ($\rho > \rho_c$) in which configuration space broken into an exponential number of different ergodic components and the system is partially frozen, i.e. there exist infinite clusters of forever blocked particles. An analysis of this dynamical transition, which has aspects of both first and second order transition, follows. Finally, we extend above results to KA model on decorated Bethe lattices, i.e. on random graphs with finite size loops.

5.1 Bethe lattices

Bethe lattice is defined as a random simple graph with N sites and fixed connectivity $z = k + 1$ [29]. "Simple" means there are neither multiple edges (no two edges joining the same sites) nor trivial loops joining a site to itself. Since the typical size of the loops is of order $\log N$, when N is large typical random graphs look locally (on finite length scale) like Cayley trees with a fixed branching ratio[1]. The presence of loops is crucial since it induces geometric frustration which assures a statistically homogeneous structure and prevents the problems arising in the Cayley lattice case [30] due to sensitivity to boundary conditions. In other words, working on the

[1]Recall that a Cailey tree with connectivity $k+1$ is constructed by taking $k+1$ rooted trees and connecting a new site, the origin, to the $k+1$ roots.

Bethe lattice would be equivalent to considering a Cailey tree of size L and focusing on a core of size l around the origin in the limit $L \to \infty$, $l \to \infty$ with $\frac{l}{L} \to 0$. On the other hand, the tree–like local structure allows analytic calculation trough the solution of recursive equations.

The main motivation for studying KA on the Bethe lattice is that such lattice is considered to be a good approximation of the hypercubic lattice in the limit of high dimensionality, therefore a good mean field approximation. As we will explain in detail, results are completely different from those obtained in previous chapter for the model on an hypercubic lattice. Indeed, in the Bethe lattice case an ergodic/non–ergodic transition takes place at a finite density. The possibility of comparing results both for the finite (hypercubic lattice) and infinite (Bethe lattice) dimensional case could be a useful ground for the extension of other mean field scenarios to real glasses.

5.2 Dynamical transition

Consider a Bethe lattice with connectivity $k+1$. KA model is defined as in section 4.1, with the only difference that now $0 < m < k$ and $s = k - m$. As usual, one arranges the lattice as a tree with k branches going up and one going down. Consider one node, call it i, and define following events:

(i) site i is occupied by a particle which can never move up. Call P_1 the probability that this event occurs, conditioned to the fact that the site below is occupied;

(ii) site i is empty. Call P_2 the probability that this event occurs and, if there were a particle on the site below, it could never move to i;

(iii) site i is occupied by a particle which can never move up. Call P_3 the probability that this event occurs, conditioned to the fact that the site below is empty.

By using the tree–like structure, one can write iterative equations for these probabilities

$$
\begin{aligned}
P_1 &= \rho\left(\sum_{j=k-s}^{k} P_1^j(1-P_1)^{k-j}\binom{k}{j} + \sum_{j=k-s}^{k} P_2^j P_1^{k-j}\binom{k}{j}\right) \\
P_2 &= (1-\rho)\sum_{j=k-s+1}^{k} P_3^j(1-P_3)^{k-j}\binom{k}{j} \\
P_3 &= \rho\left(\sum_{j=k-s+1}^{k} P_1^j(1-P_1)^{k-j}\binom{k}{j} + \sum_{j=s}^{k} P_2^j P_1^{k-j}\binom{k}{j}\right)
\end{aligned} \tag{5.1}
$$

which can be reduced to independent polynomial equations for P_1, P_2 and P_3 with ρ dependent coefficients.

5.2.1 Existence of the transition

In this section we present an argument which guarantees that a dynamical transition takes place for all the choices of k and s with $s > 0$ ($s = 0$ corresponds to the trivial lattice gas case, for which no transition takes place). Consider a node i. Let i be occupied and the outgoing bond occupied too. If all the k ingoing bong, or at least $k-1$ of them, are occupied by forever blocked particles, then the particle in i can never move up. Therefore

$$P_1 \geq \rho(P_1^k + kP_1^{k-1}(1-P_1)) \tag{5.2}$$

Let $C = 1 - P_1$, former inequality is equivalent to $C \leq f(C)$ with $f(x) \equiv 1 - \rho(1-x)^k - \rho k(1-x)^{k-1}$. Since $C = 1$ is a fixed point for f at $\rho = 1$, at sufficiently large density there exists a $\bar{C} < 1$ such that $f(\bar{C}) = \bar{C}$. Let $C = G(C) \leq f(C)$ be the iterative equation for C (i.e. the polynomial equation which can be determined from (5.1)). If one iterates on this equations starting from an initial condition $C_0 = \bar{C} - \epsilon < \bar{C}$, then all the subsequent C's, $C_1 = G(C_0), C_2 = G(C_1), \ldots$, satisfy inequality $C_i < \bar{C}$. Indeed, since $f(x)$ is increasing monotone in x, $C_1 = G(C_0) = G(\bar{C} - \epsilon) \leq f(\bar{C} - \epsilon) < f(\bar{C}) = \bar{C}$ and the same is true at any subsequent step. Therefore, also the fixed point C^* with $C^* = G(C^*)$, satisfies $C^* < \bar{C} < 1$. Thus $P_1 = 1 - C^* > 0$ at sufficiently high (but finite) density. Since for low density the solution is $P_1 = 0$, this implies that at a finite density a dynamical transition occurs.

5.2.2 Discontinuity of transition for $s < k - 1$

Consider KA model with $s < k-1$ and focus on a node i. Let i be occupied and the outgoing bond occupied too. If all the sites above i and also those

one level up in the tree are empty, or if the above is true except in one of the sites, then particle on site i can move up. Therefore

$$P_1 \leq 1 - (1 - P_1)^{k+k^2} - (k + k^2)P_1(1 - P_1)^{k+k^2-1} \tag{5.3}$$

Above inequality cannot be true for P_1 arbitrarily near to zero, since for $0 < P_1 \ll 1$ it becomes $1 \leq (k + k^2 - 1)(k + k^2)P$, which cannot hold when P_1 is too small. Therefore, P_1 cannot go continuously to zero and it has a finite jump at the critical density.
Note that former argument does not apply to the case $s = k - 1$. Indeed it is not true that if the sites above i and those one level up in the tree are all empty except one, then the particle can move (inequality (5.3) is true only with second term in r.h.s. dropped, and the rest of the argument is no more valid). We will come back to this case in section 5.2.4, where we will prove that the transition is continuous.

5.2.3 A boostrap percolation procedure

Before analyzing in detail the character of the dynamical transition, we define a bootstrap procedure which helps understanding the physical mechanism underlying this phenomenon.

Consider the following procedure: pick at random an initial configuration on the Bethe lattice with Bernoulli product measure at density ρ, then remove all the particles that can move according to KA rules and iterate the process until no more particles can be removed. Note that, if some particles survive at the end of the procedure, then they are necessarily blocked forever when one starts from the same initial configuration and let the system evolve according to KA dynamics. Let p^B be the probability that at the end of the procedure an infinite particle cluster remains. By above observation, if $p^B > 0$ KA model at density ρ is not ergodic. Let ρ_c^B be the critical density, if any, at which a *bootstrap percolation transition* takes place, namely $p^B = 0$ for $\rho < \rho_c^B$ and $p^B > 0$ for $\rho > \rho_c^B$. If there exists a bootstrap transition, a dynamical transition for KA model also takes place and the correspondent critical density satisfies $\rho_c \leq \rho_B$. Moreover, a reasonable ansatz, is that the two transitions and therefore the correspondent critical densities coincide. In the rest of the section we present an argument supporting this conjecture.

Let i be a particle blocked forever with respect to KA dynamics, i.e. a particle which is blocked on any time scale after the thermodynamic limit has been taken. Than i must have more than $z - s - 1$ neighbors blocked forever, or else all the neighboring empty sites should have more than $z-s-1$ neighbors blocked forever, otherwise one could move the not forever blocked

neighbors (or next to nearest neighbors) at the same time and then move i. Moving the neighbors at the same time is possible because there should be no correlation between them, since typically there are no finite loops in a Bethe lattice, as discussed in section 5.1. In other words, moving a particle should not affect the ability of the others to move and a neighboring particle will move provided a proper set of particles that are up in the tree have moved. If the number of particles in this set is finite, this will not affect the ability to move of the other neighbors (of the particle on which we are focusing on) because there are no finite loops. Then one can repeat the same procedure and show that the neighbors must have $z-s-2$ neighbors up in the tree occupied by particles blocked forever or all the empty neighbors with more than $z-s-1$ neighbors forever blocked and so on and so forth. Therefore, the probability $\tilde{P}$ that a given site is occupied by a particle blocked forever, can be expressed in terms of P_1 and P_2 as

$$\tilde{P} = \rho \left(\sum_{j=k-s+1}^{k+1} P_1^j (1-P_1)^{k+1-j} \binom{k+1}{j} + \sum_{j=s+1}^{k+1} P_2^j P_1^{k+1-j} \binom{k+1}{j} \right) \qquad (5.4)$$

This implies that particles blocked forever coincide with those remaining after the bootstrap procedure. More precisely, last statement holds under the hypothesis that to pick away a particle during bootstrap procedure one doesn't have necessarily to pick away before an infinite (diverging with the system size) number of particles. This should be equivalent to the hypothesis that the correlation length is always finite, which seems reasonable except at the transition [2]. From (5.4) and (5.1) is then immediate to conclude that the bootstrap percolation transition, corresponding to $\tilde{P}$ from changing from zero to a finite value, coincides with the dynamical transition discussed in previous sections, correspondent to P_1 going from zero to a positive value.

5.2.4 Continuity of transition for s=k-1

Consider the choice $s = k-1$. Equation (5.4) implies that a particle blocked forever belongs to an infinite cluster of particles with two or more neighbors, i.e. to a percolating cluster (where "percolating" refers here to conventional nearest neighbor percolation). Critical density should be therefore the same as for percolation, $\rho_c = 1/k$, and the transition should be continuous. By

[2] By numerically running bootstrap procedure in the case $k = 2, s = 1$, we have checked that the density above which a cluster of particles remains at the end of the process is compatible with the critical density above which $\tilde{P}$ becomes finite. This confirms above hypothesis.

solving equations (5.1) in the cases $k = 2$ and $k = 3$, we have checked with positive result this conjecture.

5.2.5 Cases k=3, s=1 and k=5, s=2: analogy with p-spin dynamical transition

Let me consider in detail cases $k = 2$ $s = 1$ and $k = 5$ $s = 3$, which mimic the only interesting bi–dimensional case and the three-dimensional case originally introduced by Kob and Andersen, respectively.

In the case $k = 2$ $s = 1$, equations (5.1) give

$$\begin{aligned} P_1 &= \rho\left(P_1^3 + 3P_1^2(1-P_1) + P_2^3 + 3P_2^2 P_1\right) \\ P_2 &= (1-\rho)P_3^3 \\ P_3 &= \rho(P_1+P_2)^3 \end{aligned} \tag{5.5}$$

from which it is immediate to recognize that, when $P_1 > 0$ also $P_2 > 0$ and $P_3 > 0$. Therefore one can look at the transition by studying equations for $G \equiv P_1 + P_2$, which can be written as

$$G[-1+3\rho G-2\rho G^2+v\rho^3 G^8-6v\rho^4(G^9-G^{10})+3v^2\rho^7(G^{17}-G^{18})] = 0 \tag{5.6}$$

By direct analysis one can see that there is a critical density ρ_c such that: for $\rho > \rho_c$ there are two physical solutions for G, the larger one being stable and the other $G = 0$ unstable; for $\rho < \rho_c$ only the solution $G = 0$ survives. At $\rho = \rho_c$, the two solutions annihilate in a saddle-node bifurcation signaled by

$$\frac{\partial Q(G,\rho_c)}{\partial G} = 0 \tag{5.7}$$

where we let $Q(G, \rho)$ be the left hand side of equation (5.6).
The values of critical density ρ_c and critical $G_c \equiv G(\rho_c)$ are:

$$\rho_c \simeq 0.888 \qquad G_c \simeq 0.758 \tag{5.8}$$

At $\rho = \rho_c$ the value of G jumps discontinuously from the low density value $G = 0$ to G_c and then decreases with a square root cusp $G = G_c + \sqrt{\rho - \rho_c}\, 2/\rho_c$, see figure 5.1. The same behavior holds for the probabilities $\tilde{P}$ of having a site occupied by a particle forever blocked, which can be obtained by using equations (5.4) and (5.5). Therefore, though the transition is discontinuous, it has a marginal behavior.

In the case $k = 5$ $s = 2$, by solving equations (5.1), an analogous transition can be detected at a critical density $\rho_c \simeq 0.915$ (see figure 5.2).

Recalling the discussion in previous section, the interpretation of the first order/marginal behaviour of this transition should be that the cluster of forever blocked particles arising for $\rho > \rho_c$ contains a finite fraction of particles and, at the same time, is fragile (i.e. removing by hand a selected tiny fraction of particles can unblock the cluster). Note that this phenomenon is analogous to the one occurring for random quenched p-spin models at the dynamical transition, with cluster of forever blocked particles playing the same role as threshold TAP states in p-spin models. It is also natural to expect, for $\rho \to \rho_c$ from below, a diverging correlation length $\xi \sim (\rho - \rho_c)^{-\frac{1}{2}}$ associated with the rate - in tree levels - of approach to the fixed point. This should be roughly the distance over which vacancies have to be moved to make a given particle mobile.

In order to analyze in more detail the character of this transition, we have performed numerical simulations of KA dynamics on Bethe lattice in the case $k = 3$ $s = 1$, for a lattice with $N = 10^4$ sites. In particular we have computed the local density-density equilibrium correlation function

$$C(t) \equiv \frac{1}{N} \sum_{i=1}^{N} \frac{< n_i(t) n_i(0) > - \rho^2}{\rho - \rho^2} \tag{5.9}$$

and the corresponding dynamical susceptibility

$$\chi_4(t) \equiv N < \left(\frac{1}{N} \sum_{i=1}^{N} n_i(t) n_i(0) - C(t) \right)^2 > \tag{5.10}$$

introduced in [50] to unveil the possible existence of an increasing dynamical correlation length for glass forming liquids (here $< \ >$ stands for the average on Bernoulli product measure at density ρ). The results of numerical simulations indicate the existence of a transition for $\rho_c \simeq 0.89$, which is compatible with value found analytically, see (5.8). Indeed, approaching the transition from low density $C(t)$ displays a two step relaxation which gradually evolves in an infinite plateau for $\rho > \rho_c$ (see figure 5.3). This behavior is the same as the one experimentally detected for glass forming liquids (see section 2.3) and for p-spin glasses. In analogy with the p-spin case, we call Edwards Anderson parameter or q_{EA} the finite hight of the plateau. From the knowledge of the number of forever blocked particles at the critical density, $N\tilde{P}$, we can separate the contribution of these and remaining particles and obtain the following approximation for q_{EA}

$$q_{EA} \equiv \lim_{t\to\infty} C(t) = \lim_{t\to\infty} \frac{1}{N} \sum_{i=1}^{N\tilde{P}} \frac{< n_i(t)n_i(0) > -\rho^2}{\rho - \rho^2} + \\ + \frac{1}{N} \sum_{i=1}^{N-N\tilde{P}} \frac{< n_i(t)n_i(0) > -\rho^2}{\rho - \rho^2} \\ \simeq \frac{\tilde{P} - \rho^2\tilde{P}}{\rho - \rho^2} + \frac{(\rho - \tilde{P})^2}{(\rho - \rho^2)(1 - \tilde{P})} - \frac{\rho^2(1 - \tilde{P})}{\rho - \rho^2} \quad (5.11)$$

where the approximation consists in neglecting density density fluctuation in the second term of last expression. The approximation seems to work pretty well, as it is shown in Fig. 5.3 where we have drawn the approximated value of the Edwards-Anderson parameter with a straight line.

The plots of $\chi_4(t)$ for various densities is in figure 5.4. The dynamical susceptibility seems to diverge approaching the critical density from below. More precisely, what is diverging is the height of the peak and the characteristic time scales at which the peak develops. This is analogous to the behaviour occurring for p–spin fully connected models when approaching the dynamical critical temperature from above [50]. Note that in principle there could be another mechanism, beside the one considered in previous sections, inducing a dynamical transition before ρ_c. Above numerical results show that this is not the case.

5.2.6 Configurational entropy

In previous section we have mentioned that the emergence at ρ_c of fragile clusters of forever blocked particles is analogous to the emergence of fragile sets of threshold TAP states for quenched random p-spin models at the dynamical transition, which have been conjectured to be related to glass transition [53]. Indeed, in both cases this phenomenon gives rise to a dynamical first order/marginal transition and the above numerical results for $C(t)$ and $\chi_4(t)$ in the case $k = 3$ $s = 1$ are very reminiscent of those for p-spin models. For p-spin model dynamical transition is due to ergodicity breaking, which is quantified by a finite jump of configuration entropy $S_c(T) = \ln \mathcal{N}_e/V$, where V is the size of the system and $\mathcal{N}_e$ the number of different ergodic components. The evaluation of such entropy is performed by approximating $\mathcal{N}_e$ with the number of TAP states (free energy valleys) giving the leading contribution to the partition function $\mathcal{N}_{TAP}$. Indeed, $\ln \mathcal{N}_{TAP}/V$ jumps at a critical temperature from zero to a finite value and then decreases by lowering the temperature until it reaches zero at the thermodynamic transition.

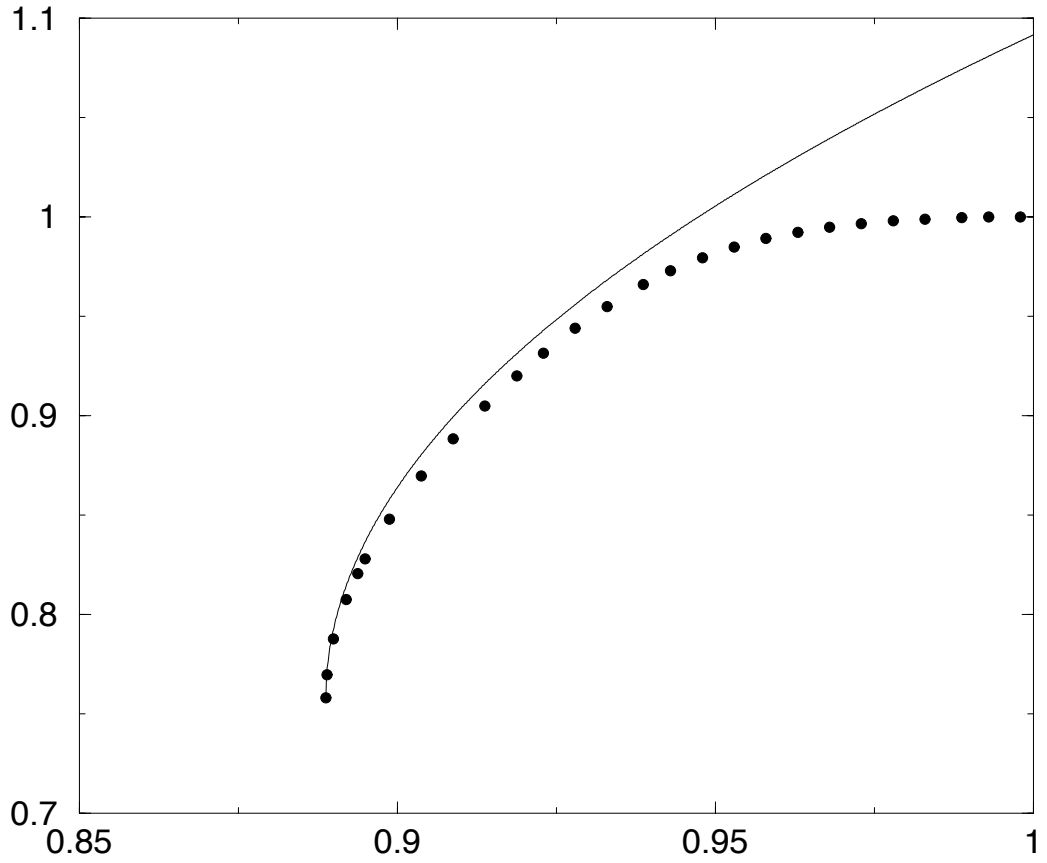

Figure 5.1: G as a function of density for $k = 3$, $s = 1$. Dots are from the stable solution of equations 5.6; solid line is the curve $G = G_c + (\rho - \rho_c)^(1/2)$, which gives the right behavior in the vicinity of ρ_c from above.

For KA model one can find a lower bound for configurational entropy by observing that all the configurations belonging to the same ergodic component must have the same cluster of particles blocked forever, therefore $\mathcal{N}_e$ has to be larger than or equal to the number $\mathcal{N}_b$ of different sets of forever blocked particles. Furthermore, by means of a saddle point evaluation, the entropy at the density ρ can be expressed as

$$S(\rho) = \max_{\rho_B} \left(S^b(\rho, \rho_B) + S^i(\rho, \rho) \right) \tag{5.12}$$

where ρ_B is the density of forever blocked particles for an equilibrium configuration at density ρ, $S^i(\rho, \rho_B)$ is $1/N$ times the logarithm of the number of configurations with the same cluster of $N\rho_B$ particles blocked forever and $S^c(\rho, \rho_B)$ is $1/N$ times the logarithm of $\mathcal{N}_b$. An upper bound on $S^i(\rho, \rho_B)$ can

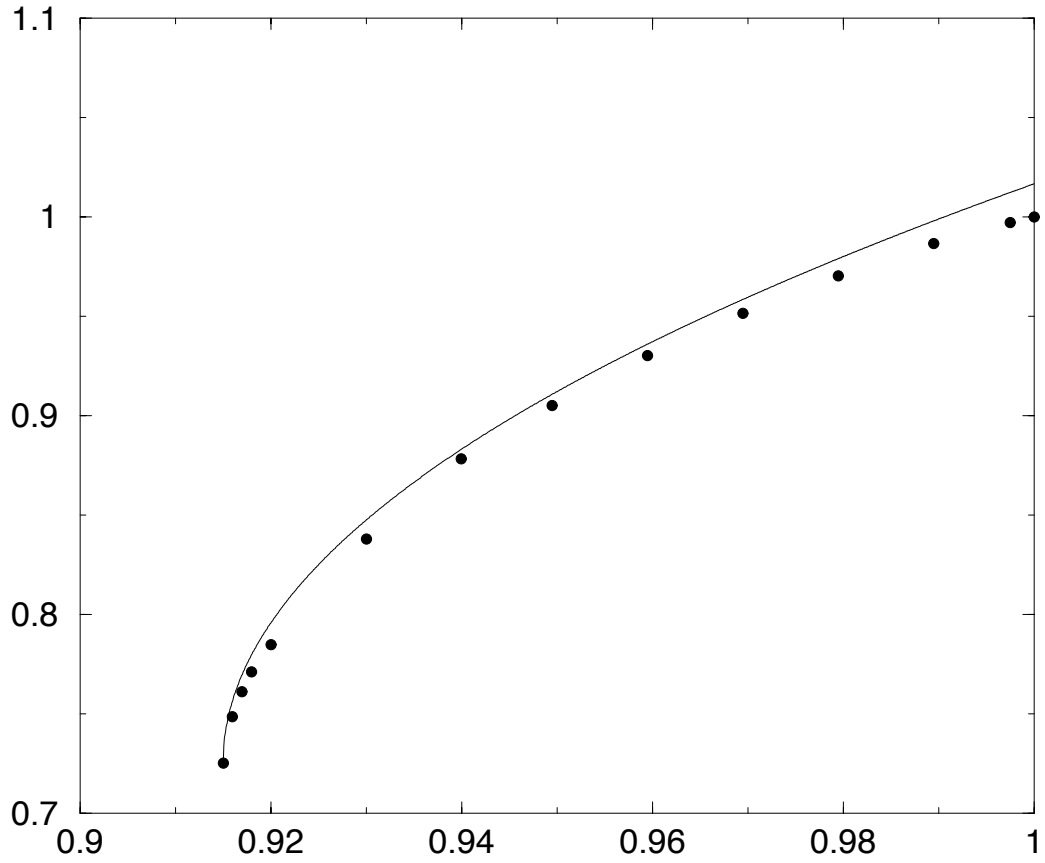

Figure 5.2: $\tilde{P}$ as a function of density for $k = 5$, $s = 2$. Dots are from the solution of equations 5.4 and 5.1; solid line is the curve $P_c + (\rho - \rho_c)^{1/2}$, $P_c \simeq 0.725$ which gives the right behavior in the vicinity of ρ_c from above.

be readily calculated by considering that $\exp NS^i(\rho, \rho_B)$ is smaller than the number of ways of putting $N\rho - N\rho_B$ particles on $N - N\rho_B$ sites, therefore

$$S^i(\rho, \rho_B) \leq (1-\rho_B)\ln(1-\rho_B) - (\rho-\rho_B)\ln(\rho-\rho_B) - (1-\rho)\ln(1-\rho) \quad (5.13)$$

where we have used Stirling formula. Since $S(\rho) = -\rho\ln\rho - (1-\rho)\ln(1-\rho)$ and the value of ρ_B which maximizes (5.12) is the typical one, i.e. $\tilde{P}$, we find the following lower bound on configuration entropy

$$S^c(\rho) \geq S^b(\rho, \tilde{P}) \geq -\rho\ln\rho - (1-\tilde{P})\ln(1-\tilde{P}) + (\rho-\tilde{P})\ln(\rho-\tilde{P}) \quad (5.14)$$

which is zero when $\tilde{P} = 0$, i.e. for $\rho > \rho_c$. In figure 5.5 we plot this lower bound as a function of density in the case $k = 3$, $s = 1$. Since, from above

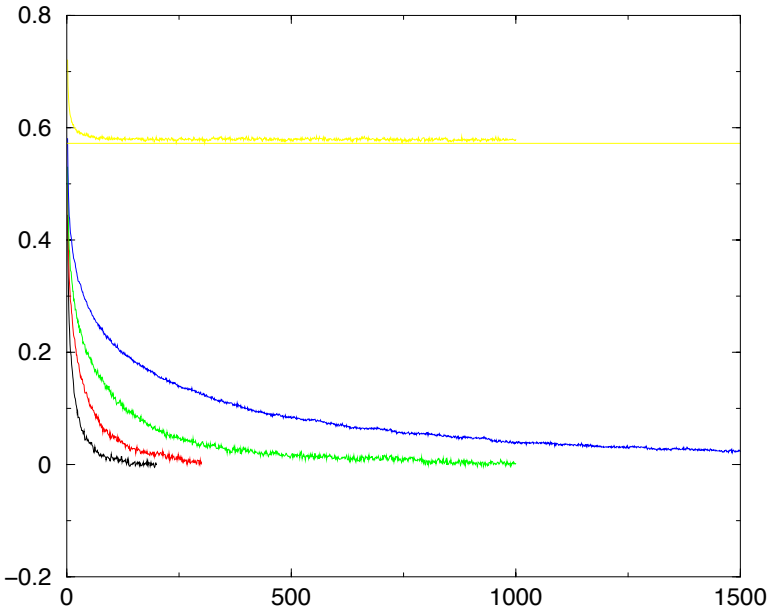

Figure 5.3: $C(t)$ as a function of time (in 50 MCS) for densities $0.85, 0.86, 0.87, 0.875, 0.9$ (N=10000) (from down to up). The dynamical transition takes place clearly between the densities 0.875 and 0.9. The straight line is the value of the Edwards-Anderson parameter obtained by the approximation discussed in the text.

numerical results, there seems to be no transition before ρ_c, it is reasonable to think that $S^c(\rho)$ is zero for $\rho < \rho_c$. Therefore, this hypothesis and above lower bound imply that the configurational entropy jumps form zero to a finite value at ρ_c. Then, for $\rho > \rho_c$, the configurational entropy decreases and goes to zero at $\rho = 1$. Note that this is exactly what happens in p-spin models, except that now there is no thermodynamic transition for $\rho < 1$.

5.3 Bethe lattice with loops

In order to investigate whether the absence of loops is the essential reason for the existence of a phase transition on Bethe lattices, one can consider a tree structure with loops.

Consider the rooted tree composed of triangles with one vertex pointing downwards and the other two vertices each being the bottom vertex of another triangle and hence the root of a tree. Then define Bethe lattice with triangular loops as the graph obtained by taking two such lattices and connecting the free vertices of the two roots (see figure 5.6). The coordination

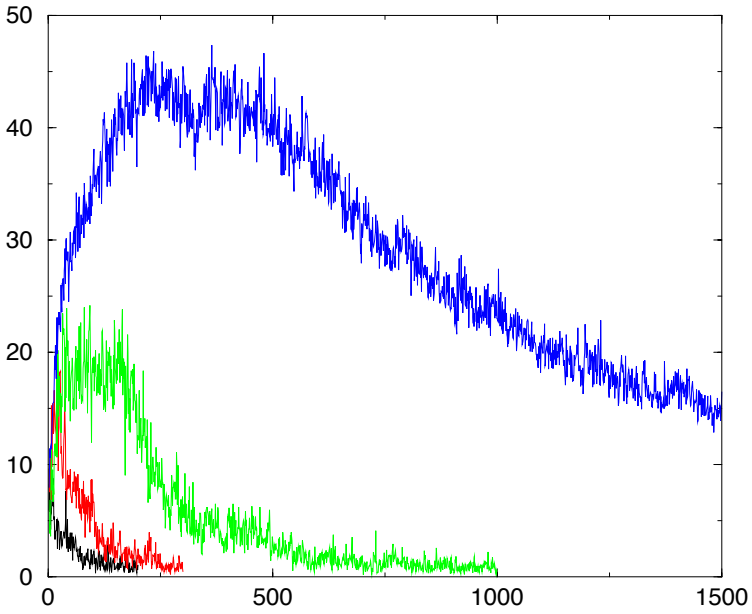

Figure 5.4: $\chi_4(t)$ as a function of time (in 50 MCS) for densities $0.85, 0.86, 0.87, 0.875$ (N=10000) (from down to up).

number of such tree is $z = 4$ and the branching ration $k = 2$. In other words, we consider a cactus tree (Husimi tree) [31] with main clusters of three vertex and three branches departing from each cluster.

Consider KA model with $s = 1$ on above defined lattice and focus on the set $\mathcal{E}_i$ including configurations for which the bottom vertex of triangle i and at least one of the top ones are occupied by particles which can never move, knowing that the other two sites of the triangle below i are occupied too. Let P be the probability of such event. If a configuration η has all the three sites of i occupied and $\eta \in \cap_{j=1}^{4} \mathcal{E}_i^j$, where $i^1, \ldots, i^4$ are the triangles two level up with respect to i, then $\eta \in \mathcal{E}_i$. The same is true for any configuration η with the three sites of i occupied and $\eta \in \cap_{j=1}^{3} \mathcal{E}_{\tilde{i}^j}$, where $\tilde{i}^1, \ldots \tilde{i}^3$ is any of the permutation of all the triangles two level up except one. Therefore

$$P \geq \rho^3 \left(P^4 + 4P^3(1-P) \right) \tag{5.15}$$

which is equivalent to $C \leq f(C)$ with $C \equiv 1-P$ and $f(x) \equiv \rho^3 \left(x^4 + 4x^3(1-x) \right)$. The same argument as in section 5.2.1 allows to prove that there exists a transition at a finite density from a region where $P = 0$ to a region where P is finite. More naturally, the critical density can be defined as the value of density at which the probability $\tilde{P}$ that a given site is occupied by a particle blocked forever goes from zero to a finite value. Such transition exists be-

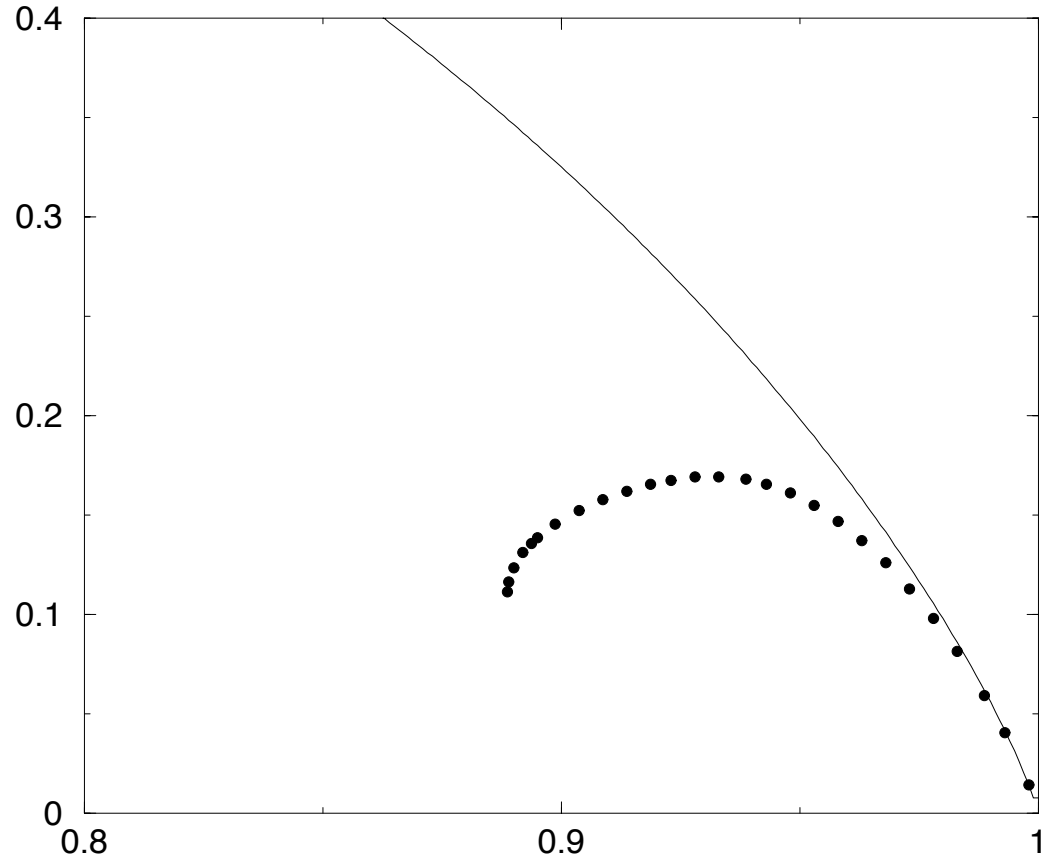

Figure 5.5: Dots indicate the lower bound $S^b(\rho)$ on configurational entropy as a function of density for $k = 5$ $s = 1$ obtained from equation (5.14) and numerical solution of equations (5.4), (5.5). Below the critical density $\rho_c \simeq 0.888$, this lower bound jumps to zero. Straight line is the equilibrium entropy.

cause $\tilde{P} \geq P_1^4 \geq P^4$, where P_1 is the probability that the bottom vertex of a triangle is occupied and the particle can never move, knowing that also the remaining two vertex of the triangle below are occupied.

Let $\mathcal{E}_i^c$ be the complement of $\mathcal{E}_i$ on the configuration space. If $\eta \in \cap_{j=1}^4 \mathcal{E}_{ij}^c$ or $\eta \in \cap_{j=1}^3 \mathcal{E}_{ij}^c$, a vacancy can be taken to the bottom vertex in i without making use of branches below. Therefore

$$P \leq 1 - (1-P)^4 - 3P(1-P)^4 \tag{5.16}$$

which implies (see section 5.2.2) that P has a finite jump at the transition.

The same arguments can be extended to KA model with any choice of s on Bethe lattices with n-polygonal loops for any n, i.e. trees composed by

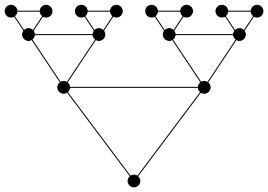

Figure 5.6: Branch of a Bethe lattice with triangular loops. Dots denotes sites, lines denotes edges of the lattice.

polygons of n vertex, each being the vertex of another polygon.
To prove the existence of the transition, it is sufficient to define the set of configurations $\mathcal{E}_i$ for which the bottom vertex and at least other $n-2$ vertex of polygon i are occupied, knowing that the other $n-1$ sites of polygon below are occupied too. By the same argument as above, we can bound the probability P of such event as

$$P \geq \rho^n \left(P^{2^n} + 2^n P^{2^n-1}(1-P)\right) \tag{5.17}$$

which implies again that $P > 0$ for sufficiently high density.
To prove that the transition is discontinuous we focus on the event that the bottom site of the polygon is occupied and the particle cannot move, knowing that all the sites of the polygon below are occupied too. The probability P_1 of this event, in all the cases $s < k-1$ can be bounded as

$$P_1 \leq 1 - (1-P_1)^{2^n} - 2^n P_1^{2^n-1}(1-P_1) \tag{5.18}$$

which implies again that the transition is discontinuous.

We could also introduce loops in a different way. Consider for example a Bethe lattice with connectivity 4 in which each site is replaced by a square lattice $\Lambda \in \mathbb{Z}^2$ with linear size L. As before, arrange the lattice as a tree with 3 branches going up and one going down. Then consider a square, I, and focus on the event that there are no vacancies at the vertices of I and, without taking advantage of the configuration in the bottom square, one cannot bring any vacancy on such vertices. Let P be the probability of such event. If all the L^2 sites of square I are filled and at least two of the squares above have all the vertices always occupied, than I will have for sure all the vertices occupied. Therefore

$$P \geq \rho^{L^2} \left(P^3 + 3P^2(1-P)\right) \tag{5.19}$$

and, by an argument analogous to the one in section 5.2.1, the existence of a transition follows. Consider than the event that, without taking advantage of

possible vacancies in the bottom square, one cannot frame the configuration in I, i.e. reach a configuration with all the boundary sites of I empty. Call P_f the probability of such event. If at least two of the three squares one level above I can be framed, then square I can be framed too. Therefore

$$P_f \leq 1 - (1 - P_f)^3 - 3(1 - P_f)^2 P_f \tag{5.20}$$

which is incompatible with a continuous transition. Therefore, also for this kind of lattices, we have proven the existence of a discontinuous transition. Note that this way of introducing loops interpolates between the simple Bethe lattice, for $L = 1$, and the square lattice $\Lambda = \mathbb{Z}^2$, for $L = \infty$. Therefore, in the limit $L \to \infty$, the critical density $\rho_c(L)$ should go to one.

In general, the existence of finite loops can make the motion of particles more easy. Indeed, there are configurations in which a collection of two or more vacancies ejected from one branch can be absorbed into another and trigger the ejection of a larger number of vacancies from the second branch. This process can depend on configurations arbitrarily far up in the two branches. The ejected vacancies could in principle extend their influence arbitrarily further down the tree and render any chosen particle mobile, even when the density is above the critical value for the Bethe lattice without loop. Nevertheless, above results show that for low enough vacancy concentration this is not the case and the system is in a partially frozen state like that of the simple Bethe lattices.

5.4 Conclusions

In this chapter we have analyzed KA model on an infinite tree–like graph with fixed connectivity $k + 1$. This corresponds to the mean field version of the usual KA model on hypercubic lattices. The tree–like structure of the lattice enables analytic calculations by iteration, from which we find that at a finite critical density ρ_c a dynamical ergodic/non–ergodic transition occurs, which corresponds to the transition from a diffusive regime to a partially frozen state. Indeed, by bootstrap percolation arguments we establish that at ρ_c an infinite cluster of forever blocked particles emerges. More precisely, below ρ_c the fraction of forever blocked particles is zero and jumps at ρ_c to a finite value[3] which goes to one for $\rho \to 1$, therefore the transition is discontinuous. However, for $\rho \to \rho_c$ from above, the fraction of blocked

[3]We have proven that these results hold for any choice of the parameter s and the connectivity, even for Bethe lattices with finite size loops. The only exception is the case $s = k - 1$ for which, as explained in section 5.2.4 the transition corresponds to a conventional percolation transition and it has a continuous character.

particles (i.e. the discontinuous order parameter) decreases with a square root cusp, which is indicative of a diverging length and time scales. This probably means that, though for $\rho > \rho_c$ there exists with finite probability an infinite cluster of blocked particles, such cluster is very fragile near ρ_c. In other words it can be unblocked by a small perturbation, like removing by hand a tiny fraction of particles. Therefore, this mean field transition has both aspects of first and second order transition. This is reminiscent of the character of the putative ideal glass transition at Kauzmann temperature (see section 2.1) and of the behaviour of p–spin models with quenched disorder at the dynamical transition (see section 2.4) [4]. In order to analyze in more detail this analogy, we have performed numerical Monte Carlo simulations focusing on the behaviour of the density density correlation function $C(t)$ and on the corresponding dynamical susceptibility $\chi_4(t)$. By approaching the transition from below $C(t)$ displays a two step relaxation and develops an infinite plateau for $\rho \to \rho_c$, while χ_4 seems to diverge. Again, these results have the same features as for p–spin models.

The results of previous chapter establish that such mean field dynamical transition is completely destroyed in finite dimensions. Moreover, the ergodicity proof allows us to identify the exponentially rare processes that restore ergodicity on the hypercubic lattice. In other words, these corresponds to the *activated processes* that allow the jump of the mean field dynamical barriers in finite dimensions (see section 2.4). This knowledge, together with the above observation that the mean field transition is analogous to the one for p–spin models, could be a useful ground to a further investigation of how the mean field results for these disordered model are modified in finite dimensions.

Note that there does not exists an *upper critical dimension* above which mean field theory gives the exact result. However, in next chapter we will explain how a ghost of the mean field transition survives on the hypercubic lattices. More precisely, we will show that the Bethe lattice transition is substituted by a dynamical crossover which is possibly very sharp for high spatial dimensions (this in some sense confirms the natural idea that Bethe lattice should crudely approximate the high dimensional hypercubic lattice).

[4] In this analogy, the cluster of forever blocked particles has the same role as the threshold TAP states for p–spin models.

Chapter 6

KA model on hypercubic lattices: dynamics

In this chapter we consider dynamics of KA model on hypercubic lattices. First we prove that there is no dynamical diffusive/non–diffusive transition at any finite density, namely the self diffusion coefficient D_S of the tagged particle is strictly positive at any $\rho \in [0,1]$. Then we analyze the density dependence of D_S, focusing on the bi–dimensional case with $s = 1$. In the high density regime, diffusion is guaranteed by the cooperative slow motion of mobile cores and D_S vanishes for $\rho \to 1$ as the density of these rare regions, which goes to zero faster than any power law of $(1 - \rho)$. For lower densities, a different diffusion mechanism is also present and a crossover to a power law behaviour for D_S takes place. Finally, we discuss a possible explanation of the stretched exponential relaxation of correlation functions which occurs in the high density regime.

6.1 Self diffusion coefficient

In section 2.5.2 we have discussed the behaviour of a tagged particle on an infinite lattice. In the diffusive rescaling, the position of the tracer converges to a Brownian motion provided the density dependent diffusion coefficient, D_S, is strictly greater than zero. In the following we analyze KA model to establish whether a transition from a positive to a zero value of D_S takes place at a finite density. Indeed, such diffusive/non–diffusive transition has been advocated by previous numerical simulations [1] for the case $d = 3$ $s = 2$. Note that both the key ingredients for diffusivity in the SSEP case, namely that a single vacancy can move freely in an otherwise totally filled lattice and that the tagged particle can move to any empty neighboring site (see section

2.5.2), do not hold. However, one can identify a different mechanism related to the cooperative motion of cores, which guarantees diffusivity.

Let us first recall the definition of cores given in chapter 4 and show that cores are mobile. Consider a frameable region constructed from an initial nucleus of empty sites through the growing procedure. The core is the hypercube of linear size ξ centered around the empty nucleus. The density dependent value of ξ, given in chapter 4 for different d and s, is chosen in order that the probability to extend the core to infinity in a frameable way is almost one. For example in the two–dimensional case with $s = 1$, ξ is such that there are with almost unit probability at least two vacancies on any row of length ξ adjacent to the core. Therefore, since to move a frameable square of one step it is sufficient to find at least two vacancies on the subsequent row in the step direction, we expect that cores can diffuse in typical regions of the system. The same argument holds in any dimension with the result that cores are always mobile. In other words, the typical diffusion time τ_ξ for a core is finite. Moreover, from the properties of frameable configurations, if the tagged particle is inside a frameable core it can be moved to any of its nearest neighbor sites through a path of at most $O(\xi^d)$ moves which involve only occupation variables inside the square. Therefore, inequality $D_S \geq n_M \, \xi^2/\tau_\xi \, 1/\xi^d > 0$ holds, where $n_M \sim 1/\Xi^d$, τ_ξ and ξ are respectively the density, the typical relaxation time and the size of mobile cores[1]. In other words, $D_S > 0$ at any density $\rho < 1$ and the tagged particle diffuses.

Above argument is turned into a proof in the following section, where we establish a lower bound for D_S which is strictly positive at any $\rho < 1$. The proof is given for the $d = 2$ $s = 1$ case, but it can be generalized to higher dimensions. In section 6.1.2 and 6.1.3 we estimate the density dependence of τ_ξ and discuss the behaviour of D_S for $\rho \to 1$. The result is that D_S goes to zero faster than any power law of $1 - \rho$, the dominant factor being the density of mobile cores. By running Monte Carlo simulations for the case $d = 2$, $s = 1$ we find a good agreement with the predicted form of D_S. Finally, in section 6.1.4, we discuss a different diffusion mechanism which is effective at low densities and gives rise to a crossover to a different behavior for D_S.

[1]Note that here $1/\xi^d$ is an adimensional number (more precisely we should write it as a^d/ξ^d with a the lattice step) which comes from the number of exchanges in the sequence needed to move the tagged particle. Therefore the diffusion coefficient has the right physical dimensions.

6.1.1 Proof of positive lower bound for d=2 s=1

In this section we consider KA model on a square lattice with parameter $s = 1$ and establish a lower bound for D_S which is strictly positive at any finite density $\rho < 1$. This rules out the possibility of a diffusive/non–diffusive transition. As already mentioned, one cannot readily generalize the proof outlined in section 2.5.2 for the SSEP case, nor the modified version of section 3.3.2. Difficulties arise from the fact that neither single vacancies, nor any finite number of vacancies can freely move trough the lattice. However, the diffusion mechanism described in previous section allows us to introduce a proper auxiliary process and then proceed by two steps. First, by using the knowledge of paths connecting any two frameable configurations, we show that the diffusion coefficient of KA is bounded from below by the diffusion coefficient of the auxiliary process, namely $D_S > D_S^{aux} c$ with $c > 0$. Then we prove that the auxiliary process is diffusive at any density, i.e. $D_S^{aux} > 0$, which allows us to conclude $D_S > 0$. This second step is performed through the mapping of the auxiliary process to a random walk in random environment. The choice of the auxiliary process is based on the following observation.

Consider a configuration on the infinite lattice $\mathbb{Z}^2$ sorted at random with Bernoulli measure at density ρ and focus on a sublattice Λ_Ξ of linear size $\Xi(\rho)$. From the results in section 4.4, we know that the restriction of the configuration to Λ_Ξ is frameable with probability almost one. Therefore in the initial configuration the tagged particle is with very high probability inside a frameable region of size Ξ. Moreover, if one divides the infinite lattice in sublattices of linear size Ξ, there exists with unit probability a percolating cluster of sublattices such that the initial configuration restricted to each sublattice is frameable. Thus, if we define an auxiliary process such that during the dynamics frameable sublattices remain frameable and the tagged particle remains always inside the percolating cluster, we can reconstruct any move of such process through a finite sequence of moves allowed by KA. Indeed, any nearest neighbor move in a frameable configuration of linear size Ξ can be performed through a sequence of elementary moves allowed by KA rules and the length of such path is at most of order Ξ^2. Therefore, through a path argument we would obtain a bound on the self diffusion coefficient for KA with the one of the auxiliary process, i.e. inequality $D_S > cD^{aux}$ with $c > 0$. The main difficulty lies in choosing an auxiliary process such that the above condition is true and at the same time the rates are not too restrictive, so that the auxiliary process itself has positive diffusion coefficient.

Let us introduce some notation. Consider the following subsets of $\mathbb{Z}^2$

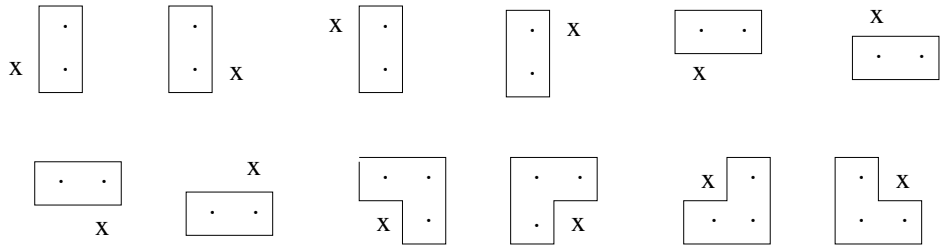

Figure 6.1: Sites inside the closed line correspond, form left to right an up down, to sets $R_x^{+1}, R_x^{-1}, R_x^{+2}, R_x^{-2}, R_x^{+3}, R_x^{-3}, R_x^{+4}, R_x^{-4}, Q_x^{+1}, Q_x^{-1}, Q_x^{+2}, Q_x^{-2}$

$$\begin{aligned}
R_x^{(\pm 1)} &:= \big\{(x_1 \pm e_1, x_2), (x_1 \pm e_1, x_2 + e_2)\big\} \\
R_x^{(\pm 2)} &:= \big\{(x_1 \pm e_1, x_2), (x_1 \pm e_1, x_2 - e_2)\big\} \\
R_x^{(\pm 3)} &:= \big\{(x_1, x_2 \pm e_2), (x_1 + e_1, x_2 \pm e_2)\big\} \\
R_x^{(\pm 4)} &:= \big\{(x_1, x_2 \pm e_2), (x_1 - e_1, x_2 \pm e_2)\big\} \\
Q_x^{(\pm 1)} &:= \big\{(x_1, x_2 + e_2) \cup R_x^{(\pm 1)}\big\} \\
Q_x^{(\pm 2)} &:= \big\{(x_1, x_2 - e_2) \cup R_x^{(\pm 2)}\big\}
\end{aligned} \tag{6.1}$$

R_x^i are the eight possible couples of neighboring sites $\{y, z\}$ such that $y, z \neq x$ and $|y-x| = 1$ or $|z-x| = 1$, in other words one among y and z is neighboring site to x and the couple does not contain x; Q_x^i are the four possible choices of three sites that, together with x, form a two by two square (see figure 6.1.1). We next define $\eta^{R_x^{+i}, R_x^{-i}}$, for $i \in \{\pm 1, \ldots, \pm 4\}$ as the configuration obtained from η by exchanging the occupation numbers in R_x^{+i} with the corresponding ones in R_x^{-i}

$$\big(\eta^{R_x^{+i}, R_x^{-i}}\big)_z := \begin{cases} \eta_{x \mp 2e_1} & \text{if } \ z \in R_x^{\pm i} \\ \eta_z & \text{if } \ z \notin R_x^{+i} \cup R_x^{-i} \end{cases} \tag{6.2}$$

Then, for $i \in \{\pm 1, \pm 2\}$, we introduce the events

$$\mathcal{A}_x^i := \big\{\eta \in \Omega \,:\, \eta_z = 0 \, \forall z \in Q_x^i\big\} \tag{6.3}$$

i.e. configurations having all the sites of set Q_x^i empty and

$$\mathcal{B}_x^i := \big\{\eta \in \Omega \,:\, \eta_z = 1 \ \ \forall z \in R_x^i, \, \eta \in \mathcal{F}_x^i\big\} \tag{6.4}$$

for $i \in \{\pm 1, \pm 2, \pm 3, \pm 4\}$, where

$$\mathcal{F}_x^i := \big\{\eta \in \Omega \,:\, \exists \Lambda \in \mathcal{S} : \ R_x^i \subset \Lambda, \ \delta(R_x^i, \partial\Lambda) \geq 3, \ \eta|_\Lambda \in \mathcal{F}_\Lambda\big\} \tag{6.5}$$

and $\mathcal{S}$ is the set of squares in $\mathbb{Z}^2$ of linear size at most Ξ. Recall that $\partial\Lambda$ is the boundary of square sublattice Λ, $\eta|_\Lambda$ is the restriction of a configuration to Λ, $\mathcal{F}_\Lambda$ is the set of frameable configuration in Λ and $d(A,B)$ is the minimum over the Euclidean distance of all the couples $\{x,y\}$ with $x \in A$ and $y \in B$. In other words, $\mathcal{B}_x^i$ is the set of configurations in which a pair of sites adjacent to x (region R_x^i) is filled and is internal to a frameable square of linear size at most Ξ. Let $\eta(0)$ be the configuration and $x(0)$ the position of the tagged particle at time zero, we define $\bar{\eta}(0)$ as

$$\bar{\eta}(0)_z = \begin{cases} 1 & \text{if } \ z \in Q_x^i \ \ \forall i \\ \eta_z & \text{otherwise} \end{cases} \tag{6.6}$$

The dynamics of the auxiliary process is chosen as follows:

(i) The tagged particle can move from x to $x+e_1$. The jump has rate one if $\eta \in \mathcal{A}_x^{+1}$ and $\bar{\eta}(0) \in \mathcal{B}_x^{+1}$ or $\eta \in \mathcal{A}_x^{+2}$ and $\bar{\eta}(0)\mathcal{B}_x^{+2}$, zero otherwise;

(ii) The tagged particle can move from x to $x-e_1$. The jump has rate one if $\eta \in \mathcal{A}_x^{-1}$ and $\bar{\eta}(0) \in \mathcal{B}_x^{-1}$ or $\eta \in \mathcal{A}_x^{-2}$ and $\bar{\eta}(0) \in \mathcal{B}_x^{-2}$, zero otherwise;

(iii) The tagged particle can move from x to $x+e_2$. The jump has rate one if $\eta \in \mathcal{A}_x^{+1}$ and $\bar{\eta}(0) \in \mathcal{B}_x^{+1}$ or $\eta \in \mathcal{A}_x^{-1}$ and $\bar{\eta}(0) \in \mathcal{B}_x^{-1}$, zero otherwise;

(iv) The tagged particle can move from x to $x-e_2$. The jump has rate one if $\eta \in \mathcal{A}_x^{-2}$ and $\bar{\eta}(0) \in \mathcal{B}_x^{-2}$ or $\eta \in \mathcal{A}_x^{+2}$ and $\bar{\eta}(0) \in \mathcal{B}_x^{+2}$, zero otherwise;

(v) Configuration η can be transformed in $\eta^{R_x^{+1},R_x^{-1}}$, namely the exchange of occupation variables in R_x^{+1} and R_x^{-1} can be performed. The move has rate one if $\eta \in \mathcal{A}_x^{+1}$ and $\bar{\eta}(0) \in \mathcal{B}_x^{-1}$ or $\eta \in \mathcal{A}_x^{-1}$ and $\bar{\eta}(0) \in \mathcal{B}_x^{+1}$, zero otherwise.

(vi) Configuration η can be transformed in $\eta^{R_x^{+2},R_x^{-2}}$, namely the exchange of occupation variables in R_x^{+2} and R_x^{-2} can be performed. The move has rate one if $\eta \in \mathcal{A}_x^{+2}$ and $\bar{\eta}(0) \in \mathcal{B}_x^{-2}$ or $\eta \in \mathcal{A}_x^{-2}$ and $\bar{\eta}(0) \in \mathcal{B}_x^{+2}$, zero otherwise.

(vii) Configuration η can be transformed in $\eta^{R_x^{+3},R_x^{-3}}$, namely the exchange of occupation variables in R_x^{+3} and R_x^{-3} can be performed. The move has rate one if $\eta \in \mathcal{A}_x^{+1}$ and $\bar{\eta}(0) \in \mathcal{B}_x^{-3}$ or $\eta \in \mathcal{A}_x^{+2}$ and $\bar{\eta}(0) \in \mathcal{B}_x^{+3}$, zero otherwise;

(viii) Configuration η can be transformed in $\eta^{R_x^{+4},R_x^{-4}}$, namely the exchange of occupation variables in R_x^{+4} and R_x^{-4} can be performed. The move has rate one if $\eta \in \mathcal{A}_x^{-1}$ and $\bar{\eta}(0) \in \mathcal{B}_x^{-4}$ or $\eta \in \mathcal{A}_x^{-2}$ and $\bar{\eta}(0) \in \mathcal{B}_x^{+4}$, zero otherwise.

In the following we will show that the above choice of the rates is a suitable choice to perform the proof of diffusivity, since the auxiliary process have a positive diffusion coefficient and any move can be reconstructed by a finite sequence of elementary moves allowed by KA.

Consider an initial configuration such that the tagged particle is inside a frameable square of size Ξ and such all the sites in at least one of the sets $Q^{(\pm 1)}_{x(0)}, Q^{(\pm 2)}_{x(0)}$ (see figure 6.1.1) are empty , where $x(0)$ is the position of the tagged particle (i.e. $\eta(0) \in \mathcal{A}^i_x$ for some i). Then, both conditions will hold at any subsequent time. Indeed, moves (i)–(iv) are such that the tagged particle remains always inside the empty two by two square. On the other hand, moves (v)–(viii) are devised in order that the only vacancies that are moved during the process are those which belong at time zero to this two by two square, therefore sublattices of size Ξ that are frameable at time zero remain frameable at later times[2]. The fact that moves for the auxiliary process occur always inside frameable regions of size at most Ξ implies that any move can be performed through a finite sequence of elementary moves allowed by KA. Indeed, by the properties of frameable configurations, any move inside a configuration of size Ξ can be performed by a sequence of order $O(\Xi^2)$ moves with positive rate for KA dynamics. By using path arguments analogous to those in section 3.3.2 it is then possible to establish inequality $D_S \geq c D_S^{aux}$, with c positive. Let us shortly recall how this argument works and emphasize an important difference occurring in this case. In section 3.3.2 we have defined an auxiliary process such that any move of the latter can be performed by a finite path of at most n nearest neighbor moves allowed for the considered model (for example $n = 16$ for the first class, $k = 1$, of models). Such path does not dependent on the choice of the configuration. Then, we have rewritten each term of the variational formula (2.15) of D_S^{aux} as a telescopic sum on the exchanges along this path. Finally, by using Cauchy Schwartz inequality, the fact that each possible move is used at most twice in the path and by performing an exchange of variables, we concluded that $D_S^{aux} \leq 2n^2 D_S$. Here things can be done analogously, with the length n of the paths at most Ξ^2. However, the path depends on the whole configuration (indeed the sequence of allowed move to connect a frameable configurations to the framed one in order to perform a pair exchange depends on the position of the vacancies, see section 4.4 and figure 4.2). This yields in the inequality among D_S^{aux} and D_S an overall factor $\Xi^2!$ besides the factor $n^2 = \Xi^4$. Let us explain in some detail this statement. With a path argument analogous to the one done before, we rewrite each term in D_S^{aux} corresponding to the

[2]More precisely, sublattices that are frameable in $\bar{\eta}(0)$ are frameable also for $\eta(t)$ at any t.

exchange of particles in R_x^i, R_x^{-i} as a telescopic sum over allowed exchanges for KA, namely

$$\Big(f(\eta^{R_x^{+i},R_x^{-i}}) - f(\eta)\Big)^2 \leq \Xi^2 \sum_{j=0}^{n} c_{x_{j-1},x_j}(\eta_j)\left(f(T_{x_{j-1},x_j}\eta_j) - f(\eta_j)\right)^2 \quad (6.7)$$

where $c_{x,y}$ are the jump rate of KA model, $\eta_0 = \eta, \eta_1, \ldots, \eta_n = \eta^{R_x^{+i},R_x^{-i}}$ is the path of allowed elementary moves which connects η to $\eta^{R_x^{+i},R_x^{-i}}$ and such that $\eta_i = \eta_{i-1}^{x_{i-1},x_i}$ for a couple of nearest neighbors $\{x_i, x_{i-1}\}$. To obtain above inequality we used Cauchy Schwartz inequality and the fact that $n \leq \Xi^2$. In order to obtain from left and right hand side the terms which appear in the variational formula (2.15) for the auxiliary process and for KA, respectively, we should average inequality (6.7) over Bernoulli measure conditioned to have a particle in zero. As we already emphasized, the sequence $x_0 \ldots x_n$ of sites in which the exchange is done, depends on the positions of vacancies in configuration η. Therefore, if we do the change of variable $\eta_i \to \eta$ in (6.7) and use the invariance of measure under exchange of variables, many different terms on the left can give rise to the same term on the right. Actually, the crucial thing to know is the following. To each configuration η for which the exchange is allowed by the auxiliary process, associate the correspondent path $\eta_0, \ldots, \eta_n$ in configuration space[3]. Then, for each elementary nearest neighbor jump e, denote by $\mathcal{N}_e$ the number of different configurations η that use such exchange and let $\mathcal{N} \equiv max_e\, \mathcal{N}_e$. Therefore $\mathcal{N}$ is the overall factor coming from possible overcounting of configuration when going from the mean of the left hand side of (6.7) to the terms in the variational formula (2.15) for D_S. Moreover, since each path is composed of moves internal to the frameable region of size $\ell \leq \Xi$ which contains the tagged particle, $\mathcal{N}$ is for sure less or equal to the total number of configurations inside a square of size Ξ, namely inequality $\mathcal{N} \leq 2^{\Xi^2}$ holds. Therefore, we finally obtain

$$D_S \geq (1-\rho)^3 \;\; \mu_{\rho,\Xi}(\mathcal{F}) \;\; \frac{1}{\Xi^2 2^{\Xi^2}} \;\; D_S^{aux} \quad (6.8)$$

The term $(1-\rho^3)\mu_{\rho,\Xi}(\mathcal{F})$ comes from the condition that the configuration at time zero should have the tagged particle with three vacancies around and be inside a frameable square of size at most Ξ and D_S^{aux} is the diffusion coefficient of the auxiliary process subject to this condition. This ends the first part of the proof.

[3]Of course there could be different sequences to perform the same move. However, one can always give a prescription associating one of them for any choice of η and any give exchange.

Let us now prove that $D_S^{aux} > 0$, i.e. that diffusivity holds for the auxiliary process. In this case, the mechanism which guarantees diffusivity is different from the one of both SSEP and the processes considered in section 3.3.2. For SSEP, the possible moves of the auxiliary process are the following. The tagged particle can move from x to $x + e_1$ or $x - e_1$ provided the final site is empty; the occupation variables of sites $x - e_1$ and $x + e_1$ can be exchanged. It is immediate to check that, by starting with at least a vacancy in the sites adjacent to the tagged particle in direction e_1, this condition will be always fulfilled at later times. Therefore it is possible to move the tagged particle in both direction e_1 and $-e_1$ either directly or via a previous exchange $\eta \to \eta^{x+e_1,x-e_1}$. This implies that the auxiliary process has a strictly positive self diffusion constant, which can be proved by mapping it to a unidimensional random walk. Analogously, the auxiliary process we introduced for KA is such that if the tagged particle is at time zero in a two by two square of vacancies (i.e. $\eta(0) \in \mathcal{A}^i_{x(0)}$ for some i) and inside a larger frameable square of size at most Ξ, both conditions will be always fulfilled at later times. However, it is not true that the tagged particle can always be moved in a chosen direction e_i through a proper path. For example, if we want to move it in direction e_1 this is possible only if $\eta \in \mathcal{A}^{+1}_x$ or $\eta \in \mathcal{A}^{+2}_x$. Otherwise, if $\eta \in \mathcal{A}^{-1}_x$ or $\eta \in \mathcal{A}^{-2}_x$, the move is allowed only if before one makes the exchange $\eta \to \eta^{R^{+1}_x, R_x - 1}$ or $\eta \to \eta^{R^{+2}_x, R_x - 2}$, respectively. However these exchanges (which are the analogous of exchange $\eta \to \eta^{x-e_i,x+e_i}$ for SSEP) are not always allowed. Indeed (see rules (v)–(viii)) they have positive rate only if in the initial configuration the rectangular regions R^{-1}_x, respectively R^{-2}_x, do not contain vacancies and are inside a frameable square of size at most Ξ. Note that the rate of such exchanges (i.e. the rate of the exchange $\eta \to \eta^{R^{+1}_x, R_x - 1}$ and $\eta \to \eta^{R^{+2}_x, R_x - 2}$ conditioned to the fact that $\eta \in \mathcal{A}^{-1}_x$ or $\eta \in \mathcal{A}^{-2}_x$ respectively) does not depend on the configuration η, but is fixed once for all by the choice of the initial configuration $\eta(0)$. In other words the choice of the initial configuration fixes the *good* rectangles, i.e. the rectangle for which this rate is one. This observation will allow us to map the motion of the two by two square of three vacancies plus tagged particle as a random walk in a random environment corresponding to the cluster of good rectangles. We emphasize that this cluster does not changes during dynamics, therefore the randomness of the environment is *quenched*. Note that the probability p_g for a given rectangle to be good is greater than ρ^2 (the probability that both the sites inside the rectangle are occupied) multiplied for the probability that it is inside a frameable region of size at most Ξ (which is almost one). Therefore in the high density regime p_g is well above the threshold of conventional site percolation. This implies that

with unit probability the initial configuration has a percolating cluster of good rectangles. By recalling that above the percolation threshold random walk on random environment has a positive diffusion coefficient [35], we will therefore prove that the diffusion coefficient of the auxiliary process is strictly positive, which ends the proof. In the following we will sketch the proof of above argument in some detail.

Let $\eta_{(0,0)} = \eta(0)$ be the initial configuration. Let us define the following sequence of configurations $\eta_{(m,n)}$ for $(m,n) \in \mathbb{Z}^2$

$$\eta_{(m+1,n)} \begin{cases} \eta_{(m,n)}^{x,x+e_1} & \text{if } \eta_{(m,n)} \in \mathcal{A}_x^{+1} \cup \mathcal{A}_x^{+2}, \quad \bar{\eta}(0) \in \mathcal{B}^{+1} \cap \mathcal{B}^{+2} \\ \eta_{(m,n)}^{R_x^{+1},R_x^{-1}} & \text{if } \eta_{(m,n)} \in \mathcal{A}_x^{-1}, \quad \bar{\eta}(0) \in \mathcal{B}_x^{+1} \\ \eta_{(m,n)}^{R_x^{+2},R_x^{-2}} & \text{if } \eta_{(m,n)} \in \mathcal{A}_x^{-2}, \quad \bar{\eta}(0) \in \mathcal{B}_x^{+1} \end{cases} \tag{6.9}$$

$$\eta_{(m,n+1)} \begin{cases} \eta_{(m,n)}^{x,x+e_2} & \text{if } \eta_{(m,n)} \in \mathcal{A}_x^{+1} \cup \mathcal{A}_x^{-1}, \quad \bar{\eta}(0) \in \mathcal{B}^{+3} \cap \mathcal{B}^{+4} \\ \eta_{(m,n)}^{R_x^{+3},R_x^{-3}} & \text{if } \eta_{(m,n)} \in \mathcal{A}_x^{+2}, \quad \bar{\eta}(0) \in \mathcal{B}^{+3} \\ \eta_{(m,n)}^{R_x^{+4},R_x^{-4}} & \text{if } \eta_{(m,n)} \in \mathcal{A}_x^{-2}, \quad \bar{\eta}(0) \in \mathcal{B}^{+4} \end{cases} \tag{6.10}$$

$$\eta_{(m-1,n)} \begin{cases} \eta_{(m,n)}^{x,x-e_1} & \text{if } \eta_{(m,n)} \in \mathcal{A}_x^{-1} \cup \mathcal{A}_x^{-2}, \quad \bar{\eta}(0) \in \mathcal{B}^{-1} \cap \mathcal{B}^{-2} \\ \eta_{(m,n)}^{R_x^{+1},R_x^{-1}} & \text{if } \eta_{(m,n)} \in \mathcal{A}_x^{+1}, \quad \bar{\eta}(0) \in \mathcal{B}^{-1} \\ \eta_{(m,n)}^{R_x^{+2},R_x^{-2}} & \text{if } \eta_{(m,n)} \in \mathcal{A}_x^{+2}, \quad \bar{\eta}(0) \in \mathcal{B}^{-2} \end{cases} \tag{6.11}$$

$$\eta^{(m,n-1)} \begin{cases} \eta_{(m,n)}^{x,x-e_2} & \text{if } \eta_{(m,n)} \in \mathcal{A}_x^{+2} \cup \mathcal{A}_x^{-2}, \quad \bar{\eta}(0) \in \mathcal{B}^{-3} \cap \mathcal{B}^{-4} \\ \eta_{(m,n)}^{R_x^{+3},R_x^{-3}} & \text{if } \eta_{(m,n)} \in \mathcal{A}_x^{+1}, \quad \bar{\eta}(0) \in \mathcal{B}^{-3} \\ \eta_{(m,n)}^{R_x^{+4},R_x^{-4}} & \text{if } \eta_{(m,n)} \in \mathcal{A}_x^{-1}, \quad \bar{\eta}(0) \in \mathcal{B}^{-4} \end{cases} \tag{6.12}$$

where $x = x(m,n)$ is the position of the tagged particle in configuration $\eta_{(m,n)}$ (we drop the dependence of x on m and n to get a more readable notation).

Note that given $\eta_{(m,n)}$ and $x(m,n)$ for a couple (m,n), using above definitions one can reconstruct the whole sequence.
Let us define a Markov process on $\mathbb{Z}^2$ with generator G acting on functions $f:(m,n)\to\mathbb{R}$ as

$$\begin{aligned} Gf(m,n) &:= \sum_{i=\pm1}\lambda_i^1(m,n)\,(f(m+i,n)-f(m,n))+ \\ &\quad \sum_{i=\pm1}\lambda_i^2(m,n)\,(f(m,n+i)-f(m,n)) \end{aligned} \tag{6.13}$$

namely a two dimensional random walk with rates $\lambda^i_{\pm1}$ for the jump in direction $\pm e_i$. We can now chose these rates in order that $\eta_{(m(t),n(t))}=\eta(t)$ for the auxiliary process. More precisely, we chose the rates in order that for any function $f(\eta)$ the expectation value over the probability μ_t evoluted with the generator of the auxiliary process coincides with the expectation over the measure on $(m(t),n(t))$ generated by (6.13). By considering the dynamics of the auxiliary process and definition (6.13), one can directly check that the choice of $\lambda^i_{\pm1}$ which satisfy above requirement is the following

$$\begin{aligned} \lambda^1_{+1}(m,n) &= \mathbb{I}_{\mathcal{A}_x^{+1}}(\eta_{(m,n)})\mathbb{I}_{\mathcal{B}_x^{+1}\cap\mathcal{B}_x^{+2}}(\eta_{(0,0)})+ \\ &\quad \mathbb{I}_{\mathcal{A}_x^{+2}}(\eta_{(m,n)})\mathbb{I}_{\mathcal{B}_x^{+1}\cap\mathcal{B}_x^{+2}}(\eta_{(0,0)})+ \\ &\quad \mathbb{I}_{\mathcal{A}_x^{-1}}(\eta_{(m,n)})\mathbb{I}_{\mathcal{B}_x^{+1}}(\eta_{(0,0)})+ \\ &\quad \mathbb{I}_{\mathcal{A}_x^{-2}}(\eta_{(m,n)})\mathbb{I}_{\mathcal{B}_x^{+2}}(\eta_{(0,0)}) \end{aligned} \tag{6.14}$$

$$\begin{aligned} \lambda^1_{-1}(m,n) &= \mathbb{I}_{\mathcal{A}_x^{-1}}(\eta_{(m,n)})\mathbb{I}_{\mathcal{B}_x^{-1}\cap\mathcal{B}_x^{-2}}(\eta_{(0,0)})+ \\ &\quad \mathbb{I}_{\mathcal{A}_x^{-2}}(\eta_{(m,n)})\mathbb{I}_{\mathcal{B}_x^{-1}\cap\mathcal{B}_x^{-2}}(\eta_{(0,0)})+ \\ &\quad \mathbb{I}_{\mathcal{A}_x^{+1}}(\eta_{(m,n)})\mathbb{I}_{\mathcal{B}_x^{-1}}(\eta_{(0,0)})+ \\ &\quad \mathbb{I}_{\mathcal{A}_x^{+2}}(\eta_{(m,n)})\mathbb{I}_{\mathcal{B}_x^{-2}}(\eta_{(0,0)}) \end{aligned} \tag{6.15}$$

$$\begin{aligned} \lambda^2_{+1}(m,n) &= \mathbb{I}_{\mathcal{A}_x^{2}}(\eta_{(m,n)})\mathbb{I}_{\mathcal{B}_x^{+3}\cap\mathcal{B}_x^{+4}}(\eta_{(0,0)})+ \\ &\quad \mathbb{I}_{\mathcal{A}_x^{-1}}(\eta_{(m,n)})\mathbb{I}_{\mathcal{B}_x^{+3}\cap\mathcal{B}_x^{+4}}(\eta_{(0,0)})+ \\ &\quad \mathbb{I}_{\mathcal{A}_x^{2}}(\eta_{(m,n)})\mathbb{I}_{\mathcal{B}_x^{+3}}(\eta_{(0,0)})+ \\ &\quad \mathbb{I}_{\mathcal{A}_x^{-2}}(\eta_{(m,n)})\mathbb{I}_{\mathcal{B}_x^{+4}}(\eta_{(0,0)}) \end{aligned} \tag{6.16}$$

$$\begin{aligned} \lambda^2_{-1}(m,n) &= \mathbb{I}_{\mathcal{A}_x^{2}}(\eta_{(m,n)})\mathbb{I}_{\mathcal{B}_x^{-3}\cap\mathcal{B}_x^{-4}}(\eta_{(0,0)})+ \\ &\quad \mathbb{I}_{\mathcal{A}_x^{-2}}(\eta_{(m,n)})\mathbb{I}_{\mathcal{B}_x^{-3}\cap\mathcal{B}_x^{-4}}(\eta_{(0,0)})+ \\ &\quad \mathbb{I}_{\mathcal{A}_x^{+1}}(\eta_{(m,n)})\mathbb{I}_{\mathcal{B}_x^{-3}}(\eta_{(0,0)}) \\ &\quad \mathbb{I}_{\mathcal{A}_x^{-1}}(\eta_{(m,n)})\mathbb{I}_{\mathcal{B}_x^{-4}}(\eta_{(0,0)}) \end{aligned} \tag{6.17}$$

Let us define also

$$\begin{aligned}
\bar{\lambda}^1_{+1}(m,n) &= \mathbb{1}_{\mathcal{B}_x^{+1}\cap\mathcal{B}_x^{+2}}(\eta_{(0,0)}) \\
\bar{\lambda}^1_{-1}(m,n) &= \mathbb{1}_{\mathcal{B}_x^{-1}\cap\mathcal{B}_x^{-2}}(\eta_{(0,0)}) \\
\bar{\lambda}^1_{+1}(m,n) &= \mathbb{1}_{\mathcal{B}_x^{+3}\cap\mathcal{B}_x^{+4}}(\eta_{(0,0)}) \\
\bar{\lambda}^1_{+1}(m,n) &= \mathbb{1}_{\mathcal{B}_x^{-3}\cap\mathcal{B}_x^{-4}}(\eta_{(0,0)})
\end{aligned} \tag{6.18}$$

and

$$\begin{aligned}
\bar{G}f(m,n) \;:=\; & \sum_{i=\pm1} \bar{\lambda}^1_i(m,n)\,(f(m+i,n)-f(m,n)) + \\
& \sum_{i=\pm1} \bar{\lambda}^2_i(m,n)\,(f(m,n+i)-f(m,n))
\end{aligned} \tag{6.19}$$

From definitions (6.14) and (6.18) it is immediate to check that $\lambda^i_{\pm1} \geq \bar{\lambda}^i_{\pm1}$, therefore

$$E\left(m(t)^2+n(t)^2\right) \geq \bar{E}\left(m(t)^2+n(t)^2\right) \tag{6.20}$$

where we let $E(f(t))$ and $\bar{E}(f(t))$ be the expectation value of $f(m,n)$ over the process $\eta(m(t),n(t))$ started at time zero from the same configuration and evoluted with generator (6.13) and (6.19), respectively. By recalling definition (6.4) and results on crossover length, we know that for sufficiently high density the probability w.r.t. Bernoulli measure of events

$$\begin{aligned}
&\mathcal{B}_x^{+1}\cap\mathcal{B}_x^{+2}, \\
&\mathcal{B}_x^{-1}\cap\mathcal{B}_x^{-2}, \\
&\mathcal{B}_x^{+3}\cap\mathcal{B}_x^{+4}, \\
&\mathcal{B}_x^{-3}\cap\mathcal{B}_x^{-4},
\end{aligned}$$

is almost one, and therefore greater then threshold probability for conventional percolation on the square lattice. Hence, by using the result in [35] which establish a central limit theorem for random walk in random environment when bond probability is greater than percolation threshold, inequality

$$\bar{E}\left(m(t)^2+n(t)^2\right) > 0 \tag{6.21}$$

follows. Above inequality, together with (6.20), implies

$$E\left(m(t)^2 + n(t)^2\right) > 0 \tag{6.22}$$

Moreover, since when m goes to m+2 (n to n+2) the first (second) coordinate of the tagged particle position increases at least of one unit, inequality

$$\mu_t\left(x_1(t)^2 + x_2(t)^2\right) \geq \frac{1}{4}E\left(m(t)^2 + n(t)^2\right) > 0 \tag{6.23}$$

holds, where μ_t is the evoluted of initial measure $\mu_{\rho,0}$ under the auxiliary process. This allows us to conclude that $D_S^{aux} > 0$ at any $\rho < 1$ which, together with inequality (6.8) implies $D_S > 0$ for KA model.

6.1.2 High density regime

As we discussed in the introduction to section 6.1, the cooperative motion of frameable cores guarantees diffusivity and the existence of this mechanism implies inequality $D_S > 1/\xi^d\ \xi^2/\tau_\xi\ n_M$, where $n_M = 1/\Xi^d$, ξ and τ_ξ are respectively the density, the size and the relaxation time of cores. In the high density limit, vacancies will be typically far apart or in small clusters that cannot move. Therefore, the tagged particle can move only when a frameable core passes by and we expect that the above lower bound gives in this regime the right dependence of the diffusion coefficient, i.e. $1/D_S \simeq \xi(d-2)\ \tau_\xi\ \Xi^d$. The density dependence of Ξ and ξ is known from results in chapter 4; the behaviour of τ_ξ will be discussed in this section. The result is that $\xi^2/\tau_\xi\ 1/\xi^d$ goes to zero for $\rho \to 1$ slower than $1/\Xi^d$, therefore the dominant factor in the self diffusion coefficient comes from the decreasing density of mobile cores, namely $D_S \simeq 1/\Xi^d$.

In order to estimate τ_ξ we evaluate the time needed to reach the most severe *bottleneck* in configuration space which, since all configurations are equiprobable, corresponds $\mathcal{N}_F/\mathcal{N}_B$, where $\mathcal{N}_F$ and $\mathcal{N}_B$ are the number of all possible configurations in the core and in the bottleneck, respectively[4]. The worst scenario, i.e. the case in which all configurations must go through the same one in order to equilibrate, yeld $\mathcal{N}_B = 1$ and therefore we obtain the upper bound $\tau_\xi \leq \mathcal{N}_F$ for the relaxation time of cores. Recalling the requirements needed to grow a frameable core starting from an empty seed, we can obtain a rough estimate of $\mathcal{N}_F$. For example, in the case $d = 2$, $s = 1$, the conditions one should satisfy to grow an optimally frameable configuration imply $\mathcal{N}_F \simeq K\ \xi!$ and therefore

[4]This corresponds to the factor $1/\mathcal{N}$ that appeared trhough the path argument performed in previous paragraph.

$$\tau_\xi \leq K\ \xi! \simeq K\ \exp\left\{\frac{-c\ln(1-\rho)}{1-\rho}\right\} \tag{6.24}$$

with K and c positive constants. However, we expect $\xi!$ to be only an upper bound on τ_ξ. Let us give an argument which supports last statement, which will be confirmed both by an alternative calculation (see section 6.1.3) and by numerical simulations (see section 6.1.3).

Let τ_ℓ be the relaxation time for a frameable ℓ by ℓ square. We expect that a recursive equation of the form

$$\tau_{\ell+2} = \tau_\ell + k\tau_{c\ell} \tag{6.25}$$

holds, with $c < 1$ and $k > 1$ and both of order one. Indeed, to equilibrate an $\ell+2$ by $\ell+2$ square, one can equilibrate the ℓ by ℓ square and then use paths that give rise to framed squares of size $c\ell$. If constant c in (6.25) were equal to one, we would obtain τ_ℓ of the order e^ℓ, therefore $\tau_\xi \simeq \exp\{-\ln(1-\rho)/(1-\rho)\}$, i.e. equal to the upper bound (6.24). However, since typically c is less than one, we expect the behaviour to be less rapid than an exponential with ℓ. This implies that $\tau < \xi! \ll \Xi^2$ and therefore in the high density regime D_S should be dominated by $n_M = 1/\Xi^2$, i.e.

$$D_S \simeq \exp\{-c_\infty/(1-\rho)\} \tag{6.26}$$

with $c_\infty \simeq 1.1$ (4.46). In order to check this prediction, we have run standard Montecarlo simulations for a 400 by 400 lattice. The result, drawn in figure 6.2, is that at high densities D_S fits well with the predicted exponential form (6.26). Moreover, by fitting $\ln D_S$ with $A/(1-\rho)$, we find $A \cong 0.9 - 0.95$ which is in good agreement with the expected $c_\infty \cong 1.1$.

For the other KA models, analogous arguments suggest that the behavior of D_S in the high density limit should again be dominated by $n_M = 1/\Xi^d$. Hence, by using formula (4.11) for Ξ, for the original cubic lattice with $s = 2$ we find

$$\ln\ln D_S^{-1} \propto 1/(1-\rho) \tag{6.27}$$

a result which has been confirmed by a recent finite size scaling analysis [56].

Note that these predictions on the density dependence of the self diffusion coefficient rely on the hypothesis that cores do not interact. Indeed, besides the hypothesis that in the high density regime the effective diffusion mechanism is due to the motion of cores, we are considering that the diffusion coefficient is given by the diffusion coefficient of cores ξ^2/τ_ξ multiplied by

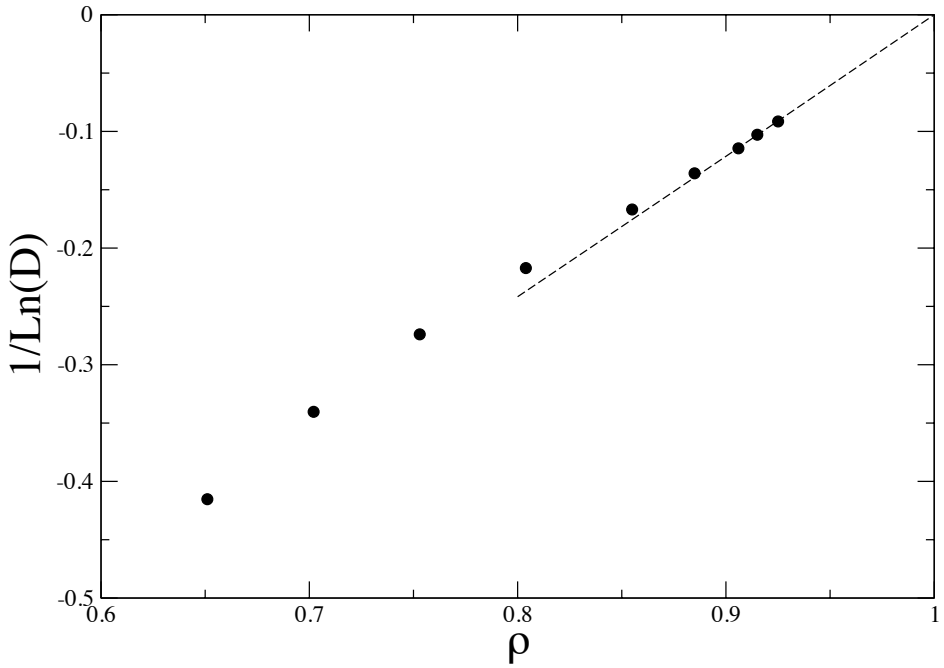

Figure 6.2: $(\ln D)^{-1}$ plotted as a function of ρ obtained for KA on a 400 by 400 square with $s = 1$. The straight line is a guide for the eye to see the $\ln D_S \propto 1/v$ behavior.

their density $1/\Xi^d$ and the length $1/\xi^d$ of the sequence needed to move of one step a tagged particle once it is inside a core. In other words, we are neglecting the possible corrections coming form the interactions of different cores. This is true for the SSEP case, with simple vacancies playing the role of cores. Indeed, the diffusion coefficient is simply proportional to their density (the diffusion coefficient for a vacancy is density independent, since they can freely move). Part of this result was discussed in section 2.5.2 where we outlined the proof [17] of a lower bound for the self diffusion coefficient of the form $1 - \rho$. To complete the argument one should establishing an upper bound of the same form. This can be easily derived by using as a test function in the variational formula (2.15) the function $f(\eta) = \eta_x$. For KA model, finding a suitable test function which gives the right upper bound is not a trivial task and we do not have a proof of above statement. However, we believe that no different interaction mechanism between *macrovacancies* (i.e. cores) should occur. This is confirmed by the good agreement of numerical results with the prediction $D_S \simeq n_M$. Moreover, for a particular version of KA model we are able to prove a lower bound which confirms the hypothesis. Consider KA model on a triangular lattice with $s = 2$. In this case pairs of

two vacancies can freely move on the lattice, therefore they play the same roles as cores in the hypercubic case and one can prove $D_S > (1-\rho)^q$ with $q = 2$. By using the same test function as for SSEP, we find a lower bound of the same form and conclude that in this case the interaction among the cluster of vacancies that allow diffusion does not modify the predicted scaling. Therefore, considering that for KA at a fixed density diffusion is guaranteed by the cooperative motion of clusters of $q = O(\xi)$ vacancies we expect that $D_S \simeq (1-\rho)^\xi$ should hold, which gives again the scaling $D_S \simeq 1/\Xi^d$ up to log corrections.

6.1.3 Diffusion of mobile cores: estimate of the diffusion times in the case d=2, s=1

In this section we consider the case $d = 2$, $s = 1$ and evaluate the typical diffusion times of cores, τ_ξ. More precisely, via an ansatz on the nature of the bottleneck and a transfer matrix technique, we perform the calculation of the number of configurations in the core and in the bottleneck, $\mathcal{N}_F$ and $\mathcal{N}_B$, whose ratio gives an estimate of τ_ξ (see previous section). The ansatz consists in assuming that the bottleneck is composed by all frameable configurations with the seed in a corner of the square. Let us outline the idea behind this assumption, which will be confirmed by the successfull comparison of our prediction for τ_ξ with numerical results (see section 6.1.3).

Consider the core of an optimally frameable region (see section 4.10). From the properties of cores, we know they are expandable into frameable larger squares and therefore there are vacancies in next lines in any direction. The presence of such vacancies enable the motion of the core itself. In order to incorporate these vacancies in an effective manner, i.e. to move the core, it is not necessary to go through the framed configuration with all the vacancies in the l-shaped configuration of figure 4.7. Indeed, using the basic moves in figures 4.8, 4.9, one can easily check that it is sufficient to bring the seed on the border in correspondence of the external vacancy. Therefore the worst case (the case which requires the longest path to bring the central empty seed near the external vacancy) is when the external vacancy is near the corner of the core. Thus, it is reasonable to assume $\mathcal{N}_B = \mathcal{N}^\angle$, where $\mathcal{N}^\angle$ is the number optimally frameable configurations with seed on a corner[5].

In the rest of this section, using a transfer matrix technique and scaling

[5]A priori it could be possible that all configuration must go trough the same configuration with seed in the corner. However, due to symmetry reasons, it is more likely to assume that we can divide the overall number of frameable configurations in $\mathcal{N}^\angle$ sets of $\mathcal{N}_F/\mathcal{N}^\angle$ configurations, each set equilibrating through a different bottleneck.

arguments, we find the density dependent values of both $\mathcal{N}_F$ and $\mathcal{N}^{\angle}$. The result for τ_ξ is subdominant with respect to $n_M = 1/\Xi^d$, as already predicted in section 6.1.2 through a different argument. Indeed, $\mathcal{N}_F$ and $\mathcal{N}^{\angle}$ have the same $\exp^{C\xi}$ factor and therefore the suppression factor in moving the seed in the corner is subexponentially small with respect to n_M. The reason why we expect the exponential factor to be the same for $\mathcal{N}_F$ and $\mathcal{N}_{\angle}$ is easily understood by considering that the number of configurations with nucleus in the corner and in the center is roughly $(2\times4\times8\times\ldots\times\ell)^2$ (expanding only two sides) and $(2\times6\times10\times\ldots\times\ell)^4$ (expanding on four sides), respectively. Therefore, since $\tau_\xi \ll n_M$, the exact density dependence of τ_ξ does not modify the diffusion coefficient which is dominated by n_M.

Estimate of $\mathcal{N}_F$: Transfer matrix technique

Let us consider a $W\times H$ rectangle. The number of frameable configurations with seed of three vacancies in the center corresponds to the number of ways vacancies can be put in the rectangle in order that, starting form the nucleus and using any sequence of growing steps, one can reach an optimally framed configuration. We recall that the possible growing steps, defined in section 4.10, are the following:

(i) expansion from a $w\times h$ to a $w\times(h+2)$ framed rectangle if there is a vacancy in a line next-nearest neighbor to one of its edges parallel to direction x;

(ii) expansion from a $w\times h$ to a $(w+2)\times h$ framed rectangle if there is a vacancy in a line next-nearest neighbor to one of its edges parallel to direction y;

(iii) expansion from a $w\times h$ to a $(w+1)\times(h+1)$ framed rectangle if there is a vacancy next nearest neighbor along a diagonal from a corner;

(iv) expansion from a $w\times h$ to a $w\times(h+1)$ framed rectangle if there is a vacancy in the line segment next to one of its edges parallel to direction x;

(v) expansion from a $w\times h$ to a $(w+1)\times h$ framed rectangle if there is a vacancy in the line segment next to one of its edges parallel to direction y.

To count the number of frameable configuration expanded form a seed in the center proceed as follows. Given a frameable configuration of size $W \times H$ with seed in the center consider first the length of the maximal expansion

performed from the seed by using steps only in the horizontal direction (i.e. steps (i) and (iv) above), let j_0 be half such length plus one, the one representing half the original width of the seed. If no horizontal expansion at all is possible, but an initial expansion from a corner or from two diagonally opposite corners is possible (step (iii)) carry out these and then expand as far as possible horizontally. For these cases define j_0 as one plus half the total expansion in the corner plus half the horizontal expansion.
Second expand as far as possible in the vertical directions. Again, if no vertical expansion is allowed but an initial corner expansion or a diagonally opposite pair of corner expansions is possible, carry these out and then expand as much as possible vertically. Define $k_0 = 1$ as half the initial vertical height, and k_1 as half the total expansion in this first vertical stage.
Third, expand again in the horizontal direction (or if not possible corner(s) plus horizontal), to increase the width by j_1 and proceed iteratively expanding by $k_2, j_2, k_3, j_3, \ldots j_n, k_n$ until the width and height are W and H.
Therefore, with the above described procedure we associate in a unique way a sequence $j_0 \ldots j_n, k_0 \ldots k_n$ to each frameable configuration with seed in the center . The overall number of frameable configurations in the $W \times H$ rectangle is obtained by summing the number $N(j_0 \ldots j_n, k_0 \ldots k_n)$ of configurations with sequence $j_0 \ldots j_n, k_0 \ldots k_n$ over all the possible choices of the sequence. Note that, the condition that the configuration has overall size $W \times H$ imposes the constraints $\sum_{i=0}^{n} 2j_i = W$ and $\sum_{i=0}^{n} 2k_i = H$.

In order to count the numbers of configuration correspondent to the different sequences, we find the recursive relation among the number of frameable configuration for different sizes. Let W_n and H_n be the width and height till which the core has been framed at step n, B_n half the deviations from square shape and s_n the running sum of $\{j_n\}$ and $\{k_n\}$, namely $B_n \equiv 1/2(W_n - H_n)$ and $s_n = \sum_{i=0}^{n}(j_i + k_i)$. In order to calculate $N(j_0, j_1, \ldots j_n, k_0, k_1, \ldots k_n)$ we should count the number of possible ways of expanding at each stage, which requires keeping track of the expansions at the previous stage in the same direction. Indeed, consider the n–step in vertical expansion starting form a framed rectangle of size $W_n \times H_{n-1}$ and leading to size $W_n \times H_n$ with an upward expansion. If the previous horizontal expansion, from $W_{n-1} \times H_{n-1}$ to $W_n \times H_{n-1}$ with $W_n = W_{n-1} + 2j_n$, did not begin with corner expansions (no use of step (iii)), the number of possible positions for a vacancy in the first step of the upward expansion is only $2j_n$ rather than the full width, W_n. Indeed, since the previous vertical expansion had stopped, we know that the other potential sites for upwards expansion are occupied. Then, any further upward expansion has W_n possibilities per step. Downward expansion is similar. On the other hand, if the previous horizontal expansion had began with a single corner expansion (step (iii)), the behavior is asymmetric for upwards

and downwards expansion. If the corner expansion in the earlier stage was in the upper left or upper right, then the potential sites for a first upwards expansion step in the next stage are the full width $W_n = W_{n-1} + 2j_n - 1$ as there was a small vertical expansion associated with the corner expansion and thus the previous stopped condition does not imply anything about sites two above the new top edge. On the bottom, however, the possible first step is limited to $2j_n - 1$ sites. Finally, if the previous horizontal expansion had begun with a double corner expansion, both upwards and downwards expansions are unrestricted so that W_n possible sites are available for each. Therefore, we will end up with a tranfer matrix which gives the number of frameable configurations of a certain size as a function of frameable configurations in smaller squares.
Let us define

$$N^o(j,B,s)\,, \qquad C^o(j,B,s) \qquad \text{and} \quad D^o(j,B,s) \tag{6.28}$$

as $1/s!$ multiplied for the number of configurations of vacancies after an horizontal expansion which stopped after length $2j$ and started from $w \times h$, with $w = s + B$ and $h = s - B$ given, respectively, that the expansion was normal (involving no corners), started with a single corner, or started with double corners. We choose the normalization factor $1/s!$ to isolate the dominant factor which we expect to be the same for the case of configurations with seed in the corner (see the rough argument in the end of section 6.1.3).
Let also

$$N^v(k,B,s)\,, \qquad C^v(k,B,s) \qquad \text{and} \quad D^v(k,B,s) \tag{6.29}$$

be $1/s!$ multiplied for the number of configurations of vacancies after an vertical expansion which stopped after increasing the hight by $2k$ and started from $w \times h$, with $w = s+B$ and $h = s-B$. Again, N^v, C^v, D^v correspond to the case in which the expansion was normal (involving no corners), started with a single corner, or started with double corners.
Consider a normal vertical expansion for a $w \times h$ rectangle. This will have w possibilities except possibly for the first step in each of the up and down directions. If the previous expansion was normal, then there are only $2j$ possibilities for each of the first steps. Therefore, if vertical expansion is by k steps in only one of the directions, this gives rise to an overall factor of

$$2(2j)(s+B)^{k-1}\frac{(s-k)!}{s!}$$

with the initial factor of two from the two possible directions and the final factor accounting for the change in normalization by $s!$. If the expansion is

both up and down, the corresponding factor is

$$(k-1)(2j)^2(s+B)^{k-2}\frac{(s-k)!}{s!}$$

with the $k-1$ arising from the possible ways of dividing the $k-2$ subsequent steps between up and down. If the previous expansion stage started with one corner, then expansion in that direction only involves

$$(s+B)^k\frac{(s-k)!}{s!}$$

while expansion in both directions includes a factor

$$k\frac{2j-1}{s}\left[\frac{s+B}{s}\right]^{k-1}\frac{(s-k)!}{s!}$$

If the previous expansion stage started with two corners, then the corresponding factor is

$$(k+1)(s+B)^k\frac{(s-k)!}{s!}$$

We thus have the recursion relation

$$\begin{aligned} N^v(k,B,s) &= \delta(A,B+k)Q(k,A,s-k)\sum_{j=1}^{s-k}\Bigg[N^o(j,A,s-k)\left(2\frac{2j}{s+B}+\right. \\ &\quad (k-1)\left(\frac{2j}{s+B}\right)^2\Bigg)+C^o(j,A,s-k)\left(1+k\frac{2j-1}{s+B}\right)+ \\ &\quad D^o(j,A,s-k)(k+1)\Bigg] \end{aligned} \tag{6.30}$$

where the overall factor Q is

$$Q(k,B,s)\equiv(s+B)^k\frac{(s-k)!}{s!} \tag{6.31}$$

If no normal vertical expansion is possible, then corner expansion must be performed for the process to continue. If only one corner has a vacancy to expand into, this will make $W+1=s+B+1$ possible sites for each further expansion, yielding a factor $Q(k,B+1,s)$ for expansion in this direction. The opposite side can, by the assumption that it was otherwise blocked, only expand if there is a vacancy the row two away from the corresponding edge and in the column of the new corner vacancy; if this does occur, then any remaining $k-2$ further vertical expansions will yield a factor of

$$(k-1)(s+B+1)^{k-2}\frac{(s-k)!}{s!}$$

from the possible ways of dividing these among up and down. Note that neither of these two cases involves the previous expansion amount, j. The contributions from previous stage expansions that themselves started with one or two corners has exactly the same form. We thus find that

$$C^v(k,B,s) = \delta(A,B+k)\ 4\ \frac{1}{s+B+1}\ Q(k,A,s)\left[1+(k-1)\frac{1}{s+B+1}\right] \sum_{j=1}^{s}[N^o(j,A,s-k)+C^o(j,A,s-k)+D^o(j,A,s-k)] \tag{6.32}$$

with the initial factor of 4 from the four possible corners.
Double corner expansions are similar except that once two diagonally opposite corners have expanded, downwards and upwards expansions are possible with $s+B+2$ possible vacancy positions. For $k-2$ such steps there is thus a factor of

$$(k-1)(s+B+2)^{k-2}\frac{(s-k)!}{s!}$$

We have therefore

$$D^v(k,B,s) = \delta(A,B+k)\ 2Q(A+1,s)\ \frac{1}{(s+B+2)^2} \sum_{j=1}^{s}[N^o(j,A,s-k)+C^o(j,A,s-k)+D^o(j,A,s-k)] \tag{6.33}$$

the initial factor of two for the possible pairs of corners. Iterating these recursion relations, with j and k and B swapping after each stage, and summing over all the possible values of j and k at each step subject to conditions $\sum_{i=0}^{n} 2j_i = W$ and $\sum_{i=0}^{n} 2k_i = H$ yields the number of configurations for any given rectangle $W \times H$ (with both W and H even). From the recursion relations we see that the j dependence enters only via the zeroth first and second j-moments of N, the zeroth and first of C and the zeroth of D. In next section, by using scaling techniques, we calculate such moments and therefore obtain the value of $\mathcal{N}_F$.

Estimate of $\mathcal{N}_F$: Scaling Limit

On large length scales it is reasonable to expect deviations from square to be small, i.e. $B \ll w \simeq h$ at any step. This can be seen from the behavior of $Q(k,B,s)$ for large s (recall that $s=(w+h)/2$):

$$Q(k,B,s) = \frac{s^k \exp\left\{\ln(1+\frac{B}{s})\right\}}{s^k(1+\frac{1}{s})\dots(1+\frac{1}{k})} \approx e^{Bk/s - k^2/s} \tag{6.34}$$

Indeed, the strong suppression of k from the gaussian factor together with the two step recursion relation for B, $B'' = B + j - k$ with positive B suppressing k and negative B suppressing j, implies that for large s

$$k \sim B \sim \sqrt{s} \tag{6.35}$$

We thus define the following rescaled variables

$$\kappa \equiv k/\sqrt{s}\ , \qquad \eta \equiv j/\sqrt{s}\ , \qquad b \equiv B/\sqrt{s} \tag{6.36}$$

Let us consider the Laplace transforms of the p-th moments $N_p(k,B,s)$, $C_p(k,B,s)$ and $D_p(k,B,s)$ and rescale them as follows

$$N_p(b,s,\nu) = s^{\frac{1}{2}(p+1)} n_p(b,\nu) \tag{6.37}$$

$$C_p(b,s,\nu) = s^{\frac{1}{2}p} c_p(b,\nu) \tag{6.38}$$

$$D_0(b,s,\nu) = s^{\frac{-1}{2}} d_0(b,\nu) \tag{6.39}$$

From the recursion relations (6.30), (6.32), (6.33) the following relations holds

$$n_p^v(b,\nu) = \int_0^\infty d\kappa \int_{-\infty}^\infty dc\ \delta(c-\kappa-b)\ e^{-\nu\kappa}\ e^{-\kappa^2+\kappa c}\left[\kappa^p J(c,\nu)\right] \tag{6.40}$$

$$c_p^v = \int_0^\infty d\kappa \int_{-\infty}^\infty dc\ \delta(c-\kappa-b)\ e^{-\nu\kappa}\ e^{-\kappa^2+\kappa c}\left[4\kappa^p n_0^o(c,\nu)\right] \tag{6.41}$$

$$d_0^v(b,\nu) = \int_0^\infty d\kappa \int_{-\infty}^\infty dc\ \delta(c-\kappa-b)\ e^{-\nu\kappa}\ e^{-\kappa^2+\kappa c}\left[2n_0^o(c,\nu)\right] \tag{6.42}$$

where

$$J(b,\nu) = 4n^o(b,\nu) + 4\kappa n_2^o(b,\nu) + c_0^o(b,\nu) + 2\kappa c_1^o(b,\nu) + \kappa d_0^o(b,\nu) \tag{6.43}$$

Taking advantage of the simple form of the kernel, we pull a factor of $e^{-a^2/2}$ out of each distribution and then Fourier transform in b, defining

$$\tilde{n}_p(\zeta,\nu) \equiv \sqrt{2\pi} \int_{-\infty}^\infty db\ e^{-ib\zeta} e^{b^2/2} n_p(b,\nu) \tag{6.44}$$

and analogous transformed functions for the p-th moments of c and d. By carrying out the integrals over κ in (6.40), (6.41), (6.42) we obtain

$$\tilde{d}_0^v(\zeta,\nu) = 2y^2\tilde{n}_0^o(-\zeta,\nu) \tag{6.45}$$

$$\tilde{c}_p^v(\zeta,\nu) = 4y^{p+1}\tilde{n}_0^o(-\zeta.\nu) \tag{6.46}$$

for $p = 0, 1$ and

$$\begin{aligned}\tilde{n}_p^v(\zeta,\nu) &= p!y^{p+1}[4\tilde{n}_1^o(\zeta,\nu) + 4y(p+1)\tilde{n}_2^o(-\zeta,\nu) + \tilde{c}_0^o(\zeta,\nu) + \\ &\quad 2y(p+1)\tilde{c}_1^o(-\zeta,\nu) + y(p+1)\tilde{d}_0^o(-\zeta,\nu)]\end{aligned} \tag{6.47}$$

with

$$y \equiv \frac{1}{\nu + i\zeta} \tag{6.48}$$

For vertical stages, as above, define the six by six transfer matrix $\mathcal{T}$ such that $\mathbf{v}^v = \mathcal{T}\mathbf{v^o}$, where $\mathbf{v}^v = (\tilde{n}_0^v, \tilde{n}_1^v, \tilde{n}_2^v, \tilde{c}_0^v, \tilde{c}_1^v, \tilde{d}_0^v)$ and $\mathbf{v}^o = (\tilde{n}_0^o, \tilde{n}_1^o, \tilde{n}_2^o, \tilde{c}_0^o, \tilde{c}_1^o, \tilde{d}_0^o)$. Note that such transfer matrix is a function only of y. On horizontal stages, one can check by direct inspection that the transfer matrix, $\overline{\mathcal{T}}$, satisfies $\overline{\mathcal{T}} = \mathcal{T}(\overline{y})$ with

$$\overline{y} \equiv \frac{1}{\nu - i\zeta} \tag{6.49}$$

We are interested in $\mathcal{N}_F$, namely on the total number of frameable configurations a square of linear size ξ, with ξ the large size of cores. Therefore, we are interested in the case of a given large $s = \xi$ and $a = b = 0$. We must thus sum over the number of possible stages, the last one being either horizontal or vertical and anti–transform in ν and ζ which gives

$$\mathcal{N}_F \sim \xi! \int_{\mathcal{C}} \frac{d\nu}{2\pi i} e^{2\nu\sqrt{\xi}} \hat{R}(\nu) \tag{6.50}$$

where the $\xi!$ factor comes from the normalization of functions N, C, D and

$$\hat{R}(\nu) = \mathbf{v}_f^T \int_{-\infty}^{\infty} \frac{d\zeta}{2\pi} \sum_n [\mathcal{I} + \overline{\mathcal{T}}][\mathcal{T}\overline{\mathcal{T}}]^n \mathbf{v}_i \tag{6.51}$$

with $\mathbf{v}_i$ a proper initial vectors and $\mathbf{v}_f$ projecting onto $\tilde{n}_0^v, \tilde{c}_0^v, \tilde{d}_0^v$ (the identity matrix, $\mathcal{I}$, is needed if the last stage is vertical). The inverse Laplace transform (6.50) to obtain $\mathcal{N}$ will be dominated for large ξ by the singularity in $\hat{R}(\nu)$ with the largest real part of ν. The singularities will occur when $y(\nu,\zeta)$

is such that $\mathcal{T}\overline{\mathcal{T}}$ has an eigenvalue $\Lambda = 1$. For $\zeta = 0$, $\overline{\mathcal{T}} = \mathcal{T}$ and one can readily find the values of y at which $\mathcal{T}$ has an eigenvalue of unity. Defining $z = y^2$ we find the condition

$$7(4z)^3 - 17(4z)^2 - 16(4z) + 8 = 0 \tag{6.52}$$

which has roots $z = -1/4$ and

$$z = z_\pm = \frac{3 \pm \sqrt{11/2}}{7} \tag{6.53}$$

The desired root with the smallest positive real part is z_- yielding a singularity at $\nu = \sigma$ with

$$\sigma = \frac{1}{\sqrt{z_-}} = \sqrt{6 + \sqrt{22}} \tag{6.54}$$

For small but non-zero ζ, the singularity in ν will only be shifted away from σ by of order ζ^2 and (6.50) therefore yields

$$\mathcal{N}_F \sim e^{2\sigma\sqrt{\xi}}\xi! \tag{6.55}$$

with σ given by (6.54) [6]. There are many sources or power law multiplicative corrections in addition to that from the integral over ζ. In particular, there are the effects of the processes that are intrinsically smaller by $1/\sqrt{s}$ and corrections to the approximations (6.34). Since we expect the cumulative effects of corrections to be of order $1/\sqrt{s}$ at each stage and integrating over steps is roughly equivalent to integrating over $d\sqrt{s}$, this gives rise to multiplicative factors of $e^{\alpha \ln \xi} = \xi^\alpha$. We thus conclude that the number of frameable configurations in an ξ by ξ square is asymptotically

$$\mathcal{N}_F \approx K\xi^\alpha e^{2\sigma\sqrt{\xi}}\xi! \tag{6.56}$$

with α computable in principle. Here K is a constant that should include the effects of configurations that do not have the simple seed of three vacancies in a two-by-two square; it could be obtained by fitting to intermediate sizes using the exact transfer matrices. The relative corrections to (6.56) are probably of order $1/\sqrt{\xi}$ and there will be other corrections suppressed by factors of $e^{-(\sigma-\sigma')\sqrt{\xi}}$ arising from other ν's at which $\Lambda = 1$.

[6] Indeed, if we switch the order of integration in (6.50) this will result in a suppression of the contributions from non-zero ζ by a factor of $e^{-c\zeta^2\sqrt{s}}$ with some positive coefficient c. The integral over ζ will then be the same order as the integrand at $\zeta = 0$ except for a factor of $1/s^{\frac{1}{4}}$. Note that the fact that the dominant values of ζ are small implies that the distribution of the asymmetry b (recall that $b = (W - H)/(2\sqrt{s})$), is asymptotically simply the gaussian factor $e^{-b^2/2}$ that was pulled out before Fourier transforming.

Estimate of $\mathcal{N}^{\angle}$

In this section we calculate the number of frameable configurations with seed on the corner. The difference with respect to the analysis in the two previous sections lye on the fact that now there is only one possible direction for each of vertical, horizontal, and corner expansions. All we need are, thus, N_0, N_1 and C_0 or, in the large s limit, the corresponding functions of ζ and ν: m_0, m_1 and f_0. Taking into account the possible moves, we write recursion relations analogous to (6.30), (6.32), (6.33), rescale variables and finally Fourier transform. We thus obtaining

$$\begin{aligned}
\tilde{n}_0^v(\zeta,\nu) &= y[2\tilde{n}_1^o(-\zeta,\nu)+\tilde{v}_0^o(-\zeta,\nu)] && (6.57)\\
\tilde{n}_1^v(\zeta,\nu) &= y^2[2\tilde{n}_1^o(-\zeta,\nu)+\tilde{c}_0^o(-\zeta,\nu)] = y\tilde{c}_0^v(\zeta,\nu) && (6.58)\\
\tilde{c}_0^v(\zeta,\nu) &= y\tilde{n}_0^o(-\zeta,\nu) && (6.59)
\end{aligned}$$

In this case, it is straightforward to work with $\mathcal{T}\overline{\mathcal{T}}$ instead and obtain the largest eigenvalue which yields for the total number of frameable configurations with the seed in one corner of the square $\mathcal{N}^{\angle}$

$$\mathcal{N}^{\angle}(\xi) \approx K^{\angle}\xi^{\alpha^{\angle}-\alpha}e^{2\sigma^{\angle}\sqrt{\xi}}\xi! \tag{6.60}$$

with

$$\sigma^{\angle} = \sqrt{3} \tag{6.61}$$

Note that the overall constants and the two power law terms are all different then in previous case. Calculating the value of $\alpha^{\angle} - \alpha$, which is in possible in principle, is difficult since one should take into account all the different corrections.

Estimate of τ_ξ and numerical results

We recall that the relaxation time of a core, τ_ξ, is given by the ratio of the overall number of possible frameable configuration inside a square of size ξ, $\mathcal{N}_F$, and the number of those which are frameable and moreover have the seed in the corner, $\mathcal{N}^{\angle}$. Therefore, by using results (6.56) and (6.60) we obtain

$$\frac{1}{\tau_\xi} \approx \frac{K^{\angle}}{K}\xi^{\alpha^{\angle}-\alpha}e^{2(\sigma^{\angle}-\sigma)\sqrt{\xi}} \tag{6.62}$$

with

$$\Sigma \equiv 2(\sigma - \sigma^{\angle}) \cong 3.075 \tag{6.63}$$

Note that above result on the relaxation time is independent on the choice of ξ and in general making in (6.62) the substitution $\xi \to \ell$ we should obtain the typical relaxation time of a frameable region of size ℓ. In order to test this result we have run numerical simulations. We start form an ℓ by ℓ frameable configuration and measure the time needed to move a particle which is in the top right position, which should correspond to τ_ℓ. Simulations are performed for different sizes from $\ell = 4$ to $\ell = 16$ on samples of about 1000 systems, in order that the error bars on the results are small. Results for $\log \tau_\ell$ are plotted in figure 6.3, which clearly shows a lower than linear variation in ℓ. Moreover, numerical data are in good agreement with the predicted square root law with coefficient Σ plus logarithmic corrections as can be seen from the result of the fit drawn as a dashed curve in figure 6.1.3. The good matching between our prediction and numerical data, suggests that our ansatz on the nature of the bottleneck–i.e. the conjecture $N^B \simeq N^\angle$ (see beginning of present section)–should be correct. Note that calculation yielding to (6.62) rely on the large ℓ approximation, this could explain why the fit is not optimal at small system sizes.

Result (6.62) implies that $1/\tau_\xi$ is subdominant with respect to n_M, therefore D_S is dominated by the low density of cores in the high density regime, i.e. $D_S \simeq n_M = 1/\Xi^d$ and (see 6.26) holds. The same result was already obtained in section 6.1.2 by a more qualitative argument. Note that, even if a diffusive/non–diffusive transition does not take place (i.e. $D_S(\rho) > 0$ at any $\rho < 1$ as proven in section 6.1.1), the self diffusion coefficient is very small at high density. Indeed, for $\rho \to 1$, D_S goes to zero faster than any power law of $1 - \rho$. This extremely slow dynamics is related to the cooperative motion of rare frameable cores.

6.1.4 Dynamical crossover, avoided transition

In this section we discuss the behaviour of the self diffusion coefficient for intermediate densities. By percolation type arguments, we establish that below a finite density another diffusion mechanism – besides the one related to the cooperative motion of cores – occurs. The reason why this mechanism is effective only below a certain density is that it requires the existence of a particular percolating cluster of vacancies. Since this new mechanism is dominant over the cooperative one, a crossover from the high density formula (6.26) to a different self diffusion coefficient takes place. This crossover can be regarded as the signature of the dynamical ergodicity breaking transition which takes place on Bethe lattices (see results in chapter 5). In other words, even if in the finite dimensional case (i.e. on hypercubic lattices) neither an ergodic/non–ergodic nor a diffusive/non–diffusive transition occurs (see

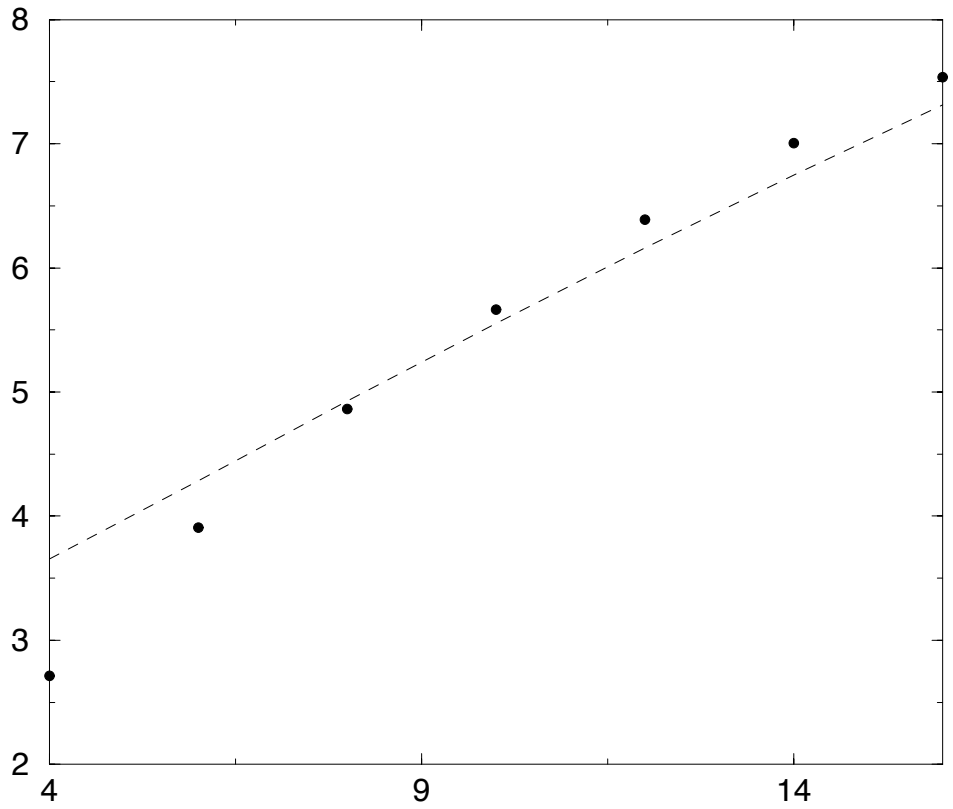

Figure 6.3: Results for $\log \tau_\ell$ as a function of ℓ for system sizes $6, 8, 10, 12, 14, 16$. Simulations are performed on samples of 1000 systems. The plot shows a variation of τ_ℓ which is clearly lower than linear in ℓ. The dashed line is the result of fitting data with formula $A\sqrt{\ell} + B \log \ell$, the values of parameters from the fit are $A \simeq 3.24794$, $B \simeq -2.04878$

results in chapter 4 and in section 6.1.1), a *ghost* of the mean field transition survives.

Consider the square lattice case with $s = 1$. In this case one can directly check (recall the moves in figures 4.7, 4.8) that a cluster of three vacancies can move along a network of empty sites that are linked no more weakly than via second neighbors along axes or diagonals. Let p_{2P} be the critical density for second neighbor percolation along axes or diagonals (namely two particles are connected if they are first, second or third neighbors one to the other). If the density of vacancies is above such threshold, i.e. $1 - \rho > p_{2P}$, there exists with unit probability in the initial configuration an infinite percolating cluster of vacancies on which a finite set of three vacancies can move freely. Therefore, we expect a power law form for the self–diffusion coeffi-

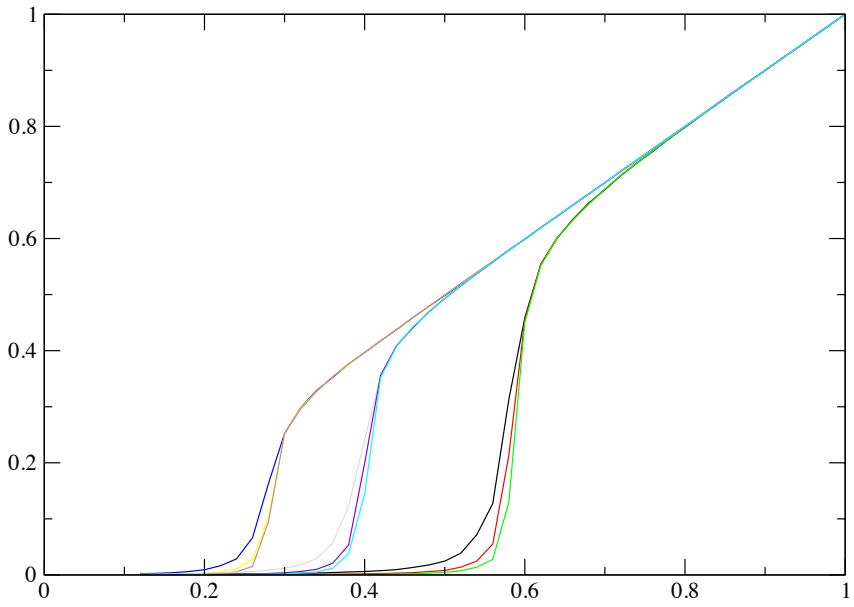

Figure 6.4: Fraction of sites $p(\rho)$ on the percolating cluster. From left to right curve correspond to second neighbor percolation along axes or diagonals (the one we are interested in), along axes, and conventional percolation. In all the cases the fraction of sites vanishes discontinuously at the threshold which corresponds, respectively, to densities $p_c \simeq 0.292$, $p_c \simeq 0.41$ $p_c \simeq 0.59$

cient. More precisely, the contribution of this mechanism to the diffusion coefficient should give a term proportional to $(1-\rho)^3$ times the probability $p(\rho)$ of being on the infinite percolating cluster of vacancies. The latter should go to zero for $\rho \to 1 - p_{2P} \equiv \rho_{2P}$ from below (i.e. for $1-\rho \to p_{2P}$ from above) like a power of $\rho - \rho_{2P}$. Indeed, we expect the second neighbor percolation transition to be second order like standard 2d percolation, therefore the probability of the infinite percolating cluster should vanish continuosly at the threshold. By running a simulation using the algorithm in [32] we have successfully checked this prediction of a continuous transition and found estimate $p_{2P} \simeq 0.292$ for the threshold probability (see figure 6.4). Therefore, coming from low density, we expect a first regime in which the diffusion slows down because the second–neighbor vacancy percolation giant cluster, on which the three–vacancy elements can move, shrinks. On the

other hand, for $\rho > \rho_{2P}$ (or slightly higher due to small scale processes), the mobile elements have to grow in order to remain mobile and they become continuously the cores of (minimal) frameable regions. In other words the only effective diffusion mechanism at high density is the cooperative motion of frameable cores which gives the predicted form (6.26) for the diffusion coefficient. In two dimensions such crossover is not sharp enough in order to determine an unambiguous power law of $\rho - \rho_{2P}$ in the vicinity of ρ_{2P}. This is probably because simulations are performed on finite size systems where the percolation transition is substituted by a crossover. Therefore, above ρ_{2P} there are still large regions of the system where clusters of three vacancies can move, while in other regions they must grow in order to be mobile.

Above argument can be generalized to other cases of KA, with the crossover density determined by more complicated types of percolation. If the crossover is sufficiently sharp–which we expect to be true at sufficiently high spatial dimensions–one should observe a substantial range of critical dependence of D_S near an apparent transition. This is a possible explanation of the numerical results for the original cubic case with $s = 2$, where for more than three decades D_S is well fitted by a power law vanishing at $\rho \sim 0.881$ [1]. Note that in this case the cooperative motion of cores in the high density regime yields a diffusion constant which is too small to be detected in numerical simulations (see equation (6.27)) . Therefor the crossover looks like a diffusive/non–diffusive transition from numerical results.

In [55] the authors proposed that the diffusion coefficient near the dynamical arrest goes like ν^2, where ν is the density of *holes* squared and a hole is a vacancy in which a particle can move (for example, for KA model, a vacancy with all the neighbors empty is not a hole but a vacancy with just one nearest neighbor occupied by a particle that can move into the vacancy is a hole). This conjecture is certainly wrong for KA model because there is no dynamical arrest before $\rho = 1$ and the diffusion coefficient does not scale as the density of holes squared near $\rho = 1$. Indeed, for the case $d = 2$ $s = 1$ the density of holes is $\nu = (1-\rho)(4(1-\rho)^3 + 6(1-\rho)^2)$, which is much higher compared to the density of frameable cores which gives the right scaling of D_S (see formula (6.26) and figure figure 6.2). However, as can be seen in figure 6.4, on a large density regime D_S is indeed proportional to ν^2 and the proportionality breaks down above a finite density. In our frame, the validity of the scaling in the intermediate regime should be due to the fact that ν^2 (which is a polynomial in $1-\rho$) approximates the density dependence of D_S in the regime where the diffusion mechanism is related to the motion of finite clusters of vacancies.

Note that the above discussed crossover between a power law to an exponential regime for the diffusion coefficient, i.e. from a normal to a much slower

dynamics, could be relevant for the study of the *activated processes* in supercooled liquids. As already recalled in section 2.4, mode coupling theory and random first order scenario predict the existence of an ideal glass transition at a finite temperature. This would correspond to an ergodic/non–ergodic transition, i.e. to the appearance of infinite barriers separating different regions of the configuration space. A widespread conjecture is that this mean field transition is substituted in real systems by a crossover between a power law to an *activated regime*. In other words for real systems a crossover would occur from a flow like relaxation to a regime in which few particles hop in a cooperative way over high (but finite) barriers. However, the nature of the activated processes which transform the mean field dynamical transition into a crossover is not clear. For KA model we have found both the mechanism which induces the mean field dynamical transition (the emergence of infinite clusters of forever blocked particles) and the cooperative processes which allow diffusion in the high density regime and replace the mean field transition with a dynamical crossover (the motion of large density dependent cores).

6.2 Dynamical heterogeneities and stretched exponential

As we already mentioned in section 2.3, the long time relaxation of the Fourier transform of density density correlation at fixed wave nuber k is non exponential for supercooled liquids in the vicinity of T_g. A possible explanation of such form is that, since the spatial structure is very heterogeneous, relaxation functions contain the superposition of many exponentials with different relaxation timescales related to an average over different local regions. Indeed, both experiments [51] and numerical simulations [52] have detected the existence of *dynamical heterogeneities*, which correspond to finite regions with correlated motion. The typical spatial extension and life time of these regions increase as the temperature is decreased. In [50] it was proposed that such inhomogeneous character could be detected by studying the four point density dynamic correlation function χ_4. Such function, defined for a generic model in [50] and corresponding for kinetically constrained models to definition (5.10), should display a maximum related to the existence of highly correlated regions. More precisely, for mean field models the maximum diverges and its position is displaced to infinite timeswhen approaching the ergodicity breaking transition (e.g., for $T \to T_d$ from above for p–spin models). On the other hand, for real system some dynamical processes should restore ergodicty and χ_4 is expected to display a maximum at a finite time.

This time should correspondent to the lifetime of cooperative regions with highly correlated motion. Indeed, such a maximum is detected is numerical simulations of Lennard–Jones liquids [50] and both its position and its height increase by decreasing the temperature.

As already mentioned in 4.2, both a stretched exponential relaxation [1] and a cusp in χ_4 [47] were detected by numerical simulations on the three–dimensional KA model with $s = 2$. However, it is not clear which is the mechanism giving rise to the heterogeneous high density relaxation and to the dynamical heterogeneities. In the following, by using the results on crossover length derived in chapter 4, we discuss a possible explanation of stretched exponential relaxation for KA models.

Consider a system at density ρ. Due to density fluctuations there will be internal regions with unusually high density and the relaxation of these rare regions will dominate the long time relaxation of correlation functions. More precisely, from the analysis in previous sections and in chapter 4, we expect that relaxation will be dominated by internal regions with linear size ℓ_i and density ρ_i such that $\ell_i \ll \Xi(\rho_i)$. Indeed, if such regions were isolated from the rest of the system they would be blocked since their configuration space is broken into an exponential number of disconnected configurations and relaxation in this regime cannot occur because the system is too small for the cooperative diffusion to take place (mobile cores are not present in such regions). However, the environment act as a source allowing vacancies to enter such regions from their boundary and unblock them. It is natural to expect that the typical time–scale τ_i of this relaxation will strongly depend on the size of ℓ_i, besides depending on both the typical density ρ of the environment and the density ρ_i of the region. To find the right dependence of τ_i on ℓ_i we have run some numerical simulations which strongly suggest the scaling $\tau_i \sim \ell_i^2$ in the square lattice case with $s = 1$.
In particular we have made two different numerical checks. The first, which is related to a sort of *persistence problem*, is the following. We have considered a completely filled region of size ℓ embedded in a low density region of size L with $L \gg \ell$ and we have measured the probability that the particle at the center has remained in its initial position until time t. The result drawn in figure 6.6 suggests that the mean *persistence time* $\tau_p(\ell)$, i.e. the time at which such probability becomes different from one, scales with ℓ^2 when ℓ is sufficiently large. Note that this behaviour is the same as for the normal lattice gas. Since we are calculating the relaxation time of completely filled regions (i.e. with choice $\rho_i = 1$), for regions at finite internal density we will have for sure $\tau_i(\ell_i, \rho_i) \leq \ell_i^2$.
Then we have calculated the density-density correlation inside a high density region $\mathcal{R}_{HD}$

$$C_{HD}(k,t) = \frac{1}{N} \sum_{x_1,x_2 \in \mathcal{R}_{HD}} exp(-ik(x_1 - x_2))\eta_{x_1}(t)\eta_{x_2}(0) \tag{6.64}$$

More precisely, we have chosen $\mathcal{R}_{HD}$ to be a square of size ℓ with density $\rho = 0.98$ embedded in a larger square L with a lower density $\rho = 0.1$. We have run the simulations for different values of ℓ, all in the range $\ell \ll \Xi(\rho = 0.98)$ (recall that the exact dependence of Ξ on ρ has been established, see section 4.10). The results can be summarized as follows

- the relaxation timescale of $C_{HD}(k,t)$ increases with the linear size ℓ of the region, see Fig. 6.7;
- the increasing of the relaxation timescale of the high density region seems to follow a ℓ^2 law. In fact in Fig. 6.8 we rescale the time to t/ℓ^2 and all the curves collapse into the same one;
- the relaxation of $C_{HD}(k,t)$ seems to be exponential in time. In Fig. 6.9 we plot the same curve that in Fig. 6.8 but using a logarithmic scale for the y-axis. The curves are well described by a linear law (a fit in a log-log scale gives back an exponent very close to one (1 ± 0.001)).

Therefore, this confirms the prediction $\tau_i \propto \ell_i^2$, already suggested by the above result on persistence times. Note that this is different from what happens for the normal lattice gas, for which the relaxation timescale of the Fourier transform of the correlation function (for $k \neq 0$) inside any region of density $\rho \neq 1$ is independent on the size of the region.

Let us present the scenario for the dynamical heterogeneity that follows from these results. One can roughly rewrite the density-density correlation function separating the contributes from internal regions of different size and density as

$$C(k,t) \sim \sum_{l_i,\rho_i} p(l_i,\rho_i,\rho) C(k,t;l,\rho_i,\rho) \tag{6.65}$$

where $p(l_i,\rho_i,\rho_o)$ is the probability of regions of linear size l_i and density ρ_i and $C(k,t;l_i,\rho_i,\rho)$ is the average density-density correlation function inside these regions (6.64). On the basis of the previous numerical results we conjecture that

$$C(k,t;l_i,\rho_i,\rho) \simeq A(K,l_i,\rho_i,\rho) \exp\left(-\frac{t}{\tau(k,l_i,\rho_i,\rho)}\right) \tag{6.66}$$

where the relaxation time $\tau(k, l_i, \rho_i, \rho)$ goes like $l_i^2 \tilde{\tau}(k, \rho_i, \rho)$ for $l_i << \Xi(\rho_i)$ and approaches a constant dependent on k, ρ for $l_i >> \Xi(\rho_i)$. Note that $\tilde{\tau}(k, \rho_i, \rho)$ should approach a constant dependent on k, ρ when $\rho_i \to 1$ and it should diverge when $\rho \to 1$. On the other hand, we expect $A(K, \ell_i, \rho_i, \rho)$ to increase like ℓ_i^d (because the contribution of a high density square is weighted with its volume) and it should roughly be of the order $\rho_i - \rho_i^2$ (which gives the right value of $C(t)$ at $t = 0$).
For simplicity in the following we will take A as a constant and we shall investigate the behaviour of (6.65) at large times. Considering that the behaviour of $p(\ell_i, \rho_i, \rho)$ should be roughly $\exp(-\ell_i^d F(\rho_i, \rho))$, we make a saddle point evaluation to determine the terms which dominates the sum (6.65). The result for the dominant length $\bar{\ell}_i$ is

$$\bar{\ell}_i(t, \rho_i) = \begin{cases} (2t/d\tilde{\tau}F)^{1/(d+2)} & \text{if } (2t/d\tilde{\tau}F)^{1/(d+2)} < \Xi(\rho_i) \\ \Xi(\rho_i) & \text{otherwise} \end{cases} \tag{6.67}$$

In the former case the contribution to $C(k, t)$ is proportional to

$$\exp\left(- (2t/d\tilde{\tau}F)^{\frac{d}{d+2}} \frac{d+2}{2} F \right) \tag{6.68}$$

whereas in the latter we find

$$\exp\left(-F\Xi^d - \frac{t}{\Xi^2 \tilde{\tau}} \right) \tag{6.69}$$

Since contribution (6.69) goes to zero at large times faster than (6.68) we will focus just on (6.68) that should give the leading behaviour at long times, provided the condition in the first line of (6.67) is satisfied. Such condition can be inverted to obtain that all the densities that gives the saddle point contribution (6.68) are larger than a certain value $\rho(t)$ which approaches one very slowly as a function of time, i.e. like $1 - c_\infty / \log(t)$ with $c_\infty \sim 1.1$ in the case $d = 2$ $s = 1$ and $1 - c/\log\log(t)$ in the case $d = 3$ $s = 2$ (where do not know the numerical value of constant c). Combining this result with the fact that $\tilde{\tau}(\rho_i, \rho)$ and $F(\rho_i, \rho)$ shouldn't diverge when $\rho_i \to 1$ but just approach a constant, we find that the contribution of the high density, rare and almost blocked regions behaves like

$$g(t, \rho_i, \rho, k) \exp\left(- \left(\frac{2t}{d\tilde{\tau}(1, \rho_o) F(1, \rho)} \right)^{\frac{d}{d+2}} \frac{d+2}{2} F(1, \rho) \right) \tag{6.70}$$

where $g(t, \rho_i, \rho, k)$ is a function of time going to zero slower than the other term in (6.70) and, thus, it can be neglected in order to have the leading behaviour at long times. As a consequence we have found that the relaxation in the system is strongly heterogeneous and this dynamical heterogeneity is responsible for the stretched exponential of the density-density correlation function.

For the original three–dimensional case with $s = 2$, Kob and Andersen reported a stretched exponential with an exponent very close to 0.6 at least for $k = 2\pi 0.5$ which is therefore in agreement with our findings. For the two–dimensional case with $s = 1$ our simulations are not conclusive about this point. The exponent is close to 0.5 for $k = 2\pi 0.1$. However for larger and smaller values of k the exponent seems to be respectively larger and smaller than 0.5. It's not clear however if what one is able to extract from the numerical simulations is the real asymptotic behaviour. The problem is that at large time the noise on the curve is of the same order of the absolute value of the curve (which is approaching zero). As a consequence we can have the behaviour up to a certain time and not after. So if the rare and slow high density regions give a very small contribution (smaller than the noise) we could miss it. It could be also that the mechanism that we have unveil is not the slowest one and there is another, much slower, physical mechanism dominating the long time behaviour.

6.3 Conclusions

In this chapter we have analyzed the typical timescale of dynamics for KA models on hypercubic lattices, focusing in particular on the density dependence of the tagged particle self diffusion coefficient D_S. We have proved that $D_S > 0$ at any finite density, ruling out the possibility that a diffusive/non–diffusive transition occurs at a finite density. Moreover, we have identified both the time and spatial scales of the cooperative processes which allow diffusivity in the high density limit. This allows us to find the density dependence of the self diffusion coefficient, which is proportional to the density of the regions involved in the cooperative motion. The predicted form for the self diffusion coefficient in the high density region (which is in good agreement with numerical results) is $D_S \propto 1/\Xi^d$, with Ξ the density dependent crossover length identified in chapter 4, which goes to zero for $\rho \to 1$ faster than any power law of $1 - \rho$. This is due to the fact that the number of vacancies that have to move in a cooperative manner to allow diffusion is larger at larger densities and diverges for $\rho \to 1$ (recall that if a cluster of q vacancies can diffuse the self diffusion coefficient should be proportional to

$(1-\rho)^q$).

The fact that $D_S > 0$ at any density seems at a first sight in disagreement with numerical prediction which suggest for the case $d = 3$ $s = 2$ a diffusion coefficient vanishing as a power law at a finite density. By percolation—type arguments we find a possible explanation of this apparent dynamical transition. At low density there exists a diffusion mechanism which does not require the cooperative motion of large density dependent clusters of vacancies. Therefore, such mechanism is faster and its contribution to the diffusion coefficient dominates on the previous one. However, this diffusion mechanism is efficient only up to a certain density since it requires the underlying presence of a percolating cluster of vacancies. Moreover, its contribution to D_S goes to zero at a finite percolation treshold where the fraction of sites on the percolating cluster shrinks to zero. Therefore, at a finite density a crossover occurs between the two different mechanism, which could explain the large range of critical behaviour (power law decreasing of D_S near a finite density) numerically detected. Note that on the Bethe lattice the crossover is substituted by a real diffusive/non–diffusive transition. Indeed the collective processes which guarantees diffusivity at high density are related to the rearrangements that restore ergodicity in finite dimension and are absent in the mean field case.

Finally, we have discussed a possible quantitative explanation of the stretched exponential high density relaxation coming from the existence of a crossover length separating the regime in which a finite size system is almost ergodic from the regime in which collective rearrangements necessary in order for the ergodicity restoring rearrangements cannot typically be performed.

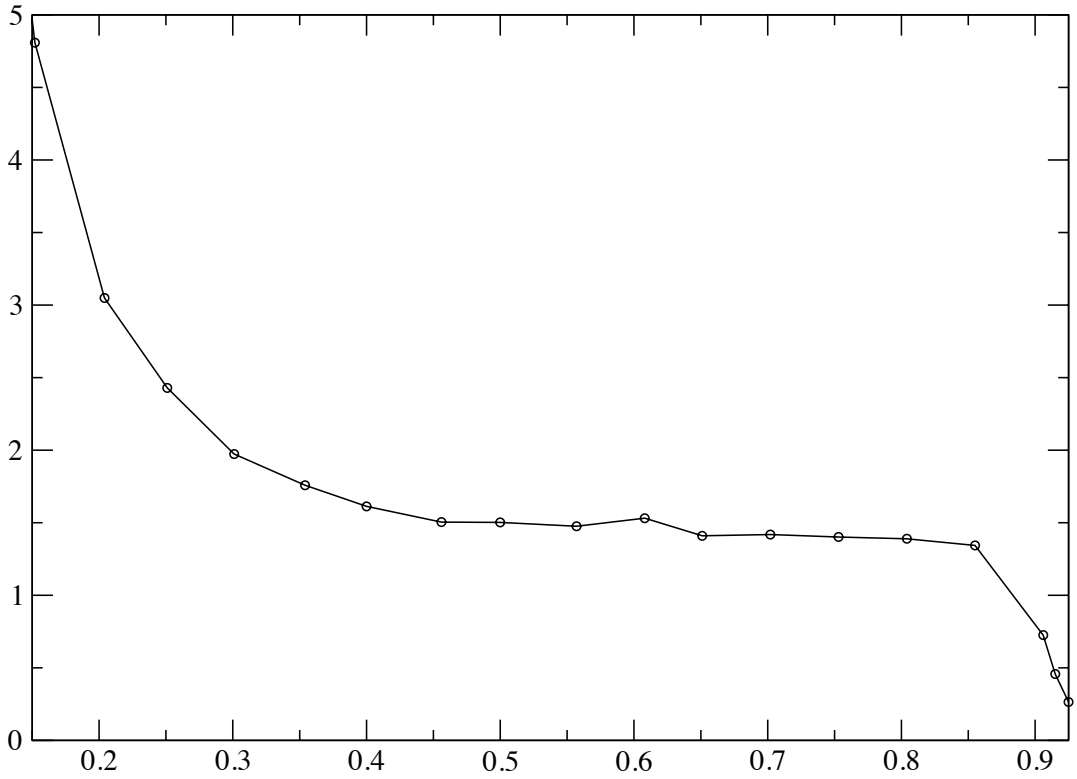

Figure 6.5: Numerical results for the ratio among D_S and ν^2 on a square lattice with parameter $s = 1$. The prediction [55], that D_S scales with ν^2 breaks down at a finite density $\rho \simeq 0.8$ above which D_S goes to zero more rapidly than any power law of $1 - \rho$, as predicted by (6.26).

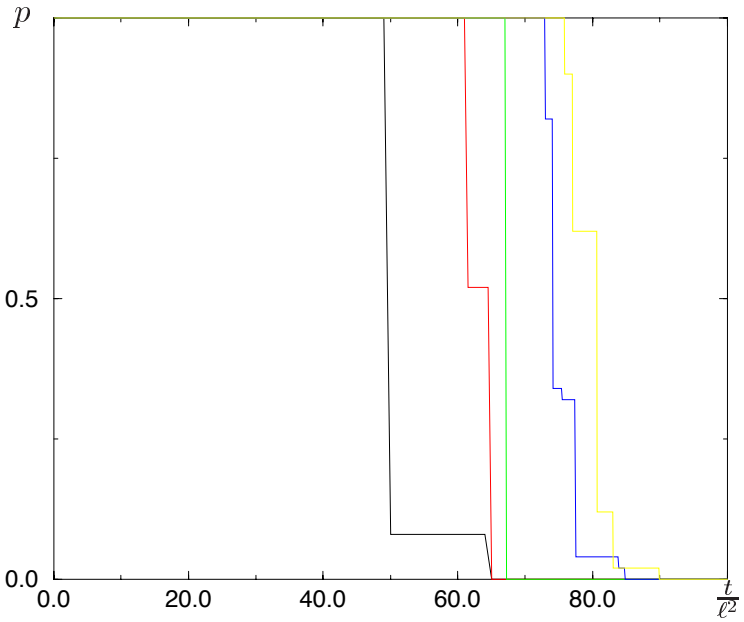

Figure 6.6: Numerical results for the persistence time. Here we plot the probability that the particle at the center has remained in its initial position until time t as a function of time for squares of linear size $\ell = 10, 14, 20, 28, 40$ (from left to right) with density $\rho = 1.$ embedded in a square $\ell = 100$ with density $\rho = 0.$ outside the high density square. The timescales has been rescaled as t/ℓ^2. For large ℓ the scaling ℓ^2 is rather well respected.

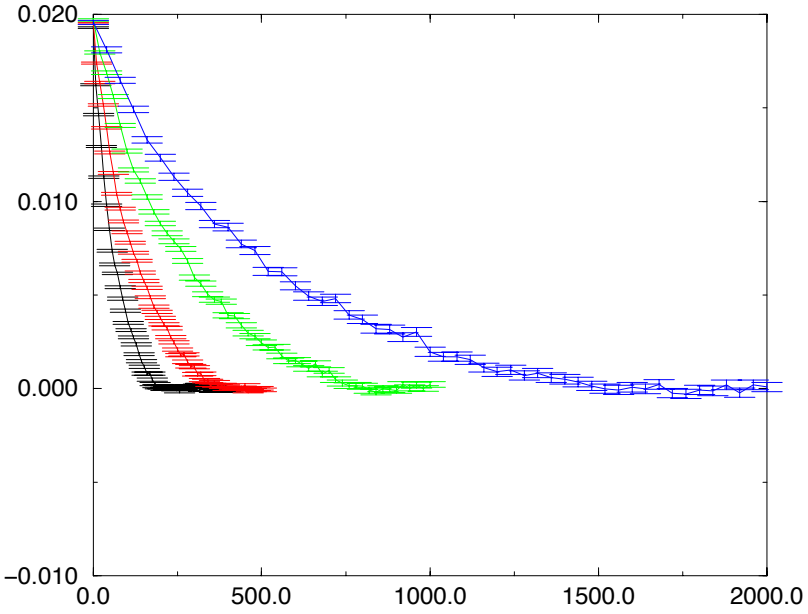

Figure 6.7: $C_{HD}(k,t)$ as a function of time on squares $\ell = 16, 22, 32, 44$ (from left to right) with density $\rho = 0.98$ embedded in a square $L = 100, 100, 100, 150$ with density $\rho = 0.1$ outside the high density square. ($k = 2\pi 0.5$)

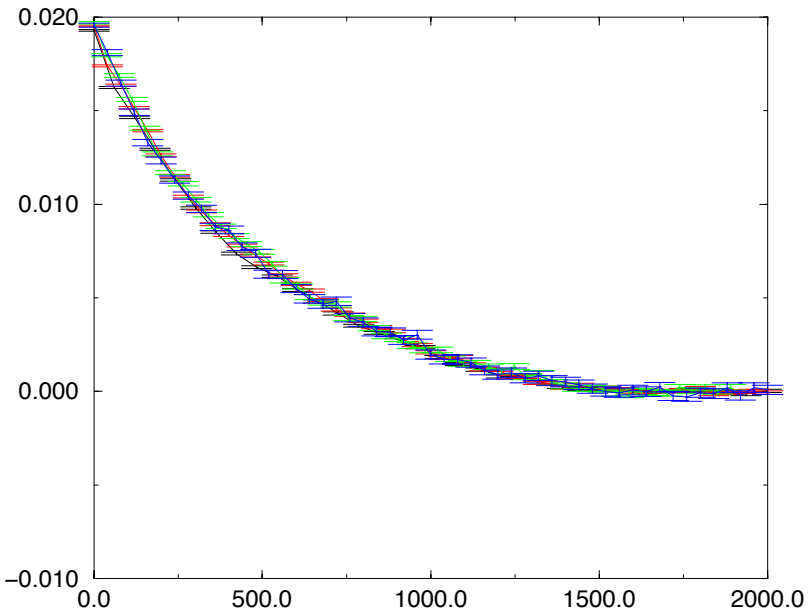

Figure 6.8: $C_{HD}(k,t)$ as a function of time on squares $\ell = 16, 22, 32, 44$ (from left to right) with density $\rho = 0.98$ embedded in a square $L = 100, 100, 100, 150$ with density $\rho = 0.1$ outside the high density square. Now the time has been rescaled as ℓ^2 (i.e. it has been rescaled as $(44/16)^2, (44/22)^2, (44/32)^2$ for $L = 16, 22, 32$).($k = 2\pi 0.5$)

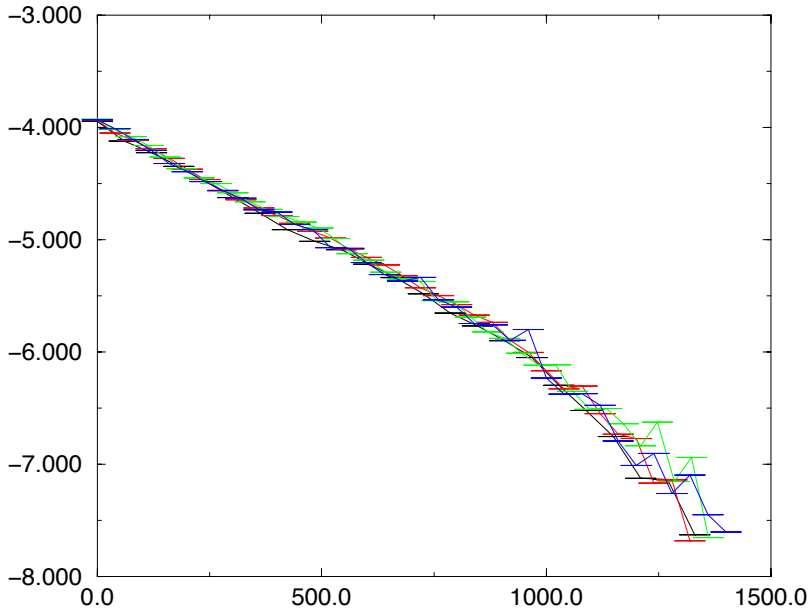

Figure 6.9: $\log C_{HD}(k,t)$ as a function of time on squares $\ell = 16, 22, 32, 44$ (from left to right) with density $\rho = 0.98$ embedded in a square $L = 100, 100, 100, 150$ with density $\rho = 0.1$ outside the high density square . Now the time has been rescaled as L^2 (i.e. it has been rescaled as $(44/16)^2, (44/22)^2, (44/32)^2$ for $L = 16, 22, 32$).($k = 2\pi 0.5$)

Chapter 7

FA model

After defining Fredrickson Andersen (FA) model on d-dimensional hypercubic lattices $\Lambda \in \mathbb{Z}^d$ and recalling previous results, we prove that also for this model irreducibility implies ergodicity. Therefore, an ergodic/non-ergodic transition *cannot take place* at any finite temperature $T > 0$. Moreover, we estimate typical relaxation times and check our predictions by numerical simulations. Then we study the mean field approximation of the model, i.e. FA on a Bethe lattice. In this case we find that there exists a critical temperature $T_c > 0$ at which an ergodic–non ergodic transition occurs. Finally, we study the character of this transition both by analytycal and numerical investigations.

7.1 Definition of the model

Let Λ be an hypercubic d–dimensional lattice and f a parameter chosen among $0, ..2d$. FA model [2] is a a spin facilitated Ising model (see section 2.6) with flip rates

$$c_x(\eta) := \begin{cases} 0 & \text{if } \sum_{\substack{d(\{z\},\{x\})=1 \\ z\in\Lambda}} (1-\eta_z) < f \\ \min\left(1, \exp -\frac{\Delta H}{T}\right) & \text{otherwise} \end{cases} \tag{7.1}$$

$\Delta H = H(\eta^x) - H(\eta)$ with $H = -h\sum_x \eta_x$ and h a positive constant. Recall that we represent up and down spins with an occupation variable taking one and zero value respectively. With this notation the configuration space is given, as for kinetically constrained model, by $\Omega_\Lambda = \{0,1\}^{|\Lambda|}$. However $\sum_{x\in\Lambda} \eta_x$ is no more conserved. Indeed the flip of a spin at site x corresponds to the birth or death of a particle at site x in the particle language. Note

that in the case $f = 0$ we would recover Glauber dynamics with Hamiltonian $H = -h\sum_x \eta_x$. On the other hand, for the above defined rates a spin in x can flip only if at least f of its nearest neighbors are in the down state (i.e. their occupation variable equals zero). For this reason, we refer to down spins as *facilitating spins* and to f as *facilitation parameter*. Since energy favors up spin (i.e. zero occupation variables), in the low temperature regime many moves will be rejected. Therefore we expect dynamics to be slow in this regime, as for the high density regime of KA models. Note that rates satisfy detailed balance with respect to equilibrium trivial product measure $\mu_{\Lambda,T}$

$$\mu_{\Lambda,T}(\eta) = \prod_{x\in\Lambda} \left(\frac{\exp(\beta h)}{1+\exp(\beta h)}\right)^{\eta_x} \left(\frac{1}{1+\exp(\beta h)}\right)^{1-\eta_x} \tag{7.2}$$

with $\beta = 1/T$, which corresponds to Bernoulli measure with density equal to the magnetization, i.e. the probability of a spin to be up. In other words the change $\rho \to \exp(\beta h)/(1+\exp(\beta h))$ transforms $\mu_T \to \mu_\rho$. However, on finite lattices this is not the unique invariant measure. Indeed, as for KA, there exist blocked configurations and the process is not ergodic.

7.2 FA on hypercubic lattices

7.2.1 Irreducibility and ergodicity

Let us recall former results for FA model on hypercubic lattices $\Lambda \in \mathbb{Z}^d$ (see [15] for a review), starting by the proof of irreducibility in the thermodynamic limit for the two and three–dimensional FA models [54]. Consider a configuration sorted at random on the lattice with Bernoulli measure and perform the boostrap procedure (see section 4.9) by removing at each step particles which have less than $2d - f$ neighbors occupied. It is immediate to check that, if at the end of such procedure no cluster of particles remains, the initial configuration belongs to the irreducible component which contains the configuration with all the spins down. Therefore, using the results for bootstrap percolation in [23], it is immediate to conclude that in the thermodynamic limit irreducibility holds (since all configurations belong with unit probability to the same irreducible component) at any temperature if $2 \le f < d$, while at any temperature irreducibility does not hold if $f \ge d$. Actually, in [54] this result was proven for the two and three–dimensional cases, but it is immediate to generalize it to higher dimensional cases using the already mentioned recent results on bootstrap percolation [26]. Note that for FA model all the moves that are allowed in bootstrap procedure are

also allowed for the true dynamics. Therefore, spins that are forever blocked up correspond to vacancies that remain after the boostrap procedure. This implies that bootstrap results are sufficient to conclude irreducibility in the thermodynamic limit, at variance with the KA case[1]. Moreover, the crossover length $L^B(\rho)$ of bootstrap procedure is in this case not only a lower bounds as for KA, but coincides with the one for FA model. In order to obtain the temperature dependence of such crossover length it is sufficient to perform the change of variables $\rho \to \exp(\beta h)/(1+\exp(\beta h))$ (see end of previous section).

As we explained in section 2.5.1, irreducibility in the thermodynamic limit is not a sufficient condition for ergodicity, which is the physically interesting property. On the other hand, a sufficient condition to establish ergodicity is proving that any eigenvectors with zero eigenvalue of the generator of the Markov process is a constant. By using the same strategy as in section 4.8 and the fact that the invariant measure (7.2) is again a product measure, we prove that for FA models irreducibility implies ergodicity. The key ingredient is that $\mu_T(\mathcal{H}) = 1$, where $\mathcal{H}$ is the irreducible component which contains the configuration with all spins down. Indeed, this allows us to establish that if $\mu_T(f\mathcal{L}f) = 0$ then $f(\eta^{xy}) = f(\eta)$ almost surely with respect to μ_T for any couple of site x, y[2]. This, using again DeFinetti's theorem on the decomposition of exchangeable measures on product measures ([42,43]), we conclude that f is constant a.s. with respect to μ_T.

7.2.2 Relaxation

Let us turn to the relaxation behaviour. For FA model on a hypercubic d–dimensional lattice it is well known from previous results and simulations that the behaviour is strongly different in the case $f = 1$ and in all the other cases. In the former case a single down spin can facilitate the flip of any of its neighbors, therefore relaxation does not require cooperative processes and times scale are proportional the density of down spins, as is confirmed by numerics. In some sense, this version of FA model is analogous to the models we have introduced in chapter 3: the single down spin plays the same role of

[1]This is due to the fact that for KA models to perform a move a requirement on the number of neighbors on the final position is also imposed and morever the dynamics conserves the number of particles. Therefore a sequence correspondent to the bootstrap procedure is not a sequence of allowed moves for KA.

[2]Note that now the generator of the process does not contain terms of the form $f(\eta^{x,x+e_i} - f(\eta)$ corresponding to the exchange of neighboring occupation variables. However, such terms can be easily reconstructed by means of two spin flips, i.e. using equality $f(\eta^{xy}) - f(\eta) = (f((\eta^x)^y - f(\eta^y)) + (f(\eta^y) - f(\eta))$.

finite clusters of vacancies that can freely move in an otherwise totally filled lattice. On the other hand, if $f > 1$ neither a single facilitating spin nor a finite cluster of them can subsequencially flip down the other spins if they are all up. Furthermore, it is natural to expect that cooperative processes are involved in relaxation at low temperature since the relaxation time does not scale as a power law of the density of up spins. However, the nature of the cooperative mechanism which guarantees relaxation and the exact scaling for the times is still an open issue (see [15]).

Consider again the cores of minimally frameable regions defined in chapter 4. It is immediate to check that using moves allowed by FA rules every occupation variable inside the core can be set to zero, i.e. every spin can be flipped to the facilitating state. Then, one can typically sequentially flip all the spins in a row of length ξ adjacent to such core. We conjecture that the diffusion of these *macro–defects* is the dominant mechanism for relaxation in the low temperature regime. Therefore, by the knowledge of the temperature dependence[3] of size and relaxation times for such defects and neglecting as for KA the interaction among two defects[4], we find the temperature dependence of relaxation times. As for KA model, these times are dominated by the large distance among the defects. For the case $d = 2$ $f = 2$, this yields

$$\tau \simeq \exp -\frac{2c_\infty}{1 - m(T)} \tag{7.3}$$

where $c_\infty \simeq 1.1$ (see equation (4.46)) and $m(T)$ is the magnetization, i.e. $1 - m(T)$ is the probability of finding a facilitating (i.e. up) spin. Therefore, we expect typical relaxation times τ to scale as

$$\tau \propto \left(L^B(\rho)(2,2)\right)^2 \tag{7.4}$$

We have run numerical simulation on a lattice to check above prediction. Relaxation time τ is measured both as the integrated persistence time and from the integrated correlation function. The two results are consistent and they are both in good agreement with above prediction (7.4), as shown in figure 7.1. Indeed, in this figure we report the logarithm of τ multiplied by $(1 - m(T))/2$ as a function of $1 - m(T)$ which converges to $c_\infty \simeq 1.1$ for $1 - m(T) \to 0$, i.e. for $T \to 0$. We recall that (7.4) gives the time relaxation

[3]Rewriting the size of typical cores as a function of density simply means substituting the particle density ρ with the temperature dependent magnetization, see section 7.1

[4]It is a priori possible that such interaction changes the typical relaxation times. Our estimate for the time corresponds to an inverse power of the facilitating spin density with the exponent given by the number of facilitating spins in a macro defect. Such interactions could slightly change this exponent as has been claimed in [40] for the easiest case $f = 1$.

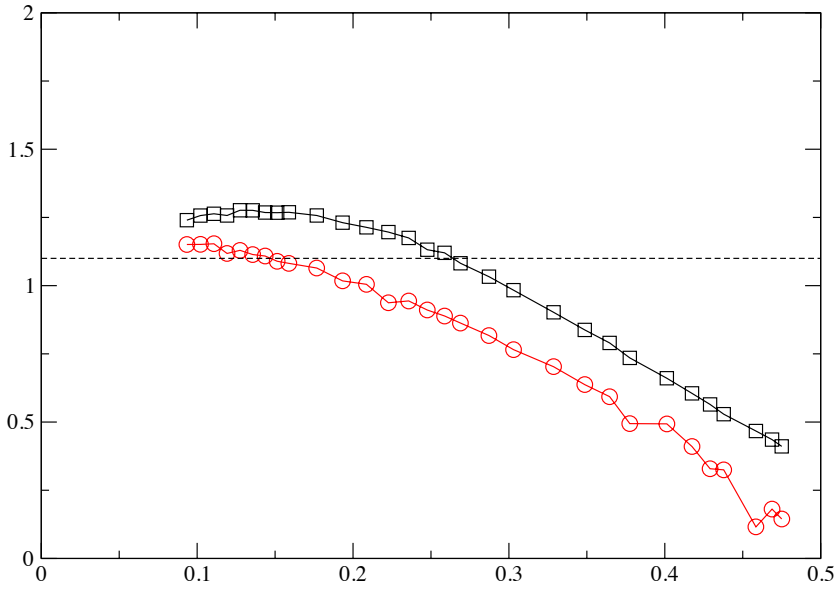

Figure 7.1: Logarithm of typical relaxation time multiplied by $1-m(T)/2$ as a function of $1-m(T)$, i.e. the probability for a spin to be down at temperature T. For $T \to 0$, prediction 7.4 is fulfilled. The two curves correspond to times obtained with the integration of persistence time (squares) and from the decay of the correlation function (circles).

only in the low temperature limit, while at higher temperatures different relaxation mechanisms are present and we do not expect (7.4) to hold (therefore our result is not in contradiction with the fact that numerical data do not follow above law for higher temperatures). Indeed, the same percolation–type arguments as for KA models assure the existence of a non–cooperative relaxation mechanism at high enough temperature. In next section we will show that this dynamical crossover is again related to the existence of a true dynamical transition in the mean field approximation.

By using arguments analogous to those in section 6.2[5] and the knowledge

[5]Note that arguments in section 6.2 rely on the fact that the time to unblock a region with size ℓ and density ρ goes like ℓ^2 if $\ell \ll \Xi(\rho)$. In a non–interacting spin system, the typical time to flip a given spin is usually independent on the size of the system. However, for FA models with $f > d$, to flip a spin inside a low temperature region one must wait until a macro–defect enters this region and "propagates" to the chosen spin. Since the diffusion of such defects involves mechanisms which are analogous to those for KA, it is

of the temperature dependence of the crossover length (see previous section), we derive a stretched exponential relaxation for spin autocorrelation functions with a stretching exponent $\beta = d/(d+2)$. This prediction for the exponent is in good agreement with previous numerical results, for example in the two dimensional case with $f = 2$ a stretching parameter $\beta = 0.5$ has been detected in [45].

7.3 FA on the Bethe lattice

Let us consider FA model on the Bethe lattice. As usual, one arranges the lattice as a tree with k branches going up from each node and one going down, and then proceeds downwards.

Let B be the probability that, without taking advantage of the configuration on the bottom, a node is in the state 0 or can be brought in this state rearranging sites above it. B verifies the iterative equation:

$$B = p_0 + p_1 \left(\sum_{i=0}^{k-f} \frac{k!}{(k-i)!i!} B^{k-i}(1-B)^i \right) \tag{7.5}$$

where we let

$$p_1 = \mu(\eta_x = 1) = \frac{\exp(\beta h)}{1+\exp(\beta h)} \tag{7.6}$$

$$p_0 = \mu(\eta_x = 0) = \frac{1}{1+\exp(\beta h)} \tag{7.7}$$

Equation (7.5) can be recovered also through the bootstrap procedure. Take a configuration at random on the Bethe lattice with the equilibrium measure and then flip to 0 all the sites for which the kinetic constraint allows the flip. The bootstrap percolation problem reduces to know if an (infinite) cluster of 1 remains at the end of this procedure (this problem has been already investigated a long time ago [25]). If this cluster exists then the FA dynamics will be non ergodic for sure. Thus, bootstrap results provide a lower bound on the temperature at which the dynamical transition takes place. We show in the following that this is not just a lower bound but it coincides with the one found solving equation (7.5) on B. Let P be the probability that a site is blocked in the state 1 because it has more than $k-f$ neighbors above blocked in the state 1. Each of this neighbors has also more than $k-f$ neighbors

reasonable to assume the same scaling for typical times. This can be checked by numerical simulations on the persistence time.

above blocked in the state 1 and so on and so forth. P verifies an iterative equation

$$P = p_1 \left(\sum_{i=0}^{f-1} \frac{k!}{(k-i)!i!} P^{k-i}(1-P)^i \right) \tag{7.8}$$

Making the change of variable $B' = 1 - P$, $i' = k - 1$ and using $p_0 + p_1 = 1$ we obtain that B' verifies the same equation of B. Thus the two transitions coincide. The reason is the following. If $P > 0$ then there will be sites blocked forever and $B < 1$. On the other hand, if $P = 0$ there exists with probability one a sequence of allowed moves that bring a random equilibrium configuration to the configuration with all sites 0 by definition (this set of configurations is the *high temperature partition* according to Fredrickson and Andersen definition). Hence, each site can flip to 0 after a certain number of allowed moves and $B = 1$[6].

By analogous arguments as in chapter 5 we can derive some general properties from the equation (7.8) on P. In particular at a finite temperature T_c (which depends on the value of k and f) a transition occurs from a finite to a zero value for P and such transition is discontinuous if $k > f$. This corresponds again to a transition from an ergodic regime (for $T > T_c$) to a non ergodic regime (for $T < T_c$) with a finite fraction of frozen spins. Furthermore, such transition has again a mixed character of first and second order. Indeed, at the transition P has again a square root singularity.

Before focusing on the particular cases $k = 3, f = 2$ and $k = 5, f = 3$, let us obtain an approximate estimate of the Edwards-Anderson parameter. After the dynamical transition the equilibrium measure is broken in different components. For each of them all the configurations have sites whose occupation variable is frozen under the FA dynamics. Therefore, at long times the correlation function

$$C = \frac{1}{N} \sum_i \langle n_i(t) n_i(0) \rangle \tag{7.9}$$

can be divided in two pieces:

- the sites that are frozen give a contribution p_1^{bf}, where p_1^{bf} is the probability that a site taken at random is in the state 1 and is blocked forever. This can be expressed in terms of P and p_1 as

[6]This corresponds to the observation of section 7.2.1 that spins that are forever blocked in the up state correspond to particles that can never be removed in the bootstrap procedure and not only vice versa.

$$p_1^{bf} = p_1 \sum_{i=0}^{f-1} \frac{(k+1)!}{(k+1-i)!i!} P^{k+1-i}(1-P) \tag{7.10}$$

- the sites not blocked forever give a contribution

$$\frac{1}{N} \sum_i \langle n_i \rangle^2 \tag{7.11}$$

where $\langle \cdot \rangle$ means the average within one of the ergodic component and we are summing only on non blocked sites. Because of the breaking of ergodicity the density profile is not flat and we do not know a priori how to calculate it. In the following we will use the approximation $\overline{\langle n_i \rangle^2} = \overline{\langle n_i \rangle}^2$ for an unblocked site i, where the overline means the average over the different ergodic components. The number of unblocked sites is $N(1 - p_1^{bf} - p_0^{bf})$, where p_0^{bf} is the probability that a site taken at random is in the state 0 and is blocked forever. It reads:

$$p_0^{bf} = p_1 \left(\sum_{i=0}^{f-1} \frac{(k+1)!}{(k+1-i)!i!} (p_1 P^3)^{k+1-i} (1 - (p_1 P^3)^i \right) \tag{7.12}$$

The number of sites in the state 1 that are not blocked is $N(p_1 - p_1^{bf})$. Thus the fraction of unblocked sites in the state 1 ($\overline{\langle n_i \rangle}$) is

$$\tilde{p}_1 = \frac{p_1 - p_1^{bf}}{1 - p_1^{bf} - p_0^{bf}} \tag{7.13}$$

Collecting all the contributions together we find the approximate estimate

$$C_\infty = p_1^{bf} + (1 - p_1^{bf} - p_0^{bf}) \tilde{p}_1^2 \tag{7.14}$$

If the correlation function is defined in such a way that in the liquid phase the long time value is zero and the value at time zero is one then

$$q_{EA} = \frac{p_1^{bf} + (1 - p_1^{bf} - p_0^{bf}) \tilde{p_1}^2 - p_1^2}{p_1 - p_1^2} \tag{7.15}$$

7.3.1 Case k=3, f=2

Consider FA model with facilitation parameter $f = 2$ on a Bethe lattice with $k = 3$ (which crudely mimics a square lattice). In this case the equation (7.8) gives

$$P = p_1 \left(P^3 + 3P^2(1-P) \right) \tag{7.16}$$

Pulling out a factor P we get the equation $1 = p_1(3P - 2P^2)$. The term in the parenthesis is maximum for $P = \frac{3}{4}$ and equals $\frac{9}{8}$. Thus the critical value of p_1 at which the transition takes place is $p_1^c = \frac{8}{9}$ which corresponds to $\beta_c = 2.07944$ and $T_c = 0.480898$. By running numerical simulations we have successfully checked this prediction. Indeed, as shown in figure 7.2, the decay of correlation becomes slower and slower at lower temperature and it develops a infinite plateau for $T \to T_c$ from above.
Note that, using the approximate formula for the q_{EA} we obtain that at the transition $q_{EA} \simeq 0.32$, which is not too far from the numerical value 0.4.

7.3.2 Case k=5, f=3

Consider FA model with facilitation parameter $f = 3$ on a Bethe lattice with $k = 5$ (which crudely mimics a cubic lattice). In this case the equation (7.8) gives

$$P = p_1 \left(P^5 + 5P^4(1-P) + 10P^3(1-P)^2 \right) \tag{7.17}$$

Pulling out a factor P we get the equation $1 = p_1(P^4 + 5P^3(1-P) + 10P^2(1-P)^2)$. The term in the parenthesis is maximum for $P \simeq 0.724022$ and equals 1.19777. Thus the critical value of p_1 at which the transition takes place is $p_1^c \simeq 0.834884$ which corresponds to $\beta_c = 1.62064$ and $T_c = 0.617038$. Using the approximate formula for the q_{EA} we obtain that at the transition $q_{EA} \simeq 0.407899$.

7.3.3 Out of equilibrium behaviour

In previous sections we have argued that, as for KA model, FA on the Bethe lattice has a dynamical ergodic/non–ergodic transition with a first order/marginal character similar to p–spin transition. Therefore, we have run some numerical simulations in the case $k = 3$ $f = 2$ to investigate whether this analogy extends also to the out of equilibrium behaviour. In figures 7.3, 7.4, 7.5 and 7.6 we draw the two–times response and correlation functions obtained when quenching the model to a temperature $T = 0.4 < T_c \simeq 0.48$. These results clearly show that the model displays the aging properties typical of disordered quenched spin models and experimentally valid for glass forming liquids (see section 2.3).

Let us discuss a possible scenario for this out of equilibrium regime. The irreducible component which contains the state with all spins in the facili-

tating state (the so called high temperature partition) has unit probability with respect to equilibrium measure above the critical temperature. On the other hand, for temperatures below the critical one there exists with finite probability an infinite cluster of forever blocked spins. Performing the quench from an initial temperature $T_i > T_c$ to a final temperature $T_f < T_c$ corresponds to take μ_{T_i} as initial configuration and then evolve it with FA dynamics with temperature $T = T_f$ in the rates (7.1). Since the initial state is concentrated on the high temperature partition it will remain there at any later time, therefore no infinite cluster of forever blocked spins can occur and the measure cannot relax to the equilibrium one at T_f. Consider the model equilibrated with rates at temperature $T = T_c + \epsilon$ with $\epsilon > 0$. For $\epsilon \to 0$ we expect that the equilibrium measure is concentrated on configurations with large clusters of up spin which are quasi blocked (the precursors of the infinite forever blocked clusters that occur when sampling configurations with μ_T with $T < T_c$), i.e. a very particular sequence of spin flips must be performed to unblock the whole cluster. We conjecture that by lowering the temperatures, i.e. for $\epsilon \to 0$, such clusters will survive while the remaining spins equilibrate and therefore the magnetization (concentration of up spins) increases towards its equilibrium value at T_c. If this conjecture is correct, chosen the value of the dynamically attained magnetization, m, one could calculate the value of other one time quantities by using a measure which is flat over all the ergodic components at temperature T_c and distributes the non–blocked spins with an equilibrium measure at a temperature such that the overall magnetization equals m. A test of such conjecture could be obtained by the numerical study of the violation of the fluctuation dissipation relation in the non–equilibrium regime. If above hypothesis is correct, this should give an effective temperature that corresponds to the derivative of the configurational entropy calculated at the critical temperature (i.e. with respect to μ_{T_c}).

7.4 Conclusions

In this chapter we have studied a kinetically constrained spin model, namely Friedrickson Andersen model. For such model bootstrap percolation procedure is exact. Indeed, all the moves that are allowed during this procedure can occur also for the real dynamics (at variance with what happens for KA model). Therefore, by using bootstrap results it is immediate to establish irreducibility in the thermodynamic limit. This, together with the fact that the equilibrium measure is trivial, implies that ergodicity also holds at any temperature. However, in the low temperature regime facilitating spins can

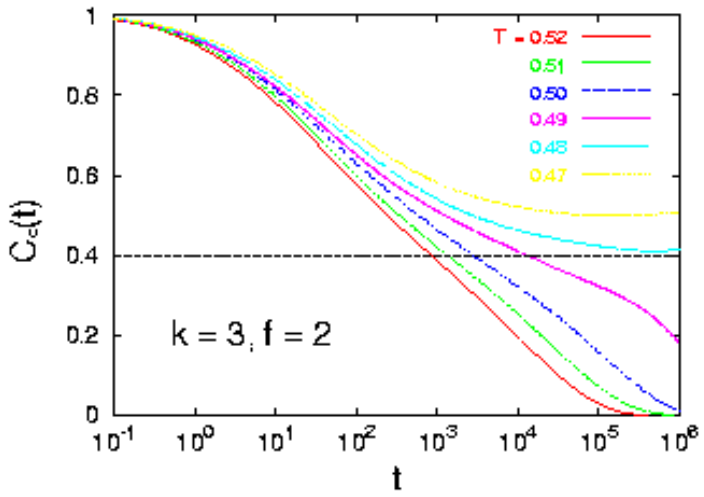

Figure 7.2: Correlation function in equilibrium in the case $k = 3$ $f = 2$ at different temperatures T

diffuse only in a cooperative way which involves large regions and the typical relaxation time diverges for $T \to 0$ as the density of these macro–defects. This scaling is confirmed by numerical results. In other words, some regions remain blocked until mobility is propagated through the sequential flip of up spins which occur in a cooperative way starting from a particular *macro–defect*, i.e. a large region containing many facilitating spins. The slowness of dynamics is due to the fact that such regions are very rare.

On the other hand, for FA model on a Bethe lattice we find that a dynamical ergodic/non–ergodic transition occurs at a finite density. As for KA on the Bethe lattice, such transition is smoothed in a dynamical crossover in finite dimensions. Moreover, the transition has again a first order/marginal character analogous to those of p–spin fully connected disordered models. Indeed, it is related again to the arising of fragile infinite clusters of forever blocked occupation variables. Here the analogy with p–spin models is strengthened by the investigation of the out of equilibrium regime, in which the system displays aging phenomena.

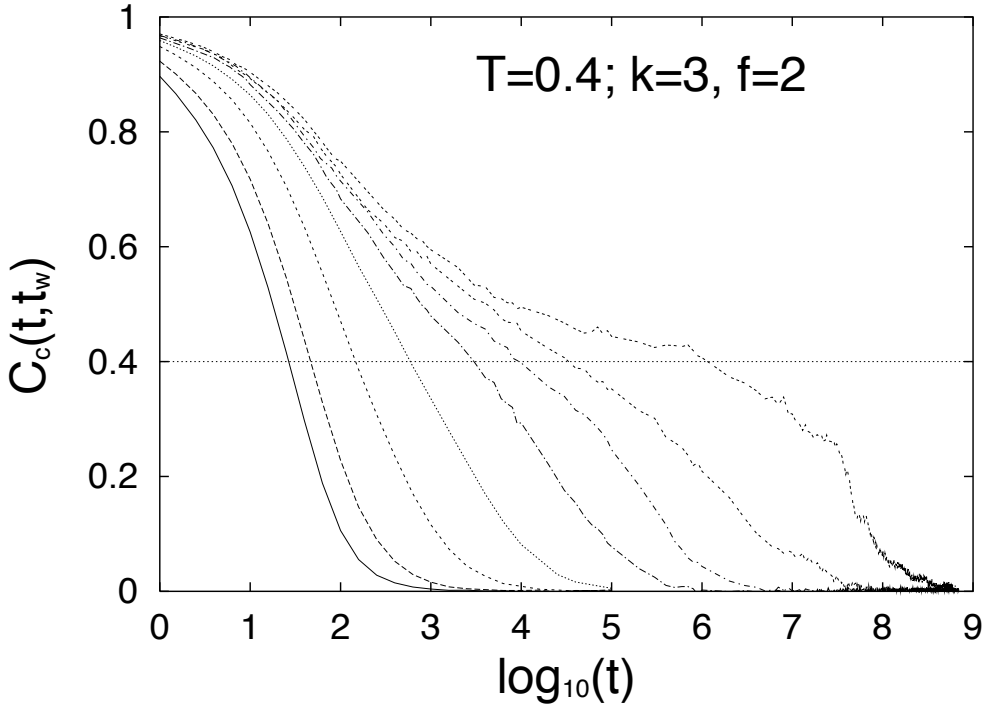

Figure 7.3: FA model on a Bethe lattice with $k = 3$, $s = 2$. Two times correlation function $C(t, t_w)$ after a quench at temperature $T = 0.4 < T_c$. The different curves correspond to different values of the waiting time $t_w = 10^k$, with $k = 1, \ldots, 8$ (from left to right).

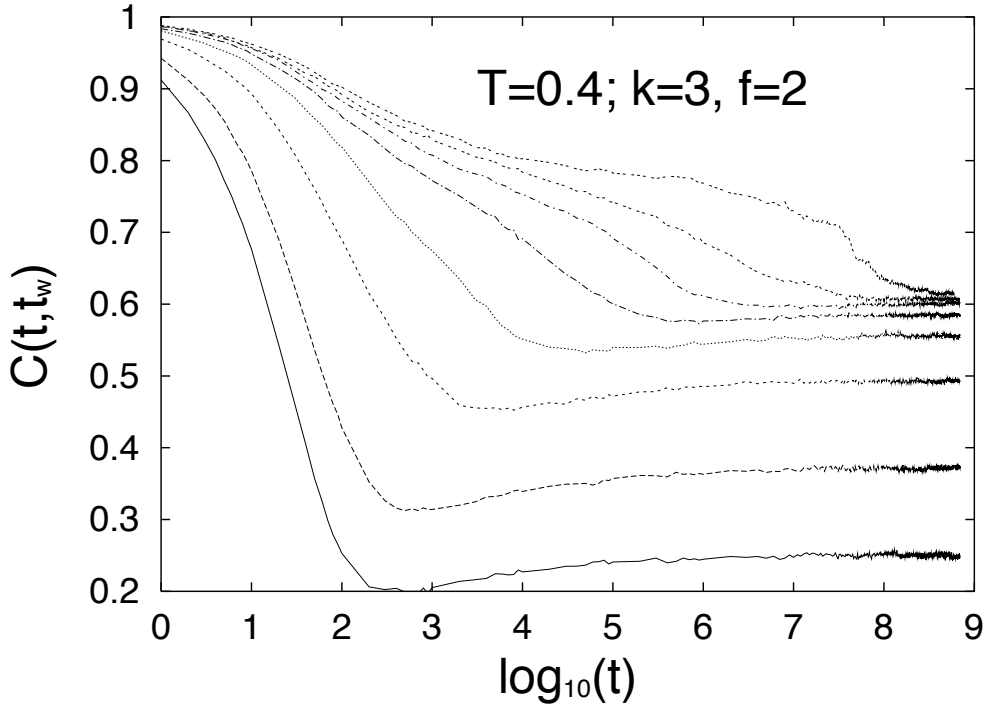

Figure 7.4: FA model on a Bethe lattice with $k = 3$, $s = 2$. Two times connected correlation function $C_c(t, t_w)$ after a quench at temperature $T = 0.4 < T_c$. The different curves correspond to different values of the waiting time $t_w = 10^k$, with $k = 1, \ldots, 8$ (from left ro right).

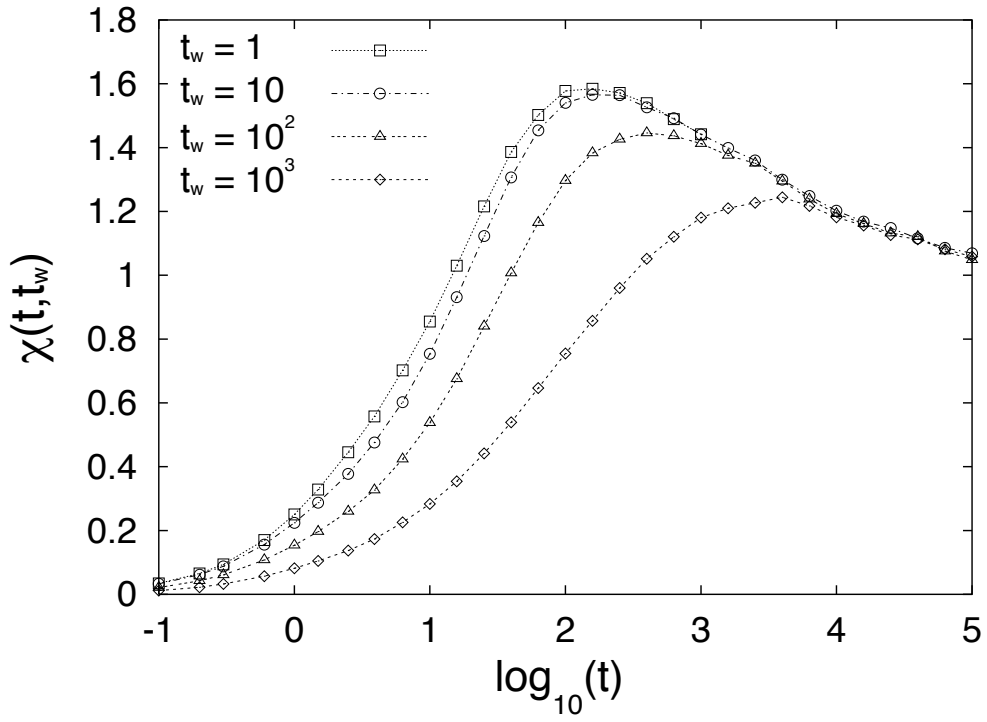

Figure 7.5: FA model on a Bethe lattice with $k = 3$, $s = 2$. Two times integrated response function $\chi(t, t_w)$ after a quench at temperature $T = 0.4 < T_c$. The different curves correspond to different values of the waiting time $t_w = 10^k$ with $k = 0, \ldots 3$ (short waiting–time behaviour).

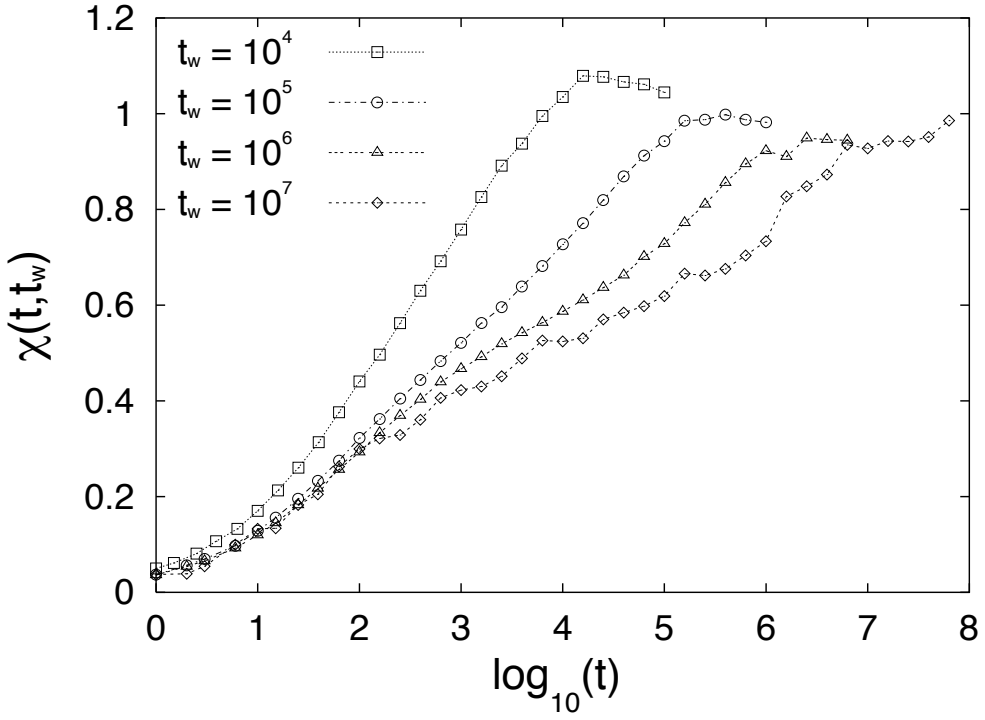

Figure 7.6: FA model on a Bethe lattice with $k = 3$, $s = 2$. Two times integrated response function $\chi(t, t_w)$ after a quench at temperature $T = 0.4 < T_c$. The different curves correspond to different values of the waiting time $t_w = 10^k$ with $k = 4, \ldots 7$ (long waiting–time behaviour).

Chapter 8

Conclusions and perspectives

In this work we have investigated the dynamical behaviour of some kinetically constrained particle and spin models. The dynamics is given through a continuous time Markov chain which allows nearest neighbors moves of particles and onsite spin flips, respectively. In particular, we focus on some models which satisfy detailed balance with respect to a trivial product measure, namely Bernoulli measure at any density for particle systems and Gibbs measure at any fixed temperature and with a non–interacting Hamiltonian for spin systems. The principal aim of the work was to investigate the mechanisms which induce a sluggish and heterogeneous dynamics for some choices of the rates in the high density (low temperature) regime. First we prove that in the thermodynamic limit an ergodic/non–ergodic transition cannot occur for such models on d–dimensional hypercubic lattices and typical relaxation times are always finite at finite density (finite temperature). However, in the high density (low temperature) regime relaxation occurs only through the cooperative motion of large rare regions and typical times scale as the distance of such regions which goes to zero faster than power law for $\rho \to 1$ ($T \to 0$). This is very reminiscent of the super–Arrhenius increase of relaxation times in supercooled liquids at low temperature. On the other hand, the scenario is different for the mean field version of such models obtained by considering them on a Bethe lattice, i.e. a random graph with fixed connectivity. Indeed, in this case an ergodic/non-ergodic transition takes place at a finite critical density (finite critical temperature). The latter separates an ergodic regime from a regime in which the system is partially frozen, namely there is a finite fraction of particles (spins) blocked forever. This transition has a first order/marginal character that is very reminiscent of the dynamical transition for p–spin models. The above mentioned ergodicity proof on hypercubic lattices allows us to identify the cooperative rearrangements which destroy such mean field transition in finite dimensions. Moreover, by percolation–

type arguments we find that the mean field transition is substituted in finite dimensions by a crossover from a non–cooperative to a cooperative relaxation mechanism. This explains the apparent dynamical transition detected by previous numerical simulations. In other words, our results unveil the cooperative processes which transform the mean field transition into a crossover in finite dimensional systems. Finally, we have discussed the heterogeneous relaxation in the high density (low temperature) regime. More precisely, by the knowledge of the density (temperature) dependent crossover length below which finite size effects are relevant, we have given a possible quantitative explanation of the stretched exponential relaxation of correlation functions.

Of course, many interesting issues remain open. In particular, the dynamical crossover and the heterogeneous relaxation deserve a further analytical and numerical investigation.

Concerning the crossover, we have run simulations for the KA model on a square lattice to check our predictions. However, in this case the crossover is not sufficiently sharp to detect an unambiguous power low of the self diffusion coefficient in the vicinity of the percolation threshold. Therefore, it could be interesting to analyze both hypercubic lattices in a higher spatial dimensions and different lattices for which we expect a sharper crossover. Indeed, gaining a further understanding of this mechanism, can be a useful ground for understating how the results obtained in other mean field approaches to glassy dynamics should be quantitatively modified in real systems. For example, dynamics near the mean field ergodic/non–ergodic transition has been extensively studied for fully connected disordered spin models and the extension of these results to the finite dimensional models is still debated.

On the other hand, concerning the heterogeneous relaxation it could be interesting to analyze the behaviour of the dynamical susceptibility χ_4 for these models. In particular, since we have sharp predictions both on the typical spatial and time scales of the cooperative processes involved in relaxation, we wish to investigate how the latter are related to the form of the dynamical susceptibility. This could be a very useful information in the study of different models of glasses, since usually analytical results are out of reach but the dynamical susceptibility can be obtained by numerical simulations.

Moreover, it would be interesting to establish the connection (if any) of our results with the out of equilibrium phenomenology that takes place when supercooled liquids are quenched below the temperature where they can equilibrate. Explaining such out of equilibrium phenomena and formulating a suitable ensemble that enables to calculate avarages of physical quantities in these regime is indeed a widely open problem. By running numerical simulations for the mean field version of FA model, we detect an out of equilibrium regime and aging features that are very similar to those of p–spin fully con-

nected disordered models. This out of equilibrium regime would deserve a further investigation. In particular, we conjecture that after a quench below the critical temperature the system is blocked on the threshold states which corresponds to the different possible ergodic components. In other words, we expect the measure to be well approximated by a flat distribution over the possible quasi–blocked clusters of up spins which dominates the equilibrium measure near (above) the critical temperature while the spins on the other sites equilibrate. Another relevant issue is to explain the aging phenomena detected for finite dimensional KA models [49]. In this case, since ergodicity holds, the measure relaxes to the equilibrium trivial one in the long time limit. However, typical diffusion times becomes very long above a finite crossover density (see section 6.1.4) and we expect the same to be true for the mixing time that controls the convergence of an initial measure to equilibrium. Therefore, aging phenomena should occur above the crossover on finite (long) times. By using the knowledge of the density dependence of time and spatial scales for relaxation, it should be possible to derive quantitative predictions on such phenomena.

Of course, it would also be interesting to extend our results to more realistic models of the physical systems which undergoes a glass transition. In this respect, one should investigate kinetically constrained models with a non trivial equilibrium measure, i.e. with interactions among particles (besides hard core constraint) or spins. Results on ergodicity should trivially generalized to these models (as long as a thermodynamic transition in the equilibrium measure does not occur), but density (temperature) dependence of typical relaxation times could be different. More importantly, one should try to extend the results to models of continuous character. The simplest among such continuous generalization is the hard sphere model. By arguments similar to those in chapter 4 and some additional work, we are able to generalize the result of irreducibility for this model. However, in the absence of an auxiliary procedure analogous to bootstrap percolation for discrete models, extending the results on typical diffusion times is a non trivial task.

Appendix A

Entropy decrease for the porous media equation

In this Appendix, by a scaling limit of the logarithmic Sobolev inequality, we deduce the exponential decrease of a suitable entropy for a nonlinear degenerate parabolic equation (porous media equation).

Let us consider the following parabolic problem, called porous media equation, on $B := [0,1]^d$ with Dirichlet boundary conditions

$$\begin{cases} \partial_t u(t,r) = \nabla_r \cdot \big(D(u(t,r)) \nabla_r u(t,r)\big) & (t,r) \in (0,\infty) \times B \\ u(t,r) = \rho & (t,r) \in (0,\infty) \times \partial B \\ u(0,r) = \varphi(r) & r \in B \end{cases} \tag{A.1}$$

where $\rho \in (0,1)$, the initial datum $\varphi \in C(B;[0,1])$ satisfies $\varphi(r) = \rho$ for $r \in \partial B$, and the diffusion coefficient $D(u) \geq 0$ is smooth and degenerates linearly for $u = 1$, namely the exists a constant $\delta \in (0,1)$ such that $\delta(1-u) \leq D(u) \leq \delta^{-1}(1-u)$, $u \in [0,1]$. Since we assumed $0 \leq \varphi \leq 1$, by the maximum principle, we have that $u \in C(\mathbb{R}_+ \times B; [0,1])$.

As discussed in the introduction, the equation (A.3) is the natural candidate for the hydrodynamic limit of the process with generator $L_\Lambda^{(k)}$, the diffusion coefficient $D(u)$ would be given by a Green–Kubo formula [17, §II.2.2]. Note that the Dirichlet boundary condition is due to the particles' reservoirs. Although we do not prove any scaling limit of the microscopic dynamics to (A.3), we show how the logarithmic Sobolev inequality (3.31) implies the exponential decrease of a suitable entropy for the nonlinear evolution (A.3).

Given $\rho \in (0,1)$, we introduce the convex functional $H_\rho : C(B;[0,1]) \to \mathbb{R}_+$ as

$$H_\rho(u) := \int_B dr \, \Big[u(r) \log \frac{u(r)}{\rho} + (1 - u(r)) \log \frac{1-u(r)}{1-\rho} \Big] \tag{A.2}$$

where we understand $0 \log 0 = 0$. It is easy to show that H_ρ is a Lyapunov functional for the evolution (A.3), moreover if $u(t,r)$ is a smooth solution of (A.3) bounded away from 0 and 1 we have

$$-\frac{d}{dt} H_\rho(u(t,\cdot)) = \int_B dr\, u(t,r)[1-u(t,r)] D(u(t,r)) \Big(\nabla_r \log \frac{u(t,r)}{1-u(t,r)} \Big)^2 =: \mathcal{Q}(u(t,\cdot)) \tag{A.3}$$

The following theorem, which states a "logarithmic Sobolev inequality" for the nonlinear evolution (A.3) is easily obtained as a scaling limit of (3.31).

Theorem A.0.1. *For each $\rho \in (0,1)$ and $\delta > 0$ there exists a constant $C' = C'(d,\delta,\rho)$ such that for any $u \in C^1\big(B;[0,1]\big)$ with $u(r) = \rho$ for $r \in \partial B$*

$$H_\rho(u) \le C' \mathcal{Q}(u) \tag{A.4}$$

Remark. The inequality (A.4) can be proven directly by reducing it to the Poincaré inequality for the Dirichlet Laplacian on B. The probabilistic proof given below, which somehow connects the evolution (A.3) to the microscopic process, shows additionally that the Lyapunov functional H_ρ is the macroscopic limit of a relative entropy.

Proof. We shall prove the bound (A.4) for $D(u) = 1-u^2$; the generic case of D degenerating linearly for $u \uparrow 1$ follows by our hypothesis on the diffusion coefficient D. By truncation, it is also enough to prove (A.4) when u is a smooth function bounded away from 0 and 1.

We set $\varepsilon := \ell^{-1}$ and apply inequality (3.31) for $k = 1$ choosing $f^2 = g_\varepsilon$ where

$$g_\varepsilon(\eta) = \prod_{x \in \Lambda} \frac{u(\varepsilon x)^{\eta_x} [1-u(\varepsilon x)]^{1-\eta_x}}{\rho^{\eta_x} [1-\rho]^{1-\eta_x}} \tag{A.5}$$

Note that $\mu^\varepsilon_{\Lambda,\rho,u}(\eta) := \mu_{\Lambda,\rho}(\eta) g_\varepsilon(\eta)$ is a product probability measure on Ω_Λ with density profile u, namely $\mu^\varepsilon_{\Lambda,\rho,u}(\eta_x) = u(\varepsilon x)$. By elementary computations which we omit, we have that the normalized relative entropy of $\mu^\varepsilon_{\Lambda,\rho,u}$ w.r.t. $\mu_{\Lambda,\rho}$ converges to $H_\rho(u)$ as $\varepsilon \to 0$, namely

$$\lim_{\varepsilon \to 0} \varepsilon^d \mu_{\Lambda,\rho} \Big(g_\varepsilon \log \frac{g_\varepsilon}{\mu_{\Lambda,\rho}(g_\varepsilon)} \Big) = H_\rho(u) \tag{A.6}$$

Moreover it is straightforward to check that

$$\lim_{\varepsilon \to 0} \varepsilon^{d-2} \mathcal{E}^{(1)}_{\Lambda,\rho}(\sqrt{g_\varepsilon}) = \mathcal{Q}(u) \tag{A.7}$$

Let $C(d,1,\rho)$ be the constant such that (3.31) holds for $k = 1$. By (A.6) and (A.7) the bound (A.4), with $C' = C(d,1,\rho)$, now follows from Theorem 3.2.3. □

The exponential decrease of the "entropy" H_ρ along the flow of the porous media equation (A.3) follows from equation (A.3) Theorem A.0.1, and a straightforward truncation argument.

Corollary A.0.2. *Let $u \in C(\mathbb{R}_+ \times B; [0,1])$ be the solution of (A.3) and $C' = C'(d, \delta, \rho)$ be the constant in (A.4). For each $\rho \in (0,1)$ we have*

$$H_\rho(u(t,\cdot)) \leq e^{-t/C'} H_\rho(\varphi) \tag{A.8}$$

for any $t \in \mathbb{R}_+$ and any $\varphi \in C(B; [0,1])$ such that $\varphi(r) = \rho$ for $r \in \partial B$.

We have assumed that the diffusion coefficient $D(u)$ degenerates linearly for $u = 1$. One can also obtain the exponential decrease of the entropy H_ρ if $D(u) \asymp (1-u)^n$, n a positive integer. This can be shown by introducing a microscopic model in which the exchange rate $c_{x,x+e_i}(\eta)$ is zero iff there exists $j = 1, \ldots, n$ such that $\eta_{x-je_i} = \eta_{x+(j+1)e_i} = 1$. It is in fact possible to prove that the logarithmic Sobolev constant for such a model is of the order ℓ^2.

Bibliography

[1] W. Kob and H.C. Andersen, Phys. Rev. E **48** (1993) 4364.

[2] G.H. Fredrickson, H.C. Andersen Phys.Rev.Lett, **53** (1984), 1244; J.Chem.Phys, **83** (1985), 5822.

[3] M. Mezard Physica A **306** (2002) 25.

[4] Recent reviews: P.G. De Benedetti and F.H. Stillinger , Nature, **410**, (2001) 267; C.A. Angell, Science, **267**, 1924 (1995); P. G. De Benedetti, *Metastable liquids*, Princeton University Press (1997); G.Tarjus and D. Kivelson, in *Jamming*, A. Lui and S. R. Nagel eds., Taylor and Francis, N.Y., 2001.

[5] A.W.Kauzman, Chem.Rev. **43** (1948) 219.

[6] L.F. Cugliandolo arXiv: cond-mat/0210312v2.

[7] W. Kob arXiv: cond-mat/0212344.

[8] R. Kohlrausch, Ann. Phys. **12** (1847) 393.

[9] G.Williams, D.C.Watts, Trans.Faraday Soc. **66** (1980) 80.

[10] S.F.Edwards in *Granular matter: an interdisciplinary approach* A. Metha Ed. (Springer Verlag, New York, 1994).

[11] Gotze W. in *Liquids Freezing and the Glass Transition* Eds. Hansen, Levesque D., J.Zinn-Justin Z., 287 (North-Holland Amsterdam, 1991).

[12] Cugliandolo L.-F., Kurchan J. Phys. Rev. Lett. **71** (1993), 173.

[13] Kirkpatrick T.R., Thirumalai D. Phys. Rev. Lett. **58** (1987), 2091; Kirkpatrick T.R., Thirumalai D., Wolynes P.G. : Phys. Rev. A **40** (1989) 1045.

[14] J.H.Gibbs, E.A. DiMarzio J.Chem.Phys **28** (1958), 373.

[15] A recent review is F. Ritort, P. Sollich *Glassy dynamics of kinetically constrained models* cond-mat/0210382.

[16] J.P. Garrahan and D. Chandler, cond-mat/0301287.

[17] Spohn H. : *Large scale dynamics of interacting particles.* Berlin: Springer 1991.

[18] H. Spohn, J. Stat. Phys. **59**, (1990) 1227; Physica A **163**, (1990) 134.

[19] Kipnis C., Varadhan S.R.S. Comm. Math. Phys. **104** (1986) 1.

[20] T.Liggett *Interacting particle systems* Springer (New York,1985).

[21] C.Ané, S.Blachère, D.Chafaï, P.Fougères, I.Gentil, F.Malrieu, C.Roberto, G.Scheffer : *Sur les inégalités de Sobolev logarithmiques.* Panoramas et Synthèses, **10**. Société Mathématique de France, Paris, 2000.

[22] C.Kipnis, C.Landim *Scaling limits of interacting particle systems*Springer (NewYork, 1999).

[23] M. Aizenmann and J.L. Lebowitz, J. Phys. A **21** (1988) 3801.

[24] J. Adler, Physica A **171**, (1991) 435.

[25] J. Chalupa, P.L. Leath and G.R. Reich, J. Phys. C **12** (1979) L31.

[26] R.Cerf, E.Cirillo, Annals. of Probab. **27 n. 4** (1999) 1837.

[27] R. Cerf, F. Manzo, Stoch. Proc. Appl. **101** (2002) 69.

[28] A.E. Holroyd, Probab. Theory Rel **125** (2003) 195.

[29] M.Mezard, G.Parisi Eur.Phys.J. B **20** (2001) 217.

[30] O.Rivoire, G.Biroli, O.C. Martin, M.Mezard arXiv: cond-mat/ 0307569.

[31] M.Pretti arXiv: cond-mat/ 0201555.

[32] J. Hoshen and R. Kopelman, Phys. Rev. B **14** (1976), 3438.

[33] H.M. Jaeger, J.B. Knight, R.P. Behringer : *Granular solids, liquids, and gases.* Rev. Mod. Phys **68** (1996) 1259.

[34] Janvresse E., Landim C., Quastel J., Yau, H.-T. Ann. Probab. **27** (1999) 325.

[35] A.De Masi, P.A. Ferrari, S.Goldstein, W.D.Wick Journ. Stat.Phys. **55** (1989), 787.

[36] Liu A.-J., Nagel S.-R. editors *Jamming and rheology: constrained dynamics on microscopic and macroscopic scales.* Taylor and Francis, London, 2001.

[37] Lu S.L., Yau H.-T. Comm. Math. Phys. **156** (1993) 399.

[38] J. Quastel Comm. Pure Appl. Math. **45** (1992) 623.

[39] M. Sellitto, J.J. Arenzon, Phys. Rev. E **62** (2000) 7793.

[40] S.Whitelam, L.Berthier, J.P.Garrahan arxiv- cond-mat 0310207.

[41] H.T. Yau Comm. Math. Phys. **181** (1996) 367.

[42] H.-O. Georgii, Lecture notes in mathematics **760** Springer, Berlin (1979).

[43] B. DeFinetti Atti R. Acc. Naz. Lincei serie 6, **4** (1931) 251.

[44] M.M. Hurley and P. Harrowell, Phys. Rev. E **52** (1995) 1694. C. Donati, S. C. Glotzer, P. H. Poole, W. Kob, and S. J. Plimpton, Phys. Rev. E **60**, (1999) 3107.

[45] P.Harrowell, Phys.Rev E**48** (1993) 4359.

[46] M. Sellitto, J-J. Arenzon, Phys. Rev. E **62**, (2000) 7793.

[47] S. Franz, R. Mulet and G. Parisi, Phys. Rev. E **65**, (2002) 021506.

[48] J. Kurchan, L. Peliti and M. Sellitto, Europhys. Lett. **39** (1997) 365.

[49] A. Barrat, J. Kurchan, V. Loreto, M. Sellitto. Phys. Rev. E **63** (2001) 051301.

[50] S. Franz and G. Parisi J. Phys.: Condens. Matter **12** (2000) 6335. C. Donati, S. Franz, G. Parisi, S.C. Glotzer, J. Non-Cryst. Solids **307-310** (2002) 215.

[51] A.H.Marcus, J.Schonfield, S.A.Rice, Phys.Rev. E **60** (1999) 5725; W.Kegel, A. Blaaderen, Science **287** (2000) 5451; E.Weeks, J.C.Crocker, A.C.Levitt, A.Schonfield, D.A.Weitz, Science **287** (2000) 627.

[52] C.Donati, S.C.Glotzer, P.H.Poole, Phys.Rev.Lett. **82** (1999) 5064; W.Kob, C.Donati, S.J.Plimpton, P.H.Poole, S.C.Glotzer, Phys.Rev.Lett. **79** (1997) 2827.

[53] J.P. Bouchaud, L.F. Cugliandolo, J. Kurchan and M. Mézard, *Spin Glasses and Random Fields*, Singapore 1998. World Scientific. L.F. Cugliandolo, cond-mat/0210312.

[54] R.H.Schonmann Ann.rob. **20** (1992), 174.

[55] A. Lawlor, D. Reagan, G. D. McCullagh, P. De Gregorio, P. Tartaglia, and K. A. Dawson , Phys. Rev. Lett. **89** (2002) 245503.

[56] L. Berthier, cond-mat/0303452.

Acknowledgments

I wish to thank Gianni Jona Lasinio for wisely guiding and constantly encouraging me during my PhD studies. I am also very grateful to him for teaching me that a clear formulation of questions is more than a half of the work.

I owe particular thanks to Lorenzo Bertini, Giulio Biroli and Daniel Fisher for their precious collaboration in the main part of this thesis. I also deeply thank Lorenzo Bertini for patiently introducing me to the mathematical techniques for interacting particle systems and Giulio Biroli for his precious and constant help during the writing of this work and his hospitality at the SPhT/CEA in Saclay.

I also acknowledge very interesting discussions with Filippo Cesi, Silvio Franz, Jorge Kurchan, Marc Mezard and Mauro Sellitto and thank Mauro Sellitto for the numerical simulations on the FA model.